

**Artificial Imine Reductases Based on the Biotin-  
(Strept)avidin Technology:  
Genetic Optimization and Applications towards *in vivo*  
Transition Metal Catalysis**

**Inauguraldissertation**

zur Erlangung der Würde eines Doktors der Philosophie

vorgelegt der

Philosophisch-Naturwissenschaftlichen Fakultät der

**Universität Basel**

von

**Marc Dürrenberger**

aus Lupsingen BL

Basel 2017

Originaldokument gespeichert auf dem Dokumentenserver der Universität Basel

[edoc.unibas.ch](http://edoc.unibas.ch)

Genehmigt von der Philosophisch-Naturwissenschaftlichen Fakultät

auf Auftrag von

Prof. Dr. T. R. Ward und Dr. Prof. A. Pfaltz

Basel, den 22.4.14

Prof. Dr. Jörg Schibler

Dekan der Philosophisch-Naturwissenschaftlichen  
Fakultät

## Acknowledgements

My special thanks goes to Prof. Dr. Thomas Ward who gave me the opportunity to perform my PhD under his supervision and inspired me with his ideas and the enthusiasm to put them into practice. To work on an interdisciplinary topic such as artificial metalloenzymes was exactly what i liked to do when i decided to perform a PhD and thus i really enjoyed to be a member of his research group.

I wish also to thank Prof. Dr. Pfaltz for agreeing to be my co-examiner.

I am very grateful to Dr. Valentin Köhler and Dr. Yvonne Wilson for interesting discussions and nice moments in- and outside the lab. Their scientific experience was a great support.

I also like to thank all my other co-workers for their help and for many funny moments: Alessia, Anamitra, Cheikh, Christian, Elisa, Ewa, Fabien, Jeremy, Martina, Maurus, Maxim, Praneth, Raphael, Sabina, Sascha, Tillmann, Thibaud, Tommaso.

For their great support I would like to thank the "biologists" Livia, Julian and Juliane.

I like to thank all my students, especially Seraina Blümli for her great work.

Many thanks goes to Kaspar Zimmermann and Dr. Daniel Häussinger for their assistance with NMR studies.

Last but not least I would like to express my gratefulness to my family and all my friends. They have been here for me all the time. Thank you for everything!



## Preface

The present PhD Thesis summarizes the scientific work performed in the research group of Prof. Dr. Ward from 2010-14 at the university of Basel. The main topic of the Ward group is the design of artificial metalloenzymes for asymmetric catalysis. These hybrid catalysts result from the incorporation of a catalytically active transition metal complex within a host protein and thus combine properties of both traditional homogenous and biocatalysis. Moreover, the genetic tuneability of the protein scaffold allows to trigger the performance of an incorporated transition metal catalyst by modification of the second coordination sphere.

The high affinity of the vitamin biotin towards the eucaryotic protein avidin (Avi) and its procaryotic counterpart streptavidin (Sav) offers an attractive strategy for the creation of artificial metalloenzymes.

The conjugation of biotin with a catalytically active transition metal complex leads to an efficient incorporation of the latter within strept(avidin). This approach was applied extensively in the Ward group to obtain effective hybrid catalysts for a variety of reactions. The present work deals with the enantioselective reduction of prochiral imines to amines by artificial transfer hydrogenases (ATHase) which result from the incorporation of piano stool complexes of ruthenium, rhodium and iridium within Sav.

The Thesis is divided into four chapters. The first chapter provides an introduction into the topic of artificial metalloenzymes and illustrates their potential in asymmetric catalysis. A review article summarizes the most recent achievements of this research field.

The following two chapters present the research performed in context of several projects which resulted in four scientific publications. A brief introduction into the respective topic is given in each chapter. The author's contribution to each publication is highlighted in a preamble. An appendix at the end of each chapter presents additional results which did not appear in the corresponding publications.

Chapter two describes the genetic optimization of the ATHase and gives mechanistic insights in its operating mode. Chapter three focuses on attempts to implement transition metal catalysis *in vivo*. This would open fascinating perspectives to enable directed evolution of artificial metalloenzymes. Detailed procedures of experiments described in the appendices are given in chapter four.

# Contents

Acknowledgements

Preface

## Chapter 1: Introduction

1.1 Background of the Thesis	1
1.1.1 Chirality	1
1.1.2 Asymmetric catalysis	3
1.1.2.1 General Principles and Definitions	3
1.1.2.2 Homogenous Transition Metal Catalysis	4
1.1.2.3 Biocatalysis	5
1.1.2.4 Complementary of Homogenous and Biocatalysis	8
1.1.3 Artificial Metalloenzymes	11
1.1.3.1 General Concepts and Design of Artificial Metalloenzymes	11
1.1.3.2 Artificial Metalloenzymes Based on the Biotin-(Streptavidin) Technology	13
1.1.4 Recent Achievements in the Design and Engineering of Artificial Metalloenzymes	18
1.2 Goal of the Thesis	27
1.3 References	28

## Chapter 2: Design and Optimization of an Artificial Transferhydrogenase (ATHase)

2.1 Introduction	33
2.1.1 Homogenous Asymmetric Transfer Hydrogenation	33
2.1.1.1 Asymmetric Transfer Hydrogenation of Ketones	33
2.1.1.2 Asymmetric Transfer Hydrogenation of Imines	35
2.1.1.3 Asymmetric Transfer Hydrogenation in Water	38
2.1.2 Artificial Transfer Hydrogenases Based on the Streptavidin-Biotin Technology	39
2.2 Artificial Transfer Hydrogenases for the Enantioselective Reduction of Cyclic Imines	43
2.2.1 Preamble: Comment on Publications	43
2.2.1.1 Optimization of an Artificial Transfer Hydrogenase for the Reduction of 6,7-dimethoxy-3,4-dihydroisoquinoline	43
2.2.1.2 Kinetics and Mechanism of the Artificial Transfer Hydrogenase	44
2.2.2 Artificial Transfer Hydrogenases for the Enantioselective Reduction of Cyclic Imines	49
2.2.3 Structural-, Kinetic- and Docking Studies of Artificial Imine Reductases based on the Biotin-Streptavidin Technology: An Induced Lock-and-Key Hypothesis	63
2.2.4 Appendix	76
2.2.4.1 pK <sub>a</sub> of 6,7-dimethoxy-1-methyl-3,4-dihydroisoquinoline	76
2.2.4.2 Michaelis-Menten Kinetics of [( $\eta^5$ -Cp*)Ir(biot- <i>p</i> -L)H]C-S112A-K121T	77
2.3 Conclusions and Outlook	79
2.4 References	80



## Chapter 3: Towards *in vivo* Transition Metal Catalysis and its Potential Applications in the Directed Evolution of Artificial Metalloenzymes

3.1 Introduction	83
3.1.1 Principles of Directed Evolution	83
3.1.2. Directed Evolution of Artificial Metalloenzymes	85
3.2 Towards <i>in vivo</i> Transition Metal Catalysis	88
3.2.1 Preamble: Comment on Publications	88
3.2.1.1 Neutralizing the Detrimental Effect of Glutathione on Precious Metal Catalysts	88
3.2.1.2 Preventing Mutual Inhibition between Organometallic Catalysts and Cellular Proteins by the Use of Artificial Metalloenzymes	89
3.2.2 Synthetic Cascades are Enabled by Combining Biocatalysts with Artificial Metalloenzymes	92
3.2.3 Neutralizing the Detrimental Effect of Glutathione on Precious Metal Catalysts	122
3.2.4 Appendix	138
3.2.4.1 ATHase-mediated Generation of Amino Acids from Enone Precursors	138
3.2.4.2 ATHase-mediated Degradation of an Antibiotic	140
3.3 Conclusions and Outlook	142
3.4 References	143

**Chapter 4: Experimental**

4.1 General Information	147
4.1.1 Reagents and Solvents	147
4.1.2 Materials	147
4.1.3 Analytical Methods	147
4.2 Synthesis	149
4.2.1 Synthesis of $[(\eta^5\text{-Cp}^*)\text{M}(\text{biot-}p\text{-L})\text{Cl}]$ (M = Rh, Ir)	149
4.2.2 Synthesis of Amino Acid Precursors	158
4.2.3 Synthesis of Reference Compounds	164
4.3 HABA and CD Titrations	166
4.3.1 HABA titrations	166
4.3.2 CD titrations	167
4.3 NMR Experiments to Elucidate the Behavior of 6,7-dimethoxy-1-methyl-3,4-dihydroisoquinoline in Aqueous Solution	170
4.3.1 HMBC experiment to confirm the ring-closed structure	170
4.3.2 $^1\text{H}$ and $^{13}\text{C}$ NMR measurements to determine the $\text{pK}_a$ value	172
4.4 Catalysis	174
4.4.1 Control Experiments	174
4.4.2 pH-dependence of $[(\eta^5\text{-Cp}^*)\text{Ir}(\text{biot-}p\text{-L})\text{Cl}]$	176
4.4.3 Transfer Hydrogenation of Amino Acid Precursors	177
4.4.4 Transfer Hydrogenation of Enrofloxacin	180
4.5. References	182

# Chapter 1: Introduction

## 1.1 Background of the Thesis

### 1.1.1 Chirality

The term "chirality" describes the property of a molecule possessing no improper rotation axis to appear in two distinct forms which are the mirror image of each other. The two mirror images of a chiral molecule are called "enantiomers" and are not superimposable. Therefore, they behave like a right and a left hand (chirality = handedness, derived from the Greek term "cheir" = hand). The most common type of chirality relies on a tetrahedral central atom (stereogenic center) bearing four different substituents ("central chirality"). Compounds bearing multiple stereogenic centers are called "diastereoisomers" and comprise isomers which differ with respect to their three-dimensional arrangement but do not behave like mirror-images.

In contrast to diastereoisomers, enantiomers exhibit the same physical properties (e.g. boiling point, solubility) apart from the fact that their interaction with linearly polarized light is different in such a way that its polarized plane is rotated by the same angle but in opposite directions. A macroscopic rotation of the polarization plane results if a single enantiomer is present or if one enantiomer is enriched compared to the other one; a phenomenon which is called "optical activity". A 1:1 mixture of two enantiomers is called "racemate" and shows no optical activity as the effect of both enantiomers on the rotation of the polarization plane cancels out. By definition, substances that rotate polarized light to the right are indicated with the prefix "(+)" whereas compounds rotating light to the left are indicated with the prefix "(-)". The current

IUPAC nomenclature for enantiomers is based on the Cahn-Ingold-Prelog rules, using "(*S*)" for *sinister* (left) and "(*R*)" for *rectus* (right).<sup>1</sup> It should be noted that this nomenclature is not related to optical rotation. Chirality is a prevalent feature in nature and many natural compounds such as amino acids, carbohydrates or nucleotides as well as their respective biopolymers (proteins, oligosaccharids, DNA/RNA) exist almost exclusively as a single enantiomer. As a consequence, the two enantiomers of a particular small molecule (e.g. a drug) will interact in a different way with such a biopolymer (e.g. a particular enzyme which may cause a certain disease). The two enantiomers of a drug can thus have dramatically different biological effects. A very prominent and often-quoted example in this context is Thalidomide, the active component in the pharmaceutical Contergan which was sold as a racemate in the late 50's and early 60's of the last century to treat ahyponosis (Figure 1.2). It turned out that only the (+)-(*R*)-enantiomer exhibited the desired sedative effect whereas the (-)-(*S*)-enantiomer was teratogenic and caused birth defects when administered to pregnant women.<sup>2</sup> It should be noted that this problem would not be solved upon administering (+)-(*R*)-Contergan as it readily racemises under physiological conditions. Another prominent example in this context is the natural product carvone: the (-)-(*R*)-enantiomer smells like spearmint, the (+)-(*S*)-counterpart on the other hand smells like caraway.<sup>3</sup> These two examples convincingly demonstrate the different effects that enantiomers display in the presence of the enantiopure macromolecules of Life.

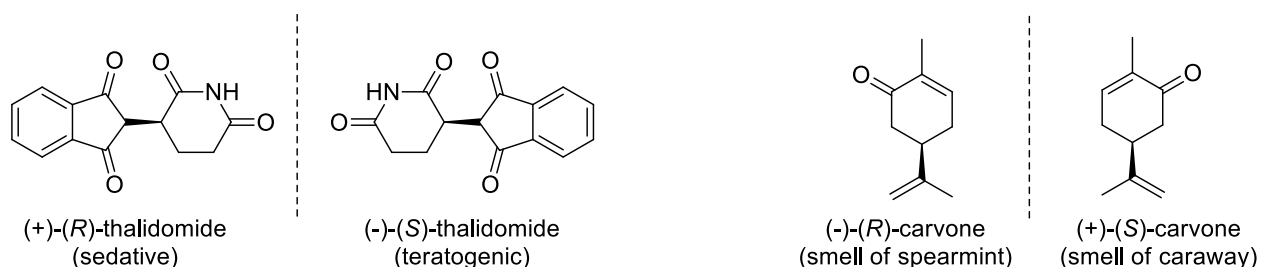


**Figure 1.1.** Selected examples of the effect of chirality on the properties of enantiopure compounds. The dashed lines indicate mirror planes.

Approximately 50 % of all pharmaceutical compounds available on the market nowadays are chiral. Although many drugs are still sold as a racemate, there is a clear trend towards marketing enantiopure drugs as the costs of studies which elucidate the toxicological and pharmacokinetic profile of the unwanted enantiomer are usually higher than the development of an enantioselective synthetic procedure.<sup>4</sup> Such a “chiral switch” strategy allows to extend the patent life of a drug without having to go through all clinical trials.

## 1.1.2 Asymmetric Catalysis

### *1.1.2.1 General Principles and Definitions*

Different approaches have been developed to introduce stereocenters into molecules for the production of drugs and fine chemicals. In some cases, chiral elements derived from enantiopure natural products such as carbohydrates and amino acids can be incorporated at a certain stage of a synthetic procedure. If not provided by the "chiral pool", enantiopure stereocenters can be generated by resolution, the use of chiral auxiliaries or asymmetric catalysis.<sup>5</sup> The latter is the most efficient method in this context as a small amount of a chiral catalyst may produce large quantities of an enantio-enriched product whereas resolution limits the maximal theoretical yield to 50% and the application of chiral auxiliaries requires additional steps to tether and cleave the auxiliary.

Two distinct classes of homogenous catalysts are predominantly used in asymmetric synthesis, namely chiral transition metal complexes and enzymes. Despite their structural and functional differences, both types of catalysts rely on the same general mechanisms of stereoselection. The interaction of the enantiopure catalyst with either one or the other prochiral face of the substrate gives rise to the formation of two diastereomeric transition states which possess different energies. The energy difference  $\Delta\Delta G^\ddagger$  of the

two transition states is directly related to the enantiomeric excess (ee) of an asymmetric catalytic transformation.<sup>6</sup>

$$ee (\%) = \frac{e^{-(\Delta\Delta G^\ddagger/RT)} - 1}{e^{-(\Delta\Delta G^\ddagger/RT)} + 1} = \frac{[\text{major enantiomer}] - [\text{minor enantiomer}]}{[\text{major enantiomer}] + [\text{minor enantiomer}]}$$

The number of moles of product a catalyst can produce before being deactivated is called "turnover number" (TON = molar ratio of product and catalyst) and is related to the life-time and activity of a catalyst. The latter property is referred to the "turnover frequency" (TOF) and is defined as the turnover number per time unit.

### 1.1.2.2 Homogenous Transition Metal Catalysis

The use of transition metal complexes in catalysis relies on the versatile reactivity and the tuneability of these compounds. Transition metals can switch between different oxidation states and therefore are able to abstract and eliminate certain fragments of molecules, thus enabling processes which are involved in catalytic cycles such as oxidative addition or reductive elimination. Moreover, by choice of the appropriate ligand the electron density and the steric environment of the metal can be influenced. This feature not only allows to fine-tune the reactivity and selectivity (e.g. chemo- and regioselectivity) of the catalyst, but also affords an opportunity to perform asymmetric catalysis using transition metals in combination with enantiopure ligands which provide the asymmetry. Frequently, both enantiomers of a chiral ligand can be prepared, e.g. by fractional recrystallisation of a diastereomeric salt,<sup>7</sup> giving access to both product enantiomers with the same asymmetric transformation.

The Nobel Prize 2001 was awarded to W.S. Knowles<sup>8</sup> and R. Noyori<sup>9</sup> who used chiral phosphine ligands for the asymmetric hydrogenation of functionalized alkenes and to B. Sharpless<sup>10</sup> who applied enantiopure ligands derived from natural products for the asymmetric epoxidation and dihydroxylation of olefins, respectively. These pioneering achievements revealed the potential of homogenous catalysts in asymmetric

synthesis and gave rise to the development of asymmetric variants of many other transformations such as Diels-Alder reactions, Michael additions, Aldol reactions, etc.<sup>11</sup> In parallel, the scope of enantiopure ligands was continuously expanded. Among these, certain scaffolds afford catalysts which provide high enantioselectivities in a wide range of asymmetric transformations and therefore are termed "privileged chiral ligands" (Figure 1.2).<sup>12</sup>

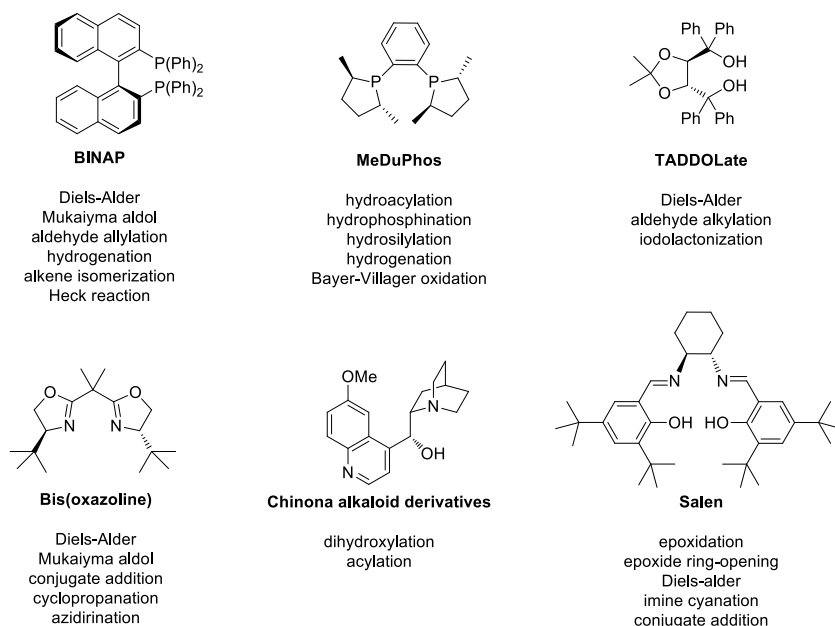


**Figure 1.2.** Privileged ligands and reactions catalyzed by corresponding transition metal complexes.<sup>12</sup>

### 1.1.2.3 Biocatalysis

Although enzymes underlie the same general principles of (asymmetric) catalysis as homogenous catalysts, they differ from the latter due to some unique features which primarily are the result of natural selection during the evolution of living organisms. Outstanding properties of biocatalysts include their high catalytic activity at ambient conditions, their substrate specificity and their high selectivity with respect to chemo-, regio- and enantioselectivity.<sup>13</sup> The rates of enzyme-catalyzed reactions can be increased by a factor of up

to  $10^{17}$  compared to the corresponding non-catalyzed reactions and enantioselectivities of 99 % ee are achieved routinely in case of asymmetric transformations.<sup>14</sup> This efficiency still outperforms by far the catalytic potential of the most chemical catalysts. Two specific features which contribute to the high effectiveness of enzymes differ significantly from homogenous catalysis and therefore are briefly summarized in the following.

First, enzymes are able to stabilize the transition state of a reaction.<sup>15</sup> This generally accepted basic mechanism of enzymatic catalysis was first formulated by Haldane<sup>16</sup> and expanded by Pauling<sup>17</sup> and Wolfenden.<sup>18</sup> According to their concept, enzymes lower the Gibbs energy  $\Delta G^\ddagger$  of a reaction by binding the corresponding transition state with higher affinity than the ground state of the substrate(s). Thereby, the fraction of the reactant in the transition state is raised. The resulting increase of the effective concentration of this intermediate is proportional to the reaction rate and therefore results in an acceleration of the reaction. This model is supported by the fact that some enzymes are strongly inhibited by transition state analogues<sup>19</sup> and is the basic concept of catalytic antibodies.<sup>20</sup>

Different catalytic features provided by enzymes directly contribute to the stabilization of the transition state (figure 1.3), including general-acid/base catalysis (proton transfer mediated by acidic and basic amino acid residues), electrostatic catalysis (stabilization of charges by complementary charged amino acid residues or hydrogen bonds) and electrophilic catalysis (stabilization of negative charges by metal ions).<sup>21</sup>

Second, enzymes may serve as an "entropic trap".<sup>22</sup> Upon binding in the active site, substrates and/or reactive amino acid residues are aligned in a relative position to each other which is favorable to promote a reaction. As the translational and rotational freedom of the reactants is restricted when bound to the enzyme, the subsequent formation of the transition state might not be expected to require as much entropy loss as for the same reaction proceeding spontaneously in dilute solution.<sup>23</sup> The consequence of substrate-binding within the enzyme can be viewed as a transformation of an intermolecular reaction into an entropically more favored and therefore faster intramolecular reaction.<sup>24</sup> Since the reacting groups are in close proximity if they are part of the same molecule or located in the active site of an enzyme, their effective concentration is increased. The rate acceleration in a monomolecular enzymatic or intramolecular



reaction compared to a bimolecular reaction may be expressed as an "effective molarity" of one reacting group or molecule relative to the other (EM = ratio between the first-order rate constant of an intramolecular reaction and the second-order rate constant of the corresponding intermolecular reaction).<sup>25</sup> However, the degree of contribution of these entropic effects to enzyme catalysis is still under discussion.<sup>26</sup>

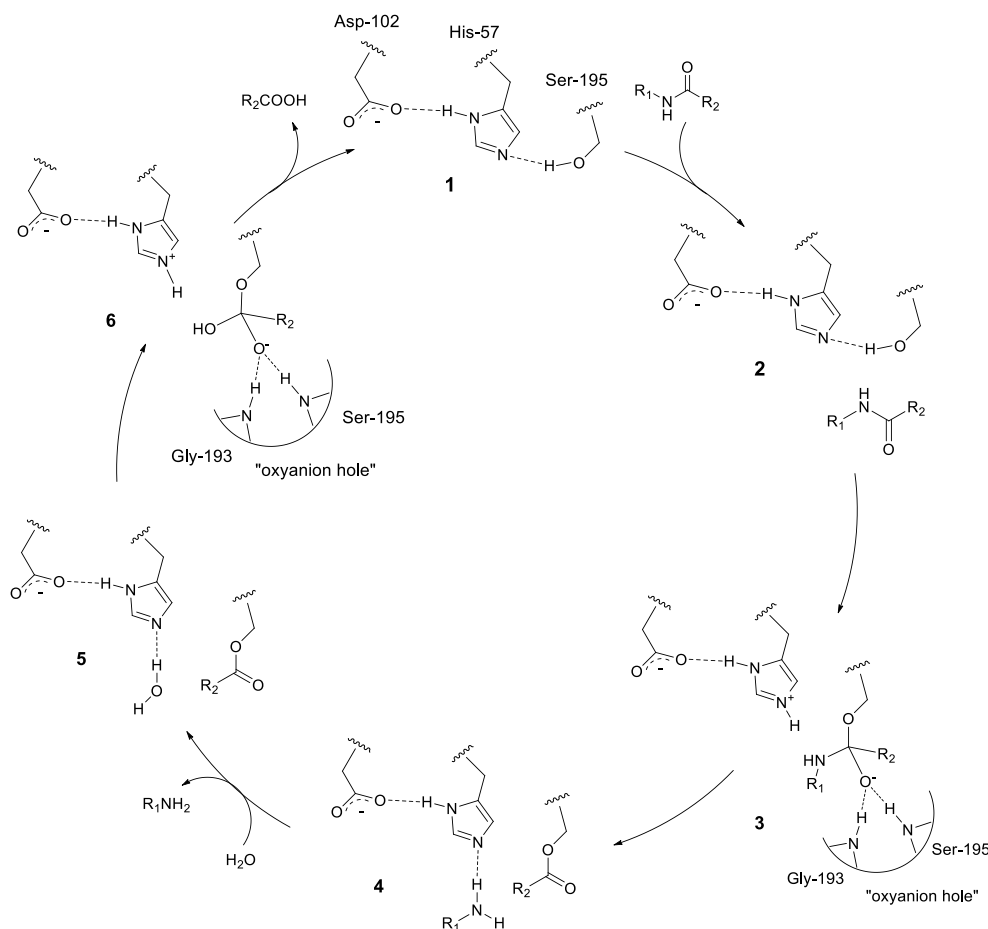


**Figure 1.3.** The catalytic cycle of serine proteases illustrates the different mechanisms of enzymatic catalysis.<sup>21</sup> The active site consists of a "catalytic triad" formed by the three conserved residues Asp-102, His-57 and Ser 195. The deprotonated hydroxyl group of the latter (acid-base catalysis) attacks the carbonyl group of the amide bond whereupon an anionic tetrahedral intermediate is formed (covalent catalysis) which is stabilized through hydrogen bondings provided by the "oxyanion hole" consisting of the backbone NH-groups of Gly-193 and Ser-195 (electrostatic catalysis). The RNH-group is activated as a leaving group after protonation by His-57 (acid-base catalysis). The resulting acylenzyme is hydrolysed by a water molecule activated as a nucleophile after deprotonation by His-57 (acid-base catalysis), yielding the second tetrahedral intermediate (electrostatic catalysis) and regenerating the enzyme.

The advent of recombinant DNA technology in the 1970s and the consecutive improvement of high-performance expression systems significantly increased the availability of biocatalysts. New protein engineering techniques such as rational design and directed evolution protocols nowadays allow to improve important features of enzymes with respect to organic chemistry (see below).<sup>27</sup> Thanks to these achievements, biocatalysis has become a versatile tool in the synthesis of fine chemicals and is used to catalyze a variety of stereoselective reactions such as hydrolysis, oxygenations, reductions, transaminations, Aldol reactions, Diels-Alder reactions etc.<sup>28</sup> Moreover, enzymes find increasing applications in industrial processes where they complement homogenous catalysts.<sup>29</sup>

#### *1.1.2.4 Complementary of Homogenous and Biocatalysis*

Despite their great catalytic potential, enzymes suffer from some major drawbacks with respect to organic synthesis. They often exhibit a narrow substrate scope and have only limited stability under conditions commonly applied in organic reactions such as the use of organic solvents, high temperatures and extreme pH-values. Additionally, only one product enantiomer is available with a given biocatalyst which applies to a lesser extent in case of homogenous transition metal catalysts (see section 1.1.2.2). Moreover, the latter often operate well at high temperatures and pressures (e.g. in hydrogenations).

With regard to the individual advantages and drawbacks of homogenous catalysts and enzymes both catalytic systems can be viewed as complementary. This statement has been illustrated recently in context of the synthesis of Sitagliptin **1** (figure 1.4). The compound is the active ingredient in Januvia, a leading drug for the treatment of type 2 diabetes.<sup>30</sup> Key step of the synthesis is the stereoselective introduction of the primary amine in the  $\beta$ -amino acid moiety of **1**. In the initial process chemistry route, this was implemented by asymmetric hydrogenation of the  $\beta$ -ketoester **2** using  $< 0.1$  mol% (*S*-BINAP)RuCl<sub>2</sub> in presence of HBr.<sup>31</sup> After ester hydrolysis the resulting  $\beta$ -hydroxyester **3** was isolated with 83 % yield and 94% ee. Although this process enabled the production of large amounts ( $> 100$  kg) of the target compound

for early clinical studies, this first generation process of Sitagliptin manufacture was discarded due to the generation of large amounts of waste in the following steps which converts the hydroxyl into the protected amine group. A collaboration between Merck and Solvias led to a second generation process which avoids the introduction of protecting groups and produced less waste. A screening of different metal precursors (Ru, Rh, Ir) and chiral ligands led to the identification of  $[\text{Rh}(\text{COD})\text{Cl}]_2$  (0.15 mol%) which in combination with *t*-BuJOSIPHOS (0.155 mol%) allowed to hydrogenate the unprotected  $\beta$ -aminoamide **4** in 98% yield 95% ee.<sup>32</sup> Subsequently, a reductive amination procedure was developed which converted **5** in presence of ammonium salicylate, hydrogen and  $[(R\text{-DM-SEGPHOS})\text{Ru}(\text{OAc})_2]$  directly to Sitagliptin in 91% yield and 99.5% ee, thus further improving the enantioselectivity and circumventing the prior formation of the enamide.<sup>33</sup> Since the asymmetric hydrogenation requires a high-pressure equipment and an additional purification process is necessary to remove the transition metal from the product, there was still room for improvement with regard to a large-scale production of the drug.

Another collaboration between Merck and Codexis provided an enzymatic route to Sitagliptin ("third generation process"). This approach relies on the *in silico* design and directed evolution of a (*R*)-selective transaminase ATA-117, a homolog of an enzyme of from *Arthrobacter sp.*<sup>34</sup> The active site of transaminases consists of two binding sites of which one accommodate the large substituent and the other one the small substituent of the ketone substrate whereas the latter is usually not larger as a methyl-group. To expand the substrate scope of the transaminase to the Sitagliptin precursor **5** a "substrate walking" approach was applied. In a first step the large binding pocket was engineered towards accommodation of a truncated version of **5** bearing a methyl group instead of the trifluorophenyl moiety. In a second step, the activity of most efficient transaminase towards **5** resulting from the first step was further evolved under consideration of the reaction conditions applied in the chemical plant such as the presence of DMSO, elevated temperatures, high substrate concentrations and high concentrations of the nitrogen donor isopropylamine. After eleven rounds of directed evolution, the original biocatalyst had been modified at 27 positions, including substitutions in the active site and the interface of the enzyme dimer which were linked with the higher stability of the catalyst under the reaction conditions. The related enzymatic process for the

production of Sitagliptin operates at  $200 \text{ g l}^{-1}$  **5** with a substrate to catalyst ratio of 2600 in presence of 50 % DMSO at  $40 \text{ }^\circ\text{C}$ , yielding the product with 92% yield and  $>99.95\%$  ee.

This impressive case study of the Sitagliptin manufacture demonstrates not only the complementary of homogenous and biocatalysis, but also illustrates the progress which has been achieved in the industrial application of biocatalysts. Applying a combination of computational enzyme design and laboratory evolution enabled the creation of an enzyme with a high activity and selectivity towards a non-native substrate and increased stability towards elevated temperatures as well as organic solvents.

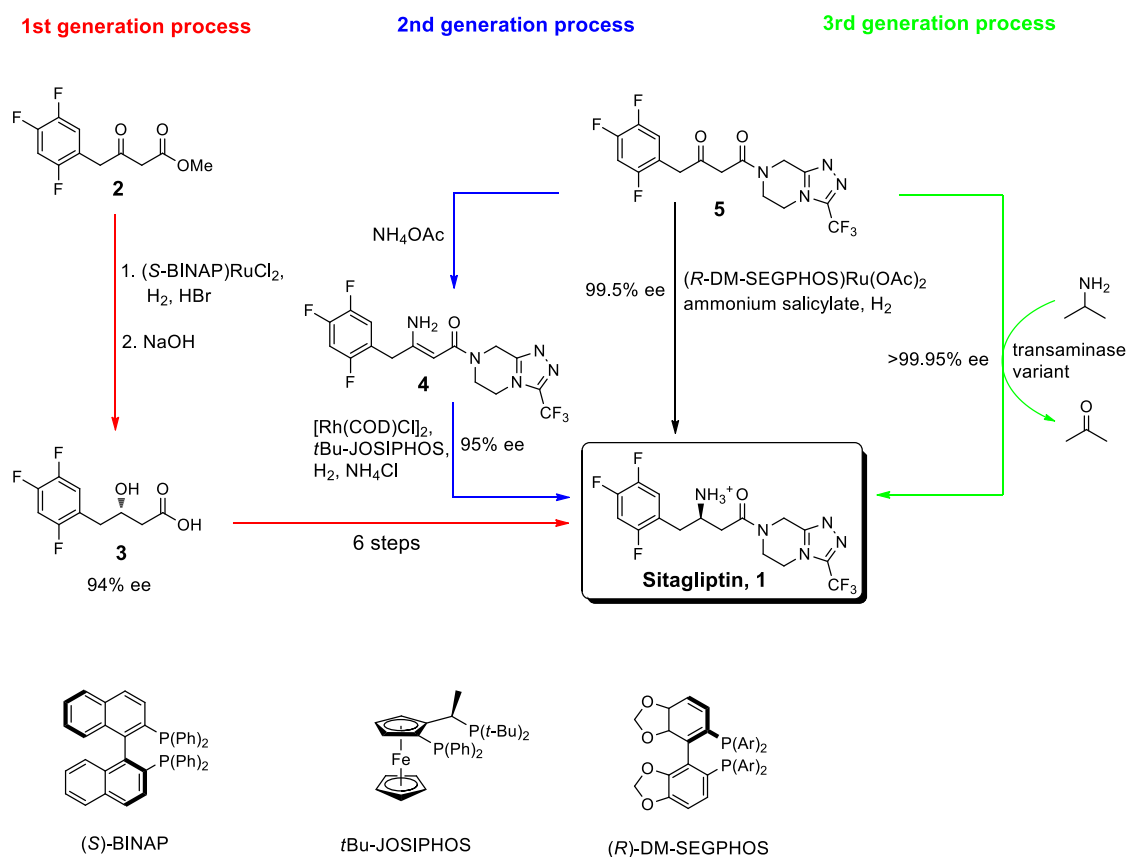


**Figure 1.4.** Enantioselective transformations in the manufacture of Sitagliptin.

### 1.1.3 Artificial Metalloenzymes

#### *1.1.3.1 General Concepts and Design of Artificial Metalloenzymes*

Almost half of all enzymes found in nature require metal ions for their catalytic function. So far, a great diversity of both main group and transition metals have been identified as a component in metalloenzymes, including Na, K, Ca, Mg, Fe, Mn, Zn, Co, Ni, Cu, V, Mo, W and Cd.<sup>35</sup> The respective ions are either coordinated by functional groups of amino acid side chains (e.g.  $\text{Zn}^{2+}$  in carbonic anhydrase) or are part of a cofactor (e.g.  $\text{Fe}^{2+}$  in heme of cytochromes). Metalloenzymes mediate various catalytic mechanisms such as electrophilic catalysis (e.g. alcohol dehydrogenase),<sup>36</sup> hydrolysis (e.g. carbonic anhydrase),<sup>37</sup> oxygen transport (e.g. hemoglobin),<sup>38</sup> hydroxylation (e.g. cytochrome P450),<sup>39</sup> methyl transfer (e.g. cobalamin-dependent methionine synthase)<sup>40</sup> and electron transport (e.g. cytochromes).<sup>41</sup> The fact that metalloenzymes are involved in fundamental biological processes including nitrogen-fixation as well as photosynthesis underlines their importance and illustrates their remarkable catalytic features.

Artificial metalloenzymes result from the incorporation of a catalytically active transition metal complex within a biomolecular scaffold (i.e. a protein or DNA/RNA).<sup>42</sup> The primary goal of this approach is to combine the reaction scope offered by traditional homogenous catalysts with the advantageous properties of biocatalysts, in particular the high activity at ambient conditions and the high selectivity (see previous section). These features are almost exclusively controlled by the ligand forming the first coordination sphere in the case of transition metal complexes. In contrast, the selectivity and activity of enzymes relies predominantly on the second coordination sphere provided by hydrophobic interactions and hydrogen bonds which are responsible for the chiral discrimination, the stabilization of the transition state of the reaction and/or the activation of the substrate by secondary interactions. In particular the last two tasks are more difficult to achieve with low molecular-weight ligands employed in homogenous catalysis. Thus, the performance of a homogenous catalyst may be improved with respect to activity and selectivity when incorporated within a protein scaffold. For instance, Zhang et al. were able to improve the chemoselectivity of a Mn-salen complex for the oxidation of thioanisole upon incorporation into apo-myoglobin.<sup>43</sup> Whereas

the free metal complex produced significant amounts of the sulfone product, over oxidation was completely suppressed in case of the corresponding hybrid catalyst, yielding exclusively the sulfide.

On the other hand, since certain activities provided by homogenous catalysts are absent in nature, artificial metalloenzymes may increase the catalytic repertoire for applications in biocatalysis and synthetic biology.

To date, many non-natural reactions including olefin metathesis could be implemented in various biomolecular scaffolds.<sup>44</sup>

Three main strategies for the creation of artificial metalloenzymes are usually applied (Figure 1.5).<sup>45</sup> In the dative anchoring strategy, a metal ion is coordinated by specific amino acid residues (e.g. histidine, aspartate) which already are present in the protein or are engineered by means of site-directed mutation. In some cases, a native metal present in the protein is exchanged by an abiotic one. An example of the latter procedure was reported by Kazlauskas who substituted the zinc ion in carbonic anhydrase by rhodium to afford a hydroformylase or hydrogenase.<sup>46</sup>

The covalent anchoring strategy relies on the covalent attachment of a catalytic moiety on a reactive amino acid residue which can be modified selectively. In this context, artificial metalloenzymes based on modification of cysteine,<sup>47</sup> serine<sup>48</sup> and lysine<sup>49</sup> have been reported.

Supramolecular anchoring takes advantage of a strong, specific interaction between a protein and a particular ligand (e.g. a substrate or inhibitor). Derivatization of the ligand with a metal complex results in the incorporation of the abiotic cofactor within the host. This strategy was applied extensively in the Ward group using the biotin-(strept)avidin technology (see below). More examples of artificial metalloenzymes and their respective anchoring strategies are provided in section 1.1.4.

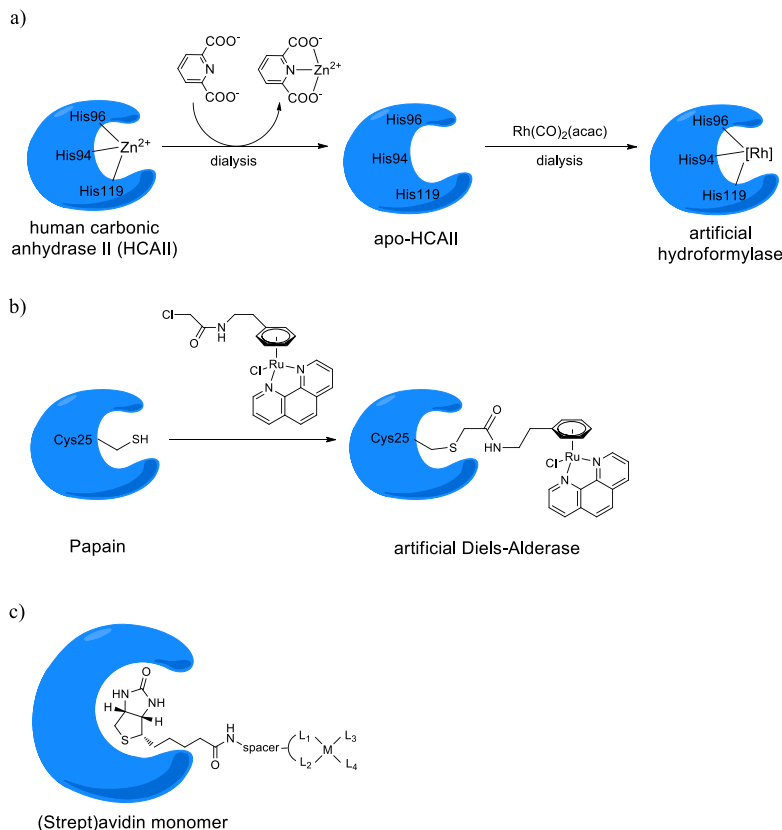


**Figure 1.5.** Selected examples of strategies to create artificial metalloenzymes. a) dative anchoring<sup>46</sup> b) covalent anchoring<sup>47</sup> c) supramolecular anchoring.

### 1.1.3.2 Artificial Metalloenzymes Based on the (Strept)avidin-Biotin Technology

Avidin (Avi, from egg-white) and streptavidin (Sav, from *Streptomyces avidinii*) are particularly well known for their high affinity towards the vitamin biotin ( $K_a = \sim 10^{15} \text{ M}^{-1}$  for Avi and  $\sim 10^{13} - 10^{14} \text{ M}^{-1}$  for Sav, respectively).<sup>50</sup> The two related proteins (32 % sequence homology) have a similar homotetrameric structure which can be described as a dimer of dimers with  $D_2$ -symmetry.<sup>51</sup> Each monomer consists of an eight-stranded  $\beta$ -barrel and binds one biotin molecule. The quaternary structure is stabilized predominately by a network of van der Waals interactions and hydrogen bonds between each individual monomer.<sup>52</sup> In contrast to streptavidin ( $M_r = 65700 \text{ D}$ ) which is devoid of sulfur-containing amino acids, avidin ( $M_r = 62400 \text{ D}$ ) contains two cysteines forming a disulfide-bridge and two methionine residues. In addition, avidin is glycosylated at Asn-17.

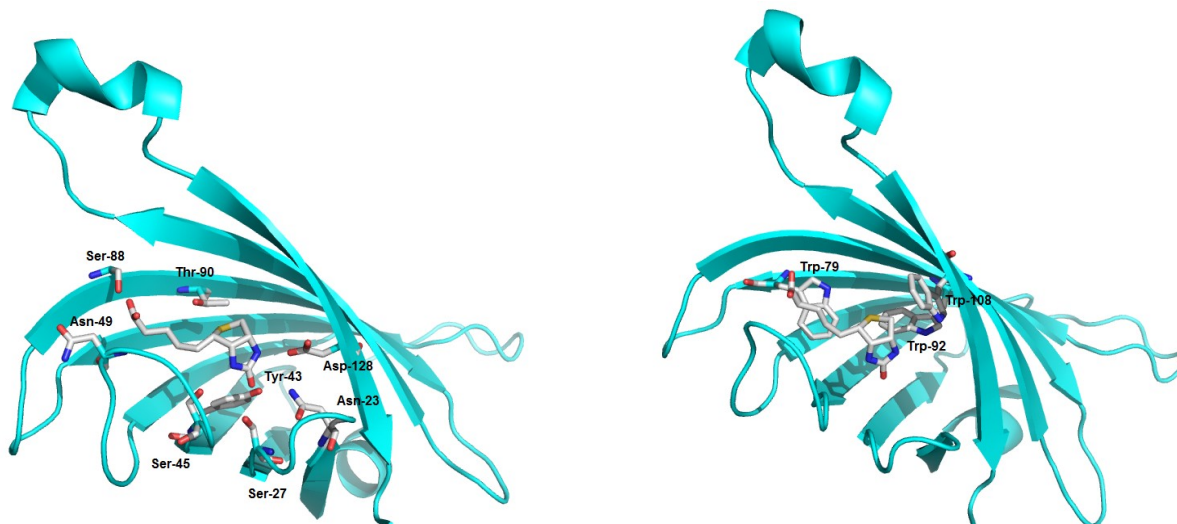


**Fig. 1.6.** X-ray crystal structure of the Streptavidin monomer (PDB-code: 1STP). Biotin and interacting amino acid residues are displayed as sticks (carbon: grey, oxygen: red, nitrogen: blue). Left: hydrophilic interactions. Right: hydrophobic interactions. Trp-120 is not shown.

In both proteins, the biotin binding sites are located at the entrance of the  $\beta$ -barrel. The network of hydrophilic interactions involved in biotin-binding is similar in both cases. As illustrated in Figure 1.6 for streptavidin, hydrogen bonds are formed with the carbonyl oxygen (Asn-23, Ser-27, Tyr-43) as well as the NH-groups (Ser-45, Asp-128) of the ureido moiety, the sulfur of the thiolane moiety (Thr-90) and the carboxyl group of the valeric acid chain (Asn-49, Ser-88).<sup>53</sup> The five hydrogen bonds of the ureido moiety act cooperatively, leading to stabilization that is larger than the sum of the individual hydrogen-bonding energies and therefore may contribute to the high affinity towards biotin.<sup>54</sup> In addition, the Trp-residues 79, 92 and 108 from one monomer as well as Trp-120 from the adjacent monomer are responsible for hydrophobic interactions between streptavidin and biotin. Energetically, the high affinity can be explained with the large activation barrier for dissociation ( $\Delta G_{\text{Sav}}^{\ddagger} = 102$  kJ/mol) which results in a high activation enthalpy ( $\Delta H_{\text{Sav}}^{\ddagger} = 134$  kJ/mol) and a favorable activation entropy ( $T\Delta S_{\text{Sav}}^{\ddagger} = 32$  kJ/mol).<sup>55</sup>



In the apoprotein of both avidin and streptavidin, the loop connecting the strands 3 and 4 of the  $\beta$ -barrel changes its conformation upon biotin-binding and thereby "closes" the binding site such that the ligand is buried almost completely. Both cooperative and non-cooperative binding of biotin to the (strept)avidin tetramer have been reported.<sup>56</sup>

Avidin and streptavidin are extremely stable over a wide pH range and with respect to high temperatures, the presence of denaturing agents as well as organic solvents.<sup>57</sup> For instance, up to 20 minutes are required to dissociate streptavidin into monomers at 100 °C in 0.2 % sodium dodecyl sulphate (SDS).<sup>58</sup> To denature the monomers and release bound biotin even more drastic conditions have to be applied (e.g. 6 M guanidinium hydrochloride, pH 1.5). Binding of biotin significantly increases the thermostability of both proteins as reflected by the increased melting temperatures which in case of streptavidin is increased from  $T_m = 75$  °C for the apoprotein to  $T_m = 112$  °C for the fully biotin-saturated complex.<sup>59</sup>

The high affinity towards biotin and the stability of (strept)avidin have led to many applications in research. These are commonly summarized under the concept of "biotin-(strept)avidin technology".<sup>60</sup> The derivatization at the carboxylic acid moiety of the valeric chain of biotin does not significantly decrease the affinity of the resulting conjugate towards (strept)avidin and therefore allows to label the host protein with a target molecule of interest. The corresponding probe (e.g. a fluorescent dye) is usually linked to the biotin anchor via an appropriate spacer (e.g. a polyethylene glycol chain) and thus does not interact with the Avi or Sav. This technique is well established nowadays and has been applied to affinity chromatography, diagnostics, immunoassays, drug targeting, etc.<sup>61</sup>

In 1978, Whitesides and coworkers reported for the first time an artificial metalloenzyme on the basis of the biotin-(strept)avidin technology.<sup>62</sup> The incorporation of an achiral biotinylated Rh(I)-bisphosphine complex into avidin resulted in an artificial hydrogenase which catalyzed the enantioselective reduction of *N*-acetamidoacrylate with 41 % ee in favor of the (*S*)-enantiomer. Inspired by this visionary work, the Ward-group adapted and extended this supramolecular anchoring strategy relying on the strength of the noncovalent (strept)avidin-biotin interaction for the creation of artificial metalloenzymes. Initial experiments using avidin in the combination with two distinct Rh(I)-complexes **Biot-1** and **Biot-2** (Figure

1.7) yielded only modest enantioselectivities in the hydrogenation of *N*-acetamidoacrylate.<sup>63</sup> The asymmetric hydrogenation was significantly improved when streptavidin was used as the host protein instead of avidin, achieving up to 96 % ee for the opposite (*R*)-enantiomer. It was concluded that the different topography of the binding pocket is responsible for the improved asymmetric induction in case of streptavidin.<sup>64</sup> The diversity of the hybrid catalysts was further increased by a chemogenetic optimization approach. For this purpose, the linker between the two phosphine ligands and the biotin anchor was modified whereby either alkylaminoacids of different chain lengths or arylaminoacids with a different substitution pattern were introduced.<sup>65</sup> Combination of the corresponding Rh(I) complexes with selected streptavidin mutants revealed that amino acid substitutions of the second coordination sphere of the biotin binding (e.g. V47G) site and those which lie in close proximity to the metal center (e.g. S112G) provide the highest variability with respect to the absolute configuration and enantiomeric excess of the product. Based on the identification of S112 as a crucial position in streptavidin with regard to the performance of the hybrid catalysts, saturation mutagenesis at this position led to the identification of mutants with increased enantioselectivity in the hydrogenation of  $\alpha$ -acetamidocinnamic acid. The introduction of chiral amino acid spacers (proline or phenylalanine) between biotin and the aminodiphosphine moiety of **Biot-1** combined with saturation mutagenesis at position S112 afforded a second generation of artificial hydrogenases with improved organic solvent tolerance, reaction rates and selectivities ( $\geq 95$  % ee for both enantiomers).<sup>66</sup> Furthermore, it could be shown that the hybrid catalysts display Michaelis-Menten behavior with increased affinities (smaller  $K_M$ -values) and rates (higher  $k_{cat}$ -values) compared to the Rh-complexes in absence of streptavidin.

This "designed evolution" approach was expanded for the optimization of artificial metalloenzymes based on the biotin-(strept)avidin technology for olefin metathesis,<sup>44</sup> asymmetric allylic alkylation,<sup>67</sup> C-H activation<sup>68</sup> and transfer hydrogenation of ketones.<sup>69</sup> Furthermore, it has been shown that (strept)avidin is also a suitable host for non-biotinylated artificial metal cofactors such as OsO<sub>4</sub> and [VO(H<sub>2</sub>O)<sub>5</sub>]<sup>2+</sup> which are also believed to bind in the biotin binding pocket via complexation to specific amino acid residues or second

coordination sphere interactions, respectively. The corresponding artificial metalloenzymes proved to be effective catalysts for the enantioselective sulfoxidation<sup>70</sup> and dihydroxylation.<sup>71</sup>

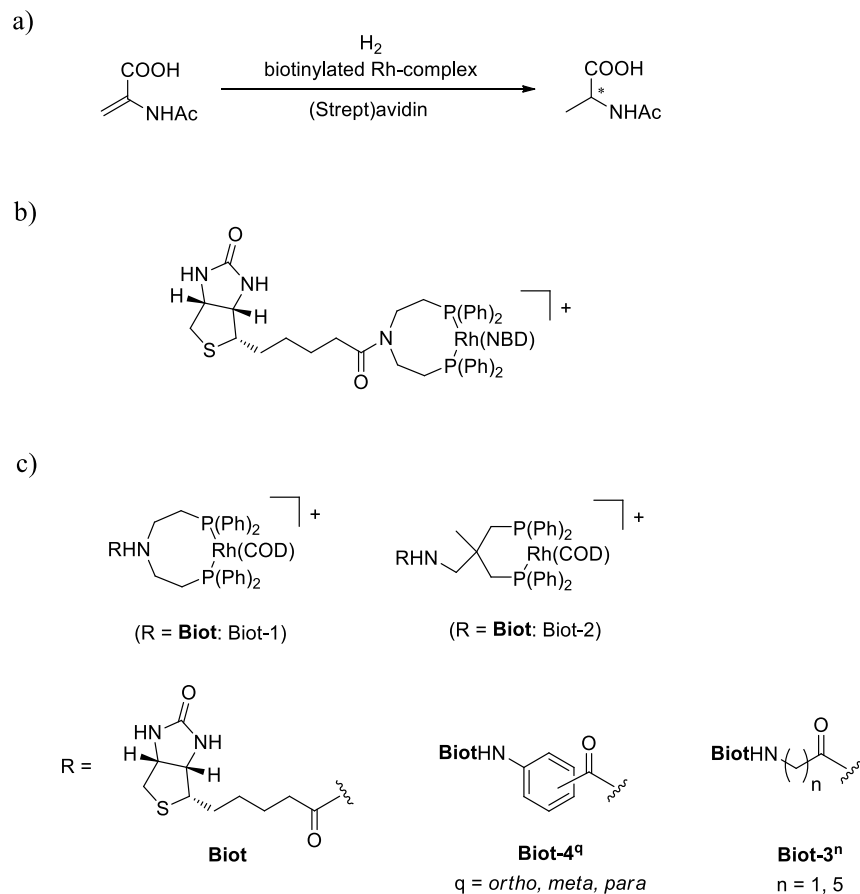


**Fig. 1.7.** Design of artificial hydrogenases based on the Biotin-(Strept)avidin technology. a) Reaction scheme showing the reduction of *N*-acetamidoacrylate by the artificial hydrogenase. b) Artificial metal cofactor reported by Whitesides. c) Design strategy to generate chemical diversity of the artificial metal cofactor reported by Ward et al.

#### 1.1.4 Recent Achievements in the Design and Engineering of Artificial Metalloenzymes

Available online at [www.sciencedirect.com](http://www.sciencedirect.com)

ScienceDirect

Current Opinion in  
Chemical Biology

## Recent achievements in the design and engineering of artificial metalloenzymes

Marc Dürrenberger and Thomas R Ward

Herein, we highlight a selection of recent successes in the creation of artificial metalloenzymes. A particular emphasis is set on different anchoring methods to incorporate the abiotic metal cofactor within the host protein as well as promising strategies for the *de novo* design of artificial metalloenzymes. Both approaches yield promiscuous catalytic activities which expand the catalytic repertoire of biocatalysis and synthetic biology. Moreover, we summarize laboratory evolution protocols which have contributed to unravel the full potential of artificial metalloenzymes.

### Addresses

Department of Chemistry, University of Basel, Spitalstrasse 51, Basel CH-4056, Switzerland

Corresponding author: Ward, Thomas R ([Thomas.Ward@unibas.ch](mailto:Thomas.Ward@unibas.ch))

Current Opinion in Chemical Biology 2014, 18:99–106

This review comes from a themed issue on **Bioinorganic chemistry**

Edited by **Elizabeth M Nolan** and **Mitsuhiro Shionoya**

For a complete overview see the [Issue](#) and the [Editorial](#)

Available online 5th March 2014

1367-5931/\$ – see front matter, © 2014 Elsevier Ltd. All rights reserved.

<http://dx.doi.org/10.1016/j.cpb.2014.01.018>

### Introduction

Enzymes are increasingly finding applications in large scale industrial processes [1,2]. Typical features associated with enzymatic transformations include: high catalytic efficiency, high selectivity and ability to operate under mild reaction conditions in water. These remarkable characteristics are the result of natural selection during the evolution of living organisms. However, enzymes also display some drawbacks with respect to organic synthesis: limited stability under typical operating conditions (e.g. organic solvents, high temperatures), narrow substrate scope, *etc.* In this context, transition metal catalysts, despite their own set of limitations, can be regarded as complementary to enzymes. Combining both catalytic strategies may allow to overcome some of the limitations of both enzymes and organometallic catalysts.

Artificial metalloenzymes result from the incorporation of a catalytically active transition metal complex within a biomolecular scaffold (either protein or oligonucleotide) and thus provide an attractive approach to explore the potential of merging homogenous and biocatalysis. To date, a variety of biohybrid catalysts have been reported,

relying either on dative, covalent or supermolecular anchoring of a transition metal complex [3].

To complement these strategies, more recently *de novo* design algorithms have been applied to metalloproteins [4].

In this review we present a selection of achievements in the field of artificial metalloenzymes which were published in the past two years.

### New strategies for the creation of artificial metalloenzymes

The Diels-Alder reaction has extensively been used as a benchmark reaction in context of Cu(II)-based artificial metalloenzymes [5,6]. Most recent contributions in this area include a study by Roelfes and coworkers. They introduced an acetamide-functionalized copper phenanthroline complex at the dimer interface of the transcription factor LmrR by covalent anchoring relying on cysteine bioconjugation (Table 1, entry 1). The resulting artificial Diels-Alderase mediates the [4+2] cycloaddition between azachalcone and cyclopentadiene with excellent enantioselectivity (up to 97%) and diastereoselectivity (*endo/exo* 95:5) [7]. This approach represents a novel design strategy of an active site at the interface of a dimeric biomolecular scaffold. The biohybrid also catalyzes the enantioselective conjugate addition of water to enones to yield the corresponding chiral  $\beta$ -hydroxy ketones with up to 84% ee [8].

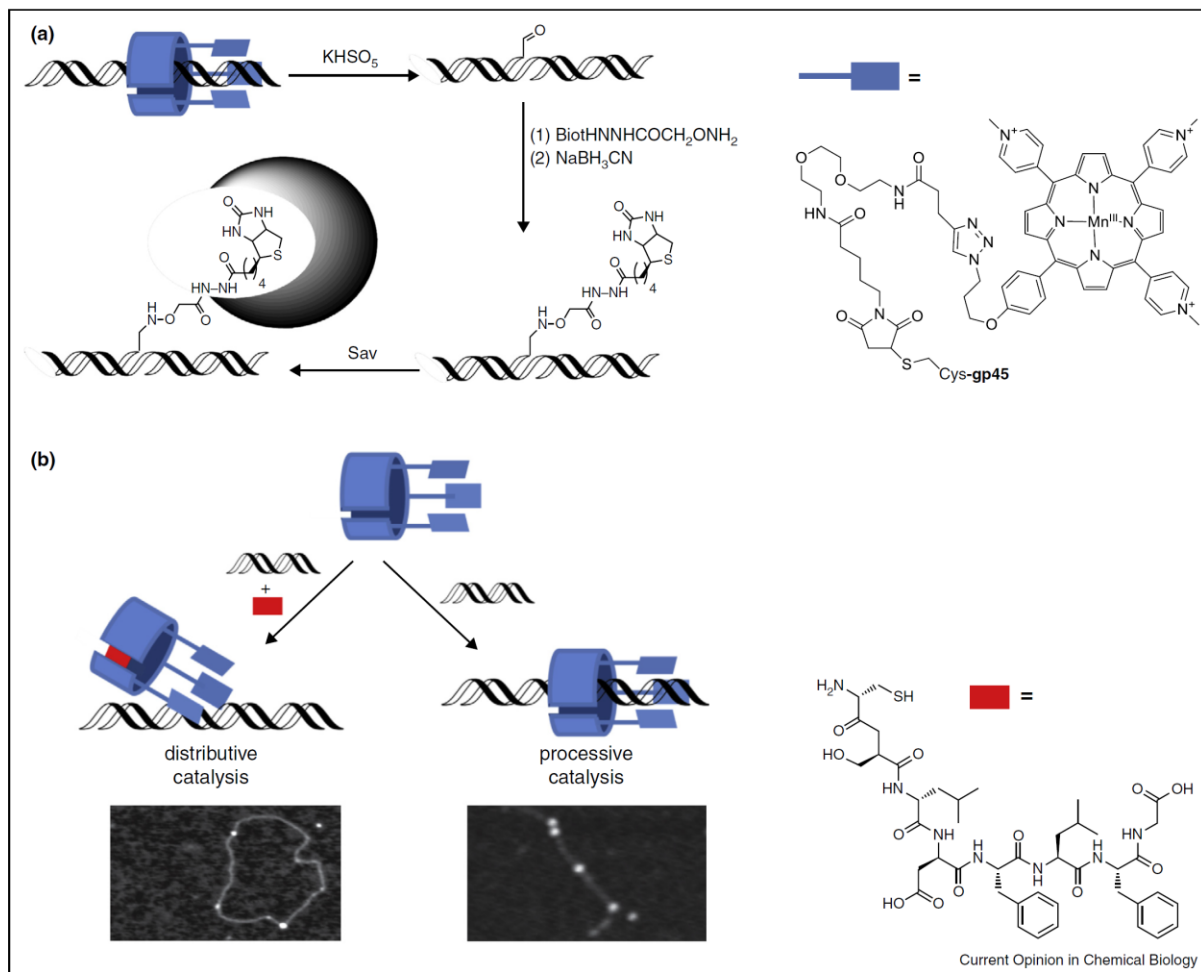
As exemplified by DNA polymerases and exonucleases, processive catalysis is a widely exploited feature in Nature. The corresponding enzymes often possess a toroid structure which allows them to wrap around DNA and translocate along the polynucleotide template during processing. The properties of these clamp proteins are utilized by van Dongen *et al.* to develop a biohybrid catalyst for plasmid DNA oxidation (Figure 1). For this purpose, a cysteine containing gp45 sliding clamp variant originating from the bacteriophage T4 was conjugated with a maleimide-functionalized manganese (III) porphyrin complex [9]. The oxidative DNA single strand cleavage activity of the resulting construct produced aldehyde moieties which were derivatized with hydroxylamine-bearing biotin and subsequently labeled with streptavidin. This procedure allowed them to detect the oxidative cleavage sites by atomic force microscopy (AFM). The catalytic behaviour of the biohybrid catalyst could be modulated by adding a structural mimic of the

Table 1					
Summary of artificial metalloenzymes and corresponding reactions highlighted in this review					
Entry	Protein	Engineered active site	Substrate(s)	Product(s)	Reference
1	LmrR				[7]
2	$\alpha$ -Chymo-trypsin				[8]
3	Nitrobindin				[14]
4	Sav				[15**]
5	Sav		Imine + HCOOH NAD <sup>+</sup> + HCOOH	Amine + CO <sub>2</sub> NADH + CO <sub>2</sub>	[16*]
6	Cytochrome P450 <sub>BM3</sub>				[20**,21]
7	DFsc	Engineered His <sub>2</sub> Glu <sub>2</sub> Fe(III)OFe(III)Glu <sub>2</sub> His active site			[22*]
8	Adenosine desaminase	Reengineered Zn(II)His <sub>3</sub> Asp active site			[23**]
9	3SCC-oligopeptide	Reengineered Zn(II)His <sub>3</sub> active site			[24**,25]
10	Myoglobin	HemeFe-CuHis <sub>3</sub> binuclear metal center	O <sub>2</sub> + reductant	H <sub>2</sub> O + oxidized reductant	[26,27]
11	HydF-HydA1		H <sup>+</sup> + reductant	H <sub>2</sub> + oxidized reductant	[28**,29]

C-terminus of the T4 polymerase, an octapeptide that blocks the subunit interface of trimeric gp45. In the absence of the peptide the clamp binds to DNA and mediates processive catalysis as reflected by streptavidin molecules found to be in close proximity on the plasmid. Such streptavidin clusters were absent when the inhibitor

peptide was present, suggesting randomly distributed oxidative cleavage along the plasmid. Introduction of mirrored recognition sites on each of the complementary DNA-strands allowed to determine the direction in which the biohybrid catalyst performs processive oxidation on the plasmid.

Figure 1



Artificial catalytic clamp for DNA-oxidation developed by van Dongen *et al.* (a) The catalytic clamp consists of a homotrimeric gp45-E212C variant (blue cylinder) conjugated with a Mn(III)-porphyrin. The oxidative single-strand cleavage of DNA produces aldehyde-moieties which are derivatized with hydroxylamine-biotin and subsequently labeled with streptavidin (Sav, for clarity only one monomer shown), allowing to detect the oxidation sites by AFM. (b) The presence of a peptidic structural analogue of the C-terminus of the T4 polymerase (red rectangle) inhibits the clamp and leads to distributive oxidation events as the clamp cannot wrap around the DNA. As a consequence, Sav molecules (white dots in the AFM pictures) are randomly distributed along the plasmid. In absence of the peptide, the clamp is loaded on DNA and performs processive oxidation leading to Sav-clusters (adapted with permission from Ref. [9\*]).

### Artificial metalloenzymes catalyze bioorthogonal reactions

The scope of reactions catalyzed by artificial metalloenzymes has significantly expanded in the past two years. With the aim of complementing the enzymatic repertoire, hybrid catalysts that mediate abiotic reactions are of particular interest as these may find in synthetic biology to complement metabolic pathways.

The olefin metathesis represents a very attractive bioorthogonal reaction [10–12]. An elegant method for the side-specific modification of a serine protease was

published by Matsuo *et al.* (Table 1, entry 2). Derivatization of a Hoveyda–Grubbs catalyst with an inhibitor based on *N*-tosyl L-phenylalanyl chloromethylketone (TPCK) directs the ruthenium complex into the peptide binding cleft of  $\alpha$ -chymotrypsin. There, it is covalently attached to the enzyme via nucleophilic attack at the chloromethyl moiety by the imidazole of a catalytically active histidine residue [13]. The corresponding decrease in protease activity supports the incorporation of the Hoveyda–Grubbs catalyst into  $\alpha$ -chymotrypsin. Unfortunately, only moderate turnover numbers were achieved in ring closing metathesis (RCM) of water soluble olefins.

Engineering a very hydrophobic active site for the metathesis cofactor may allow to overcome this widespread limitation of olefin metathesis in water.

Onoda *et al.* covalently linked a rhodium(I) complex bearing a maleimide-functionalized cyclopentadienyl ligand with a cysteine residue introduced in the apo-form of the  $\beta$ -barrel protein nitrobindin (Table 1, entry 3). The biohybrid catalyzes the stereospecific polymerization of phenylacetylene [14]. Whereas the free rhodium complex produces mostly *cis*-poly(phenylacetylene) (PPA), the content of the *trans*-product increases notably for the artificial polymerase (*trans:cis* ratio up to 53:47). The authors speculate that the content of the *trans* isomer can be further increased by engineering the active site bearing the Rh-moiety as, in the current design, it adopts two different conformations within the entrance of the  $\beta$ -barrel.

The potential of artificial metalloenzymes to improve homogenous catalytic systems with respect to activity and selectivity was illustrated by Ward and Rovis. On the basis of the biotin–streptavidin technology, a biotinylated Cp<sup>\*</sup>Rh(III) pianostool complex, where Cp<sup>\*</sup> is pentamethylcyclopentadienyl, was incorporated within Streptavidin (Sav) to create a bifunctional hybrid catalyst. It catalyzes an asymmetric benzannulation reaction between pivaloyl-activated benzhydroxamic acid and acrylates (Table 1, entry 4). Both the activity and the selectivity of the artificial metalloenzyme were improved by site-directed mutagenesis [15<sup>\*\*</sup>]. Guided by docking-studies, they engineered a basic residue at position K121 which was shown to be critical in deprotonating the Rh-activated C–H bond of the benzamide. This, combined with steric bulk introduced at position S112 resulted in an artificial benzannulase (i.e. S112Y–S112E) which affords the dihydroisquinolone product in 93:7 enantiomeric ratio and with nearly a 100-fold increased rate compared to the activity of the rhodium cofactor alone.

### Enzyme cascades which include an artificial metalloenzyme

Despite of the synthetic potential of combining chemo- and biocatalysts, the practical realization of concurrent cascade reactions combining both systems remains elusive, due to mutual inhibition. To circumvent this, Hollmann, Turner and Ward combined an artificial transferhydrogenase (ATHase) with a variety of NADH-dependent, FAD-dependent and heme-dependent enzymes [16<sup>\*</sup>]. The ATHase consists of [Cp<sup>\*</sup>Ir(biot-*p*-L)Cl] embedded in streptavidin (Sav) variants, thus efficiently compartmentalizing the organometallic moiety and the natural enzyme (Table 1, entry 5 and Figure 2). Examples include: firstly, double stereoselective deracemisation of amines in combination with evolved monoamine oxidases (MAO-N) and secondly,

regeneration of NADH in the presence of a monooxygenase to catalyze an aromatic oxyfunctionalisation.

### De novo design of metalloenzymes

Catalytic promiscuity has been elegantly exploited to engineer and evolve new catalytic function in enzymes [17–19]. In the past two years, this strategy has been successfully extended to metalloenzymes.

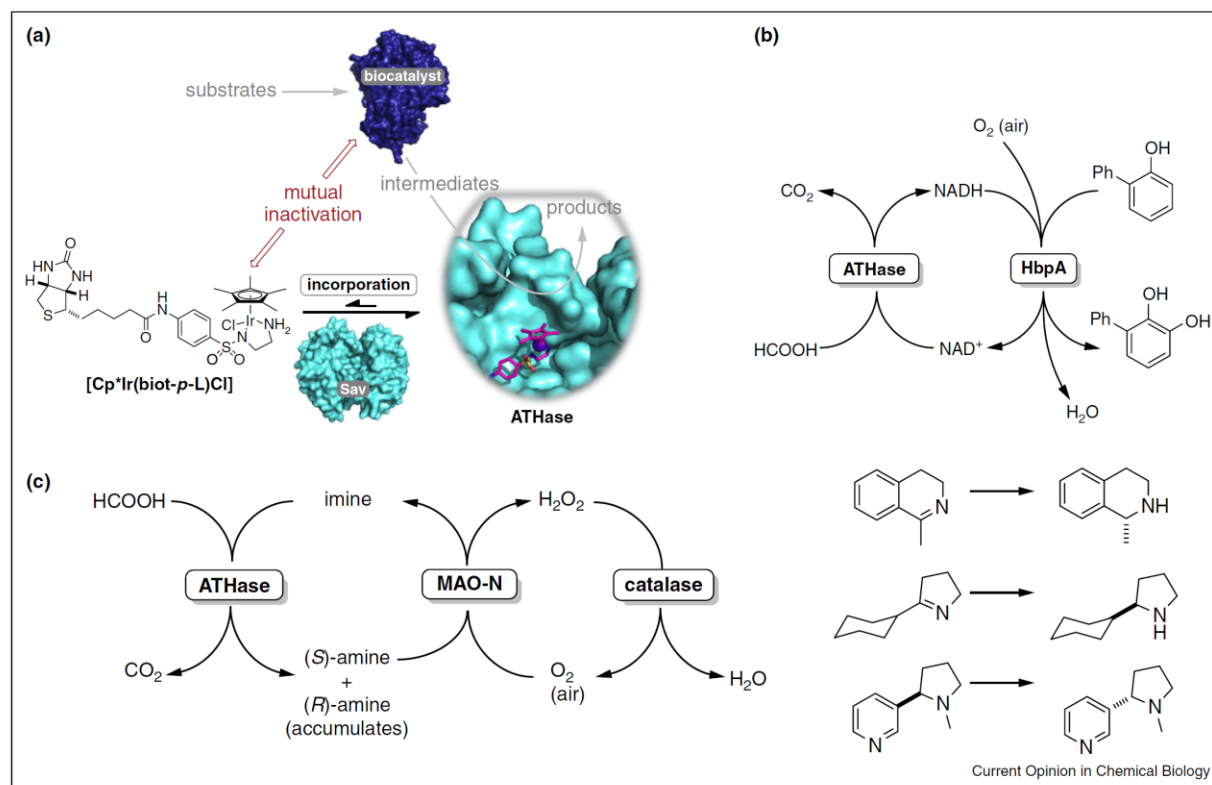
As the M=CHR and M=O fragments are isoelectronic, Coelho and coworkers reasoned that monooxygenases may be reprogrammed into cyclopropanating enzymes. With this goal in mind, they screened heme proteins for the asymmetric cyclopropanation of styrene in the presence of ethyldiazoacetate (Table 1, entry 6). A cytochrome P450 fatty acid monooxygenase (P450<sub>BM3</sub>) was found to be a suitable scaffold to further engineer the active site around the iron center of the heme cofactor [20<sup>\*\*</sup>]. Mutation T268A is the key mutation to achieve high cyclopropanation activity. Other active site alanine mutations influence the product distribution with respect to diastereo- and enantioselectivity. Individual saturation mutagenesis of the wild type enzyme finally provides a variant with a *cis:trans* ratio of 92:8 and an ee<sub>cis</sub> of 97% for the cyclopropanation of styrene by ethyl diazoacetate. Replacement of the iron ligating cysteine by a weakly coordinating serine residue reduced the monooxygenase activity and raised the Fe<sup>III/II</sup> potential to enable NAD(P)H-driven reduction [21]. This further engineered “P411<sub>BM3</sub>”-variant catalyzes the olefin cyclopropanation *in vivo* in *E. coli* cells.

Inspired by the structure of the native *p*-aminobenzoate *N*-oxygenase AurF the hydroquinone-oxidizing activity of a di-iron carboxylate model protein of the Due Ferri family was reprogrammed to catalyze the *N*-hydroxylation of activated aryl amines by Reig and coworkers (Table 1, entry 7 and Figure 3). Crucial mutations included four alanine to glycine substitutions to enlarge the substrate access cavity, introduction of a third iron-ligating histidine residue in the active site and three mutations in the second- and third shell to accommodate the additional histidine [22<sup>\*</sup>]. The redesigned oxygenase showed no apparent reactivity towards the oxidation of hydroquinones whereas the activity of the hydroxylation of *p*-anisidine was similar as to AurF.

Another very elegant approach to redesign a metalloprotease was reported by Khare *et al.* (Table 1, entry 8 and Figure 3). Suitable native protein scaffolds offering a mononuclear zinc center with at least one free coordination site were extracted from the protein data bank (PDB). Transition state models corresponding to the organophosphate substrate diethyl 7-hydroxycoumaryl phosphate (DECP) were then computed into the zinc sites of selected scaffolds and additional hydrogen-bond interactions were identified using the RosettaMatch



Figure 2



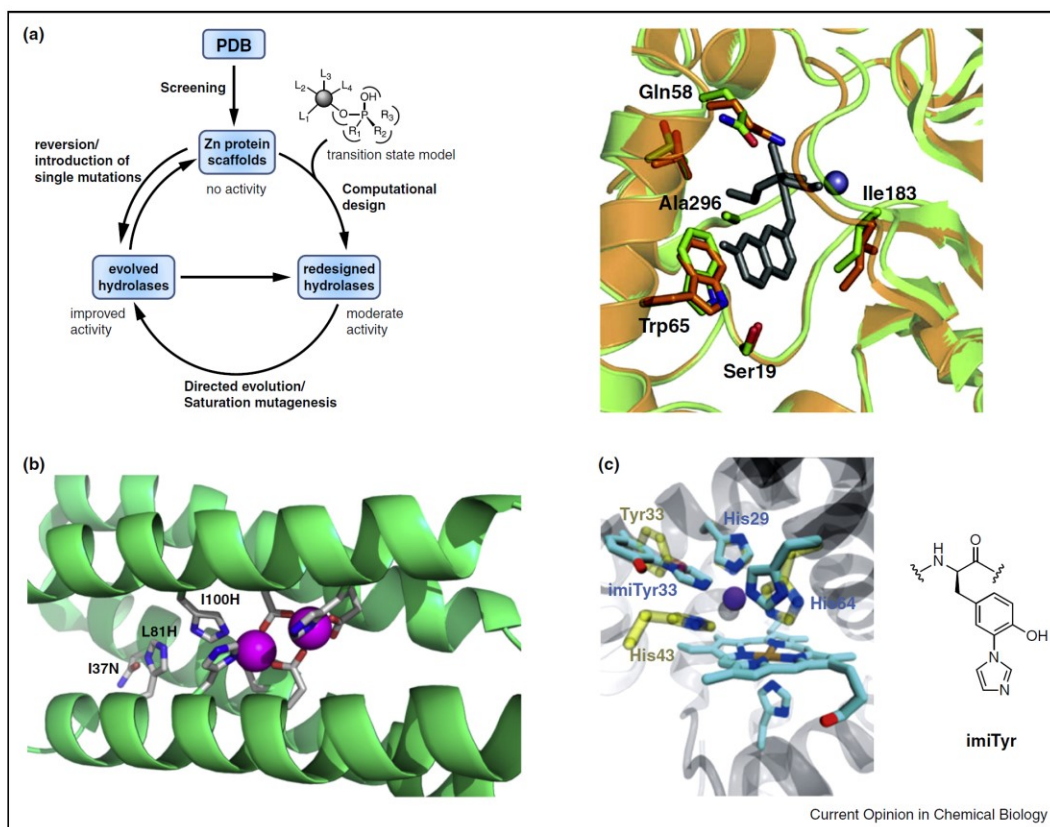
Reaction cascades which include an artificial transferhydrogenase (ATHase) as reported by Köhler *et al.* (a) Incorporation of a biotinylated transfer hydrogenation catalyst  $[\text{Cp}^*\text{Ir}(\text{biot-}p\text{-L})\text{Cl}]$  within streptavidin (Sav) shields the organometallic moiety and prevents mutual inhibition of native enzymes, thus allowing concurrent reaction cascades. (b) Concurrent regeneration of NADH by the ATHase in the presence of a monooxygenase (HbpA) for the hydroxylation of 2-hydroxybiphenyl. (c) Reaction cascades resulting from the combination of a moderately (*R*)-selective ATHase and a highly (*S*)-selective monoamine oxidase (MAO-N) for the double stereoselective deracemisation of amines or the stereoinversion of nicotine. Addition of a catalase prevents inactivation of the Ir-center by  $\text{H}_2\text{O}_2$  generated by the catalytic action of MAO-N (adapted with permission from Ref. [16\*\*]).

algorithm. The redesigned metalloenzyme showed moderate hydrolytic activity. Directed evolution combined with saturation mutagenesis led to a significant improvement of the catalytic activity. Reversion of single mutations back to the wild-type sequence and generation of a library of variants in which the substitutions were present in random combinations revealed the minimal set of mutations required for increased hydrolase activity [23\*\*]. The power of this general and readily applicable protocol was demonstrated by the successful redesigning of a native adenosin deaminase to yield an organophosphatase with a catalytic efficiency ( $k_{\text{cat}}/K_m$ ) of  $10^4 \text{ M}^{-1} \text{ s}^{-1}$ .

In view of the vast catalytic repertoire offered by transition metals, transposing the concepts of catalytic promiscuity to metalloenzymes promises fascinating developments in the near future. This may prove particularly powerful in transformation for which no natural enzyme exists.

In recent years, Pecoraro and coworkers have reported very efficient carbonic anhydrase mimics consisting of the incorporation of a  $\text{Zn}(\text{His})_3$  site with a three-stranded coiled-coil oligopeptide (3-SCC). The biohybrid includes a structural  $\text{Hg}(\text{II})\text{Cys}_3$ -site and a catalytic  $\text{Zn}(\text{II})\text{His}_3$ -site. The resulting hydrolase displays remarkable catalytic properties for both the hydration of  $\text{CO}_2$  and the hydrolysis of *p*-nitrophenylacetate (Table 1, entry 9) [24\*\*]. In order to scrutinize the subtle second coordination sphere interactions on catalytic performance, both structural and catalytic sites were systematically translocated along the  $\alpha$ -helical sequence of the peptide [25]. While the  $\text{Hg}(\text{II})$ -site has a negligible impact on both the binding affinity and catalytic performance, the position of the  $\text{Zn}(\text{His})_3$ -site is critical as a 10-fold variation of Zn-affinity was observed. In contrast, the catalytic efficiencies were retained upon shifting the active site along the 3-SCC. Remarkably, these artificial metallohydrolases display efficiencies approaching that of the native carbo-

Figure 3



Redesign and engineering of artificial metalloenzymes. **(a)** Computational *de novo* design of an organophosphate hydrolase based on a native deaminase as described by Khare *et al.* Left: schematic summary of the design strategy. Right: superposition of the designed hydrolase (gold) and the corresponding X-ray structure (green, PDB code 3T1G) highlighting the near perfect match between both structures (except Gln 58). Relevant amino acids and the DECP substrate are highlighted as sticks and the zinc ion is depicted as a blue sphere (with permission from Ref. [23\*\*]). **(b)** Structure of an arylamine *N*-oxidase (3His-G2DFsc, PDB code 2LFD) redesigned from DFsc reported by Reig *et al.* The native HisGlu<sub>2</sub>Fe(III)OFe(III)Glu<sub>2</sub>His reaction center are highlighted as sticks as well as the engineered additional coordinating His100 and the supporting second- and third shell residues His81 and Asn37, respectively. The side chains of the residues are indicated as sticks. The two iron ions are shown as magenta spheres (with permission from Ref. [22\*]). **(c)** Designed myoglobin heme-copper oxidase (HCO) model resulting from the introduction of a Cu<sub>B</sub>-site (pink sphere) and the non-natural amino acid imiTyr which mimics the posttranslational Tyr-His crosslink found in HCO (imiTyrCu<sub>B</sub>Mb). The overlay contains a Cu<sub>B</sub>-myoglobin variant lacking imiTyr, bearing a tyrosine residue at the same position (F33YCu<sub>B</sub>Mb, PDB code 4FWX). Amino acid side chains are shown as sticks (carbon atoms are indicated in cyan for imiTyrCu<sub>B</sub>Mb or light blue for F33YCu<sub>B</sub>Mb, respectively; nitrogen atoms in blue, oxygen atoms in red, iron atom in brown). The Cu ion is depicted as pink sphere (with permission from Ref. [26]).

nic anhydrase, one of the most efficient natural enzymes (kinetic parameters at pH 9 for the catalytic hydrolysis of *p*-nitrophenylacetate:  $k_{\text{cat}} = 0.038 \text{ s}^{-1}$ ,  $K_{\text{M}} = 2.1 \text{ mM}$  for the 3-SCC-derived artificial hydrolase,  $k_{\text{cat}} = 56 \text{ s}^{-1}$ ,  $K_{\text{M}} = 24 \text{ mM}$  for carbonic anhydrase II).

Due to their ability to activate small molecules including O<sub>2</sub> and H<sub>2</sub> under mild conditions, redox-active metalloenzymes may find applications in the development of fuel cells. In this context, artificial oxidases and hydrogenases have been intensively investigated in recent years.

Heme-copper oxidase (HCO) performs the reduction of oxygen to water. The corresponding active site consists of

a heterobinuclear metal center containing a heme Fe and a histidine ligated Cu (Cu<sub>B</sub>) as well as a post-translationally installed crosslink between carbon atom C6 of a tyrosine residue and nitrogen atom Nε2 of a close lying histidine residue. To investigate the role of the post-translational modification, Liu and coworkers engineered a related moiety in myoglobin by genetic incorporation of (*S*)-2-amino-3-(4-hydroxy-3-(1*H*-imidazole-1-yl)phenyl)propanoic acid (Table 1, entry 10 and Figure 3). The myoglobin HCO model catalyzed the reduction of oxygen with a threefold increase in turnovers and an eightfold increase in selectivity (with respect to ROS generation) compared to a myoglobin variant which harbors an individual histidine and tyrosine residue at the same positions

[26]. This work complements a related study whereby a tyrosine residue was mutated into myoglobin in proximity to one of the copper ligating histidine residues, thus affording an artificial metalloenzyme that reduces oxygen to water with over one thousand turnovers [27].

In the context of hydrogenases, many structural and functional small molecule [FeFe]-mimics have been reported. These however, which lack the crucial second coordination sphere interactions, fail to reproduce the remarkable efficiency of natural hydrogenases. An original approach was recently reported by Berggren *et al.* They rely on the assembly of a semisynthetic [FeFe]-hydrogenase HydA1 (Table 1, entry 11) which does not require the entire maturation machinery. For this purpose, they loaded one of the maturation enzymes HydF with a synthetic [FeFe] bearing a azadithiolate bridging ligand [28<sup>\*\*</sup>,29]. Incubating the loaded HydF with apo-HydA1 leads to the transfer of the diiron cofactor. The resulting hydrogenase displays a specific activity of up to 800  $\mu\text{mol H}_2$  per minute and mg HydA1, comparable to that of the natural HydA1. This fascinating strategy may allow to test the effect of small changes in [FeFe]-mimics in the natural hydrogenase environment.

## Conclusions

The present review summarizes the impressive progress achieved in the past two years in the area of artificial metalloenzymes. Functional constructs can be obtained either by incorporation of abiotic cofactors within a variety of protein scaffolds using either covalent or supramolecular anchoring strategies or redesigning proteins applying sophisticated computational methods or exploiting catalytic promiscuity to unravel abiotic reactivity from natural enzymes. Most importantly, directed evolution protocols were applied to optimize a nascent catalytic activity. Catalytic efficiencies approaching that of natural enzymes were obtained, a remarkable feat considering the youth of the artificial metalloenzyme's field.

## References and recommended reading

Papers of particular interest, published within the period of review, have been highlighted as:

- of special interest
  - of outstanding interest
1. Zaks A: **Industrial biocatalysis.** *Curr Opin Chem Biol* 2001, **5**:130-136.
  2. Savile CK, Janey JM, Mundroff EC, Moore CM, Tam S, Jarvis WR, Colbeck JC, Krebber A, Fleitz FJ, Brands J *et al.*: **Biocatalytic asymmetric synthesis of chiral amines from ketones applied to Sitagliptin manufacture.** *Science* 2010, **329**:305-309.
  3. Lewis JC: **Artificial metalloenzymes and metallopeptides catalysts for organic synthesis.** *ACS Catal* 2013 <http://dx.doi.org/10.1021/cs400806a>.
  4. Kiss G, Celebi-Ölcüm N, Moretti R, Baker D, Houk KN: **Computational enzyme design.** *Angew Chem Int Ed* 2013, **52**:5700-5725.
  5. Reetz MT: **Artificial metalloenzymes as catalysts in stereoselective Diels-Alder reactions.** *Chem Rec* 2012, **12**:391-406.
  6. Deus PJ, Popa G, Slawin AMZ, Laan W, Kamer PCJ: **Artificial copper enzymes for asymmetric Diels-Alder reactions.** *ChemCatChem* 2013, **5**:1184-1191.
  7. Bos J, Fusetti F, Driessen AJM, Roelfes G: **Enantioselective artificial metalloenzymes by creation of a novel active site at the protein dimer interface.** *Angew Chem Int Ed* 2012, **51**:7472-7475.
  8. Bos J, Garcia-Herraiz A, Roelfes G: **An enantioselective artificial metallo-hydratase.** *Chem Sci* 2013, **4**:3578-3582.
  9. van Dongen SFM, Clerx J, Norgaard K, Bloemberg TG, Cornelissen JJLM, Trakselis MA, Nelson SW, Benkovic SJ, Rowan AE, Nolte RJM: **A clamp-like biohybrid catalyst for DNA-oxidation.** *Nat Chem* 2013, **5**:945-951.
- Highly sophisticated artificial oxidase based on a clamp-like protein that can translocate along DNA and perform processive catalysis.
10. Lo C, Ringenberg MR, Gndant D, Wilson Y, Ward TR: **Artificial metalloenzymes for olefin metathesis based on the biotin-(strept)avidin technology.** *Chem Commun* 2011, **47**:12065-12067.
  11. Mayer C, Gillingham DG, Ward TR, Hilvert D: **An artificial metalloenzyme for olefin metathesis.** *Chem Commun* 2011, **47**:12068-12070.
  12. Philipart F, Arit M, Gotzen S, Tenne SJ, Bocola M, Chen HH, Zhu L, Schwaneberg U, Okuda J: **A hybrid ring-opening methesis polymerization catalyst based on an engineered variant of the  $\beta$ -barrel protein FhuA.** *Chem Eur J* 2013, **19**:13865-13871.
  13. Matsuo T, Imai C, Yoshida T, Saito T, Hayashi T, Hirota S: **Creation of an artificial metalloprotein with a Hoveyda-Grubbs catalyst moiety through the intrinsic inhibition mechanism of  $\alpha$ -chymotrypsin.** *Chem Commun* 2012, **48**:1662-1664.
  14. Onoda A, Fukumoto K, Arit M, Schwaneberg U, Hayashi T: **A rhodium complex-linked  $\beta$ -barrel protein as a hybrid biocatalyst for phenylacetylene polymerization.** *Chem Commun* 2012, **48**:9756-9758.
  15. Hyster TK, Knörr L, Ward TR, Rovis T: **Biotinylated Rh(III) complexes in engineered streptavidin for accelerated asymmetric C-H activation.** *Science* 2012, **338**:500-503.
- An artificial benzannulase that demonstrates the full potential of artificial metalloenzymes by improving the catalytic performance of a Cp\*Rh(III)-catalyst with respect to the enantioselectivity and, most importantly, the activity towards an abiotic C-H activation reaction.
16. Köhler, Wilson YM, Dürrenberger M, Ghislieri D, Churakova E, Quinto T, Knörr L, Häussinger D, Hollmann F, Turner NJ, Ward TR: **Synthetic cascades are enabled by combining biocatalysts with artificial metalloenzymes.** *Nat Chem* 2013, **5**:93-99.
- Incorporation of a biotinylated Cp\*Ir(III) transfer hydrogenation catalyst within streptavidin prevents mutual inhibition between the organometallic moiety and a variety of natural enzymes; therefore enabling synthetic cascades.
17. Khersonsky O, Tawfik DS: **Enzyme promiscuity: a mechanistic and evolutionary perspective.** *Annu Rev Biochem* 2010, **79**:471-505.
  18. Toscano MD, Woycechowsky KJ, Hilvert D: **Minimalist active-site redesign: teaching old enzymes new tricks.** *Angew Chem Int Ed* 2007, **46**:3212-3236.
  19. Bornscheuer UT, Kazlauskas RJ: **Catalytic promiscuity in biocatalysis: using old enzymes to form new bonds and follow new pathways.** *Angew Chem Int Ed* 2004, **43**:6032-6040.
  20. Coelho PS, Brustad EM, Kannan A, Arnold FH: **Olefin cyclopropanation via carbene transfer catalyzed by engineered cytochrome P450 enzymes.** *Science* 2013, **339**:307-310.
- Exploiting Fe=CHR as an isoelectronic surrogate for Fe=O enables cyclopropanation with monooxygenase enzymes.
21. Coelho PS, Wang ZJ, Ener ME, Baril SA, Kannan A, Arnold FH, Brustad EM: **A serine-substituted P450 catalyzes highly efficient carbene transfer to olefins *in vivo*.** *Nat Chem Biol* 2013, **9**:485-487.

## 106 Bioinorganic chemistry

22. Reig AJ, Pires MM, Snyder RA, Wu Y, Jo H, Kulp DW, Butch SE, Calhoun JR, Szyperski TG, Solomon EI, DeGerado WF: **Alteration of the oxygen-dependent reactivity of *de novo* *de* ferri proteins.** *Nat Chem* 2012, **4**:900-906.
- Reprogramming a di-iron carboxylate hydroquinone oxidase into a *de novo* enzyme for the *N*-oxidation of activated aryl amines.
23. Khare SD, Kipnis Y, Greisen PJ, Takeuchi R, Ashani Y, Goldsmith M, Song Y, Gallaher JL, Silman I, Leader H *et al.*: **Computational redesign of a mononuclear zinc metalloenzyme for organophosphate hydrolysis.** *Nat Chem Biol* 2012, **8**:294-300.
- Extending the Rosetta enzyme design algorithms to metalloenzymes.
24. Zastrow ML, Peacock AFA, Stuckey JA, Pecoraro VL: **Hydrolytic catalysis and structural stabilization in a designed metalloprotein.** *Nat Chem* 2012, **4**:118-123.
- A remarkable *de novo* designed artificial hydrolase with native-like catalytic efficiency.
25. Zastrow ML, Pecoraro VL: **Influence of active site location on catalytic activity in *de novo*-designed metalloenzymes.** *J Am Chem Soc* 2013, **135**:5895-5903.
26. Liu X, Yu Y, Hu C, Zhang W, Lu Y, Wang J: **Significant increase of oxidase activity through the genetic incorporation of a tyrosine-histidine cross-link in a myoglobin model of heme-copper oxidase.** *Angew Chem Int Ed* 2012, **51**:4312-4316.
27. Miner KD, Mukherjee A, Gao YGG, Null EL, Petrik ID, Zhao X, Yeung N, Robinson H, Lu Y: **A designed functional metalloenzyme that reduces O<sub>2</sub> to H<sub>2</sub>O with over one thousand turnovers.** *Angew Chem Int Ed* 2012, **51**:5589-5592.
28. Berggren G, Adamska A, Lambert C, Simmons TR, Esselborn J, Atta M, Gambarelli S, Muesca JM, Reijerse E, Lubitz W *et al.*: **Biomimetic assembly and activation of [FeFe]-hydrogenases.** *Nature* 2013, **499**:66-70.
- Synthetic di-iron cofactors can be loaded into natural [FeFe]-hydrogenases via a single maturation enzyme *in vitro*.
29. Esselborn J, Lambert C, Adamska-Venkatesh A, Simmons T, Berggren G, Noth J, Siebel J, Hemschemeler A, Artero V, Reijerse E *et al.*: **Spontaneous activation of [FeFe]-hydrogenases by an inorganic [2Fe] active site mimic.** *Nat Chem Biol* 2013, **9**:607-610.

## 1.2 Goal of the Thesis

Artificial transfer hydrogenases (ATHase) result from the incorporation of biotinylated piano stool metal complexes  $[(\eta^6\text{-arene})\text{M}(\text{biot-}p\text{-L})\text{Cl}]$  ( $\text{M} = \text{Ru}, \text{Rh}, \text{Ir}$ ) into strept(avidin). These hybrid catalysts were successfully applied for the asymmetric transfer hydrogenation of prochiral ketones in the Ward group in the last decade (see below). In this context, the aims of the present Thesis are:

- i) expanding the substrate scope of artificial transfer hydrogenases to the asymmetric reduction of prochiral imines
- ii) optimization of the artificial imine reductase with respect to the amino acid composition of the active site and the reaction conditions
- iii) performing the Michaelis-Menten kinetics of ATHases catalysts to gain information about the mechanism of the hybrid catalysts
- iv) enable catalysis with the ATHases in cellular environments (cell free extracts and cell lysates) by identification of reagents which neutralize the dentrimetal effect of glutathione (GSH) on precious metal catalysts
- v) illustrating the compatibility of homogenous and biocatalysis by performing reaction cascades with ATHases in combination with several natural enzymes

## 1.3 References

- 1) International Union of Pure and Applied Chemistry.
- 2) Stephens, T.D.; Bunde, C.J.W.; Fillmore, B.J. *Biochem. Pharmacol.* **2000**, *59*, 1489.
- 3) Leitereg, T.J.; Guadagni, D.G.; Harris J.; Mon T.R.; Teranishi, R. *J. Agr. Food Chem.* **1971**, *19*, 785.
- 4) Farina, V.; Reeves, T.R.; Senanayake, C.H.; Song, J.J. *Chem. Rev.* **2006**, *106*, 2734.
- 5) Hawkins, J.M.; Watson, T.J.N. *Angew. Chem. Int. Ed.* **2004**, *43*, 3224.
- 6) Hartwig, J. *Organotransition Metal Chemistry: From Bonding to Catalysis*. University Science Books, Sausalita, **2010**.
- 7) Miyashita, A.; Yasuda, A.; Takaya, H.; Toriumi, K.; Ito, T.; Souchi, T.; Noyori, R. *J. Am. Chem. Soc.* **1980**, *102*, 7932.
- 8) Knowles, W.S. *Angew. Chem. Int. Ed.* **2002**, *41*, 1998.
- 9) Noyori, R. *Angew. Chem. Int. Ed.* **2002**, *41*, 2008.
- 10) Kolb, H.C.; VanNieuwenhze, M.S.; Sharpless, K.B. *Chem. Rev.* **1994**, *94*, 2483.
- 11) Ojima, I. *Catalytic Asymmetric Synthesis*, 2nd Edition, Wiley-VCH, **2000**.
- 12) Yoon, T.P.; Jacobsen, E.N. *Science* **2003**, *299*, 1691.
- 13) Bommarius, A.S.; Riebel, B.R.; *Biocatalysis. Fundamentals and Applications*. Wiley-VCH, **2004**.
- 14) Radzicka, A.; Wolfenden, R. *Science* **1995**, *267*, 90.
15. a) Truhlar, D.G.; Garrett, B.C.; Klippenstein, S.J. *J. Phys. Chem.* **1996**, *100*, 12771. b) Bruice, T.C.; *Acc. Chem. Res.* **2002**, *35*, 139. c) Andrews, P.R.; Smith, G.D.; Young, I.G. *Biochemistry* **1973**, *12*, 3492. d) Robertus, J.D.; Kraut, J.; Alden, R.A.; Birktoft, J.J. *Biochemistry* **1973**, *11*, 4293.
- 16) Haldane, J. *Enzymes*, **1930** New York, Longmans, Green and Co.
- 17) Pauling, L. *Nature* **1948**, *4097*, 707.
- 18) Wolfenden, R. *Biophys. Chem.* **2003**, *105*, 559.
19. a) Schramm, V.L. *Annu. Rev. Biochem.* **2011**, *80*, 703. b) Cama, E.; Shin, H.; Christianson, D.W. *J. Am. Chem. Soc.* **2003**, *125*, 13052. c) Singh, S.; Lee, J.E.; Nunez, S.; Howell, P.L.; Schramm, V.L. *Biochemistry* **2005**, *44*, 11649. d) Holden, H.M.; Tronrud, D.E.; Monzingo, A.F.; Weaver, L.H.; Matthews, B.W. *Biochemistry* **1987**, *26*, 8542.

- 20) Keinan, E. *Catalytic Antibodies*. Weinheim: Wiley-VCH; **2005**.
- 21) Fersht, A. *Structure and Mechanism in Protein Science: A Guide to Enzyme Catalysis and Protein Folding*; 1<sup>st</sup> Ed.; W.H. Freeman and Company, New York, **1998**.
- 22) Westheimer, F. H. *Adv. Enzymol. Relat. Areas Mol. Biol.* **1962**, *24*, 455.
- 23) Snider, M.J.; Lazarevic, D.; Wolfenden, R. *Biochemistry* **2002**, *41*, 3925.
- 24.a) Page, M.I.; Jencks, W.P. *Proc. Nat. Am. Soc. U.S.A* **1971**, *68*, 1678. b) Page, M.I. *Angew. Chem. Int. Ed. Engl.* **1977**, *16*, 449. c) Menger, F.M. *Acc. Chem. Res.* **1985**, *18*, 128.
- 25) Krishnamurthy, V.M.; Semetey, V.; Bracher, P.J.; Shen, N.; Whitesides, G.M. *J. Am. Chem. Soc.* **2007**, *129*, 1312.
- 26) Villa, J.; Strajbl, M.; Glennon, T.M.; Sham, Y.Y.; Chu, Z.T.; Warshel, A. *Proc. Nat. Am. Soc. U.S.A.* **2000**, *97*, 11899.
- 27.a) Hult, K.; Berglund, P.; *Curr. Op. Biotech.* **2003**, *14*, 395. b) Jaeger, K.E.; Eggert, T. *Curr. Op. Biotech.* **2004**, *1*, 305. c) Otten, L.G.; Quax, W.J. *Biomolecular Engineering* **2005**, *22*, 1. d) Jiang, L.; Althoff, E.A.; Clemente, F.R.; Doyle, L.; Röthlisberger, D.; Zanghellini, A.; Gallaher, J.L.; Betker, J.L.; Tanaka, F.; Barbas, C.F.; Hilvert, D.; Houk, K.N.; Stoddard, B.L., Baker, D. *Science* **2008**, *319*, 1387.
- 28) Faber, K. *Biotransformations in Organic Chemistry*, 6<sup>th</sup> Ed., Springer, **2011**.
- 29.a) Zaks, A. *Curr. Op. Chem. Biol.* **2001**, *5*, 130. b) Straathof, A.J.J.; Panke, S.; Schmid, A. *Curr. Op. Biotech.* **2002**, *13*, 548. c) Bornscheuer, U.T.; Huisman, G.W.; Kazlauskas, R.J.; Lutz, S.; Moore, J.C.; Robins, K. *Nature* **2012**, *485*, 185. d) Reetz, M.T. *J. Am. Chem. Soc.* **2013**, *135*, 12480.
- 30) Kim, D.; Wang, L.; Beconi, M.; Eiermann, G.J.; Fisher, M.H.; He, H.; Hickey, G.J.; Kowalchick, J.E.; Leiting, B.; Lyons, K.; Marsilio, F.; McCann, M.E.; Patel, R.A.; Petrov, A.; Scapin, G.; Patel, S.B.; Roy, R.S.; Wu, J.K.; Wyvratt, M.; Zhang, B.B.; Zhu, L.; Thornberry, N.A.; Weber, A.E. *J. Med. Chem.* **2005**, *48*, 141.
- 31) Hansen, K.B.; Balsells, J.; Dreher, S.; Hsiao, Y.; Kubryk, M.; Palucki, M.; Rivera, N.; Steinhuebel, D.; Armstrong III, J.D.; Askin, D.; Grabowski, E.J.J. *Org. Process Res. Dev.* **2005**, *9*, 634.
- 32) Hansen, K.B.; Hsiao, Y.; Xu, F.; Rivera, N.; Clausen, A.; Kubryk, M.; SKrska, S.; Rosner, T.; Simmons, B.; Balsells, J.; Ikemoto, N.; Sun, Y.; Spindler, F.; Malan, C.; Grabowski, E.J.J.; Armstrong III, J.D. *J. Am. Chem. Soc.* **2009**, *131*, 8798.
- 33) Steinhuebel, D.; Sun, Y.; Matsumura, K.; Sayo, N.; Saito, T. *Am. Chem. Soc.* **2009**, *131*, 11316.

- 34) Savile, C.K.; Janey, J.M.; Mundorff, E.C.; Moore, J.C.; Tam, S.; Jarvis, W.R.; Colbeck, J.C.; Krebber, A.; Fleitz, F.J.; Brands, J.; Devine, P.N.; Huisman, G.W.; Hughes, G.J. *Science* **2010**, *329*, 305.
- 35) Waldron, K.J.; Rutherford, J.C.; Ford, D.; Robinson, N.J. *Nature* **2009**, *460*, 823.
- 36) Leskovac, V.; Trivic, S.; Pericin, D. *FEMS Yeast Research* **2002**, *2*, 481.
- 37) Lindskog, S. *Pharmacol. Ther.* **1997**, *74*, 1.
- 38) Epstein, F. H.; Hsia, C. C. W. *New England Journal of Medicine* **1998**, *338*, 239.
- 39) Sono, M.; Roach, M.P.; Coulter, E.D.; Dawson, J.H. *Chem. Rev.* **1996**, *96*, 2841.
- 40) Banerjee, R.V.; Matthews, R.G. *FASEB J.* **1990**, *4*, 1450.
- 41) Margoliash, E. *Proc. Natl. Acad. Sci. U.S.A.* **1963**, *50*, 672.
- 42.a) Rosati, F.; Roelfes, G. *ChemCatChem* **2010**, *2*, 916. b) Pordea, A.; Ward, T.R. *Synlett* **2009**, *20*, 3225. c) Köhler, V.; Wilson, Y.M.; Lo, C.; Sardo, A.; Ward, T.R. *Curr. Op. Chem. Biol.* **2010**, *21*, 744. d) Heinisch, T.; Ward, T.R. *Op. Chem. Biol.* **2010**, *14*, 184.
- 43) Zhang, J.L.; Garner, D.K.; Liang, L.; Chen, Q.; Lu, Y. *Chem. Commun.* **2008**, 1665.
- 44) Lo, C.; Ringenberg, M.R.; Gnanndt, D.; Wilson, Y.M.; Ward, T.R. *Chem. Commun.* **2011**, *47*, 12065.
- 45) Steinreiber, J.; Ward, T.R. *Coord. Chem. Rev.* **2008**, *252*, 751.
- 46) Jing, Q.; Kazlauskas, R.J. *ChemCatChem* **2010**, *2*, 953.
- 47.a) Talbi, B.; Haquette, P.; Martel, A.; Montigny, F.; Fosse, C.; Cordier, S.; Roisnel, T.; Jaouena, G.; Salmain, M. *Dalton Trans.* **2010**, *39*, 5605. b) Bos, J.; Fusetti, F.; Driessen A.J.M.; Roelfes, G. *Angew. Chem. Int. Ed.* **2012**, *51*, 7472.
- 48.a) Wu, Z.P.; Hilvert, D. *J. Am. Chem. Soc.* **1989**, *111*, 4513.
- 49) Nicholas, K.M. *Natl. Acad. Sci.* **2002**, *99*, 2648.
- 50.a) Green, N.M.; *Adv. Protein Chem.* **1975**, *29*, 85. b) Wilcheck, M.; Bayer, E.A. *Biomol. Eng.* **1999**, *16*, 1. c) Green, N.M. *Methods. Enzymol.* **1990**, *184*, 51. d) Green, N.M. *Biochem. J.* **1963**, *89*, 585. e) Chaiet, L.; Wolf, F.J. *Arch. Biochem. Biophys.* **1964**, *106*, 1.
- 51) Livnah, O.; Bayer, E.A.; Wilcheck, M.; Sussman, J.L. *Proc. Natl. Acad. Sci.* **1993**, *90*, 5076.
- 52.a) Chilkoti, A.; Tan, P.H.; Stayton, P.S. *Proc. Natl. Acad. Sci.* **1995**, *92*, 1754. b) Laitinen, O.H.; Airene, K.J.; Marttila, A.T.; Kulik, T.; Porkka, E.; Bayer, E.A. Wilcheck, M.; Kulomaa, M.S. *FEBS Lett.* **1999**, *461*, 52.



- 53.a) Weber, P.C.; Ohlendorf, D.H.; Wendoloski, J.J.; Salemme, F.R. *Science* **1989**, *243*, 85. b) Hendrickson, W.A.; Pähler, A.; Smith, J.L.; Satow, Y.; Merritt, E.A.; Phizackerley, R.P. *Proc. Natl. Acad. Sci.* **1989**, *86*, 2190.
- 54) DeChancie, J.; Houk, K.N. *J. Am. Chem. Soc.* **2007**, *129*, 5419.
55. a) Chilkoti, A.; Stayton, P.S. *J. Am. Chem. Soc.* **1995**, *117*, 10622. b) Stayton, P.S.; Freitag, S.; Klumb, L.A.; Chilkoti, A.; Chu, V.; Penzotti, J.E.; To, R.; Hyre, D.; Le Trong, I.; Lybrand, T.P.; Stenkamp, R.E. *Biomol. Eng.* **1999**, *16*, 39.
- 56.a) Chignell, C.F.; Starkweather, D.K.; Sinha, B.K. *J. Biol. Chem.* **1975**, *250*, 5622. b) Zhao, S.; Walker, D.S., Reichert, W.M. *Langmuir* **1993**, *9*, 3166. c) Zhao, S.; Reichert, W.M. *Biophys. J.* **1994**, *66*, 305. d) Sano, T.; Cantor, C.R. *J. Biol. Chem.* **1990**, *265*, 3369. e) Sano, T.; Cantor, C.R. *Proc. Natl. Acad. Sci.* **1995**, *92*, 3180. f) Jones, M.L.; Kurzban, G.P. *Biochemistry* **1995**, *34*, 11750.
- 57.a) Kohler, V. *Curr. Op. Biotechnol.* **2010**, *21*, 744.
- 58) Bayer, E.A.; Ben Hur, H.; Gitlin, G.; Wilcheck, M.J. *Chem. Biophys. Methods* **1986**, *13*, 103.
- 59) Gonzalez, M.; Bagatolli, L.A.; Echabe, I.; Arrondo, J.L.R.; Argarana, C.E.; Cantor, C.R.; Fidelio, G.D. *J. Biol. Chem.* **1997**, *272*, 11288.
- 60) Dundas, C.M.; Demonte, D.; Park, S. *Appl. Microbiol. Biotechnol.* **2013**, *97*, 9343.
- 61) McMahon, R.J. *Avidin-biotin Interactions (Methods in Molecular Biology)*, Springer **2008**, New York
- 62) Wilson, M.E.; Whitesides, G.M. *J. Am. Chem. Soc.* **1978**, *100*, 306.
- 63) Collot, J.; Gradinaru, J.; Humbert, N.; Skander, M.; Zocchi, A.; Ward, T.R. *J. Am. Chem. Soc.* **2003**, *125*, 9030.
- 64) Skander, M.; Humbert, N.; Collot, J.; Gradinaru, J.; Klein, G.; Loosli, A.; Sauser, J.; Zocchi, A.; Gilardoni, F.; Ward, T.R. *J. Am. Chem. Soc.* **2004**, *126*, 14411
- 65) Klein, G.; Humbert, N.; Gradinaru, J.; Ivanova, A.; Gilardoni, F.; Rusbandi, U.E.; Ward, T.R. *Angew. Chem. Int. Ed.* **2005**, *44*, 7764.
- 66) Rusbandi, U.E.; Lo, C.; Skander, M.; Ivanova, A.; Creus, M.; Humbert, N.; Ward, T.R. *Adv. Synth. Catal.* **2007**, *349*, 1923.
- 67) Pierron, J.; Malan, C.; Creus, M.; Gradinaru, J.; Hafner, I.; Ivanova, A.; Sardo, A.; Ward, T.R. *Angew. Chem.* **2008**, *120*, 713.
- 68) Hyster, T.; Knörr, L.; Ward, T.R.; Rovis, T. *Science* **2012**, *338*, 500.
- 69) Letondor, C.; Humbert, N.; Ward, T.R. *Proc. Natl. Acad. Sci.* **2005**, *102*, 4683.

70) Pordea, A.; Creus, M.; Panek, J.; Duboc, C.; Mathis, D.; Novic, M.; Ward, T.R. *J. Am. Chem. Soc.* **2008**, *130*, 8085.

71) Köhler, V.; Mao, J.; Heinisch, T.; Pordea, A.; Sardo, A.; Wilson, Y.M.; Knörr, L.; Creus, M.; Prost, J.C. Schirmer, T.; Ward, T.R. *Angew. Chem. Int. Ed.* **2011**, *50*, 10863.

## Chapter 2: Design and Genetic Optimization of an Artificial Transfer Hydrogenase (ATHase)

### 2.1 Introduction

#### 2.1.1 Homogenous Asymmetric Transfer Hydrogenation

##### 2.1.1.1 Asymmetric Transfer Hydrogenation of Ketones

Asymmetric transfer hydrogenation can be viewed as a transition metal catalyzed asymmetric variant of the Meerwein-Ponndorf-Verley reduction in which ketones and aldehydes are reduced to alcohols using isopropanol as a reducing agent and aluminium alkoxides as catalysts.<sup>1</sup> Therefore, this reaction provides a versatile alternative to classic hydrogenation using hazardous hydrogen gas. First attempts to develop asymmetric transfer hydrogenation date back to the 1970s and utilized rhodium and ruthenium phosphine complexes in the presence of enantiopure carbohydrates as a hydride source.<sup>2</sup> However, these catalytic systems afforded only modest enantioselectivities. Since then, many types of homogenous asymmetric transfer hydrogenation catalysts mainly based on transition metal complexes of Ru(II), Rh(III) and Ir(III) have been reported. The most active and selective catalysts available nowadays are those contain bisphosponites **1**<sup>3</sup>, pyridine derivatives **2**<sup>4</sup>, aza-norbornyl alcohols **3**<sup>5</sup>, amino alcohols **4**<sup>6</sup> and tosylated diamines **5**<sup>7</sup> (TsDPEN, *N*-tosyl 1,2-diphenyldiamine) (Figure 2.1).

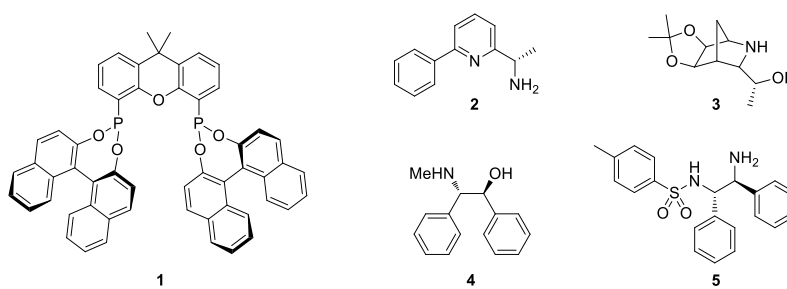


**Fig. 2.1.** Selected ligands used in asymmetric transfer hydrogenation.

The ruthenium  $\eta^6$ -arene piano-stool complexes of TsDPEN developed by Noyori and related catalysts such as  $[(\eta^5\text{-Cp}^*)\text{M}(\text{TsDPEN})\text{Cl}]$  ( $\text{M} = \text{Rh, Ir}$ ;  $\text{Cp}^* = \text{pentamethyl cyclopentadienyl}$ )<sup>8</sup> are maybe the most prominent examples in this context. In presence of isopropanol or a formic acid/triethylamine azeotrope as a hydride source, these catalysts reduce aromatic ketones<sup>9</sup>, acetylenic carbonyl compounds<sup>10</sup> and imines (see below) with high enantioselectivities. The generally accepted mechanism for the reduction of ketones by  $[(\eta^6\text{-benzene})\text{Ru}(\text{S,S-TsDPEN})\text{Cl}]$  is shown in Figure 2.2<sup>11</sup>. Upon formal loss of HCl, the precatalyst **1** forms a planar 16 electron amido complex **2** which reacts readily with isopropanol to yield the tetrahedral 18 electron Ru-hydride species **3**. The bifunctional constitution of the catalyst then promotes the concerted delivery of the hydride and a proton provided by the amine group of the ligand to the carbonyl moiety of the substrate via a six-membered transition state **4**, thereby yielding the alcohol and regenerating the 16 electron complex. This process occurs with an outer-sphere mechanism whereby neither the ketone substrate nor the alcohol interacts with the metallic center throughout the reduction. Studies by Wills showed that corresponding complexes in which the amino group of TsDPEN is alkylated are poor transfer hydrogenation catalysts, thus confirming the functional role of the ligand.<sup>12</sup>

The hydride complex is sterically controlled by the enantiopure ligand, resulting in the formation of a single diastereomer that is chiral at Ru. Thereby, two structural features of the catalyst are responsible for the chiral induction. The enantiodiscrimination of the prochiral faces of the aromatic ketone depends on i) the chiral geometry of the five-membered chelate which determines the absolute configuration of the metal and ii) is mediated by an energetically favorable CH/ $\pi$ -interaction between a hydrogen atom of the  $\eta^6$ -arene and the aromatic moiety of the substrate.<sup>13</sup>

It should be noted that recent computational studies by Ikariya suggest that the above mechanism is only valid in the gas-phase.<sup>14</sup> Under consideration of solvation effects, calculations based on density functional theory suggest that the reaction proceeds in two steps whereby the enantioselectivity determining hydride transfer to the carbonyl moiety is followed by protonation of the resulting alkoxide. The proton source for

the latter process is probably a protic solvent molecule rather than the amine moiety of the ligand. This would imply that the catalytic cycle does not proceed necessarily via a 16 electron amido complex.

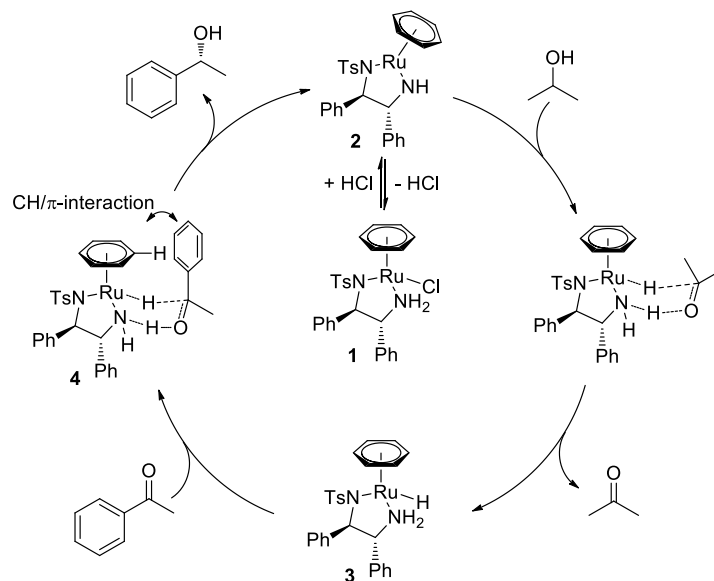


**Fig. 2.2.** Suggested catalytic cycle of the asymmetric transfer hydrogenation of acetophenone with  $[(\eta^6\text{-benzene})\text{Ru}(\text{R,R-TsDPEN})\text{Cl}]$ . According to recent studies by Ikariya, this mechanism may only be valid in the gas phase.

### 2.1.1.2 Asymmetric Transfer Hydrogenation of Imines

In contrast to asymmetric transfer hydrogenation of ketones, this reaction is relatively undeveloped for the reduction of imines. In 1996, Noyori showed that  $[(\eta^6\text{-arene})\text{Ru}(\text{S,S-TsDPEN})\text{Cl}]$ -catalysts effectively reduce imines in the presence of a 5:2 formic acid-triethylamine azeotropic mixture in acetonitrile, achieving up to 97 ee for the reduction of various isoquinolines.<sup>15</sup> Thereby, the reactivity of the catalysts was found to be much higher towards imine reduction compared to ketone reduction.

Two different mechanisms have been proposed for the asymmetric transfer hydrogenation of imines, namely a concerted outer-sphere mechanism similar to the one operating in ketone-reduction and an ionic pathway where the nitrogen of the imine is protonated prior to hydride delivery from the metal to the carbon

of the polarized C=N bond. So far, experiments supporting either one or the other mechanism have been reported. Bäckvall used the isolated hydride species  $[(\eta^6\text{-}p\text{-cymene})\text{Ru}(\text{S,S-TsDPEN})\text{H}]$  for the stoichiometric reduction of imines.<sup>16</sup> The reaction proceeded only under acidic conditions or in the presence of Lewis acids, thus supporting an ionic mechanism as the activation barrier may be too high for the delivery of the hydride to the non-protonated imine. This result contrasts with several other studies which suggest a concerted mechanism analogous to ketone reduction. Blackmond and coworkers performed kinetic experiments for the reduction of 6,7-dimethoxy-1-methyl-3,4-dihydroisoquinoline using  $[(\eta^5\text{-Cp}^*)\text{Rh}(\text{S,S-TsDPEN})\text{Cl}]$  as a catalyst in presence of formic acid and triethylamine in methanol.<sup>17</sup> According to this study, the reaction rates depend on the different acid-base equilibria between formic acid and the imine, the amine and triethylamine, respectively. Thereby it was suggested that the catalyst displays saturation kinetics towards the formation of the hydride intermediate even at low concentrations of formic acid and that the latter reactant protonates the imine substrate. Keeping the formic acid concentration low by slow addition during the reaction or performing the reaction at high triethylamine concentration, resulted in higher reaction rates whereby the formed  $\text{Et}_3\text{NH}^+\text{HCOO}^-$ -salt is thought to act as a reservoir for HCOOH. Based on these results, it was proposed that the free amine rather than the iminium was the actual substrate for the catalyst.

As the opposite enantiomers are produced when compared to the reduction of prochiral alcohols, Wills suggested that the mechanism for the reduction of the imine substrate cannot be the same as the one for ketone reduction (Figure 2.3).<sup>18</sup> Based on this hypothesis, he suggested two transition states which both lead to the observed enantiomers in the reduction of 6,7-dimethoxy-1-methyl-3,4-dihydroisoquinoline using  $[(\eta^6\text{-benzene})\text{Ru}(\text{R,R-TsDPEN})\text{Cl}]$ : i) the imine is reduced via concerted six-membered transition state where the imine moiety is orientated relative to the catalyst in a way to allow a simultaneous delivery of hydrogen atoms to the C=N bond (Figure 2.3.C) ii) the imine is reduced by a ionic mechanism in which the C=N bond of the iminium is oriented away from the amine group of the ligand without adopting a six-membered transition state. This arrangement would allow the CH/ $\pi$  interaction observed in ketone reduction

to operate (Figure 2.3.D). However, experiments using *N*-alkylated *R,R*-TsDPEN derivatives to probe which of the two mechanisms is operative did not settle the question.

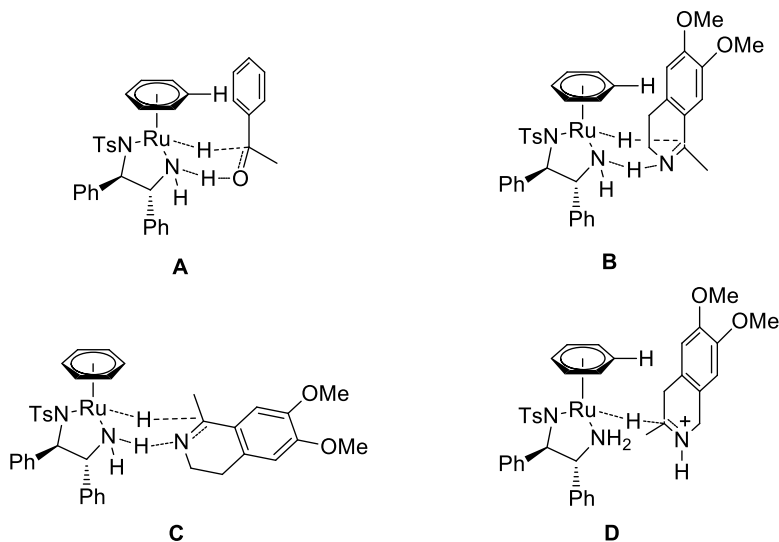


**Fig. 2.3.** Proposed transition states for the transfer hydrogenation of imines using  $[(\eta^6\text{-benzene})\text{Ru}(\text{R,R-TsDPEN})\text{Cl}]$  suggested by Wills et al. A) concerted mechanism with a CH/ $\pi$ -interaction between the arene of the catalyst and the aromatic moiety of the substrate for the reduction of acetophenone, yielding (*R*)-phenylethanol. B) the corresponding hypothetical transition state for the reduction of 6,7-dimethoxy-3,4-dihydroisoquinoline would afford the same absolute configuration of the product as in A which contrasts to the observed (*S*)-enantiomer. A plausible concerted non-ionic transition state without CH/ $\pi$ -interaction (C) and a non-concerted ionic mechanism with CH/ $\pi$ -interaction both deliver the observed (*S*)-product amine.<sup>18</sup>

Further experiments addressing this issue were performed by Casey who applied a related bifunctional Ru-catalyst ("Shvo's catalyst") to the transfer hydrogenation of imines.<sup>19</sup> Whereas his detailed mechanistic investigations support a concerted mechanism, Bäckvall proposed a stepwise transfer of hydrogen atoms from this catalyst to the imine moiety whilst the nitrogen atom of the substrate is coordinated to the Ru-center.<sup>20</sup>

However, these examples show an ambiguous picture of the exact mechanism of the transfer hydrogenation of imines and illustrate the need for further investigations on this particular topic.

### 2.1.1.3 Asymmetric Transfer Hydrogenation in Water

Asymmetric transfer hydrogenation in water has been reported for ketones as well as imines by various research groups using either Noyori type complexes or related catalysts of which some bearing modified ligands with improved water solubility (e.g. sulfonated TsDEPN).<sup>21</sup>

Xiao and coworkers extensively investigated the pH-dependence of  $[(\eta^6\text{-}p\text{-cymene})\text{Ru}(\text{R,R-TsDEPN})\text{Cl}]$  and  $[(\eta^5\text{-Cp}^*)\text{M}(\text{TsDEPN})\text{Cl}]$  (where M = Rh, Ir) in the asymmetric transfer hydrogenation of ketones and imines in the presence of formate as a hydride source. Whereas the Ru-catalyst performed best at pH-values above 10 for the reduction of acetophenone<sup>22</sup>, the Rh and Ir counterparts display the highest activity and selectivity around neutral pH in ketone reduction<sup>23</sup> and around pH 5 in imine reduction.<sup>24</sup> At very acidic or basic conditions the performance of the latter catalysts was poor for both substrates. In the case of imine reduction this observation was traced back to two conflicting equilibria between the protonated and deprotonated forms of either formic acid and the imine substrate. At pH-values above 5.4, the fraction of protonated imine is low whereas at pH-values below 3.6 the concentration of formate decreases, on one hand leading to a lower concentration of reactive iminium and on the other hand resulting in a decreased rate at which the metal-formate complex and thus the hydride intermediate is formed. A pH-value between 3.6 and 5.4 would be expected to afford high concentrations of both reactants and could therefore provide higher reaction rates. In addition, it was proposed that at low pH-values the nitrogen of the sulfonamide moiety of the TsDEPN ligand may be protonated and therefore dissociates from the metal. The resulting monodentate amine complex would be less rigid and therefore may explain the poor enantioselectivity at low pH-values. Furthermore, it has to be considered that the hydride intermediate also may be protonated to yield H<sub>2</sub> and that this competing reaction contributes to the low transfer hydrogenation activity under these conditions.<sup>25</sup>

The low reaction rate at high pH-values may be explained by formation of the inactive hydroxo-species resulting from deprotonation of the corresponding cationic aquo-complex. The corresponding processes are outlined in Figure 2.4.



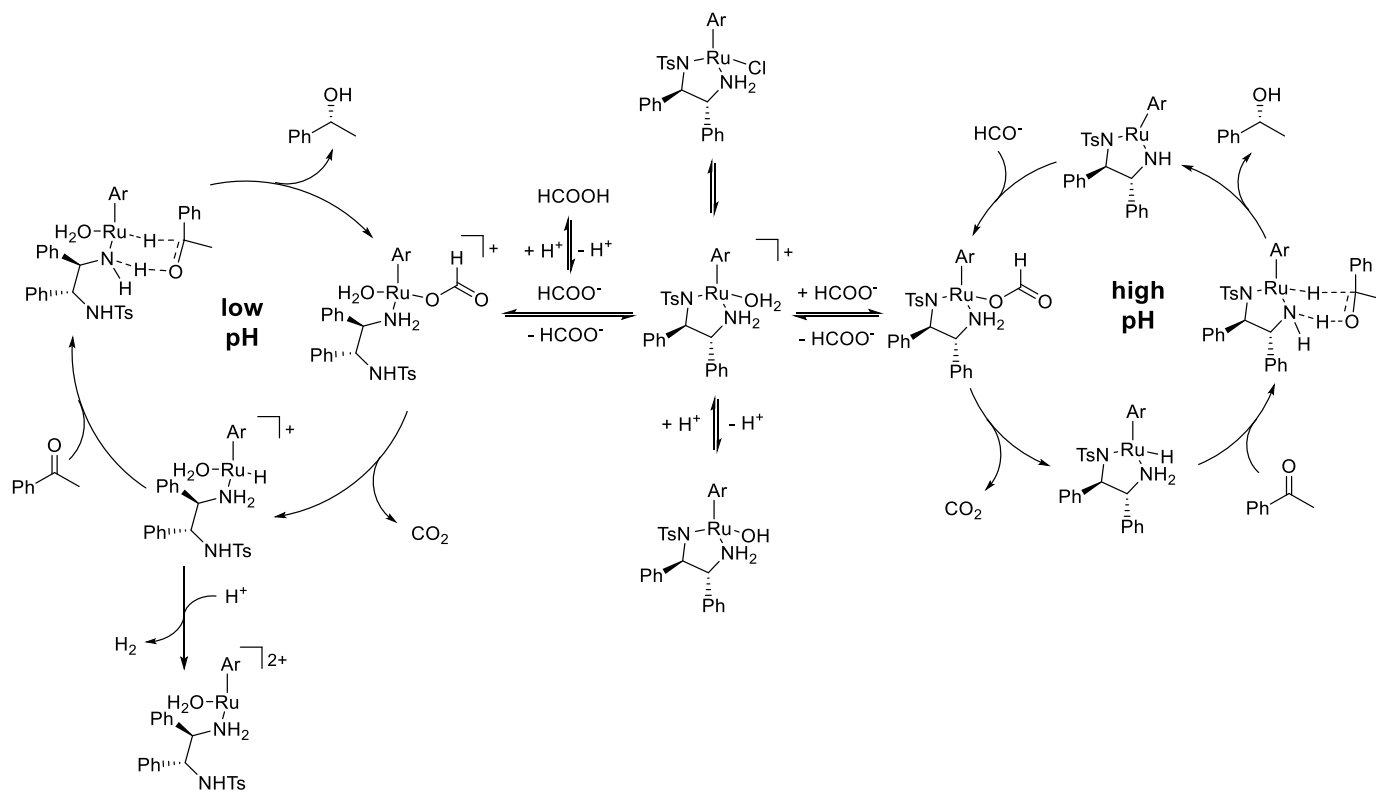
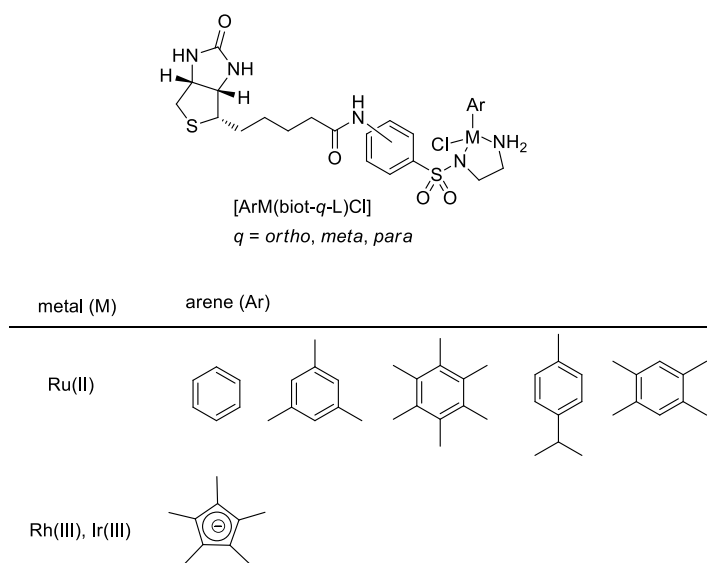


Fig 2.4. pH-dependence of asymmetric transfer hydrogenation in water.<sup>22</sup>

### 2.1.2 Artificial Transferhydrogenases Based on the Biotin-(Strept)avidin Technology for the Asymmetric Reduction of Ketones (Previous Work)

In a similar approach as applied for artificial hydrogenases (see section 1.1.2.2), a chemogenetic optimization strategy led to the development of artificial transferhydrogenases (ATHase) for the asymmetric reduction of ketones in the second half of the last decade within the Ward group. The chemical diversity of the racemic biotinylated Noyori-type catalyst  $[(\eta^n\text{-Arene})\text{M}(\text{biot-}p\text{-L})\text{Cl}]$  was generated by variation of the metal ( $\text{M} = \text{Ru}^{\text{II}}, \text{Rh}^{\text{III}}, \text{Ir}^{\text{III}}$ ), the  $n = 6$  (Arene = benzene, *p*-cymene, mesitylene, durene, hexamethyl benzene for  $\text{M} = \text{Ru}$ ,  $n = 5$  pentamethylcyclopentadienyl for  $\text{M} = \text{Rh}, \text{Ir}$ ) and the substitution

pattern of the biotin moiety ( $q = \textit{ortho}, \textit{meta}, \textit{para}$ ) (figure 2.5).<sup>26</sup> These complexes were prepared *in situ* from the corresponding metal precursors  $[(\eta^n\text{-arene})\text{MCl}_2]_2$  and the achiral ligands in refluxing isopropanol. Applying the twenty one resulting racemic metal complexes to the reduction of acetophenone, *p*-bromoacetophenone and *p*-methylacetophenone in presence of streptavidin revealed that only the *para*-substituted complexes afforded significant reaction products and that the capping arene had a great influence on the activity and selectivity of the ATHase.



**Fig. 2.5.** Chemical diversity of the metal cofactor of the artificial transfer hydrogenase (ATHase).

Docking studies of  $[(p\text{-cymene})\text{Ru}(\text{biot-}p\text{-L})\text{H}]$  within wild type streptavidin showed that the residues S112 and S122 lie in closest proximity to the Ru-center. Nineteen streptavidin mutants resulting from saturation mutagenesis at position 112 were subsequently combined with a selection of five complexes (Ru in combination with either *p*-cymene, durene or benzene and Rh/Ir in combination with Cp\*) and the resulting artificial metalloenzymes were tested in the reduction of the three acetophenone derivatives. The main

trends which emerged from this screening include: i) the absolute configuration of the reaction products is strongly dependent on the  $\eta^6$ -arene present in the Ru-complexes whereas the induced selectivity of the corresponding ATHase can be reverted by the presence of cationic residues at position 112 (e.g.  $[(\eta^6\text{-}p\text{-cymene})\text{Ru}(\text{biot-}p\text{-L})\text{Cl}]$  yields (*R*)-phenylethanol with 90% ee in case of Sav-S112A and (*S*)-phenylethanol with 20% ee when the S112K mutant is present). ii) the hybrid catalysts with Ru-complexes generally afford better results in terms of activity and selectivity compared to the Rh and Ir derived ATHases iii) ATHases with Sav-mutants offering a coordinating amino acid residue at position 112 (e.g. cysteine, histidine) are inactive, therefore confirming the proximity of this position to the metal center. The X-ray crystal structure of the most promising (*S*)-selective ATHase  $[(\eta^6\text{-benzene})\text{Ru}(\text{biot-}p\text{-L})\text{Cl}]\subset\text{Sav-S112K}$  confirmed the proximity of the K112 residue to the metal-center and identified K121 of an adjacent monomer as another close-lying residue.<sup>27</sup> In addition, L124 was found to display a close contact to the SO<sub>2</sub>-moiety of the ligand (figure 2.6). The absolute configuration of the Ru-atom is (*S*) which is also observed in the (*S*)-selective homogenous system with chiral TsDPEN-ligands. Based on these observations, a "second generation" of ATHases was designed by saturation mutagenesis of Sav-WT, Sav-S112A (yields (*R*)-selective ATHases) and Sav-S112K (yields (*S*)-selective ATHases) at either the 121 and 124 position. The resulting 120 Sav isoforms were combined with either  $[(\eta^6\text{-}p\text{-cymene})\text{Ru}(\text{biot-}p\text{-L})\text{Cl}]$  or  $[(\eta^6\text{-benzene})\text{Ru}(\text{biot-}p\text{-L})\text{Cl}]$  and tested for the reduction of different aromatic and dialkyl ketones. The screening revealed that the K121 position is more crucial to optimization of enantioselectivity whereby up to 90% ee for the reduction of was achieved using  $[(\eta^6\text{-}p\text{-cymene})\text{Ru}(\text{biot-}p\text{-L})\text{Cl}]\subset\text{S112A-K121T}$ . As the CH- $\pi$ -interaction between *p*-cymene and the non-aromatic substrate cannot operate in this case, it was concluded that the selectivity is induced by the second coordination sphere of the host protein.

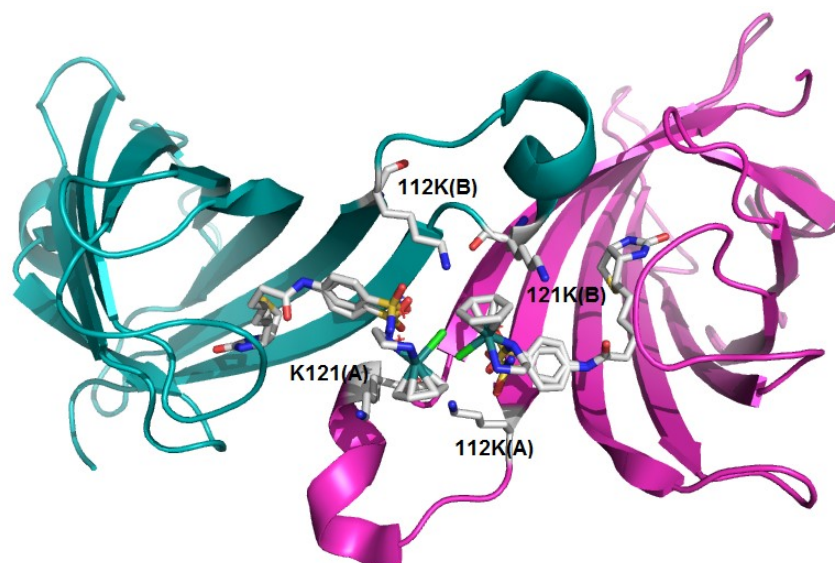


**Fig. 2.6.** Crystal structure of  $[(\eta^6\text{-benzene})\text{Ru}(\text{biot-}p\text{-L})\text{Cl}]_2\text{-Sav-S112K}$  (PDB-code:2QCB). Two symmetry-related monomers are highlighted in magenta (monomer A) and cyan (monomer B). The metal cofactors and the closely lying residues K112 and K121 are shown as sticks (carbon: grey, oxygen: red, nitrogen: blue, chlorine: green, Ru: cyan).

## 2.2 Artificial Transfer Hydrogenases based on the Biotin-(Strept)avidin Technology for the Asymmetric Reduction of Imines

### 2.2.1 Preamble: Comment on Publications

#### 2.2.1.1 Optimization of an Artificial Transfer Hydrogenase for the Reduction of 6,7-dimethoxy-3,4-dihydroisoquinoline

Based on the results obtained previously for the ketone reduction, the ATHase system was tested for the asymmetric transfer hydrogenation of cyclic imines. In order to identify suitable metal cofactors for this purpose, a selection of biotinylated d<sup>6</sup> piano stool complexes have been screened in presence of WT-Sav for the reduction of 6,7-dimethoxy-1-methyl-3,4-dihydroisoquinoline to salsolidine in previous work. In contrast to ketone reduction, the  $[(\eta^5\text{-Cp}^*)\text{M}(\text{biot-}p\text{-L})\text{Cl}]$  complexes (where M = Rh<sup>III</sup>, Ir<sup>III</sup>) afforded better results in terms of activity and selectivity than the corresponding  $[(\eta^6\text{-arene})\text{Ru}(\text{biot-}p\text{-L})\text{Cl}]$  counterparts. For all but one metal complex the same absolute product configuration was observed for the reduction of phenylethanol and the imine substrate which contrasts with the corresponding homogenous system where aromatic imines and ketones are reduced with opposite selectivity, thus again illustrating the influence of the protein environment to the performance of the metal cofactors (see section 2.2.2).

Control experiments indicated that the biotinylated complexes are localized within the biotin-binding site of the host protein and that it is the second coordination sphere which induces the selectivity of the artificial transfer hydrogenase: i) catalysis with  $[(\eta^5\text{-Cp}^*)\text{Ir}(\text{biot-}p\text{-L})\text{Cl}]$  in absence of Sav affords (*rac*)-salsolidine, ii) racemic product in low yield was obtained with the non-biotinylated achiral counterpart  $[(\eta^5\text{-Cp}^*)\text{Ir}(\text{TsEN})\text{Cl}]$  in presence of Sav iii) addition of biotin decreases the selectivity of the artificial transfer hydrogenases drastically (see experimental part).

The artificial transfer hydrogenase was genetically optimized for the transfer hydrogenation of 6,7-dimethoxy-1-methyl-3,4-dihydroisoquinoline by screening a library of Sav isoforms resulting from

saturation mutagenesis at position S112 (see section 2.2.2). Similar trends with the mutant ATHases were observed as for ketone-reduction.  $[(\eta^5\text{-Cp}^*)\text{Ir}(\text{biot-}p\text{-L})\text{Cl}]_{\text{S112A}}$  (*R*-selective) and  $[(\eta^5\text{-Cp}^*)\text{Ir}(\text{biot-}p\text{-L})\text{Cl}]_{\text{S112K}}$  (*S*-selective) provided the highest enantioselectivity and their performance could be further improved with respect to the reaction temperature and the Sav-tetramer/[Ir] ratio.

### 2.2.1.2 Kinetics and Mechanism of the Artificial Transfer Hydrogenase

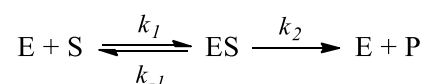
HABA-titrations and circular dichroism (CD) spectroscopy where the biotinylated Ir-complex was added stepwise to a solution of Sav confirmed that the biotinylated complex is indeed incorporated within a well-defined second coordination sphere. The maximal molar ration between  $[(\eta^5\text{-Cp}^*)\text{Ir}(\text{biot-}p\text{-L})\text{Cl}]$  and tetrameric Sav was found to be 4:1 in both experiments, indicating that all four biotin-binding sites of the tetramer can accommodate the metal complex (see experimental part). Unfortunately, due to their complexity it was not possible to deconvolute the CD-spectra of  $[(\eta^5\text{-Cp}^*)\text{Ir}(\text{biot-}p\text{-L})\text{Cl}]_{\text{S112A}}$  and  $[(\eta^5\text{-Cp}^*)\text{Ir}(\text{biot-}p\text{-L})\text{Cl}]_{\text{S112K}}$  to extract binding constants.

The crystal structure of  $[(\eta^5\text{-Cp}^*)\text{Ir}(\text{biot-}p\text{-L})\text{Cl}]_{\text{S112A}}$  (see section 2.2.2) shows that the Ir-atoms of two adjacent monomers are located in close proximity (distance  $\text{Ir}\cdots\text{Ir} = 5.2 \text{ \AA}$ ) and therefore may interact during the catalytic process. Indeed, the molar ratio  $[(\eta^5\text{-Cp}^*)\text{Ir}(\text{biot-}p\text{-L})\text{Cl}]$  vs. Sav-tetramer was found to have a great influence on the catalytic performance of the hybrid catalysts. In case of the S112A variant, a gradual erosion of the enantioselectivity was observed when increasing this ratio from 1:1 to 4:1 (where all biotin binding sites of the tetramer are occupied with the Ir-complex). In contrast, the enantioselectivity of the S112K-ATHase remains nearly constant. In case of both hybrid catalysts, the enantioselectivity decreases when an excess of complex is present which is due to the production of racemic product by unbound  $[(\eta^5\text{-Cp}^*)\text{Ir}(\text{biot-}p\text{-L})\text{Cl}]$ .

With regard to these observations, the following questions with respect to the mechanistic features of the hybrid catalysts arise: i) how do adjacent active sites of the Sav-tetramer influence each other during catalysis? ii) how is the enantioselectivity of the reaction induced? iii) what is the absolute configuration at Ir in  $[(\eta^5\text{-Cp}^*)\text{Ir}(\text{biot-}p\text{-L})\text{H}]$  in the transition state? iv) which mechanism of the hydride transfer is operative (ionic or concerted)?

To gain further information on how the enantioselectivity is induced in the S112A and S112K derived ATHases, the enzyme kinetics of  $[(\eta^5\text{-Cp}^*)\text{Ir}(\text{biot-}p\text{-L})\text{H}]$  within both mutants at different  $[\text{Ir}]/\text{Sav-tetramer}$  ratios was determined (see section 2.2.3).

A basic kinetic model of enzymes was developed by L. Michaelis and M.L. Menten.<sup>28</sup> According to their underlying mechanism, the substrate (S) and the enzyme (E) form a complex (ES) in a first step (whereby  $k_1$  denotes the association rate and  $k_{-1}$  denotes the dissociation rate of ES). In a second step, the chemical transformation takes place with a first-order rate ( $k_2$ ) before the product (P) is released by the enzyme. Assuming that the second step is rate-limiting ( $k_{-1} \gg k_2$ ), the enzyme-substrate complex ("Michaelis complex") is in thermodynamic equilibrium with free enzyme and substrate.



whereby

$$\frac{k_1}{k_{-1}} = \frac{[\text{E}][\text{S}]}{[\text{ES}]} = K_s$$

is the corresponding equilibrium constant. Since in biotransformations the concentration of the substrate is typically much higher than the concentration of the enzyme ( $[\text{E}] \ll [\text{S}]$ ), the concentration of the enzyme-substrate complex remains constant during the reaction:

$$\frac{d[\text{ES}]}{dt} = 0$$

This "steady-state" approximation formulated by G.E. Haldane and B.S. Briggs<sup>29</sup> in 1925 is more general than the assumption of an equilibrium and the rate of an enzyme-catalyzed reaction can therefore be expressed with the Michaelis-Menten equation:

$$v = \frac{V_{\max} [S]}{K_M + [S]}$$

Plotting the initial rate  $v$  against the substrate concentration  $[S]$  yields a hyperbolic curve indicating saturation kinetics with the maximal reaction rate at  $V_{\max}$ . In the case of the above mentioned Michaelis-Menten mechanism in which only one particular enzyme-substrate complex is formed and all binding steps are fast,  $k_2$  represents the catalytic constant  $k_{cat}$  which is defined as

$$k_{cat} = \frac{V_{\max}}{[E]_0}$$

where  $[E]_0$  is the total enzyme concentration ( $[E]_0 = [E] + [ES]$ ).  $k_{cat}$  is often called the "turnover number" of an enzyme. However, since  $k_{cat}$  is related to the number of conversions per time unit, it is actually the equivalent of the turnover frequency (TOF) used in context of homogenous catalysis.  $K_M$  denotes the Michaelis constant and represents the substrate concentration at which the rate  $v$  is equal to  $1/2 V_{\max}$ .  $K_M$  can be alternatively expressed as

$$K_M = \frac{k_{-1} + k_2}{k_1} = \frac{K_s + k_2}{k_1}$$

If  $k_{-1} \gg k_2$ , the dissociation constant  $K_s$  of the Michaelis-Komplex becomes equal to the Michaelis constant ( $K_s = K_M$ ). The Michaelis constant therefore can be viewed as a measure of the substrate affinity towards the enzyme.

The assumption of interacting metal cofactors located in neighboring active sites is supported by the observation that the  $k_{cat}$  values decrease upon raising the  $[Ir]/\text{Sav-S112A}$  ratio from 2:1 to 4:1 (see section



2.2.3). The significantly higher  $K_M$ -value in the fully [Ir]-saturated ATHase suggests that the affinity of the substrate towards the artificial metal cofactor decreases, possibly due to sterical hindrance between two Ir-Cp\*-moieties. This interaction may also explain the observed concurrent decrease of the enantioselectivity, indicating a different second coordination sphere around the metal at high [Ir]/Sav-S112A ratios as the complex adopts a different conformation. In contrast,  $[(\eta^5\text{-Cp}^*)\text{Ir}(\text{biot-}p\text{-L})\text{Cl}]$  seems to operate independently in case of the S112K mutant as the ee- and  $k_{\text{cat}}$ -values remain constant upon increasing the [Ir]/Sav-S112A ratio from 1:1 to 4:1. The different behavior implies that the amino acid residue at position 112 close to the active site dictates the conformation of the metal cofactor which in turn determines the relative alignment between the latter moiety and the substrate in the transition state and thus the absolute configuration of the amine product produced.

With a critical look at the kinetic results obtained from catalysis at different [Ir]/Sav ratios, it has to be mentioned that incubation of  $[(\eta^5\text{-Cp}^*)\text{Ir}(\text{biot-}p\text{-L})\text{Cl}]$  with Sav in case where this ratio is lower than 4:1 results in a statistical distribution of Sav-tetramers with either no, one, two, three or four bound metal cofactors. Therefore, it may be likely that the concentration of Sav-tetramer at a certain ratio of complex and Sav might be slightly different as one would expect from the molar ratio which was obtained by applying a given relative concentration in the experiment. In addition, the obtained kinetic parameters ( $k_{\text{cat}}$ ,  $K_M$ ) are apparent constants as transfer hydrogenation involves the consumption of actually two substrates (imine and formate) to yield two products (amine and  $\text{CO}_2$ ). Therefore, this reaction might not be applicable *per se* to the Michaelis-Menten mechanism on which the respective kinetic law relies.

Another question that arises in this context what is the absolute configuration of the metal center in the transition state of the reaction. The catalytic cycle of transfer hydrogenation involves a planar 16 electron complex to which the hydride can be delivered from both bottom and top face. Ikariya showed that prior to hydride formation formate binds to the metal in the 16 electron amido complex  $[(p\text{-cymene})\text{Ru}(R,R\text{-TsNCHPhCHPhNH})]$  yielding the corresponding 18 electron formato complex as a single diastereomer.<sup>30</sup> This intermediate subsequently decarboxylates to afford enantiopure  $[(\eta^6\text{-}p\text{-cymene})\text{Ru}(R,R\text{-TsDPEN})\text{H}]$

and CO<sub>2</sub>. In the homogenous system the chiral ligand thus dictates the absolute configuration of the metal hydride which in turn determines the enantioselectivity in the reduction of the substrate (see section 2.1.1.1). In contrast, the Ir-center of  $[(\eta^5\text{-Cp}^*)\text{Ir}(\text{biot-}p\text{-L})\text{H}]$  is not configurationally stable in absence of Sav as it affords racemic-at metal intermediate in the transfer hydrogenation. In principle, two possible enantioselectivity determining mechanisms may operate in the case of the ATHase which both may contribute to the enantiodiscrimination: i) the second coordination sphere of the host protein favors the formation of a single  $[(\eta^5\text{-Cp}^*)\text{Ir}(\text{biot-}p\text{-L})\text{H}]$ -diastereomer which then induces the enantioselectivity similar to the homogenous system or ii) there is no influence of the second coordination sphere on the selectivity of the hydride formation but one of the two resulting ATHase-isomers (obtained from the combination of the racemic metal cofactor and the enantiopure protein) is more reactive towards the substrate. The situation becomes even more complex in case where the molar ratio of [Ir]/Sav-tetramer is greater than 1:4 as more than two isomers exist. The finding that only one configuration of the metal center is observed in the crystal structure of  $[(\eta^5\text{-Cp}^*)\text{Ir}(\text{biot-}p\text{-L})\text{Cl}]\subset\text{S112A}$  (see section 2.2.2) suggests that the host protein discriminates between two diastereomers of  $[(\eta^5\text{-Cp}^*)\text{Ir}(\text{biot-}p\text{-L})\text{H}]$  and therefore it seems unlikely that different diastereoisomers of the hybrid catalyst are formed. This leads to the hypothesis that the protein environment in ATHases dictates the absolute configuration of the metal in  $[(\eta^5\text{-Cp}^*)\text{Ir}(\text{biot-}p\text{-L})\text{H}]$ . The observation that the enantioselectivity of the reaction decreases above [Ir]/Sav ratios of 2:1 in the case of the S112A-ATHase may thus indicate that metal complexes located in adjacent active sites of the Sav-tetramer may influence each other when the absolute configuration at Ir is determined. This is not the case in the S112K counterpart as the individual active sites operate independently. The resulting "induced key-and-lock" mechanism is not only supported by the Michaelis-Menten behavior (see above) but also by additional data obtained from the crystal structure of the S112K-ATHase as well as docking studies and is discussed in detail in section 2.2.3.

Further investigations concerning the question if an ionic or concerted mechanism is operative in the ATHase-mediated transfer hydrogenation are presented in section 2.2.4.

### 2.2.2 Artificial Transfer Hydrogenases for the Enantioselective Reduction of Cyclic Imines

Author contribution: synthesis of biotinylated metal complexes, screening of Sav mutants (in collaboration with Annette Mutschler), optimization of the reaction conditions for  $[(\eta^5\text{-Cp}^*)\text{Ir}(\text{biot-}p\text{-L})\text{Cl}]\subset\text{S112A}$ , HABA-assays

## Communications

## Artificial Metalloenzyme

DOI: 10.1002/anie.201007820

## Artificial Transfer Hydrogenases for the Enantioselective Reduction of Cyclic Imines\*\*

Marc Dürrenberger, Tillmann Heinisch, Yvonne M. Wilson, Thibaud Rossel, Elisa Nogueira, Livia Knörr, Annette Mutschler, Karoline Kersten, Malcolm Jeremy Zimbron, Julien Pierron, Tilman Schirmer, and Thomas R. Ward\*

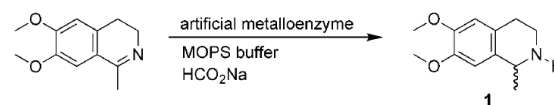
Enantiopure amines are privileged compounds which find wide use in the pharmaceutical, agrochemical, and flavor and fragrance industries. In this context, enzymatic,<sup>[1]</sup> homogeneous,<sup>[2]</sup> and chemoenzymatic<sup>[3]</sup> approaches offer complementary means for the preparation of these targets.

The asymmetric transfer hydrogenation (ATH) of ketones using d<sup>6</sup> piano stool complexes as catalyst has been the subject of numerous studies,<sup>[4]</sup> leading to a unified picture of the reaction mechanism.<sup>[5]</sup> The ATH of imines, however, has received less attention.<sup>[6]</sup> Interestingly, the reaction proceeds through a different enantioselection mechanism: for a given aminosulfonamide ligand configuration, the opposite enantiomers (alcohol vs amine) are produced.<sup>[7]</sup> In addition, it has been argued that the imine must be protonated for the reaction to proceed.<sup>[8]</sup>

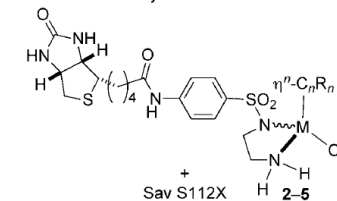
In recent years, artificial metalloenzymes, resulting from the introduction of a catalyst within a protein environment, have attracted attention as potential alternatives to traditional catalysts.<sup>[9]</sup> Based on our experience in artificial ATHs for the reduction of ketones,<sup>[10]</sup> we set out to test these systems toward the enantioselective reduction of imines and to compare their salient features with related homogeneous systems.

As a starting point, we screened d<sup>5</sup> and d<sup>6</sup> piano stool complexes bearing the biotinylated aminosulfonamide ligand (abbreviated Biot-*p*-L) combined with wild-type streptavidin (Sav) for the production of salsolidine **1** (Scheme 1).<sup>[11]</sup>

This screening led to the identification of [Cp\*Ir(Biot-*p*-L)Cl] (**5**; Sav) as the most promising catalyst. This contrasts with ATH of ketones for which [(η<sup>6</sup>-arene)Ru(Biot-*p*-L)Cl] **2** and **3** proved superior (Table 1).<sup>[12]</sup> In all but one case, both amine **1** and 1-phenylethanol **6** were produced with the same configuration for a given artificial metalloenzyme.



artificial metalloenzyme:



M	η <sup>n</sup> -C <sub>n</sub> R <sub>n</sub>	Abbreviation
Ru	η <sup>6</sup> - <i>p</i> -cymene	[( <i>p</i> -cymene)Ru(Biot- <i>p</i> -L)Cl] <b>2</b>
Ru	η <sup>6</sup> -benzene	[(benzene)Ru(Biot- <i>p</i> -L)Cl] <b>3</b>
Rh	η <sup>5</sup> -C <sub>5</sub> Me <sub>5</sub>	[Cp*Rh(Biot- <i>p</i> -L)Cl] <b>4</b>
Ir	η <sup>5</sup> -C <sub>5</sub> Me <sub>5</sub>	[Cp*Ir(Biot- <i>p</i> -L)Cl] <b>5</b>

**Scheme 1.** Artificial metalloenzymes based on the biotin-streptavidin technology for the ATH of imines. MOPS = 3-morpholinopropanesulfonic acid.

Next, we screened complex **5** with the saturation mutagenesis library S112X (Table 2 and Supporting Information, Table S1). Noteworthy features include:

- 1) Incorporation of [Cp\*Ir(Biot-*p*-L)Cl] (**5**) into Sav S112X produces predominantly (*R*)-**1**.
- 2) The best (*R*)-selectivities are obtained for the smallest amino acids at position 112 (S112G, S112A). The optimal pH is 6.50, affording the product in 85% *ee* at 55°C (Table 2, entries 3 and 14).
- 3) The active biotinylated catalyst resides in the biotin-binding vestibule: addition of four equivalents of biotin to

[\*] M. Dürrenberger,<sup>[1]</sup> T. Heinisch,<sup>[4]</sup> Y. M. Wilson,<sup>[4]</sup> T. Rossel, E. Nogueira, L. Knörr, A. Mutschler, K. Kersten, M. J. Zimbron, J. Pierron, T. Schirmer, Prof. Dr. T. R. Ward  
Institut für Anorganische Chemie, Universität Basel  
Spitalstrasse 51, 4056 Basel (Switzerland)  
Fax: (+41) 61-267-1005  
E-mail: thomas.ward@unibas.ch

[†] These authors contributed equally to this work.

[\*\*] This research was supported by the Swiss National Science Foundation (Grant 200020-126366), the Cantons of Basel, and Marie Curie Training Networks (FP7-ITN-238531, FP7-ITN-238434). We thank Prof. C. R. Cantor for the Sav gene.

Supporting information for this article is available on the WWW under <http://dx.doi.org/10.1002/anie.201007820>.

**Table 1:** Results for the chemical optimization of artificial transfer hydrogenases.

Entry	Complex	<i>ee</i> [%] [conv.] <b>1</b> <sup>[a]</sup>	<i>ee</i> [%] [conv.] <b>6</b> <sup>[b]</sup>
1	<b>2</b>	22 ( <i>R</i> ) [97]	70 ( <i>R</i> ) [84]
2	<b>3</b>	12 ( <i>R</i> ) [76]	45 ( <i>S</i> ) [56]
3	<b>4</b>	52 ( <i>R</i> ) [94]	15 ( <i>R</i> ) [26]
4	<b>5</b>	57 ( <i>R</i> ) [quant.]	13 ( <i>R</i> ) [47]

[a] The reaction was carried out at 55°C for 15 h using 1 mol% complex **2–5** (690 μM final concentration) and 0.33 mol% tetrameric WT Sav at pH 8.0 (MOPS buffer 2.9 M) containing 3.65 M HCO<sub>2</sub>Na (see Supporting Information for experimental details). [b] Data from Ref. [12].

**Table 2:** Selected results for the genetic optimization of artificial transfer hydrogenases for the production of Salsolidine **1**.<sup>[a]</sup>

Entry	Sav mutant	T [°C]	t [h]	pH	Conv. [%]	ee [%]
1	no prot.	25	5	7.25	quant.	rac.
2	WT Sav	55	2	7.25	quant.	57 (R)
3	S112G	55	2	7.25	quant.	60 (R)
4	S112R	55	2	7.25	quant.	19 (S)
5	S112K	55	2	7.50	94	35 (S)
6	S112K	55	64	7.25	30 <sup>[b]</sup>	6 (S)
7	S112K	5	48	7.50	quant.	78 (S)
8	S112K	25	24	7.25	39 <sup>[c]</sup>	44 (S)
9	S112K <sup>[d]</sup>	25	24	7.25	30 <sup>[c]</sup>	42 (S)
10	empty plasmid	25	24	7.25	43 <sup>[c]</sup>	1 (S)
11	S112A	55	2	7.25	quant.	79 (R)
12	S112A	55	64	7.25	69 <sup>[b]</sup>	27 (R)
13	S112A	55	2	7.25	59 <sup>[c]</sup>	14 (R)
14	S112A	55	2	6.50	quant.	85 (R)
15	S112A	5	24	6.50	quant.	91 (R)
16	S112A	5	24	6.50	quant. <sup>[f]</sup>	93 (R)
17	S112A	5	24	6.50	quant. <sup>[d]</sup>	88 (R)
18	S112A	5	96	6.50	quant. <sup>[h]</sup>	96 (R)
19	S112A	5	115	6.50	86 <sup>[h,i]</sup>	96 (R)
20	S112A	25	24	7.25	77 <sup>[j]</sup>	64 (R)
21	S112A <sup>[d]</sup>	25	24	7.25	65 <sup>[d]</sup>	61 (R)
22	H87A	55	2	7.25	quant.	48 (R)
23	H127A	55	2	7.25	quant.	54 (R)
24	S112AK121T	5	24	6.50	90	54 (R)

[a] See Table 1 and Supporting Information for full experimental details; S112P was expressed as inclusion bodies and thus was not tested. [b] Acetophenone reduction yielding 1-phenylethanol **6**. [c] 50  $\mu\text{M}$  [Cp\*Ir(Biot-*p*-L)Cl] (**5**; i.e. 1 mol% vs **1**) and 25  $\mu\text{M}$  S112K (tetramer). [d] Precipitated protein from cell free extracts (Supporting Information). [e] Four equivalents (vs tetrameric Sav) biotin added. [f] 0.25 mol% complex **5** and 0.25 mol% S112A tetramer. [g] 1 mol% complex **5** and 0.25 mol% S112A tetramer. [h] 0.025 mol% complex **5** and 0.025 mol% S112A tetramer. [i] 86% yield of isolated product on 100 mg scale. [j] 39  $\mu\text{M}$  [Cp\*Ir(Biot-*p*-L)Cl] (**5**; i.e. 1 mol% vs **1**) and 20  $\mu\text{M}$  S112A (tetramer).

[Cp\*Ir(Biot-*p*-L)Cl]C<S112A affords (*R*)-**1** in low *ee* (Table 2, entry 13).

- (*S*)-selectivities result from the presence of a cationic residue at position S112 (e.g. S112K and S112R, Table 2, entries 4 and 5).
- Decreasing the temperature to 5 °C allows improvement of the enantioselectivity to 91% (*R*) for **5**C<S112A and 78% (*S*) for **5**C<S112K (Table 2, entries 7 and 15). Importantly, these reactions are not sensitive to traces of oxygen: no degassing is required prior to catalysis.
- Up to 4000 turnovers can be achieved with no erosion of selectivity (Table 2, entry 18). On a preparative scale (100 mg substrate, 0.025 mol% catalyst), the *ee* could be further increased to 96%, with an isolated yield of 86% (Table 2, entry 19).
- [Cp\*Ir(Biot-*p*-L)Cl]C<S112A produces the same preferred enantiomer for alcohol (*R*)-**6** and amine (*R*)-**1**. Similarly, [Cp\*Ir(Biot-*p*-L)Cl]C<S112K affords (*S*)-**6** and amine (*S*)-**1**, respectively (Table 2, entries 6 and 12). This suggests that both imine and ketone reduction proceed through the same enantioselection mechanism. We thus conclude that the second coordination sphere interactions provided by

the host protein outweigh the preference of the related homogeneous catalyst.

- Increasing the ratio of [Cp\*Ir(Biot-*p*-L)Cl] vs Sav tetramer from one to four leads to a gradual erosion of enantioselectivity (93 to 88% *ee*, Table 2, entries 16 and 17). This suggests that an empty biotin binding site adjacent to a [Cp\*Ir(Biot-*p*-L)Cl] moiety within Sav may be favorable for selectivity.
- Performing catalysis with Sav mutants obtained from an ethanol precipitation step on a dialyzed protein extract yields results very similar to those obtained with dilute samples of pure protein for both S112K and S112A (Table 2, compare entries 8–10 and 20–21). This finding demonstrates that [Cp\*Ir(Biot-*p*-L)Cl] (**5**) tolerates cellular components.<sup>[13]</sup> This opens fascinating perspectives for parallel screening as it significantly shortens the protein purification effort (from 12 to 3 days).

To gain structural insight into the best (*R*)-selective artificial metalloenzyme, crystals of S112A Sav were soaked with a solution containing an excess of cofactor **5**. The X-ray crystal structure was solved to 1.9 Å resolution. Strong residual density in the  $F_o - F_c$  map indicated that all biotin-binding sites are fully occupied by ligand Biot-*p*-L (Figure 1 a,

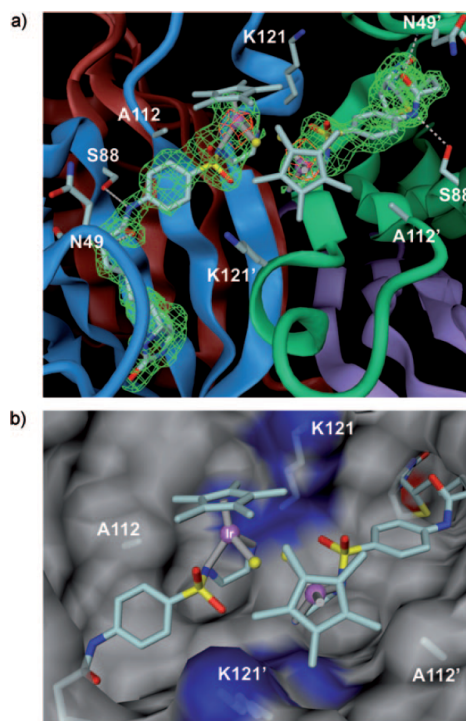


**Figure 1.** Close-up view of the X-ray crystal structure (PDB: 3pk2) of complex **5**C<S112A Sav showing two symmetry-related cofactors in the biotin-binding pocket of the protein tetramer.  $F_o - F_c$  omit map colored in green (contoured at 3  $\sigma$ ) and anomalous difference density map (5  $\sigma$ ) in red (a). Surface representation with basic residues in blue, acidic in red, polar and apolar in gray (b); (chloride: yellow sphere).

## Communications

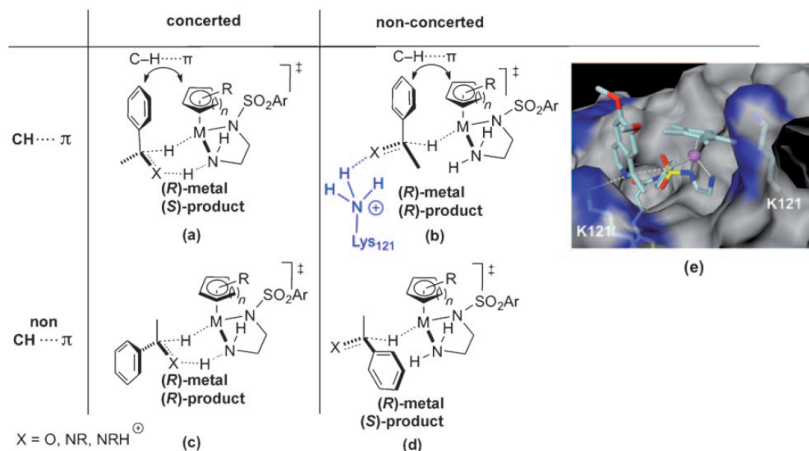


**Figure 2.** Possible transition states for the  $d^6$  piano stool catalyzed asymmetric transfer hydrogenation of ketones and imines a–d. a)  $\text{CH}\cdots\pi$  interaction combined with a contact between the imine N and K121 affords (*R*)-products (b and e; latter viewed from the empty biotin-binding pocket).

note that due to crystallographic symmetry all Sav monomers are identical). Adjacent to the ethylenediamine moiety of Biot-*p*-L a strong peak ( $15\sigma$ ) in the anomalous difference map suggested the position of iridium. To avoid negative  $F_o - F_c$  density the iridium atom occupancy was set to 50%. This most likely indicates partial dissociation of the  $[\text{IrCp}^*\text{Cl}]$  fragment upon soaking, since alternative conformations appear sterically not possible. The iridium atoms of two symmetry-related cofactors (face-to-face) are separated by 5.2 Å. Despite the purity of the complex used for soaking, no  $F_o - F_c$  density was found for  $\text{Cp}^*$  and chloride ligands. To prevent steric clashes between symmetry-related  $\text{Cp}^*$  groups, this bulky moiety was modeled with a dihedral angle  $\text{S-N-Ir-Cp}^*_{\text{centroid}} = 98.3^\circ$  (and  $\text{S-N-Ir-Cl} = -34.2^\circ$ ). This sets the configuration at Ir in the structure to (*S*)- $[\text{Cp}^*\text{Ir}(\text{Biot-}p\text{-L})\text{Cl}]$  (and correspondingly (*R*)- $[\text{Cp}^*\text{Ir}(\text{Biot-}p\text{-L})\text{H}]$ ).

Compared to the recently characterized  $[(\eta^6\text{-benzene})\text{Ru}(\text{Biot-}p\text{-L})\text{Cl}]$  (**3**; S112K; PDB: 2qcb, an (*S*)-selective ATH),<sup>[10]</sup> the absolute configuration at the metal is (*S*) in both cases, but the metal fragment is rotated along the aryl–S bond by about  $150^\circ$ . This prevents steric clashes between the benzene moiety and K121 of the adjacent monomer B (Figure S2b).

Additional anomalous difference density indicating iridium was found in the vicinity of the  $N_\epsilon$  atoms of H87 and H127 (Figure S2c,d). These species, however, are not involved in catalysis, as demonstrated by the results obtained with the H87A and H127A mutants which are nearly identical to those obtained with WT Sav (Table 2, entries 22 and 23).

Assuming that the absolute configuration revealed in the X-ray structure is catalytically active, two transition states leading to the observed (*R*)-products (alcohol or amine) can be envisaged: non-concerted +  $\text{CH}\cdots\pi$  or concerted + non- $\text{CH}\cdots\pi$ , respectively (Figure 2b,c). Qualitative modeling of the imine substrate into a vacated neighboring biotin site was carried out for both possible transition states leading to (*R*)-**1**. For the concerted + non- $\text{CH}\cdots\pi$  mechanism, steric clashes

between the substrate's aromatic group and the protein project the imine moiety into the  $\text{Cp}^*$  fragment (Figure S2e). In contrast, for the non-concerted +  $\text{CH}\cdots\pi$  interaction, no steric clashes with the protein are apparent (Figure 2e). Interestingly, the imine functionality lies close to the ammonium group of K121 (of the adjacent monomer). This contact may replace the amine group of the ligand for the delivery of a proton to the substrate (Figure 2b,e). To test this possibility, the double mutant S112AK121T was tested in catalysis (Table 2, entry 24). The erosion in enantioselectivity suggests that the non-concerted +  $\text{CH}\cdots\pi$  mechanism is operative both for the ATH of ketones and imines.

In summary, introduction of a biotinylated iridium piano stool complex  $[(\eta^5\text{-Cp}^*)\text{Ir}(\text{Biot-}p\text{-L})\text{Cl}]$  (**5**) within streptavidin affords an artificial imine reductase. Both (*R*)-**1** (96% *ee*) and (*S*)-**1** (78% *ee*) are accessible with the same organometallic moiety. This corresponds to a  $\delta\Delta G^\ddagger$  of  $3.3 \text{ kcal mol}^{-1}$  for a single-point mutation. With the implementation of laboratory evolution protocols for the optimization of artificial metalloenzymes for the reduction of more challenging imines in mind,<sup>[1,14]</sup> we have shown that the screening can be performed in air with up to 4000 TON and, most importantly, on precipitated protein rather than on rigorously purified Sav samples used thus far. Based on X-ray structural data, we suggest that the reaction proceeds, both for the imine and the ketone reduction, through a non-concerted +  $\text{CH}\cdots\pi$  interaction,<sup>[7b,15]</sup> whereby the residue K121 may be involved in the protonation step.

Received: December 12, 2010

Published online: February 24, 2011

**Keywords:** artificial metalloenzymes · asymmetric catalysis · imine reduction · piano stool complexes · transfer hydrogenation

- [1] N. J. Turner, *Nat. Chem. Biol.* **2009**, *5*, 567–573.
- [2] a) T. C. Nugent, M. El-Shazly, *Adv. Synth. Catal.* **2010**, *352*, 753–819; b) N. Fleury-Brégeot, V. de La Fuente, S. Castillon, C. Claver, *ChemCatChem* **2010**, *2*, 1346–1371.
- [3] L. K. Thalén, D. Zhao, J.-B. Sortais, J. Paetzold, C. Hoben, J.-E. Bäckvall, *Chem. Eur. J.* **2009**, *15*, 3403–3410.
- [4] R. Noyori, S. Hashiguchi, *Acc. Chem. Res.* **1997**, *30*, 97–102.
- [5] a) M. Yamakawa, I. Yamada, R. Noyori, *Angew. Chem.* **2001**, *113*, 2900–2903; *Angew. Chem. Int. Ed.* **2001**, *40*, 2818–2821; b) M. Yamakawa, I. Yamada, R. Noyori, *Angew. Chem.* **2001**, *113*, 2900–2903; c) S. E. Clapham, A. Hadzovic, R. H. Morris, *Coord. Chem. Rev.* **2004**, *248*, 2201–2237; d) T. Ikariya, A. J. Blacker, *Acc. Chem. Res.* **2007**, *40*, 1300–1308.

- ] a) N. Uematsu, A. Fujii, S. Hashiguchi, T. Ikariya, R. Noyori, *J. Am. Chem. Soc.* **1996**, *118*, 4916–4917; b) C. Li, J. Xiao, *J. Am. Chem. Soc.* **2008**, *130*, 13208–13209; c) L. Evanno, J. Ormala, P. M. Pihko, *Chem. Eur. J.* **2009**, *15*, 12963–12967; d) C. Wang, C. Li, X. Wu, A. Pettman, J. Xiao, *Angew. Chem.* **2009**, *121*, 6646–6650; *Angew. Chem. Int. Ed.* **2009**, *48*, 6524–6528; e) C. Wang, C. Li, X. Wu, A. Pettman, J. Xiao, *Angew. Chem.* **2009**, *121*, 6646–6650; *Angew. Chem. Int. Ed.* **2009**, *48*, 6524–6528; f) J. Wu, F. Wang, Y. Ma, X. Cui, L. Cun, J. Zhu, J. Deng, B. Yu, *Chem. Commun.* **2006**, 1766–1768.
- ] a) J. Mao, D. C. Baker, *Org. Lett.* **1999**, *1*, 841–843; b) J. E. D. Martins, G. J. Clarkson, M. Wills, *Org. Lett.* **2009**, *11*, 847–850.
- ] a) J. B. Aberg, J. S. M. Samec, J. Bäckvall, *Chem. Commun.* **2006**, 2771–2773; b) D. G. Blackmond, M. Ropic, M. Stefinovic, *Org. Process Res. Dev.* **2006**, *10*, 457–463.
- ] a) Y. Lu, N. Yeung, N. Sieracki, N. M. Marshall, *Nature* **2009**, *460*, 855–862; b) F. Rosati, G. Roelfes, *ChemCatChem* **2010**, *2*, 916–927; c) M. T. Reetz, *Top. Organomet. Chem.* **2009**, *25*, 63–92; d) S. Abe, T. Ueno, Y. Watanabe, *Top. Organomet. Chem.* **2009**, *25*, 25–43; e) Q. Jing, R. J. Kazlauskas, *ChemCatChem* **2010**, *2*, 953–957; f) P. J. Deuss, G. Popa, C. H. Botting, W. Laan, P. C. Kamer, *Angew. Chem.* **2010**, *122*, 5443–5445; *Angew. Chem. Int. Ed.* **2010**, *49*, 5315–5317; g) P. J. Deuss, G. Popa, C. H. Botting, W. Laan, P. C. Kamer, *Angew. Chem.* **2010**, *122*, 5443–5445; *Angew. Chem. Int. Ed.* **2010**, *49*, 5315–5317; h) J. Podtetenieff, A. Taglieber, E. Bill, E. J. Reijerse, M. T. Reetz, *Angew. Chem.* **2010**, *122*, 5277–5281; *Angew. Chem. Int. Ed.* **2010**, *49*, 5151–5155; i) J. Podtetenieff, A. Taglieber, E. Bill, E. J. Reijerse, M. T. Reetz, *Angew. Chem.* **2010**, *122*, 5277–5281; *Angew. Chem. Int. Ed.* **2010**, *49*, 5151–5155; j) T. Heinisch, T. R. Ward, *Curr. Opin. Chem. Biol.* **2010**, *14*, 184–199; k) P. Fournier, R. Fiammengo, A. Jäschke, *Angew. Chem.* **2009**, *121*, 4490–4493; *Angew. Chem. Int. Ed.* **2009**, *48*, 4426–4429; l) P. Fournier, R. Fiammengo, A. Jäschke, *Angew. Chem.* **2009**, *121*, 4490–4493; *Angew. Chem. Int. Ed.* **2009**, *48*, 4426–4429.
- [10] a) M. Creus, A. Pordea, T. Rossel, A. Sardo, C. Letondor, A. Ivanova, I. LeTrong, R. E. Stenkamp, T. R. Ward, *Angew. Chem.* **2008**, *120*, 1422–1426; *Angew. Chem. Int. Ed.* **2008**, *47*, 1400–1404; b) M. Creus, A. Pordea, T. Rossel, A. Sardo, C. Letondor, A. Ivanova, I. LeTrong, R. E. Stenkamp, T. R. Ward, *Angew. Chem.* **2008**, *120*, 1422–1426; *Angew. Chem. Int. Ed.* **2008**, *47*, 1400–1404.
- [11] T. S. Kaufman, *Tetrahedron: Asymmetry* **2004**, *15*, 1203–1237.
- [12] C. Letondor, A. Pordea, N. Humbert, A. Ivanova, S. Mazurek, M. Novic, T. R. Ward, *J. Am. Chem. Soc.* **2006**, *128*, 8320–8328.
- [13] a) C. Streu, E. Meggers, *Angew. Chem.* **2006**, *118*, 5773–5776; *Angew. Chem. Int. Ed.* **2006**, *45*, 5645–5648; b) C. Streu, E. Meggers, *Angew. Chem.* **2006**, *118*, 5773–5776; *Angew. Chem. Int. Ed.* **2006**, *45*, 5645–5648; c) V. Köhler, Y. M. Wilson, C. Lo, A. Sardo, T. R. Ward, *Curr. Opin. Biotechnol.* **2010**, *21*, 744–752.
- [14] M. T. Reetz, J. J.-P. Peyerlans, A. Maichele, Y. Fu, M. Maywald, *Chem. Commun.* **2006**, 4318–4320.
- [15] J. E. D. Martins, M. A. C. Redondo, M. Wills, *Tetrahedron: Asymmetry* **2010**, *21*, 2258–2264.



Supporting Information

© Wiley-VCH 2011

69451 Weinheim, Germany

**Artificial Transfer Hydrogenases for the Enantioselective Reduction of Cyclic Imines\*\***

*Marc Dürrenberger, Tillmann Heinisch, Yvonne M. Wilson, Thibaud Rossel, Elisa Nogueira, Livia Knörr, Annette Mutschler, Karoline Kersten, Malcolm Jeremy Zimbron, Julien Pierron, Tilman Schirmer, and Thomas R. Ward\**

anie\_201007820\_sm\_miscellaneous\_information.pdf



## SUPPORTING INFORMATION

Synthesis of complexes 2-5 was carried out as described in Letondor et al.,<sup>1</sup> expression and purification of Sav mutants as described by Humbert et al.<sup>2</sup> and Klein et al.<sup>3</sup>

### CATALYSIS

#### Preparation of Stock Solutions

The reaction buffer was prepared by mixing 3-(N-morpholino)propane sulfonic acid (MOPS, final concentration 1.2 M) and sodium formate (final conc. 3 M) in milliQ water. The pH was adjusted with NaOH and the solution was thoroughly degassed (flushing with nitrogen).

A substrate stock solution was prepared by dissolving 6,7-dimethoxy-1-methyl-3,4-dihydroisoquinoline in milliQ water to a final concentration of 2 M.

Metal complexes were dissolved in degassed DMF to a final concentration of 39.5 mM.

#### General Procedure for the Asymmetric Transfer Hydrogenation

Lyophilized streptavidin S112X corresponding to 0.83 mM final concentration of free binding sites (3 - 5.6 mg) was weighed into reaction tubes. The reaction buffer (200  $\mu$ L) was added and the mixture was stirred until all protein was dissolved. The metal complex stock solution was added (3.7  $\mu$ L, final conc. 0.69 mM; 0.83 equivalents [Ru]/[Rh]/[Ir] vs. Sav free binding sites) and the mixture was stirred for 5 minutes. Finally, the substrate stock solution was added (7.5  $\mu$ L, final conc. 69 mM). The tubes were placed in a magnetically stirred

multireactor (RR 98072, Radleys Discovery Technologies), which was purged three times with nitrogen (and was heated up to 55 °C if required). After completion, 0.5 mL of milliQ water and 50  $\mu$ L of 20 % NaOH were added to the reaction mixture, which was then extracted four times with 1.5 mL of CH<sub>2</sub>Cl<sub>2</sub>. The organic phase was dried over Na<sub>2</sub>SO<sub>4</sub>, filtered with a syringe filter and subjected to HPLC analysis, using a Chiralpak IC column (20  $\mu$ m, 250 x 4.5 mm, Daicel Chemical Industries, Tokyo) with CH<sub>2</sub>Cl<sub>2</sub>/iPrOH/DEA 98:2:0.1 as an eluent at 1 mL/min ( $t_s$  = 6.86 min,  $t_{\text{substrate}}$  = 8.37 min,  $t_R$  = 10.19 min, UV-detection at 280 nm). The absolute configurations were assigned by comparison with commercial enantiopure samples of (*R*)/(*S*)-salsolidine. Reactions at 5 °C were performed in thoroughly nitrogen-flushed and sealed tubes which were cooled using a cryostat (Julabo F12). A summary of the catalysis results are given in Supporting Table 1.

Supporting Table 1: Summary of Catalysis Results for the Production of 1 and 6

Entry	Complex $\subset$ Sav mutant	Temp (°C)	Time (hrs)	pH	Conv. (%)	ee (%)
1	5 no protein	25	5	7.25	quant.	rac.
2	5 $\subset$ WT Sav	55	2	7.25	quant. <sup>a</sup>	57 ( <i>R</i> )
3	5 $\subset$ S112G	55	2	7.25	quant. <sup>a</sup>	60 ( <i>R</i> )
4	5 $\subset$ S112L	55	2	7.25	87 <sup>a</sup>	14 ( <i>R</i> )
5	5 $\subset$ S112I	55	2	7.25	75 <sup>a</sup>	5 ( <i>S</i> )
6	5 $\subset$ S112F	55	2	7.25	quant. <sup>a</sup>	37 ( <i>R</i> )
7	5 $\subset$ S112Y	55	2	7.25	quant. <sup>a</sup>	50 ( <i>R</i> )
8	5 $\subset$ S112W	55	2	7.25	quant. <sup>a</sup>	7 ( <i>R</i> )
9	5 $\subset$ S112T	55	2	7.25	15 <sup>a</sup>	46 ( <i>R</i> )
10	5 $\subset$ S112C	55	2	7.25	75 <sup>a</sup>	25 ( <i>R</i> )
11	5 $\subset$ S112M	55	2	7.25	26 <sup>a</sup>	19 ( <i>S</i> )
12	5 $\subset$ S112N	55	2	7.25	quant. <sup>a</sup>	20 ( <i>R</i> )
13	5 $\subset$ S112Q	55	2	7.25	47 <sup>a</sup>	16 ( <i>S</i> )
14	5 $\subset$ S112D	55	2	7.25	quant. <sup>a</sup>	29 ( <i>R</i> )
15	5 $\subset$ S112E	55	2	7.25	80 <sup>a</sup>	5 ( <i>R</i> )
16	5 $\subset$ S112H	55	2	7.25	13 <sup>a</sup>	9 ( <i>R</i> )
17	5 $\subset$ S112R	55	2	7.25	quant. <sup>a</sup>	19 ( <i>S</i> )
18	5 $\subset$ S112V	55	2	7.25	quant. <sup>a</sup>	19 ( <i>R</i> )
19	5 $\subset$ S112A	55	2	7.25	quant. <sup>a</sup>	79 ( <i>R</i> )
20	5 $\subset$ S112A	55	64	7.25	69 <sup>b</sup>	27 ( <i>R</i> )

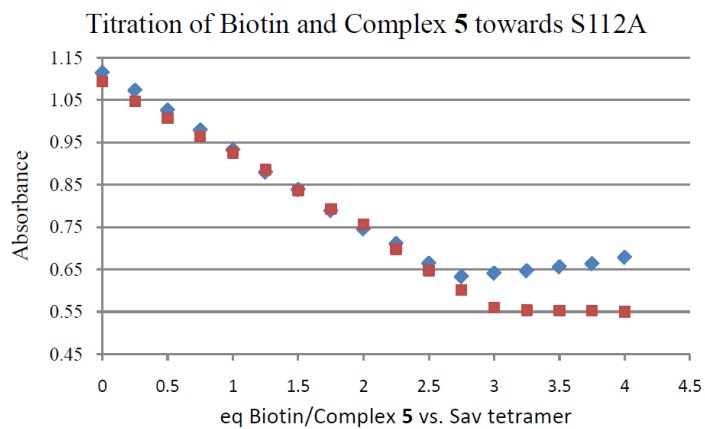
21	5 $\subset$ S112K	55	2	7.25	quant. <sup>a</sup>	25 (S)
22	5 $\subset$ S112K	55	64	7.25	30 <sup>b</sup>	6 (S)
23	5 $\subset$ S112A	55	2	7.25	quant. <sup>c</sup>	14(R)
24	5 $\subset$ S112K	55	2	7.25	quant. <sup>c</sup>	rac.
25	5 $\subset$ S112A	55	2	6.50	quant. <sup>a</sup>	85 (R)
26	5 $\subset$ S112A	25	5	6.50	quant.	89 (R)
27	5 $\subset$ S112A	5	24	6.50	quant.	91 (R)
28	5 $\subset$ S112A	5	24	6.50	quant. <sup>d</sup>	93 (R)
29	5 $\subset$ S112A	5	24	6.50	quant. <sup>e</sup>	92 (R)
30	5 $\subset$ S112A	5	24	6.50	quant. <sup>f</sup>	91 (R)
31	5 $\subset$ S112A	5	24	6.50	quant. <sup>g</sup>	88 (R)
32	5 $\subset$ S112A	5	96	6.50	quant. <sup>h</sup>	96 (S)
33	5 $\subset$ S112A	5	115	6.50	86 <sup>h,i</sup>	96 (R)
34	5 $\subset$ S112K	55	2	7.50	quant. <sup>a</sup>	35 (S)
35	5 $\subset$ S112K	25	24	7.50	quant.	62 (S)
36	5 $\subset$ S112K	5	48	7.50	quant.	78 (S)
37	5 $\subset$ S112K	25	24	7.25	39 <sup>j</sup>	44 (S)
38	5 $\subset$ S112K <sup>l</sup>	25	24	7.25	30 <sup>j</sup>	42 (S)
39	5 + empty plasmid <sup>l</sup>	25	24	7.25	43 <sup>j</sup>	1 (S)
40	5 $\subset$ S112A	25	24	7.25	77 <sup>k</sup>	64 (R)
41	5 $\subset$ S112A <sup>l</sup>	25	24	7.25	65 <sup>k</sup>	61 (R)
42	5 $\subset$ H87A	55	2	7.25	quant. <sup>a</sup>	48(R)
43	5 $\subset$ H127A	55	2	7.25	quant. <sup>a</sup>	54(R)

44	5 c S112A K121T	55	2	6.50	quant. <sup>a</sup>	54 ( <i>R</i> )
----	-----------------	----	---	------	---------------------	-----------------

<sup>a</sup>The reaction was carried out at 55°C for 2 h using 1 mol % complex 2-5 and 0.33 mol % tetrameric WT Sav containing 3.65 M HCO<sub>2</sub>Na in 1.46 M MOPS buffer; <sup>b</sup>acetophenone reduction yielding 1-phenylethanol 6; <sup>c</sup>four equivalents (vs. tetrameric Sav) biotin added; <sup>d</sup>0.25 mol % complex 5 and 0.25 mol % S112A, <sup>e</sup>0.50 mol % complex 5 and 0.25 mol % S112A; <sup>f</sup>0.75 mol % complex 5 and 0.25 mol % S112A; <sup>g</sup>1 mol % complex 5 and 0.25 mol % S112A; <sup>h</sup>0.025 mol % complex 5 and 0.025 mol % S112A, <sup>i</sup>86 % isolated yield on a 487 mM scale, <sup>j</sup>50 μM [Cp\*Ir(Biot-*p*-L)Cl] 5 (ie. 1 mol % vs 1) and 25 μM S112K (tetramer), <sup>k</sup>39 μM [Cp\*Ir(Biot-*p*-L)Cl] 5 (ie. 1 mol % vs 1) and 20 μM S112A (tetramer), <sup>l</sup>precipitated protein from cell free extracts (See SI).

#### HABA TITRATION EXPERIMENTS

Aliquots (5 μL, 0.25 equivalents vs. tetrameric Sav S112A) of a biotin solution (0.69 mM in a 0.5 M sodium phosphate-buffer, pH 7.4) or a solution of [Cp\*Ir(Biot-*p*-L)Cl] 5 (0.69 mM in DMF), respectively, were added stepwise to a mixture of 2.4 mL of a streptavidin S112A solution (8 μM in 0.5M sodium phosphate-buffer, pH 7.4) and 300 μL of a 4-hydroxyazobenzene-2-carboxylic acid-solution (HABA, 9.6 mM in water) in a cuvette. The decrease of absorption was monitored at 506 nm (**Supporting Figure 1**). Based on the equivalence point of 3.0 determined with biotin, the molecular weight of tetrameric Sav was back-calculated to obtain an equivalence point at 4.0 equivalents ( $MW_{\text{apparent Sav tetramer}}: (65700 \times 4.0)/3.0$ ). This apparent molecular weight was used for all experiments.



**Supporting Figure 1:** HABA displacement titration with biotin (red squares) and complex 5 (blue diamonds).<sup>4</sup>

## REFERENCES

- (1) C. Letondor, A. Pordea, N. Humbert, A. Ivanova, S. Mazurek, M. Novic, T. R. Ward, *J. Am. Chem. Soc.* **2006**, *128*, 8320-8328.
- (2) N. Humbert, A. Zocchi, T. R. Ward, *Electrophoresis* **2005**, *26*, 47-52.
- (3) G. Klein, N. Humbert, J. Gradinaru, A. Ivanova, F. Gilardoni, U. E. Rusbandi, T. R. Ward, *Angew. Chem. Int. Ed.* **2005**, *44*, 7764-7767; G. Klein, N. Humbert, J. Gradinaru, A. Ivanova, F. Gilardoni, U. E. Rusbandi, T. R. Ward, *Angew. Chem.* **2005**, *117*, 7942-7945.
- (4) M. Skander, N. Humbert, J. Collot, J. Gradinaru, G. Klein, A. Loosli, J. Sauser, A. Zocchi, F. Gilardoni, T. R. Ward, *J. Am. Chem. Soc.* **2004**, *126*, 14411-14418.
- (5) *Acta Crystallogr., Sect. D: Biol. Crystallogr.* **1994**, *50*, 760-763.
- (6) G. N. Murshudov, A. A. Vagin, E. J. Dodson, *Acta Crystallogr., Sect. D: Biol. Crystallogr.* **1997**, *53*, 240-255.
- (7) M. Creus, A. Pordea, T. Rossel, A. Sardo, C. Letondor, A. Ivanova, I. LeTrong, R. E. Stenkamp, T. R. Ward, *Angew. Chem. Int. Ed.* **2008**, *47*, 1400-1404; M. Creus, A. Pordea, T. Rossel, A. Sardo, C. Letondor, A. Ivanova, I. LeTrong, R. E. Stenkamp, T. R. Ward, *Angew. Chem.* **2008**, *120*, 1422-1426.
- (8) A. T. Brünger, *Acta Crystallogr., Sect. D: Biol. Crystallogr.* **1993**, *49*, 24-36.
- (9) T. A. Jones, J.-Y. Zou, S. W. Cowan, M. Kjeldgaard, *Acta Crystallogr., Sect. A: Found. Crystallogr.* **1991**, *47*, 110-119.
- (10) P. Emsley, K. Cowtan, *Acta Crystallogr., Sect. D: Biol. Crystallogr.* **2004**, *60*, 2126-2132.
- (11) A. C. Wallace, R. A. Laskowski, J. M. Thornton, *Protein Eng.* **1995**, *8*, 127-134.
- (12) S. Freitag, I. LeTrong, L. Klumb, P. S. Stayton, R. E. Stenkamp, *Protein Sci.* **1997**, *6*, 1157-1166.

- (13) P.C. Weber, D. H. Ohlendorf, J. J. Wendoloski, F.R. Salemme, *Science* **1989**, *243*, 85-88.
- (14) G. Kada, K. Kaiser, H. Falk, H. J. Gruber, *Biochim. Biophys Acta* **1999**, *1427*, 44-48.



### 2.2.3 Structural-, Kinetic- and Docking Studies of Artificial Imine Reductases Based on the Biotin-Streptavidin Technology: An Induced Lock-and-Key Hypothesis

Author contributions: Michaelis-Menten kinetics of  $[(\eta^5\text{-Cp}^*)\text{Ir}(\text{biot-}p\text{-L})\text{Cl}]\text{C}112\text{A}$  and  $[(\eta^5\text{-Cp}^*)\text{Ir}(\text{biot-}p\text{-L})\text{Cl}]\text{C}112\text{K}$  for the transfer hydrogenation of 6,7-dimethoxy-1-methyl-3,4-dihydroisoquinoline, catalysis

## Structural, Kinetic, and Docking Studies of Artificial Imine Reductases Based on Biotin–Streptavidin Technology: An Induced Lock-and-Key Hypothesis

Victor Muñoz Robles,<sup>†,||</sup> Marc Dürrenberger,<sup>‡,||</sup> Tillmann Heinisch,<sup>§</sup> Agustí Lledós,<sup>†</sup> Tilman Schirmer,<sup>§</sup> Thomas R. Ward,<sup>\*,‡</sup> and Jean-Didier Maréchal<sup>\*,†</sup>

<sup>†</sup>Departament de Química, Universitat Autònoma de Barcelona, Edifici C.n., 08193 Cerdanyola del Vallés, Barcelona, Spain

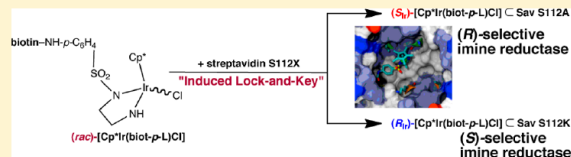
<sup>‡</sup>University of Basel, Spitalstrasse 51, CH-4056 Basel, Switzerland

<sup>§</sup>Biozentrum, University of Basel, Klingelbergstrasse 50/70, CH-4056 Basel, Switzerland

### Supporting Information

**ABSTRACT:** An artificial imine reductase results upon incorporation of a biotinylated Cp\*Ir moiety (Cp\* = C<sub>5</sub>Me<sub>5</sub><sup>−</sup>) within homotetrameric streptavidin (Sav) (referred to as Cp\*Ir(Biot-*p*-L)Cl) ⊂ Sav). Mutation of S112 reveals a marked effect of the Ir/streptavidin ratio on both the saturation kinetics as well as the enantioselectivity for the production of salsolidine. For [Cp\*Ir(Biot-*p*-L)Cl] ⊂ S112A

Sav, both the reaction rate and the selectivity (up to 96% ee (*R*)-salsolidine,  $k_{\text{cat}}$  14–4 min<sup>−1</sup> vs [Ir],  $K_{\text{M}}$  65–370 mM) decrease upon fully saturating all the biotin binding sites (the ee varying between 96% ee and 45% ee *R*). In contrast, for [Cp\*Ir(Biot-*p*-L)Cl] ⊂ S112K Sav, both the rate and the selectivity remain nearly constant upon varying the Ir/streptavidin ratio [up to 78% ee (*S*)-salsolidine,  $k_{\text{cat}}$  2.6 min<sup>−1</sup>,  $K_{\text{M}}$  95 mM]. X-ray analysis complemented with docking studies highlight a marked preference of the S112A and S112K Sav mutants for the S<sub>Ir</sub> and R<sub>Ir</sub> enantiomeric forms of the cofactor, respectively. Combining both docking and saturation kinetic studies led to the formulation of an enantioselection mechanism relying on an “induced lock-and-key” hypothesis: the host protein dictates the configuration of the biotinylated Ir-cofactor which, in turn, by and large determines the enantioselectivity of the imine reductase.

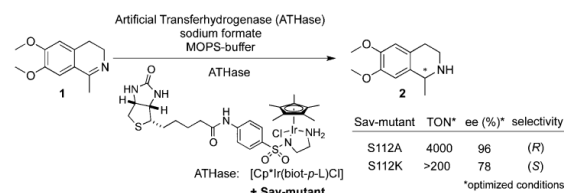


## INTRODUCTION

Artificial metalloenzymes result from the incorporation of a catalytically competent organometallic moiety within a macromolecule.<sup>1–13</sup> Thus far, three anchoring strategies have been pursued to ensure localization of the abiotic cofactor within a well-defined second coordination sphere environment:<sup>14</sup> covalent, dative, or supramolecular. One of the most attractive features of such systems results from combining both chemical and genetic optimization strategies. In this context, the biotin–streptavidin technology has provided a propitious playground for the creation and optimization of artificial metalloenzymes.<sup>1,15–18</sup> Tethering a biotin anchor to a catalyst precursor ensures that, in the presence of streptavidin (Sav hereafter), the metal moiety is quantitatively incorporated within the host protein. Importantly, the dimer of dimers nature of the Sav homotetramer provides two ideally sized biotin-binding vestibules, each capable of accommodating (up to) two biotinylated catalysts as well as the corresponding substrates. However, as the biotin-binding vestibule is fairly shallow, upon incorporation, the biotinylated catalyst tends to be poorly localized, as reflected by the low metal occupancy in the corresponding X-ray structures.<sup>19–22</sup> This ill-defined cofactor localization, combined with the vast genetic optimization potential, offers an opportunity but also a challenge for rational structure-based design.

We recently reported on an artificial imine reductase, asymmetric transfer hydrogenase (ATHase hereafter), resulting from incorporation of a biotinylated Cp\*Ir-moiety within streptavidin ([Cp\*Ir(Biot-*p*-L)Cl] ⊂ Sav hereafter) (Cp\* = C<sub>5</sub>Me<sub>5</sub><sup>−</sup>, Scheme 1). We showed that, upon substituting Sav Ser112 with either an alanine or a lysine (i.e., S112A or S112K), both enantiomers of salsolidine **2** could be produced in 96% ee (*R*)- and 78% ee (*S*)-configuration, respectively (Scheme 1).<sup>21,23</sup> This single-point mutation thus leads to a difference in transition state Gibbs energy  $\delta\Delta G^\ddagger = 3.5$  kcal·mol<sup>−1</sup> between both enantiomers at room temperature.<sup>24</sup> Herein, we present

### Scheme 1. Artificial Imine Reductase (ATHase) for the Production of Both Enantiomers of Salsolidine 2



Received: August 20, 2014

Published: October 15, 2014

our efforts to rationalize the effect of point mutations on the structure and catalytic performance of both ATHases.

## RESULTS AND DISCUSSION

**Michaelis–Menten Behavior of ATHase.** In order to gain insight on the kinetics of the two ATHases, we set out to determine the saturation kinetics and the corresponding enantioselectivity for both  $[\text{Cp}^*\text{Ir}(\text{Biot-}p\text{-L})\text{Cl}] \subset \text{S112A}$  and  $[\text{Cp}^*\text{Ir}(\text{Biot-}p\text{-L})\text{Cl}] \subset \text{S112K}$  at various Ir/Sav ratios. In previous screening studies, we typically set this ratio to 2. The fully loaded X-ray structure of  $[\text{Cp}^*\text{Ir}(\text{Biot-}p\text{-L})\text{Cl}] \subset \text{S112A}$  (PDB code 3PK2)<sup>21</sup> suggests that the four biotinylated cofactors are arranged as two pairs with the Cp\* moieties of each pair within van der Waals contact. We thus speculated that the Ir loading (i.e., Ir/Sav ratio) may have a significant influence on the catalytic performance of the ATHase.<sup>25</sup> The Michaelis–Menten behavior and enantioselectivity were determined in triplicate at four different Ir/Sav ratios (1, 2, 3, and 4 vs tetrameric streptavidin) for both S112A and S112K ATHase as well as for the bare catalyst  $[\text{Cp}^*\text{Ir}(\text{Biot-}p\text{-L})\text{Cl}]$ . The data is displayed in Figure 1 and collected in Table 1.

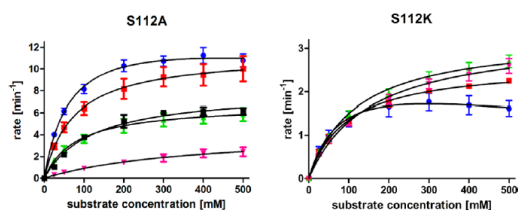


**Figure 1.** Saturation kinetics profiles of  $[\text{Cp}^*\text{Ir}(\text{Biot-}p\text{-L})\text{Cl}] \subset \text{S112A}$  (left) and  $[\text{Cp}^*\text{Ir}(\text{Biot-}p\text{-L})\text{Cl}] \subset \text{S112K}$  (right) for the production of salsolidine. The initial rates are displayed with respect to the concentration of iridium.  $[\text{Sav}] = 25 \mu\text{M}$  (corresponding to [biotin binding sites] =  $100 \mu\text{M}$ ) was held constant, varying the Ir/Sav ratio from 1.0 (blue data points) to 2.0 (red data points), 3.0 (green data points), and 4.0 (magenta data points). For comparison, the initial rates for the free  $[\text{Cp}^*\text{Ir}(\text{Biot-}p\text{-L})\text{Cl}]$  catalyst are displayed ( $50 \mu\text{M}$ , black data points). The black solid lines correspond to the fit obtained either using the Michaelis–Menten or the Haldane equation (see Table 1).

As can be appreciated from these data, the kinetic and selectivity behavior of both ATHases differ markedly. The following trends emerge:

(i) For  $[\text{Cp}^*\text{Ir}(\text{Biot-}p\text{-L})\text{Cl}] \subset \text{S112A}$ , upon increasing the Ir/Sav ratio beyond 2, the rate decreases ( $k_{\text{cat}}$  determined vs  $[\text{Ir}]$ ) and the Michaelis constant  $K_M$  increases. These observations suggest that neighboring  $[\text{Cp}^*\text{Ir}(\text{Biot-}p\text{-L})\text{Cl}]$  moieties experience significant steric interaction, leading to a decrease in enzyme–substrate affinity and rate. The modest substrate inhibition (derived from fitting the saturation kinetics behavior with the Haldane equation)<sup>26</sup> at Ir/Sav = 1.0 suggests that the biotin-binding vestibule may accommodate the prochiral imine substrate within the empty biotin-binding site. Strikingly, the ee drops sharply to 45% (*R*)-salsolidine **2** at Ir/Sav = 4.0. This suggests that, upon saturating all biotin-binding sites with  $[\text{Cp}^*\text{Ir}(\text{Biot-}p\text{-L})\text{Cl}]$ , the second coordination sphere environment around the metal, which is responsible for the enantioselection, differs significantly from that at lower Ir/Sav ratios.

(ii) For  $[\text{Cp}^*\text{Ir}(\text{Biot-}p\text{-L})\text{Cl}] \subset \text{S112K}$ , upon increasing the Ir/Sav ratio,  $k_{\text{cat}}$ ,  $K_M$ , and ee remain essentially constant. These observations suggest that all four  $[\text{Cp}^*\text{Ir}(\text{Biot-}p\text{-L})\text{Cl}]$  moieties operate largely independently, irrespective of the presence or absence of a catalytic moiety in the adjacent biotin-binding site. The substrate inhibition, observed at Ir/Sav = 1.0, is lifted upon increasing the metal loading.

A possible explanation for the striking difference in behavior of the S112A- and S112K-derived ATHases may lie in different binding affinities of the biotinylated cofactor  $[\text{Cp}^*\text{Ir}(\text{Biot-}p\text{-L})\text{Cl}]$  for the respective host proteins. Indeed, if only two cofactors bind to S112A with high affinity, one would anticipate an erosion of enantioselectivity upon increasing the Ir:S112A ratio beyond 2. To test this hypothesis, we estimated the binding affinity of  $[\text{Cp}^*\text{Ir}(\text{Biot-}p\text{-L})\text{Cl}]$  for both S112A and S112K using the 2-(4-hydroxyphenylazo)benzoic acid (HABA) displacement assay.<sup>27</sup> HABA displays millimolar affinity for streptavidin. The resulting host–guest complex HABA  $\subset$  Sav exhibits an absorbance at 506 nm. Addition of a biotinylated probe (with higher affinity than HABA) leads to a gradual decrease of the absorbance at  $\lambda_{\text{max}} = 506 \text{ nm}$ .

This displacement titration procedure was performed with  $[\text{Cp}^*\text{Ir}(\text{Biot-}p\text{-L})\text{Cl}]$  using both S112A and S112K. In both cases, the displacement titration curves were nearly identical to those obtained for biotin (see Figure S11, Supporting Information). Most importantly, they reached a minimum at ca. 4.0 equiv, unambiguously demonstrating that up to four  $[\text{Cp}^*\text{Ir}(\text{Biot-}p\text{-L})\text{Cl}]$  cofactors have similar affinities for both S112A and S112K. Unfortunately, the linear profiles of the displacement assay precluded a precise determination of the

**Table 1.** Michaelis–Menten Parameters and Enantioselectivity for the Production of Salsolidine **2** Using Artificial ATHase

entry	Sav mutant	eq $[\text{Ir}]^a$	ee <sup>c</sup>	$k_{\text{cat}}/[\text{Ir}]$ (min <sup>-1</sup> ) <sup>d,e</sup>	$K_M$ (mM) <sup>d</sup>	$K_I$ (mM) <sup>d</sup>
1	no Sav	– <sup>b</sup>	0	$8 \pm 0.41$	$120 \pm 18$	0
2	S112A	1.0	93	$14.1 \pm 1.7$	$65 \pm 16$	$3201 \pm 3015$
3		2.0	92	$11.4 \pm 0.7$	$74 \pm 17$	0
4		3.0	89	$6.8 \pm 0.5$	$80 \pm 19$	0
5		4.0	45	$4.3 \pm 1.1$	$370 \pm 175$	0
6	S112 K	1.0	–70	$2.7 \pm 0.83$	$82 \pm 47$	$1073 \pm 1138$
7		2.0	–74	$2.6 \pm 0.08$	$95 \pm 9$	0
8		3.0	–76	$3.3 \pm 0.13$	$119 \pm 14$	0
9		4.0	–78	$3.3 \pm 0.17$	$151 \pm 21$	0

<sup>a</sup>Eq  $[\text{Cp}^*\text{Ir}(\text{biot-}p\text{-L})\text{Cl}]$  versus free biotin binding sites. <sup>b</sup>Corresponds to an  $[[\text{Cp}^*\text{Ir}(\text{biot-}p\text{-L})\text{Cl}]] = 50 \mu\text{M}$ , no Sav present. <sup>c</sup>Positive values correspond to (*R*)-salsolidine **2**, negative values correspond to (*S*)-salsolidine **2**. <sup>d</sup>Errors represent standard errors derived from triplicate measurements. <sup>e</sup> $k_{\text{cat}}$  determined vs  $[\text{Ir}]$ .

affinity. Such a linear profile, however, sets a lower limit for the affinity constant (i.e.,  $K_a > 10^9 \text{ M}^{-1}$ ) and thus ensures that >99% of the cofactor is bound to either S112A or S112K at full saturation.

Taken together, these results suggest that the second coordination sphere around S112K ATHase differs significantly from that of the S112A mutant. With the X-ray structure of this latter mutant at hand, we set out to structurally characterize  $[\text{Cp}^*\text{Ir}(\text{Biot-}p\text{-L})\text{Cl}] \subset \text{S112K}$  by X-ray crystallography.

**X-ray Structure of  $[\text{Cp}^*\text{Ir}(\text{Biot-}p\text{-L})\text{Cl}] \subset \text{S112K}$ .** Crystals of complex  $[\text{Cp}^*\text{Ir}(\text{Biot-}p\text{-L})\text{Cl}] \subset \text{S112K Sav}$  were obtained by the soaking technique at pH 8.0, and diffraction data were collected at the synchrotron to 2.5 Å resolution. Upon refining the streptavidin structure, residual electron density in the  $2F_o - F_c$  map remained in the biotin-binding cavity (Figure 2). The anomalous dispersion density map revealed two peaks (4.5 and 4.0 Å) in the vestibule that coincided with two strong peaks in the  $F_o - F_c$  omit map (11.5 and 5.4  $\sigma$ ). The density was modeled with the  $[\text{Cp}^*\text{Ir}(\text{Biot-}p\text{-L})\text{Cl}]$  cofactor in two

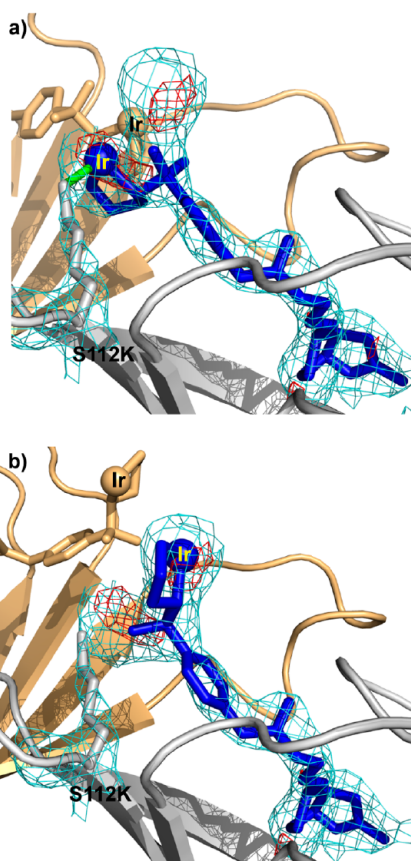


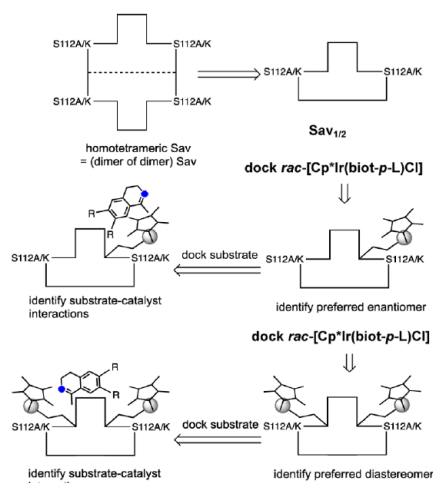
**Figure 2.** Close-up view of the cofactor conformations A (a) and B (b) in stick-representation modeled into the biotin binding site in the crystal structure of  $[\text{Cp}^*\text{Ir}(\text{Biot-}p\text{-L})\text{Cl}] \subset \text{S112K Sav}$  (PDB code 4OKA). Only one Sav dimer (monomers are highlighted in gray and brown, respectively) is depicted for clarity, the  $\text{Cp}^{*-}$  and  $\text{Cl}^-$  could not be located and are thus not displayed. The green cylinder highlights the  $\text{N}\zeta\text{-Lys112}\cdots\text{Ir}$  contact. The  $2F_o - F_c$  electron density and the anomalous difference density map are highlighted in aquamarine and red and are contoured at 1  $\sigma$  and 2.5  $\sigma$ , respectively.

conformations (A and B with occupancies of 60% and 40%, respectively) related by a rotation of 180° around the  $\text{C}_{\text{benzene}}\text{-S}_{\text{sulfonamide}}$  bond (Figure 2). No electron density for any additional ligands at iridium (e.g.,  $\text{Cp}^*$ ,  $\text{Cl}^-$  or  $\text{H}_2\text{O}$  etc.) could be detected in the  $F_o - F_c$  omit map. We hypothesize that this may be due to the flexibility of the cofactor within the shallow biotin-binding vestibule. In the  $F_o - F_c$  omit map, no residual electron density was detected to model the side chain of Lys112, suggesting a high flexibility. However, upon modeling its side chain in an extended conformation, electron density became visible in the  $2F_o - F_c$  map (Figure 2). In this conformation, the distance  $\text{N}\zeta\text{-Lys112-Ir}$  is 2.3 Å, suggesting a bonding interaction between  $\text{Ir-N}$ . We assume that the three remaining free coordination sites are occupied by  $\text{Cp}^{*-}$ , thus suggesting an absolute configuration of the metal of  $R_{\text{Ir}}$ . Orientation A produced similarities to the cofactor in structure  $[\text{Cp}^*\text{Ir}(\text{Biot-}p\text{-L})\text{Cl}] \subset \text{S112A Sav}$  (PDB code 3PK2,<sup>21</sup> Figure S12a, Supporting Information) while the cofactor conformation B shares similarities with its counterpart in structure  $[(\eta^6\text{-benzene})\text{Ru}(\text{Biot-}p\text{-L})\text{Cl}] \subset \text{Sav-S112K}$  (PDB code 2QCB,<sup>19</sup> Figure S12b, Supporting Information).

Unfortunately, the absence of the substrate in the crystal structure and the apparent flexibility of both the cofactor and the lysine 112, as well as the lack of  $\text{Cp}^*$  and  $\text{Cl}^-$  densities, do not allow one to establish a molecular relationship for the ee and rates observed for both mutants. We thus turned to docking simulations to gain further structural insight.

**Docking Simulations.** In order to analyze the kinetic- and ee profiles, several molecular features of the ATHase were addressed by computational means, as summarized in Scheme 2: (i) Do Sav S112A and Sav S112K have any preference for binding  $[\text{Cp}^*\text{Ir}(\text{Biot-}p\text{-L})\text{Cl}]$  in a given absolute configuration at the metal? (ii) What is the complementarity between the cofactor and the substrate? (iii) What is the influence of the occupation of one biotin binding site on the catalytic profile of the adjacent cofactor?

**Scheme 2. Stepwise Docking Strategy Used to Identify (i) Enantiodiscrimination between a Model Dimeric Streptavidin Sav<sub>1/2</sub> and (rac)- $[\text{Cp}^*\text{Ir}(\text{Biot-}p\text{-L})\text{Cl}]$  and (ii) Critical Interactions between the ATHase and the Prochiral Imine Substrate**



To address these questions, a stepwise computational process was performed. Calculations were first carried out for S112A and S112K with a single biotinylated catalyst  $[\text{Cp}^*\text{Ir}(\text{Biot-}p\text{-L})\text{Cl}]$  per Sav dimer (Sav<sub>1/2</sub> hereafter: Sav is best described as a dimer of dimers with two close-lying biotin binding sites) with either (*R*<sub>Ir</sub>)- or (*S*<sub>Ir</sub>)-metal configuration. In a second step, an additional  $[\text{Cp}^*\text{Ir}(\text{Biot-}p\text{-L})\text{Cl}]$  moiety, either with an (*R*<sub>Ir</sub>)- or an (*S*<sub>Ir</sub>)-configuration, was docked in the host dimer model for both S112A Sav<sub>1/2</sub> and S112K Sav<sub>1/2</sub>. At both stages, the dihydroisoquinoline substrate **1** was docked to identify how the prochiral substrate may reach a reactive location in the various ATHases (Scheme 2). The dockings were performed with allowing full flexibility of the iridium complex. For the S112K mutant, the lysine was also allowed to freely move using a library of rotameric states.<sup>28</sup> Finally, in order to study the possible coordination between Lys112 and the iridium atom upon binding, dockings were performed first using an pseudoatom type implemented in GOLD and simulating an electron deficient metal and then optimizing the best energy complexes using the QM/MM approach ONIOM-(PBE:AMBER) with an extended basis set and a flexible binding sphere of out 10 Å around the metal center.<sup>30</sup>

**Identification of the Preferred Metal Configuration for  $[\text{Cp}^*\text{Ir}(\text{Biot-}p\text{-L})\text{Cl}]$  in S112A Sav.** Despite the absence of density for the Cp\* and the Cl<sup>-</sup> of the organometallic cofactor, the X-ray structure of  $[\text{Cp}^*\text{Ir}(\text{Biot-}p\text{-L})\text{Cl}]$  in S112A<sup>21</sup> suggests the presence of a diastereopure complex, (*S*<sub>Ir</sub>)- $[\text{Cp}^*\text{Ir}(\text{Biot-}p\text{-L})\text{Cl}]$ , snugly embedded within Sav S112A. Because a “racemic at iridium” biotinylated cofactor was used for soaking the Sav crystals, this result implies an enantiodiscrimination by the protein environment on the metal center. In order to better ascertain this configurational preference, (*R*<sub>Ir</sub>)- and (*S*<sub>Ir</sub>)-pseudoenantiomers were docked within S112A Sav<sub>1/2</sub> (see the Supporting Information). The lowest energy orientations for the (*S*<sub>Ir</sub>)- and (*R*<sub>Ir</sub>)-moieties were predicted to have good binding affinities (about 40 scoring units) with a slight preference for the (*S*<sub>Ir</sub>)-metal over the (*R*<sub>Ir</sub>)-cofactor (no more than 1.2 scoring units; see Table 2). However, this preference may be higher than predicted by the pure scoring function. Indeed, analysis of the energetic breakdown of both binding modes shows a clear preference for *S*<sub>Ir</sub> in absolute energetic terms  $\Delta G$  (about 5 kJ·mol<sup>-1</sup> as reported in Table S12,

**Table 2. Summary of the Docking Results of the Pseudoenantiomers of  $[\text{Cp}^*\text{Ir}(\text{Biot-}p\text{-L})\text{Cl}]$  Catalyst in the S112A and S112K Sav**

host protein	cofactor config	score <sup>a</sup>	RMSD <sup>b</sup> (Å)
S112A	<i>S</i> <sub>Ir</sub>	44.4	1.0
	<i>R</i> <sub>Ir</sub>	43.2	2
S112 K	<i>S</i> <sub>Ir</sub>	51.5	1.7 <sup>A</sup>
	<i>R</i> <sub>Ir</sub>	58.6	1.4 <sup>A</sup>
<i>(S</i> <sub>Ir</sub> )- $[\text{Cp}^*\text{Ir}(\text{Biot-}p\text{-L})\text{Cl}]$ in S112A	<i>S</i> <sub>Ir</sub>	43.1	1.3
	<i>R</i> <sub>Ir</sub>	43.9	3.2
<i>(R</i> <sub>Ir</sub> )- $[\text{Cp}^*\text{Ir}(\text{Biot-}p\text{-L})\text{Cl}]$ in S112K	<i>S</i> <sub>Ir</sub>	42.5	2.8 <sup>B</sup>
	<i>R</i> <sub>Ir</sub>	44.4	3.0 <sup>B</sup>

<sup>a</sup>Scores correspond to dimensionless ChemScore values as established in GOLD.<sup>29,34</sup> <sup>b</sup>Root mean square deviations (RMSD) for lowest energy docking solution vs X-ray structures. For S112K, the RMSD values are for the experimental binding modes that present the best structural overlap with conformer A (indicated by A) and with conformer B (indicated by B).

Supporting Information). Only corrective terms associated with internal degrees of freedoms penalize this binding mode, something for which scoring functions are currently not accurate for organometallic compounds (i.e., no relaxation of the first coordination sphere upon binding).<sup>29</sup>

The most stable binding modes of the cofactor in the  $[\text{Cp}^*\text{Ir}(\text{Biot-}p\text{-L})\text{Cl}]$  in S112A structure were superposed with the X-ray structure.<sup>21</sup> The resulting RMSD is 1.0 and 2.0 Å for *S*<sub>Ir</sub> and *R*<sub>Ir</sub>, respectively [Figures SI3a (Supporting Information) and 3a]. Both energetic and RMSD considerations suggest that the (*S*<sub>Ir</sub>)-metal center better fits the protein vestibule.

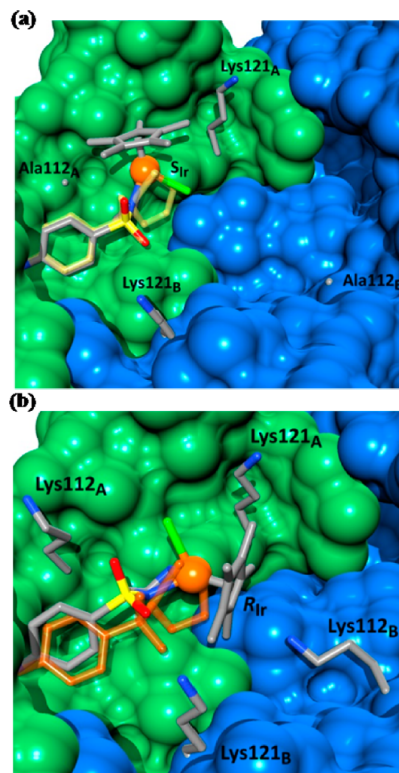


**Figure 3.** Representation of the lowest-energy orientation obtained for the docking of the preferred pseudoenantiomers in both the S112A (*(S*<sub>Ir</sub>)- $[\text{Cp}^*\text{Ir}(\text{Biot-}p\text{-L})\text{Cl}]$ , top) and the S112K mutants (*(R*<sub>Ir</sub>)- $[\text{Cp}^*\text{Ir}(\text{Biot-}p\text{-L})\text{Cl}]$ , bottom). Monomers A and B are depicted in green and blue, respectively. For comparison, the crystallographically determined position of the cofactors is highlighted as yellow and orange ghost structures in the S112A and S112K models, respectively (in the latter case only conformation A is depicted for clarity).

To understand how this complementarity could impact the enantioselectivity observed experimentally, docking of the imine **1** substrate was performed on both (*R*<sub>Ir</sub>)- and (*S*<sub>Ir</sub>)-cofactor-loaded streptavidin. The conformational search was restrained to a reasonable distance for hydride transfer with all the remaining degrees of freedom entirely allowed. It is important to mention that the chloride was substituted by its corresponding hydride in those calculations, hence leading to an inversion of the configuration at the metal by virtue of the Cahn–Ingold–Prelog priorities: (*S*<sub>Ir</sub>)- $[\text{Cp}^*\text{Ir}(\text{Biot-}p\text{-L})\text{Cl}]$  becomes (*R*<sub>Ir</sub>)- $[\text{Cp}^*\text{Ir}(\text{Biot-}p\text{-L})\text{H}]$ . The best docked structures

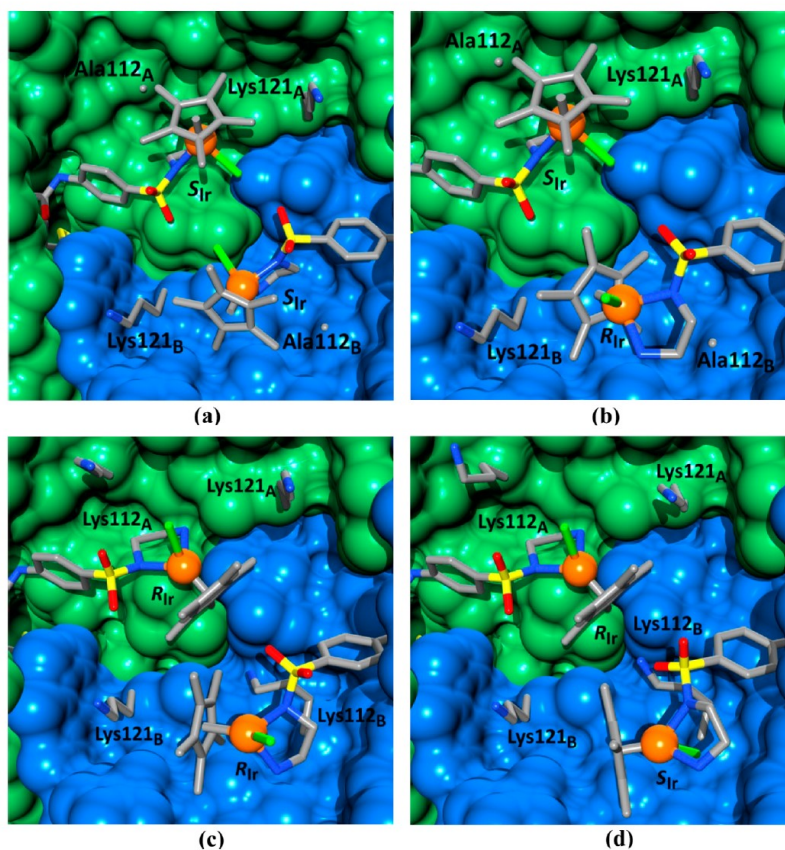


**Figure 4.** Representation of the models of a fully loaded dimer of the Sav tetramer. Most relevant residues are in stick representation. Monomer A is depicted in green and monomer B in blue. Top: Mutant S112A with two ( $S_{Ir}$ )-[Cp\*Ir(Biot-*p*-L)Cl] cofactors (a) or one ( $S_{Ir}$ )- and one ( $R_{Ir}$ )-[Cp\*Ir(Biot-*p*-L)Cl] (b). Bottom: Mutant S112K with two ( $R_{Ir}$ )-[Cp\*Ir(Biot-*p*-L)Cl] cofactors (c) or one ( $R_{Ir}$ )- and one ( $S_{Ir}$ )-[Cp\*Ir(Biot-*p*-L)Cl] (d).

for the ( $R_{Ir}$ )-[Cp\*Ir(Biot-*p*-L)H]  $\subset$  S112A reveals substrate **1** located deep inside the opposite biotin binding cavity (Figure SI3a, Supporting Information), while the same calculation for ( $S_{Ir}$ )-[Cp\*Ir(Biot-*p*-L)H]  $\subset$  S112A leads to a highly solvent exposed prochiral imine **1** with limited interactions with surface residues of the host protein, a situation unlikely to provide the highly enantioenriched product **2** (Figure SI3b, Supporting Information).

Taken together, the docking studies suggest that with a unique cofactor loaded monomer per dimer of S112A the reaction proceeds via an ( $R_{Ir}$ )-[Cp\*Ir(Biot-*p*-L)H]  $\subset$  S112A Sav to afford highly enantioenriched (*R*)-salsolidine **2**. These observations are consistent with the experimental results, thus giving us confidence to model the [Cp\*Ir(Biot-*p*-L)H]  $\subset$  S112K ATHase.

**Identification of the Preferred Metal Configuration for [Cp\*Ir(Biot-*p*-L)Cl]  $\subset$  S112K Sav.** The above methodology was applied to analyze the ATHase derived from the S112K Sav mutant, considering both the ( $R_{Ir}$ )- and ( $S_{Ir}$ )-[Cp\*Ir(Biot-*p*-L)Cl] cofactor configurations. Calculations were first performed with a coordinatively saturated metal (i.e., no coordination with amino acid side chains).

For both pseudoenantiomers, the lowest energy binding modes of the biotinylated catalyst fit well with the conformation A observed in the X-ray structure (Table 2).

The predicted lowest energy binding modes for the ( $S_{Ir}$ )- and ( $R_{Ir}$ )-[Cp\*Ir(Biot-*p*-L)Cl] cofactors were 51.5 and 58.6 score units, respectively, thus suggesting that the ( $R_{Ir}$ )-pseudoenantiomer is energetically favored (Table 2 and Figure 3b).

As suggested by the X-ray data, we further explored the ability of Lys112 to coordinate the iridium metal by reproducing in silico this phenomenon. To this end, and because of the need to account for the formation of a coordination bond, we applied an integrative protocol suited to simulate interactions between organometallic cofactors and protein residues, a feature absent from usual protein–ligand docking approaches.<sup>30</sup>

A protein–ligand docking with optimized parameters for treating metals with a vacant coordination site allied with QM/MM refinements (see the Supporting Information) suggests that Lys112 can interact only with the cofactor leading to an ( $S_{Ir}$ )-configuration upon coordination (resulting from Cl<sup>−</sup> substitution from ( $R_{Ir}$ )-[Cp\*Ir(Biot-*p*-L)Cl]). The QM/MM simulation confirmed an Ir–Lys112<sub>A</sub> contact with an Ir–N $_{\zeta}$ <sub>Lys112A</sub> distance of 2.2 Å. The calculated RMSD between the QM/MM-minimized structure and the A conformation in the S112K X-ray structure is 0.8 Å, suggesting that the experimental orientation is compatible with a coordination of the catalyst by Lys112<sub>A</sub> (Figure SI4, Supporting Information).

Interestingly, the dockings with and without direct interaction between  $N_{C_{Lys112A}}$  and the metal led to nearly overlapping orientations (RMSD 0.7 Å). This suggests that the coordination of the lysine to the metal is not determinant in fixing the orientation of the cofactor within the binding site but likely that an equilibrium exists in solution between bound and unbound iridium center. At this stage, however, none of the docking solutions led to the alternative conformation B of the cofactor as identified in the X-ray structure.

To decipher the influence of the absolute metal configuration of the cofactor in determining the catalytic environment, the dihydroisoquinoline **1** was docked on both  $(R_{Ir})$ - and  $(S_{Ir})$ -[Cp\*Ir(Biot-*p*-L)H]  $\subset$  S112K ATHases (Figure S13c,d, Supporting Information). The results show that the substrate is challenged to reach the hydride only in the  $(R_{Ir})$ -[Cp\*Ir(Biot-*p*-L)H] configuration (Figure S13c, Supporting Information). We thus hypothesize that the  $(S_{Ir})$ -[Cp\*Ir(Biot-*p*-L)H]  $\subset$  S112K is the preferred metal configuration, both in terms of stability and activity. However, protein–ligand dockings are not accurate enough to predict the enantioselectivity for the reduction process. Simulations involving quantum mechanical based techniques and a wide exploration of the precatalytic state of the enzyme would be needed for this purpose.

Taken together, this first part of the computational analysis of the ATHases suggests that S112K and S112A mutants stabilize different pseudoenantiomers of the embedded catalyst. This in turn offers different second coordination sphere environments for the approach of the substrate **1**. For the homogeneous transfer-hydrogenation catalyst pioneered by Noyori and co-workers, the critical role of the chirality of the metal is well-documented:<sup>31,32</sup> the enantiopure aminosulfonamide ligand enforces one configuration at the metal that, in turn, dictates which prochiral face of the substrate can approach the hydride to afford the preferred enantiomer of the product. In the present case, we hypothesize that the host protein influences the enantiodiscriminating step in a similar way: incorporation of a configurationally labile piano stool moiety<sup>33</sup> [Cp\*Ir(Biot-*p*-L)Cl] within the host protein favors one configuration at the metal:  $(S_{Ir})$ -[Cp\*Ir(Biot-*p*-L)Cl]  $\subset$  S112A and  $(R_{Ir})$ -[Cp\*Ir(Biot-*p*-L)Cl]  $\subset$  S112K. This by and large dictates which enantiomer of salsolidine **2** is produced. Additional interactions between the substrate and the host protein contribute to fine-tune the enantioselectivity, eventually leading to salsolidine **2** in up to 96% ee *R* and 78% ee *S* for S112A and S112K ATHases, respectively.

**Structural Consequences of Increasing the Ir/Sav Ratio in [Cp\*Ir(Biot-*p*-L)Cl]  $\subset$  S112A and S112K.** Additional docking simulations were performed on  $(S_{Ir})$ -[Cp\*Ir(Biot-*p*-L)Cl]  $\subset$  S112A to identify how a second cofactor may affect the structure and the corresponding activity of the fully loaded Sav<sub>1/2</sub> (which in turn helps rationalize the mechanism of the fully loaded tetrameric Sav). Both the  $(S_{Ir})$ - and the  $(R_{Ir})$ -cofactors were docked in the second pocket of Sav<sub>1/2</sub> (Figure 4a,b). The small difference in scores (Table 2) shows that there is no significant chiral discrimination for the binding of the second cofactor. Inspection of the structure reveals that for the  $(S_{Ir},S_{Ir})$ -system, both chlorides point toward each other with a short Cl–Cl distance (3.8 Å) (Figure 4a). In this configuration, there is little space for the dihydroisoquinoline **1** to approach the catalyst. Therefore, it is expected that the fully loaded  $(S_{Ir},S_{Ir})$ -[Cp\*Ir(Biot-*p*-L)Cl]<sub>2</sub>  $\subset$  S112A ATHase displays limited activity (Figure S15a, Supporting Information). In

stark contrast, in the  $(S_{Ir},R_{Ir})$ -[Cp\*Ir(Biot-*p*-L)Cl]<sub>2</sub>  $\subset$  S112A, the  $(R_{Ir})$ -cofactor better fits into the adjacent cavity offering its chloride face accessible for the substrate. However, the Cp\* ligand of this same catalyst impedes the access of the substrate **1** to the hydride of the adjacent  $(S_{Ir})$ -enantiomer, thus eroding the activity rate of the Sav<sub>1/2</sub> [Figures 4b and S15b (Supporting Information)].

Protein–ligand dockings were also performed with  $(S_{Ir})$ - and  $(R_{Ir})$ -metal cofactors on the  $(R_{Ir})$ -[Cp\*Ir(Biot-*p*-L)Cl]  $\subset$  S112K model. Although little energy differences were observed (Table 2), structural differences were substantial (Figure 4c). The  $(R_{Ir},R_{Ir})$ -[Cp\*Ir(Biot-*p*-L)Cl]<sub>2</sub>  $\subset$  S112K hybrid presented both chlorides facing the Lys112 of the same monomer where the biotinylated cofactor is bound, whereas in the  $R_{Ir},S_{Ir}$  combination the docked  $(S_{Ir})$ -cofactor has its chloride facing the interface of the two monomers (Figure 4d). Docking calculations with the dihydroisoquinoline **1** substrate in both hybrids revealed that in the  $R_{Ir},R_{Ir}$  case, each monomer is active and behaves independently with no interaction between the adjacent cofactors (Figure S15c, Supporting Information), while in the  $R_{Ir},S_{Ir}$  model, only the  $(R_{Ir})$ -cofactor embedded monomer should be catalytically active, as the substrate is challenged to reach the  $(S_{Ir})$ -cofactor (Figure S15d, Supporting Information). Therefore, only the  $(R_{Ir},R_{Ir})$ -[Cp\*Ir(Biot-*p*-L)Cl]<sub>2</sub>  $\subset$  S112K model is consistent with the experimental data gathered for the S112K ATHase, where a nearly constant rate irrespective of the number of Ir equivalents (Table 1) is observed. Those results are essentially unaltered when considering the possibility of Lys112 to coordinate to the iridium center. Those calculations actually predict that two homogeneous catalysts could bind the same Sav<sub>1/2</sub> dimer, each one of them interacting with a different Lys112. We hypothesize that the Ir–lysine interactions might favor the rapid epimerization of the piano stool moiety during the catalytic cycle. More insight on the regeneration of the catalyst through the use of formic acid would be needed and should answer whether this contact has a role in the catalytic cycle or it is just an artifact created by the crystallization conditions.

Interestingly, in most calculations of the  $(R_{Ir},R_{Ir})$ -[Cp\*Ir(Biot-*p*-L)Cl]<sub>2</sub>  $\subset$  S112K model with or without the metal coordinated by Lys112, low-energy solutions present the second cofactor in a binding mode closer to orientation B, with some of them reaching an RMSD < 1 Å. Since this binding mode is absent in the simulations performed for the binding of the first cofactor, these results suggest that a B-like conformation could be stabilized when the adjacent monomer is loaded. This suggests that the two monomers of a fully loaded dimer present a mixture of A and B-like orientations and have different second coordination sphere environments for the metal. Simulations to reproduce two cofactors with an orientation B as it stands in the X-ray structure lead to no enantioselectivity for the metal center by the protein scaffold [both  $(R_{Ir})$ - and  $(S_{Ir})$ -enantiomers of the cofactors have similar binding energies]. In the resulting orientations, the chloride is systematically exposed to the solvent and neither the chirality of the metal nor the contacts of the protein in its second coordination sphere can help rationalize the enantioselectivity observed experimentally.

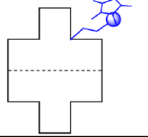
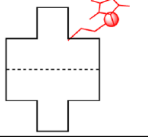
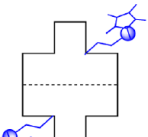
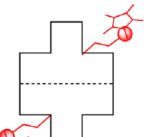
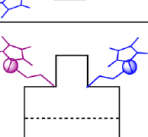
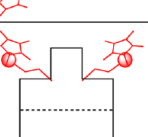
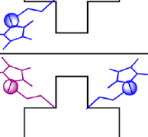
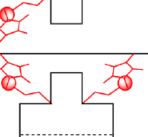
For both cofactors, the respective protein environment surrounding the substrate docked in the  $(R_{Ir},R_{Ir})$ -[Cp\*Ir(Biot-*p*-L)Cl]<sub>2</sub>  $\subset$  S112K hybrid are slightly different, and in both cases, the prochiral imine is exposed to the solvent. This suggests that the enantioselectivity is by and large dictated by

the chirality at the metal rather than second coordination sphere interactions between the prochiral imine and the protein. This contrasts with  $(S_{Ir})$ -[Cp\*Ir(Biot-*p*-L)Cl]  $\subset$  S112A, where the substrate **1** is surrounded by a protein cavity, thus contributing to fine-tune the enantioselectivity (up to 96% ee)

## CONCLUSION AND OUTLOOK

Combining structural and kinetic data with the docking simulations, the following mechanistic insights can be inferred for the ATHases (Table 3).

**Table 3. Phenomenological Rationalization of the Rate and Enantioselectivity of ATHase as a Function of Ir/Sav Ratio and Mutant<sup>a</sup>**

S112A		S112K	
Equivalents of cofactor	ee Rate	Equivalents of cofactor	ee Rate
	Max. Max.		Max. Max.
	Max. Max.		Max. Max.
	Max. Decreases		Max. Max.
	Decreases Decreases		Max. Max.

<sup>a</sup>Blue, red, and violet cofactors symbolize  $(S_{Ir})$ -[Cp\*Ir(Biot-*p*-L)Cl],  $(R_{Ir})$ -[Cp\*Ir(Biot-*p*-L)Cl], and  $(rac)$ -[Cp\*Ir(Biot-*p*-L)Cl], respectively.

**1. [Cp\*Ir(Biot-*p*-L)Cl]  $\subset$  S112A.** (i) The first cofactor binds with an  $(S_{Ir})$ -configuration of the metal (Figure 3a). In this situation the system reaches its maximum rate and highest enantioselectivity (Table 1, entry 2). Relying on a QM/MM study, we recently analyzed the subtle details of enantioselectivity for this system, highlighting the critical involvement of Lys121 in stabilizing the substrate via cation- $\pi$  interactions.<sup>23</sup>

(ii) On the basis of the above docking studies, we anticipate that the second cofactor binds to the opposite dimer of the tetrameric streptavidin, thus minimizing clashes between the

two cofactors. In this situation, we predict a combination of two  $(S_{Ir})$ -[Cp\*Ir(Biot-*p*-L)Cl]  $\subset$  S112A dimeric units forming an ATHase operating at the same rate (vs [Ir]) and yielding similar enantioselectivities (Table 3). This prediction is largely verified experimentally (Table 1, entry 3).

(iii) No enantiopreference is predicted for the binding of a third cofactor within Sav S112A (Figure 4a,b). Due to close contacts between the adjacent catalysts, the substrate is challenged to reach the hydride in the  $(S_{Ir}S_{Ir})$ -Sav<sub>1/2</sub> and only in the  $(S_{Ir}R_{Ir})$ -hybrids it could reach the  $(R_{Ir})$ -cofactor in a solvent-exposed way. In this situation the performance of the ATHase should be negatively affected and the observed activity and selectivity for [Cp\*Ir(Biot-*p*-L)Cl]<sub>3</sub>  $\subset$  S112A can thus be generally traced back to the singly occupied Sav<sub>1/2</sub> (Table 1, entry 4).

(iv) As in point iii, fully loading the four biotin binding sites leads to [Cp\*Ir(Biot-*p*-L)Cl]<sub>4</sub>  $\subset$  S112A with significantly eroded rate and selectivity (Table 1, entry 5).

**2. [Cp\*Ir(Biot-*p*-L)Cl]  $\subset$  S112K.** The docking studies performed on the S112K ATHase suggest that the first and second catalysts bound to the homotetrameric Sav are in an  $(R_{Ir})$ -configuration (Figure 4c). Importantly and in stark contrast to the S112A ATHase, all four biotin-binding sites can accommodate an  $(R_{Ir})$ -[Cp\*Ir(Biot-*p*-L)Cl] cofactor. In this situation, each catalytic event is by and large confined within one monomer and thus little affected by the Sav:Ir ratio. However, the substrate **1** is highly solvent exposed with limited contacts with the protein environment. A nearly constant rate (vs [Ir]) and enantioselectivity are thus predicted, irrespective of the Ir/Sav ratio. These predictions are largely corroborated experimentally (Table 1, entries 5–9). The localization the cofactor is close enough to Lys112 so that this residue can interact with the metal. However, the absence of clear density and the relatively little impact of this coordination on the geometry of the system suggest a transient structure that rapidly converts to catalytically competent systems.

Considering that the ATHases derived from S112A and S112K mutants afford opposite enantiomers, we suggest that it is the absolute configuration at Ir which for the most part determines the preferred enantiomer of the reduction product. This situation may be viewed as an “induced lock-and-key” fit, whereby the second coordination sphere provided by the Sav mutant induces an enantiopure configuration at the metal center which, in turn, governs to which prochiral face of the substrate the hydride is delivered. Subtle substrate–protein interactions further contribute to fine-tune the enantioselectivity.

It is gratifying that, despite the qualitative nature of the docking simulations, the kinetic and structural data all in all corroborate the predictions. Current efforts are aimed at producing a heterotetrameric Sav with only two functional biotin-binding sites and engineering additional weak interactions between the substrate and the host protein.

## ASSOCIATED CONTENT

### Supporting Information

Material and methods for kinetics measurements and crystallography protocol and resolution, as well as details on the molecular modeling tools and procedure followed; Tables S11 and S12 for X-ray data collection and extended docking analysis, respectively; and figures associated with HABA displacement titration (Figure S11), binding site comparison between cofactor-loaded Sav mutants S112A and S112K



(Figure SI2), docking solutions of [Cp\*Ir(Biot-*p*-L)H] interacting with substrate for Sav<sub>1/2</sub> mutants (Figure SI3), depiction of the doubly occupied S112K Sav<sub>1/2</sub> ATHase (Figure SI4) with the Lys112 coordinated to the metal center and representation of the models of a fully loaded dimer of the Sav tetramer (Figure SI5). This material is available free of charge via the Internet at <http://pubs.acs.org>.

## AUTHOR INFORMATION

### Corresponding Authors

thomas.ward@unibas.ch.

JeanDidier.Marechal@uab.cat.

### Author Contributions

<sup>¶</sup>V.M.R. and M.D. contributed equally to this work.

### Notes

The authors declare no competing financial interest

## ACKNOWLEDGMENTS

T.R.W. thanks Umicore for a loan of [Cp\*IrCl<sub>2</sub>]<sub>2</sub>, Prof. C. Cantor for the streptavidin gene, and Prof. K. Faber for suggesting the “induced lock-and-key” term. Generous funding was provided by the SNF (grant 200020\_144354) and the Cantons of Basel and the Swiss Nanoscience Institute. Financial support from the Spanish Ministerio de Economía y Competitividad (Project CTQ2011-23336) is acknowledged. V.M.R. is grateful to the Spanish MINECO for a FPI Fellowship.

## REFERENCES

- (1) Wilson, M. E.; Whitesides, G. M. *J. Am. Chem. Soc.* **1978**, *100*, 306–307.
- (2) Levine, H. L.; Kaiser, E. T. *J. Am. Chem. Soc.* **1978**, *100*, 7670–7677.
- (3) Qi, D.; Tann, C.-M.; Haring, D.; Distefano, M. D. *Chem. Rev.* **2001**, *101*, 3081–3112.
- (4) Köhler, V.; Wilson, Y. M.; Lo, C.; Sardo, A.; Ward, T. R. *Curr. Opin. Biotechnol.* **2010**, *21*, 744–752.
- (5) Reetz, M. T. *Top. Organomet. Chem.* **2009**, 63–92.
- (6) Jing, Q.; Okrasa, K.; Kazlauskas, R. J. *Top. Organomet. Chem.* **2009**, 45–61.
- (7) Jing, Q.; Okrasa, K.; Kazlauskas, R. J. *Chem. An Eur. J.* **2009**, *15*, 1370–1376.
- (8) Ueno, T.; Abe, S.; Yokoi, N.; Watanabe, Y. *Coord. Chem. Rev.* **2007**, *251*, 2717–2731.
- (9) Mayer, C.; Gillingham, D. G.; Ward, T. R.; Hilvert, D. *Chem. Commun.* **2011**, 47, 12068–12070.
- (10) Lu, Y.; Yeung, N.; Sieracki, N.; Marshall, N. M. *Nature* **2009**, *460*, 855–862.
- (11) Boersma, A. J.; Megens, R. P.; Feringa, B. L.; Roelfes, G. *Chem. Soc. Rev.* **2010**, *39*, 2083–2092.
- (12) Rosati, F.; Roelfes, G. *ChemCatChem* **2010**, *2*, 916–927.
- (13) Fournier, P.; Fiammengo, R.; Jäschke, A. *Angew. Chem. Int. Ed.* **2009**, *48*, 4426–4429.
- (14) Steinreiber, J.; Ward, T. R. *Coord. Chem. Rev.* **2008**, *252*, 751–766.
- (15) Ward, T. R. *Acc. Chem. Res.* **2011**, *44*, 47–57.
- (16) Lin, C.-C.; Lin, C.-W.; Chan, A. S. C. *Tetrahedron: Asymmetry* **1999**, *10*, 1887–1893.
- (17) Hyster, T. K.; Knörr, L.; Ward, T. R.; Rovis, T. *Science* **2012**, *338*, 500–503.
- (18) Podtetenieff, J.; Taglieber, A.; Bill, E.; Reijerse, E. J.; Reetz, M. T. *Angew. Chem. Int. Ed.* **2010**, *122*, 5277–5281.
- (19) Creus, M.; Pordea, A.; Rossel, T.; Sardo, A.; Letondor, C.; Ivanova, A.; Letrong, I.; Stenkamp, R. E.; Ward, T. R. *Angew. Chem. Int. Ed.* **2008**, *47*, 1400–1404.
- (20) Zimbron, J. M.; Sardo, A.; Heinisch, T.; Wohlschlager, T.; Gradinaru, J.; Massa, C.; Schirmer, T.; Creus, M.; Ward, T. R. *Chem. An Eur. J.* **2010**, *16*, 12883–12889.
- (21) Dürrenberger, M.; Heinisch, T.; Wilson, Y. M.; Rossel, T.; Nogueira, E.; Knörr, L.; Mutschler, A.; Kersten, K.; Zimbron, M. J.; Pierron, J.; Schirmer, T.; Ward, T. R. *Angew. Chem. Int. Ed.* **2011**, *50*, 3026–3029.
- (22) Zimbron, J. M.; Heinisch, T.; Schmid, M.; Hamels, D.; Nogueira, E. S.; Schirmer, T.; Ward, T. R. *J. Am. Chem. Soc.* **2013**, *135*, 5384–5388.
- (23) Muñoz Robles, V.; Vidossich, P.; Lledós, A.; Ward, T. R.; Maréchal, J.-D. *ACS Catal.* **2014**, *4*, 833–842.
- (24) Balcells, D.; Maseras, F. *New J. Chem.* **2007**, *31*, 333–343.
- (25) As the biotin-binding event is essentially noncooperative, a statistical distribution of [Cp\*Ir(Biot-*p*-L)Cl] within Sav is expected upon varying the Ir/Sav ratio from 1 to 4.
- (26) Haldane, J. *Enzymes*; Longman, Green and Co.: New York, 1930.
- (27) Skander, M.; Humbert, N.; Collot, J.; Gradinaru, J.; Klein, G.; Loosli, A.; Sauser, J.; Zocchi, A.; Gilardoni, F.; Ward, T. R. *J. Am. Chem. Soc.* **2004**, *126*, 14411–14418.
- (28) Chase, F.; Avenue, B. *Curr. Opin. Struct. Biol.* **2002**, *12*, 431–440.
- (29) Ortega-Carrasco, E.; Lledós, A.; Maréchal, J.-D.; Ortega Carrasco, E.; Maréchal, J.-D. *J. Comput. Chem.* **2014**, *35*, 192–198.
- (30) Muñoz Robles, V.; Ortega-Carrasco, E.; Fuentes, E. G.; Lledós, A.; Maréchal, J.-D. *Faraday Discuss.* **2011**, *148*, 137.
- (31) Martins, J. E. D.; Clarkson, G. J.; Wills, M. *Org. Lett.* **2009**, *11*, 847–850.
- (32) Yamakawa, M.; Ito, H.; Noyori, R. *J. Am. Chem. Soc.* **2000**, *122*, 1466–1478.
- (33) Ward, T. R.; Schafer, O.; Daul, C.; Hofmann, P. *Organometallics* **1997**, *16*, 3207–3215.
- (34) Verdonk, M. L.; Cole, J. C.; Hartshorn, M. J.; Murray, C. W.; Taylor, R. D. *Proteins: Struct. Funct. Bioinf.* **2003**, *52*, 609–623.

## Structural-, Kinetic- and Docking Studies of Artificial Imine Reductases Based on the Biotin-Streptavidin Technology: An Induced Lock-and-Key Hypothesis

*Victor Muñoz Robles,<sup>a,∇</sup> Marc Dürrenberger,<sup>b,∇</sup> Tillmann Heinisch,<sup>c</sup> Agustí Lledós,<sup>a</sup> Tilman Schirmer,<sup>c</sup> Thomas R. Ward<sup>b,\*</sup> and Jean-Didier Maréchal<sup>a,∇</sup>*

*Received (in XXX, XXX) Xth XXXXXXXXX 20XX, Accepted Xth XXXXXXXXX 20XX*

DOI: 10.1039/b000000x

### Supplementary information

Materials and Methods .....	S2
Table SI1 .....	S5
Table SI2 .....	S5
Figure SI1 .....	S6
Figure SI2 .....	S7
Figure SI3 .....	S8
Figure SI4 .....	S9
Figure SI5 .....	S10
References .....	S11

## Materials and Methods

### Michaelis-Menten Kinetics General Considerations

6,7-dimethoxy-1-methyl-3,4-dihydroisoquinoline **1** was purchased from Acros and used as received. Streptavidin (Sav) mutants were produced, purified and characterized as previously described.<sup>1</sup> The Sav used in this work and on which all variants were based is the T7-tagged core Sav described by Gallizia et al.<sup>2</sup> (referred to as WT Sav). For a detailed synthesis of [Cp\*Ir(Biot-*p*-L)Cl], see reference.<sup>3</sup> HPLC measurements were performed on Agilent instruments equipped with modules from the 1100 and 1200 series and diode array detectors.

### Stock solutions and buffers MOPS/formate buffer

5.0225 g of 3-(*N*-morpholino)propanesulfonic acid (MOPS) and 8.1612 g of sodium formate were dissolved in 40 ml water and the pH was adjusted by addition of NaOH (final concentration: 0.6 M MOPS, 3 M formate).

### [Cp\*Ir(Biot-*p*-L)Cl]

[Cp\*Ir(biot-*p*-L)Cl] was dissolved in degassed DMF to a final concentration of 10, 20, 30, or 40 mM, respectively. These solutions were stored under nitrogen at 4 °C and used within 5 days.

### Substrate

6,7-dimethoxy-1-methyl-3,4-dihydroisoquinoline **1** (410.5 mg), MOPS (251.12 mg) and sodium formate (408.1 mg) were dissolved in 2 ml water in a volumetric flask and the pH was adjusted by addition of concentrated sulfuric acid (final concentrations: 1 M 6,7-dimethoxy-1-methyl-3,4-dihydroisoquinoline **1**, 0.6 M MOPS, 3 M formate).

### ATHase

Sav mutants were weighted into 2 mL PP-tubes and dissolved in the MOPS/formate buffer to a concentration of 200 mM streptavidin free biotin binding sites (the average of free binding sites per Sav tetramer was determined with a biotin-4-fluorescein assay).<sup>4</sup> An appropriate volume of the corresponding [Cp\*Ir(Biot-*p*-L)Cl] stock solution was added (5 µL/ml) in order to adjust the desired [Ir]/Sav biotin binding sites ratio and the mixture was vigorously vortexed.

### General procedure

For an individual kinetic measurement at a particular substrate concentration, 100 µl of the ATHase stock solution was added to a glass tube equipped with a mechanical stirrer and MOPS/formate buffer was added to adjust the final volume of 200 µL (between 0-95 µL). The reaction was initiated by adding an appropriate volume of the substrate stock solution (between 5-100 µl) and the mixture was stirred at 25 °C (final concentrations: 99.5 µM Sav biotin binding sites, between 24.88 and 99.5 µM [Cp\*Ir(biot-*p*-L)Cl]). Aliquots of 50 µl were collected at 15, 30 and 45 minutes and were added to PP-tubes containing 40 µl of a freshly prepared glutathione solution (250 mM) which was found to be an effective inhibitor of the catalyst. Water (300 µl) was added and 200 µl of the resulting solution was further diluted with water (500 µl) before analysis by RP-HPLC using an Eclipse XDB-C18 column (5 µm, 4.6 × 150 mm, Agilent); solvent A: H<sub>2</sub>O with 0.1 % TFA, solvent B: MeOH with 0.1 % TFA; 87.5 % B at 0 min, 87.5 % B at 20 min, 60 % B at 21.5 min, 60 % B at 23.5 min, 12.5 % B at 25 min, 12.5 % B at 30 min; 1 ml/min; 25 °C, 280 nm; T<sub>R</sub> 12.3 min (6,7-dimethoxy-1-methyl-1,2,3,4-tetrahydroisoquinoline), 16.4 min (6,7-dimethoxy-1-methyl-3,4-dihydroisoquinoline).

For a given Sav mutant at a given [Ir]/Sav biotin binding sites ratio, the kinetic measurements using different substrate concentrations (between 25 and 500 mM) were performed simultaneously by starting the reactions staggered every minute. All measurements were performed in triplicate.

Product concentrations were determined under consideration of the response factor and plotted against the corresponding reaction times (see above). Initial rates at a given initial substrate concentration were obtained by linear regression of the resulting data points. The average value of these rates was plotted as a function of the substrate concentration. The apparent Michaelis-Menten parameters  $V_{max}$ ,  $K_m$  and  $K_i$  were obtained applying nonlinear regression (least squares method) using GraphPad Prism 5.0<sup>®</sup> corresponding to the Michaelis-Menten equation<sup>5</sup> or to Haldane's equation for substrate inhibition.<sup>6</sup>

### Determination of the enantioselectivity

For a given Sav mutant at a given [Ir]:Sav biotin binding sites ratio, reactions were set up as described above at a particular substrate concentration and run for 7 hours at 25 °C before water was added (500 µl) followed by 50 µl of a 20% NaOH solution. The mixture was extracted two times with dichloromethane (1 ml), the combined organic fractions dried over anhydrous sodium sulfate, filtered and analysed by chiral HPLC using a Chiralpak IC column (5 µm, 4.6 mm ·

25 mm) and dichloromethane containing 1 % isopropanol and 0.06 % diethylamine as an eluent; 1 ml/min; 25 °C, 280 nm,  $T_R$  8.6 min ((*S*)- 6,7-dimethoxy-1-methyl-1,2,3,4-tetrahydroisoquinoline **2**), 9.5 min (6,7-dimethoxy-1-methyl-3,4-dihydroisoquinoline **1**), 15.6 ((*R*)-6,7-dimethoxy-1-methyl-1,2,3,4-tetrahydroisoquinoline **2**, referred to as salsolidine).

#### HABA Displacement titration for the estimation of the $K_d$ of $[\text{Cp}^*\text{Ir}(\text{biot-}p\text{-L})\text{Cl}]^7$

Sav-mutants were dissolved in phosphate buffer (20 mM, pH 7) to a tetrameric concentration of 8  $\mu\text{M}$ . The solution was added to a quartz cuvette (2.4 ml) and treated with 0.3 ml of a 2-(4-hydroxyphenylazo)benzoic acid solution (HABA, 9.6 mM in phosphate buffer pH 7). To this mixture was added stepwise 5  $\mu\text{L}$  of either a biotin solution (0.96 mM in phosphate buffer) or 1.7  $\mu\text{L}$  of a  $[\text{Cp}^*\text{Ir}(\text{biot-}p\text{-L})\text{Cl}]$  solution (2.9 mM in DMF), corresponding to 0.25 equivalents vs. Sav tetramer. The solution was mixed at each step by means of pipetting up and down. After 5 minutes, the absorbance at 506 nm was measured.

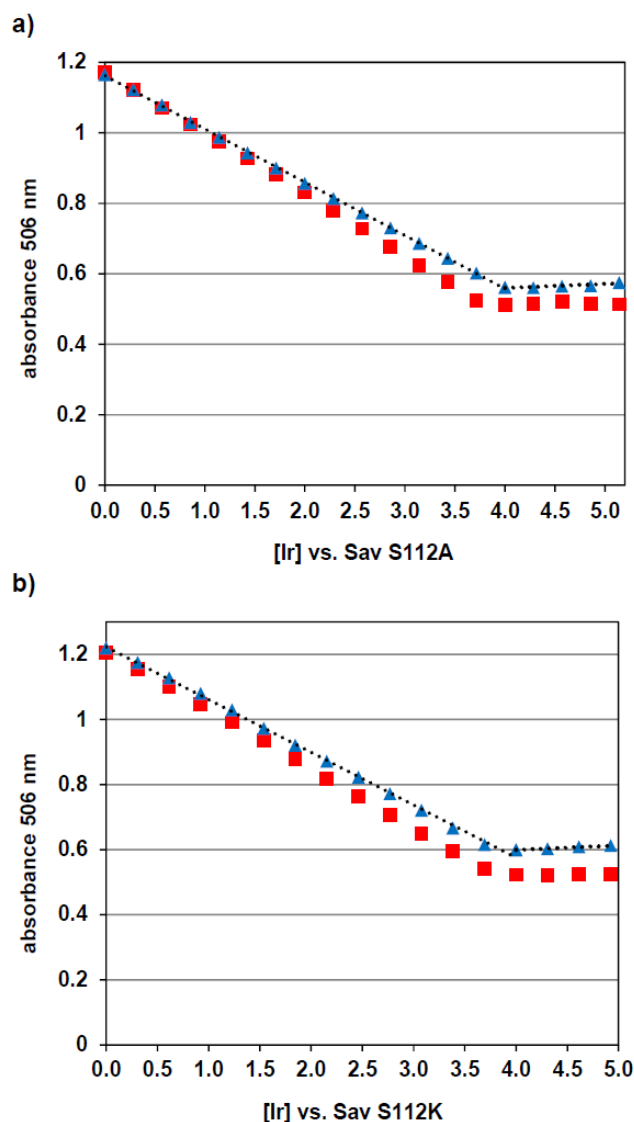


Figure S11 HABA-displacement titration assay by  $[\text{Cp}^*\text{Ir}(\text{biot-}p\text{-L})\text{Cl}]$  ( $\blacktriangle$ , blue triangles) and biotin ( $\blacksquare$ , red squares) in the presence of Sav S112 A a) and Sav S112K b). The linear decrease (dotted line) of the absorbance at  $\lambda_{\text{max}}$  506 nm (caused by the quantitative displacement of HABA  $\subset$  Sav by  $[\text{Cp}^*\text{Ir}(\text{biot-}p\text{-L})\text{Cl}]$ ) precludes the determination of a precise dissociation constant but sets a lower limit at  $K_d > 10^9 \text{ M}^{-1}$ . The molecular weight of Sav was adjusted to take into consideration the presence of residual salts.<sup>7</sup>

## References

- (1) Köhler, V.; Mao, J.; Heinisch, T.; Pordea, A.; Sardo, A.; Wilson, Y. M.; Knörr, L.; Creus, M.; Prost, J.-C.; Schirmer, T.; Ward, T. R. *Angew. Chemie Int. Ed.* **2011**, *123*, 11055–11058.
- (2) Galizia, A.; de Lalla, C.; Nardone, E.; Santambrogio, P.; Brandazza, A.; Sidoli, A.; Arosio, P. *Protein Expr. Purif.* **1998**, *14*, 192–196.
- (3) Wilson, Y. M.; Dürrenberger, M.; Ward, T. R. In *Engineering Handbook, Volume III*; Wiley-VCH: Weinheim, 2012.
- (4) Kada, G.; Kaiser, K.; Falk, H.; Gruber, H. J. *Biochim. Biophys. Acta* **1999**, *1427*, 44–48.
- (5) Michaelis, L.; Menten, M. M. L. *Biochem. Z.* **1913**, *49*, 333–369.
- (6) Haldane, J. *Enzymes*; Longman, Green and Co: New York, 1930.
- (7) Skander, M.; Humbert, N.; Collot, J.; Gradinaru, J.; Klein, G.; Loosli, A.; Sauser, J.; Zocchi, A.; Gilardoni, F.; Ward, T. R. *J. Am. Chem. Soc.* **2004**, *126*, 14411–14418.
- (8) Batty, T. G. G.; Kontogiannis, L.; Johnson, O.; Powell, H. R.; Leslie, A. G. W. *Acta Crystallogr. D* **2011**, *67*, 271–281.
- (9) Evans, P. *Acta Crystallogr. D* **2011**, *67*, 282–292.
- (10) McCoy, A. J.; Grosse-Kuntze, R. W.; Adams, P. D.; D., W. M.; Storoni, C. L.; Read, R. J. *J. Appl. Cryst.* **2007**, *40*, 658–674.
- (11) Creus, M.; Pordea, A.; Rossel, T.; Sardo, A.; Letondor, C.; Ivanova, A.; Letrong, I.; Stenkamp, R. E.; Ward, T. R. *Angew. Chemie Int. Ed.* **2008**, *47*, 1400–1404.
- (12) Murshudov, G. N.; Vagin, A. A.; Dodson, E. J. *Acta Cryst. D.* **1997**, *53*, 240–255.
- (13) Adams, P. D.; Afonine, P. V.; Bunkóczi, G.; Chen, V. B.; Davis, I. W.; Echols, N.; Headd, J. J.; Hung, L.-W.; Kapral, G. J.; Grosse-Kuntze, R. W.; McCoy, A. J.; Moriarty, N. W.; Oeffner, R.; Read, R. J.; Richardson, D. C.; Richardson, J. S.; Terwilliger, T. C.; Zwart, P. H. *Acta Crystallogr. D* **2010**, *66*, 213–221.
- (14) Emsley, P.; Cowtan, K. *Acta Crystallogr. D* **2004**, *60*, 2126–2132.
- (15) Zhao, Y.; Truhlar, D. G. *J. Chem. Phys.* **2006**, *125*, 1–18.
- (16) Frisch, M. J.; Trucks, G. W.; Schlegel, H. B.; Scuseria, G. E.; Robb, M. A.; Cheeseman, J. R.; Scalmani, G.; Barone, V.; Mennucci, B.; Petersson, G. A.; Nakatsuji, H.; Caricato, M.; Li, X.; Hratchian, H. P.; Izmaylov, A. F.; Bloino, J.; Zheng, G.; Sonnenberg, J. L.; Hada, M.; Ehara, M.; Toyota, K.; Fukuda, R.; Hasegawa, J.; Ishida, M.; Nakajima, T.; Honda, Y.; Kitao, O.; Nakai, H.; Vreven, T.; Montgomery, J. A., Jr.; Peralta, J. E.; Ogliaro, F.; Bearpark, M.; Heyd, J. J.; Brothers, E.; Kudin, K. N.; Staroverov, V. N.; Kobayashi, R.; Normand, J.; Raghavachari, K.; Rendell, A.; Burant, J. C.; Iyengar, S. S.; Tomasi, J.; Cossi, M.; Rega, N.; Millam, J. M.; Klene, M.; Knox, J. E.; Cross, J. B.; Bakken, V.; Adamo, C.; Jaramillo, J.; Gomperts, R.; Stratmann, R. E.; Yazyev, O.; Austin, A. J.; Cammi, R.; Pomelli, C.; Ochterski, J. W.; Martin, R. L.; Morokuma, K.; Zakrzewski, V. G.; Voth, G. A.; Salvador, P.; Dannenberg, J. J.; Dapprich, S.; Daniels, A. D.; Farkas, Ö.; Foresman, J. B.; Ortiz, J. V.; Cioslowski, J.; Fox, D. J. *Gaussian 09, Revision A.1*, 2009.
- (17) Weigend, F.; Ahlrichs, R. *Phys. Chem. Chem. Phys.* **2005**, *7*, 3297–3305.
- (18) Hehre, W. J. *J. Chem. Phys.* **1972**, *56*, 2257–2261.
- (19) Verdonk, M. L.; Cole, J. C.; Hartshorn, M. J.; Murray, C. W.; Taylor, R. D. *PROTEINS Struct. Funct. Bioinforma.* **2003**, *52*, 609–623.
- (20) Eldridge, M. D.; Murray, C. W.; Auton, T. R.; Paolini, G. V.; Mee, R. P. *J. Comput. Aided. Mol. Des.* **1997**, *11*, 425–445.
- (21) Baxter, C. A.; Murray, C. W.; Clark, D. E.; Westhead, D. R.; Eldridge, M. D. *Proteins* **1998**, *33*, 367–382.
- (22) Zimbron, J. M.; Sardo, A.; Heinisch, T.; Wohlschlagler, T.; Gradinaru, J.; Massa, C.; Schirmer, T.; Creus, M.; Ward, T. R. *Chem. An Eur. J.* **2010**, *16*, 12883–12889.
- (23) Zimbron, J. M.; Heinisch, T.; Schmid, M.; Hamels, D.; Nogueira, E. S.; Schirmer, T.; Ward, T. R. *J. Am. Chem. Soc.* **2013**, *135*, 5384–5388.
- (24) Dürrenberger, M.; Heinisch, T.; Wilson, Y. M.; Rossel, T.; Nogueira, E.; Knörr, L.; Mutschler, A.; Kersten, K.; Zimbron, M. J.; Pierron, J.; Schirmer, T.; Ward, T. R. *Angew. Chemie Int. Ed.* **2011**, *50*, 3026–3029.
- (25) Pierron, J.; Malan, C.; Creus, M.; Gradinaru, J.; Hafner, I.; Ivanova, A.; Sardo, A.; Ward, T. R. *Angew. Chemie Int. Ed.* **2008**, *47*, 701–705.
- (26) Muñoz Robles, V.; Ortega-Carrasco, E.; Fuentes, E. G.; Lledós, A.; Maréchal, J.-D. *Faraday Discuss.* **2011**, *148*, 137.
- (27) Chase, F.; Avenue, B. *Curr. Opin. Struct. Biol.* **2002**, *12*, 431–440.
- (28) Dapprich, S.; Komáromi, I.; Byun, K. S.; Morokuma, K.; Frisch, M. J. *J. Mol. Struct.* **1999**, *461-462*, 1–21.
- (29) Bakowies, D.; Thiel, W. *J. Phys. Chem.* **1996**, *3654*, 10580–10594.
- (30) Perdew, J. P.; Emzerhof, M.; Burke, K. *J. Chem. Phys.* **1996**, *105*, 9982–9985.
- (31) Perdew, J.; Burke, K.; Emzerhof, M. *Phys. Rev. Lett.* **1996**, *77*, 3865–3868.
- (32) Muñoz Robles, V.; Vidossich, P.; Lledós, A.; Ward, T. R.; Maréchal, J.-D. *ACS Catal.* **2014**, *4*, 833–842.
- (33) Cornell, W. D.; Cieplak, P.; Bayly, C. I.; Gould, I. R.; Metz, K. M.; Ferguson, D. M.; Spellmeyer, D. C.; Fox, T.; Caldwell, J. W.; Kollman, P. A. *J. Am. Chem. Soc.* **1995**, *117*, 5179–5197.
- (34) Jitř Václavík; Marek Kuzma, J. P.; Kačer, P. *Organometallics* **2011**, *30*, 4822–4829.
- (35) Martins, J. E. D.; Clarkson, G. J.; Wills, M. *Org. Lett.* **2009**, *11*, 847–850.
- (36) Pettersen, E. F.; Goddard, T. D.; Huang, C. C.; Couch, G. S.; Greenblatt, D. M.; Meng, E. C.; Ferrin, T. E. *J. Comput. Chem.* **2004**, *25*, 1605–1612.

## 2.2.4 Appendix

The crystal structure of  $[(\eta^5\text{-Cp}^*)\text{Ir}(\text{biot-}p\text{-L})\text{Cl}]\subset\text{S112A}$  revealed that the absolute configuration of Ir is (*S*) which yields (*R*)- $[(\eta^5\text{-Cp}^*)\text{Ir}(\text{biot-}p\text{-L})\text{H}]$  upon reaction with formate. Based on this finding, a non-concerted mechanism was suggested for the hydride transfer whereby a CH- $\pi$  interaction between Cp\* and the aromatic moiety of the substrate is operating (see section 2.2.2). In addition, it was hypothesized that the lysine-residue K121 of an adjacent monomer may be involved in the protonation of the imine nitrogen. Further experiments were performed to examine if this lysine residue serves as a proton-donor, namely the determination of the  $pK_a$ -value of the imine substrate and kinetic studies of the double-mutant S112A-K121T in which the critical lysine residue is replaced by threonine.

2.2.4.1  $pK_a$  of 6,7-dimethoxy-1-methyl-3,4-dihydroisoquinoline

The behavior of cyclic imines in aqueous solution may be described by three equilibrium constants: a hydrolysis constant  $K_H$  which describes the hydrolysis of the C=N bond and two acid-base equilibrium constants which describe the protonation of either the imine ( $K_1$ ) or the open-chain amino ketone ( $K_2$ )<sup>31</sup>:

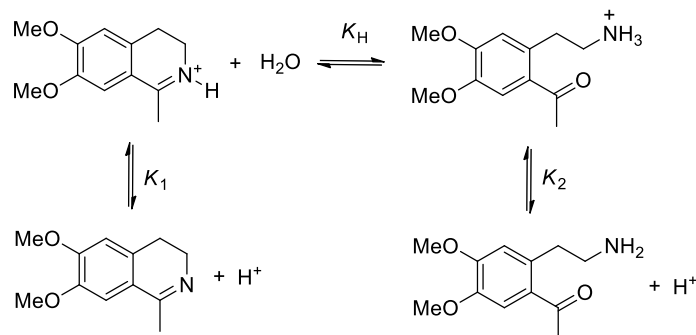


**Figure 2.7** Possible equilibria of 6,7-dimethoxy-1-methyl-3,4-dihydroisoquinoline in water.

The titration of 6,7-dimethoxy-1-methyl-3,4-dihydroisoquinoline with HCl resulted in a typical sigmoidal titration curve with a corresponding  $pK_a$  of approximately 8.5, indicating the existence of a single equilibrium. Two dimensional NMR-experiments (HMBC) performed in water indicate that the imine substrate exists exclusively in its ring-closed form under acidic (pH 2.5) as well as basic (pH 11.5) conditions (see experimental part). This somehow unexpected result may be explained by an unfavorable loss of entropy upon hydrolysis. The chemical shifts obtained for selected  $^1\text{H}$  and  $^{13}\text{C}$  signals at different pH-values between 3 and 11 allowed to locate the  $pK_{a1}$  within a range of 8.5-9 which is in good agreement with the value obtained from the titration (see experimental part).

#### 2.2.4.2 Michaelis-Menten Kinetics of $[(\eta^5\text{-Cp}^*)\text{Ir}(\text{biot-}p\text{-L})\text{H}]\text{C}_{\text{S112A-K121T}}$

If the lysine residue K121A of the adjacent Sav-monomer would act as a proton donor in the transfer hydrogenation process of  $[(\eta^5\text{-Cp}^*)\text{Ir}(\text{biot-}p\text{-L})\text{H}]\text{C}_{\text{S112A}}$ , one would assume that replacing this residue by another polar amino acid downgrades the performance of the resulting double mutant. Indeed,  $[(\eta^5\text{-Cp}^*)\text{Ir}(\text{biot-}p\text{-L})\text{H}]\text{C}_{\text{S112A-K121T}}$  showed an erosion of enantioselectivity compared to the S112A-counterpart (see section 2.2.2). To find out if the double mutant as well displays a lower activity towards the transfer hydrogenation of 6,7-dimethoxy-1-methyl-3,4-dihydroisoquinoline, the Michaelis-Menten kinetics of this ATHase isoform was determined (see section 2.2.3 for a detailed experimental procedure). As observed for the S112A-ATHase, the activity of the metal cofactor within the double mutant decreases when raising the molar ratio  $[\text{Ir}]/\text{Sav-tetramer}$  from. Comparison of the kinetic profiles of  $[(\eta^5\text{-Cp}^*)\text{Ir}(\text{biot-}p\text{-L})\text{H}]$  within the two variants did not show a significant difference in activity as similar  $k_{\text{cat}}$ -values were observed ( $k_{\text{cat}} = 14.1$  and  $11.4 \text{ min}^{-1}$  in case of S112A vs.  $k_{\text{cat}} = 11.5$  and  $9.7 \text{ min}^{-1}$  in case of S112A-K121T).

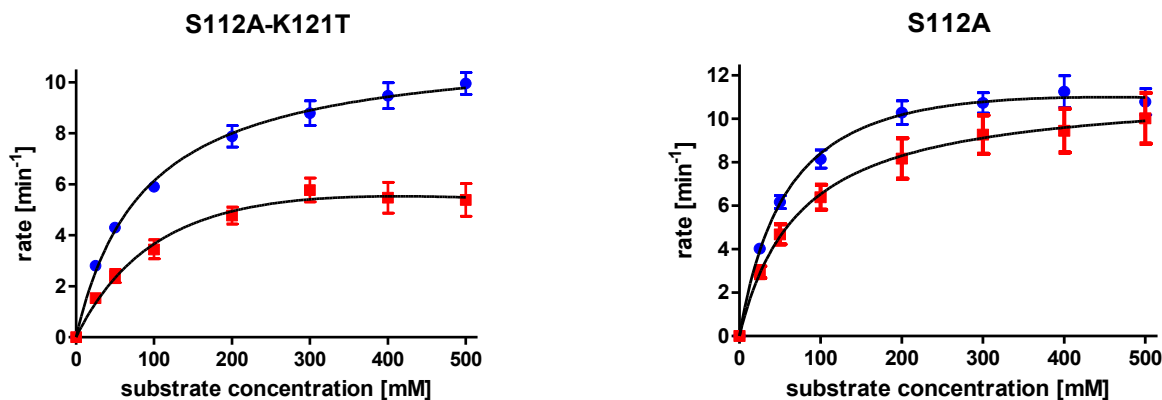


**Figure 2.8** Michaelis-Menten plots of  $[(\eta^5\text{-Cp}^*)\text{Ir}(\text{biot-}p\text{-L})\text{H}]\text{cSav-S112A-K121T}$  (left) and  $[(\eta^5\text{-Cp}^*)\text{Ir}(\text{biot-}p\text{-L})\text{H}]\text{cSav-S112A}$  (right, see section 2.2.2) for the transfer hydrogenation of 6,7-dimethoxy-1-methyl-3,4-dihydroisoquinoline. The color scheme represents kinetic profiles at different molar ratios of the Ir-complex versus free Sav biotin binding sites: blue trace 0.25 eq [Ir], red trace 0.5 eq [Ir]. Initial rates were plotted with respect to the concentration of the Ir-complex. The concentration of Sav free biotin binding sites was 100  $\mu\text{M}$ .

In conclusion, these results on one hand support that an ionic, non-concerted mechanism is operative in the transfer hydrogenation of 6,7-dimethoxy-1-methyl-3,4-dihydroisoquinoline catalyzed by  $[(\eta^5\text{-Cp}^*)\text{Ir}(\text{biot-}p\text{-L})\text{Cl}]\text{cS112A}$  as the imine nitrogen seems to be protonated under the experimental conditions (typically pH 6.5-7.5). Both the activity and selectivity of the S112A-ATHase decrease significantly above pH 8 (see experimental part). This behavior is not necessarily explained by a decreased fraction of the protonated imine as other processes such as deprotonation of amino acid residues of Sav may have an influence on the performance of the hybrid catalyst.

The functional role of lysine 121K could not be confirmed as its absence does not decrease the reaction rate with respect to the S112A-K121T isoform. However, when comparing the two ATHase variants it has to be considered that additional beneficial effects (e.g. structural changes) may have an impact on the activity of the double mutant ATHase which counterbalance the possible reduced activity caused by the absence of the lysine residue.



## 2.3 Conclusions and Outlook

The substrate scope of artificial transfer hydrogenases based on the biotin-(strept)avidin technology could successfully be expanded from the reduction of ketones to cyclic imines. The introduction of a biotinylated iridium pincer complex  $[(\eta^5\text{-Cp}^*)\text{Ir}(\text{Biot-}p\text{-L})\text{Cl}]$  within streptavidin affords an artificial imine reductase which was optimized by saturation mutagenesis at position 112. Thereby, both enantiomers of the corresponding imine are accessible using the same organometallic moiety, affording 96% ee in favor of the (*R*)-enantiomer in case of  $[(\eta^5\text{-Cp}^*)\text{Ir}(\text{Biot-}p\text{-L})\text{Cl}]_{\text{S112A}}$  and 78% ee in case of  $[(\eta^5\text{-Cp}^*)\text{Ir}(\text{Biot-}p\text{-L})\text{Cl}]_{\text{S112K}}$  for the production of salsolidine.

Although the observed Michaelis-Menten behavior may rely on a simplified mechanistic model, the obtained kinetic parameters in combination with structural data and docking studies allowed to establish a qualitative model of the mode of action of these hybrid catalysts. Nevertheless, the role of the formate concentration should be investigated in prospective kinetic studies.

The high robustness and activity of the ATHases (up to 4000 TON could be achieved) renders them to ideal candidates for laboratory evolution protocols. This procedure eventually may allow to further optimize ATHases in order to identify catalysts for the enantioselective reduction of more challenging substrates.

## 2.4 References

1. a) Meerwein, H.; Schmidt, R. *Justus Liebigs Annalen der Chemie* **1925**, *444*, 221. b) Verley, A. *Bull. Soc. Chim. Fr.* **1925**, *37*, 537. c) Ponndorf, W. *Angew. Chem.* **1926**, *39*, 138.
- 2) Descottes, G.; Sinou, D. *Tetrahedron Lett.* **1976**, *45*, 4083.
- 3) Reetz, M. T.; Li, X. *J. Am. Chem. Soc.* **2006**, *128*, 1044.
- 4) Baratta, W.; Benedetti, F.; Del Zotto, A.; Fanfoni, L.; Felluga, F.; Magnolia, S.; Putignano, E.; Rigo, P. *Organometallics* **2010**, *29*, 3563.
- 5) Nordin, S. J. M.; Roth, P.; Tarnai, T.; Alonso, D. A.; Brandt, P.; Andersson, P. G. *Chem. Eur. J.* **2001**, *7*, 1431.
- 6) Takehara, J.; Hashiguchi, S.; Fujii, A.; Inoue, S.; Ikariya, T.; Noyori, R. *J. Chem. Soc., Chem. Commun.* **1996**, 233.
- 7) Hashiguchi, S.; Fujii, A.; Takehara, J.; Ikariya, T.; Noyori, R. *J. Am. Chem. Soc.* **1995**, *117*, 7562.
8. a) Mashima, K.; Abe, T.; Tani, K. *Chemistry Lett.* **1998**, 1199. b) Mashima, K.; Abe, T.; Tani, K. *Chemistry Lett.* **1998**, 1201.
- 9) Noyori, R.; Hashiguchi, S. *Acc. Chem. Res.* **1997**, *30*, 97.
- 10) Matsumura, K.; Hashiguchi, S.; Ikariya, T.; Noyori, R. *J. Am. Chem. Soc.* **1997**, *119*, 8738
11. a) Haack, K.J.; Hashiguchi, S.; Fujii, A.; Ikariya, T.; Noyori, R. *Angew. Chem. Int. Ed. Engl.* **1997**, *36*, 285. b) Yamakawa, M.; Ito, H.; Noyori, R. *J. Am. Chem. Soc.* **2000**, *122*, 1466. c) Alonso, D.A.; Brandt, P.; Nordin, S.J.M.; Andersson, P.G. *J. Am. Chem. Soc.* **1999**, *121*, 9580.
- 12) Soni, R.; Cheung, F.K.; Clarkson, G.C.; Martins, J.E.D.; Grahamband, M.A.; Wills, M. *Org. Biomol. Chem.*, **2011**, *9*, 3290.
- 13) Yamakawa, M.; Yamada, I.; Noyori, R. *Angew. Chem. Int. Ed.* **2001**, *40*, 2818.
- 14) Dub, P.A.; Ikariya, T. *J. Am. Chem. Soc.* **2013**, *135*, 2604.
- 15) Uematsu, N.; Fujii, A.; Hashiguchi, S.; Ikariya, T.; Noyori, R. *J. Am. Chem. Soc.* **1996**, *118*, 4916.
- 16) Aberg, J.B.; Samec, J.S.M.; Bäckvall, J.E. *Chem. Commun.* **2006**, 2771.
- 17) Blackmond, D.G.; Ropic, M.; Stefinovic, M. *Organic Process Research & Development* **2006**, *10*, 457.

- 18) Martins, J.E.D.; Clarkson, G.J.; Wills, M. *Org. Lett.* **2009**, *11*, 847.
- 19.a) Casey, C.P.; Singer, S.W.; Powell, D.R.; Hayashi, R.K.; Kavana, M. *J. Am. Chem. Soc.* **2001**, *123*, 1090. b) Casey, C.P.; Clark, T.B.; Guzei, I.A. *J. Am. Chem. Soc.* **2007**, *129*, 11821.
- 20.a) Samec, J.S.M.; Ell, A.H.E.; Bäckvall, J.E. *Chem. Commun.* **2004**, 2748. b) Éll, A.H.E.; Johnson, Bäckvall, J.E. *Chem. Commun.* **2003**, 1652.
- 21.a) Canivet, J.; Süss-Fink, G. *Green Chem.* **2007**, *9*, 391. b) Li, L.; Wu, J.; Wang, F.; Liao, J.; Zhang, H.; Lian, C.; Zhu, J.; Deng, J. *Green Chem.* **2007**, *9*, 23. c) Romain, C.; Gaillard, S.; Elmkaddem, M.K.; Toupet, L. Fischmeister, C.; Thomas, C.M.; Renaud, J.L. *Organometallics* **2010**, *29*, 1992.
- 22) Wu, X.; Li, X.; King, F.; Xiao, J. *Angew. Chem. Int. Ed.* **2005**, *44*, 3407.
- 23.a) Wu, X.; Li, X.; Zanotti-Gerosa, A.; Pettman, A.; Liu, J.; Mills, A.J.; Xiao, J. *Chem. Eur. J.* **2008**, *14*, 2209.
- 24) Wang, C.; Li, C.; Wu, X.; Pettman, A.; and Xiao, J. *Angew. Chem. Int. Ed.* **2009**, *48*, 6524.
- 25) Abura, T.; Ogo, S.; Watanabe, Y.; Fukuzumi, S. *J. Am. Chem. Soc.* **2003**, *125*, 4149.
- 26) Letondor, C.; Pordea, A.; Humbert, N.; Ivanova, A.; Mazurek, S.; Novic, M.; Ward, T.R. *J. Am. Chem. Soc.* **2006**, *128*, 8320.
- 27) Creus, M.; Pordea, A.; Rossel, T.; Sardo, A.; Letondor, C.; Ivanova, A.; LeTrong, I.; Stenkamp, R.E.; Ward, T.R. *Angew. Chem. Int. Ed.* **2008**, *47*, 1400.
- 28) Michaelis, L.; Menten, M.L. *Biochem Z* **1913**, *49*, 333.
- 29) Briggs, G.E.; Haldane, J.B.S. *Biochem J* **1925**, *19*, 338.
- 30) Koike, T.; Ikariya, T. *Adv. Synth. Catal.* **2004**, *346*, 37.
- 31) Zoltewicz, J.A.; Bloom, L.B.; Kem, W.R. *J. Org. Chem.* **1989**, *54*, 4462.



## Chapter 3: Towards *in vivo* Transition Metal Catalysis and its Potential Applications for the Directed Evolution of Artificial Metalloenzymes

### 3.1 Introduction

#### 3.1.1 Principles of Directed Evolution

The outstanding catalytic properties of enzymes result from natural selection which is the "driving force" of evolution. The introduction of mutations may lead to improved or even new catalytic functions which will survive if the related enzyme provides a beneficial feature to the host organism with respect to its adaptability to a particular environment ("survival of the fittest"). Evolution of life therefore can be seen as a random "trial-and-failure" process which selects for the fittest. In contrast, laboratory evolution protocols have a defined goal in order to improve certain properties of an enzyme such as its stability (e.g. towards the presence of organic solvents), activity and selectivity (e.g. towards non-native substrates).<sup>1</sup> Apart from this important difference, directed evolution protocols mimic Darwinian evolutionary processes by performing iterative cycles of mutagenesis and identifying mutants with desired properties. A typical experimental cycle of directed evolution is given in Figure 3.1. Starting point is an enzyme with a desired activity that is wished to be increased or modified. In a first step, sequence diversity is created by mutagenesis of the corresponding DNA sequence. Given the 20 standard proteinogenic amino acids, a protein with an average number of 250 residues gives rise to  $20^{250}$  possible combinations. Even if only a

small part of the resulting proteins is functional, a great variety of structures and functionalities can be obtained.<sup>2</sup> Mutations can either be introduced at certain positions in the primary structure using site-directed mutagenesis (e.g. to replace amino acid residues close to the active site) or throughout the entire gene using random mutagenesis (e.g. by error-prone mutagenesis).<sup>3</sup> Additional diversity may be generated by techniques which recombines homologous DNA fragments to generate new genes such as DNA shuffling<sup>4</sup> or RACHITT (random chimeragenesis on transient templates).<sup>5</sup> After the mutated genes have been cloned into an expression vector and transformed into a suitable host bacterium, the activity of the expressed enzyme variants is determined either by high-throughput screening (HTS)<sup>6</sup> or selection.<sup>7</sup> The advantage of screening is that the enzymatic reaction can eventually be detected directly in the cell cultures or on agar plates. The simplest approach in this context includes visual screens in which the enzymatic reaction generates a product of a different color from the starting material (e.g. *p*-nitrophenyl derivatives to monitor hydrolase activity).<sup>8</sup> In cases where no chromogenic substrate is available for a particular enzyme, other methods such as high performance liquid chromatography (HPLC),<sup>9</sup> nuclear magnetic resonance (NMR),<sup>10</sup> mass spectrometry (MS),<sup>11</sup> gas chromatography (GC),<sup>12</sup> circular dichroism (CD)<sup>13</sup> or fluorescence assisted cell sorting (FACS)<sup>14</sup> etc. have been applied for HTS purposes. However, the major drawback of screening is that each individual clone has to be tested for a desired enzymatic transformation, including those which do not provide a functional biocatalyst. In contrast, selection uncovers only mutants of interest. The principle relies on the circumstance that bacteria experience an advantage in survival if a particular catalyzed transformation produces an essential nutrient that the corresponding cell strain cannot produce itself (auxotrophy)<sup>15</sup> or degrades a toxic compound.<sup>14,16</sup> Growth of single bacterial clones in a medium containing a corresponding precursor or a toxin thus indicates the expression of a highly active enzyme variant ("chemical complementation"). If a given enzymatic reaction allows to apply a selection mechanism, it is usually the method of choice as up to  $10^{13}$  mutants can be analysed whereas screening limits the size of the library to about  $10^4$  variants.<sup>17</sup> Independently of which methodology is used, the consistence of the corresponding model substrate should be as similar as possible to the target substrate

which is desired to convert with the evolved biocatalyst ("you get what you select/screen for").<sup>18</sup> Many laboratory evolution protocols therefore often do not lead to the desired result.

Nevertheless, directed evolution has a great potential to improve particular features of enzymes without the need to know their molecular structure and has been applied successfully to increase the thermal stability,<sup>19</sup> the stability towards organic solvents,<sup>20</sup> the oxidative stability,<sup>21</sup> the alkaline tolerance,<sup>22</sup> and the selectivity as well as the activity towards non-native substrates.<sup>23</sup>

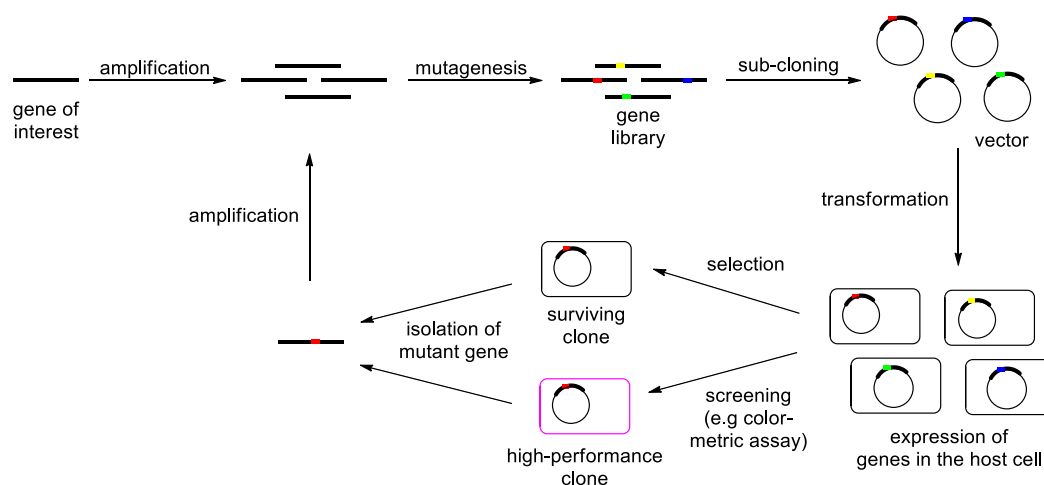


**Fig. 3.1.** Schematic outline of the directed evolution procedure. Colored dots indicate different mutations.

### 3.1.2 Directed Evolution of Artificial Metalloenzymes

The artificial metalloenzymes reported so far by various research groups generally perform as effectively as their homogenous counterparts at best. As outlined in chapter 1, the actual potential of these hybrid catalysts lies in the high tuneability of the respective host protein by means of genetic diversification of the second coordination sphere. Although considerable improvement has been achieved by rational design (see chapter 1), directed evolution protocols for artificial metalloenzymes are highly desirable as a much higher

number of variants can be obtained. This technology was applied successfully to numerous biocatalysts used in academic laboratories and industry.<sup>24</sup> In contrast, to date only one proof-of-principle approaches have been reported to expand directed evolution to hybrid catalysts.

Reetz and coworkers used a "laboratory evolution protocol" to improve the enantioselectivity of an artificial hydrogenase based on the biotin-(strept)avidin technology towards the reduction of  $\alpha$ -acetamido-acrylic acid methyl ester.<sup>25</sup> Selected residues in proximity of the active site were randomized specifically in an iterative manner by applying CAST (combinatorial active site saturation test). The corresponding positions were identified by modelling the biotinylated Rh(I)-diphosphine complex into the X-ray crystall structure of streptavidin-biotin and comprise residues close to the metal center which directly influence the conformation of the metal cofactor-substrate complex as well as more distant amino acids potentially having an impact on the protein structure as they are involved in hydrogen bondings of secondary elements. In each saturation mutagenesis experiment about two to three hundred clones were tested in the hydrogenation, thereby covering >95 % of all possible mutants. Saturation mutagenesis was performed at positions 110, 112 and 124, leading to the artificial hydrogenase variant Sav-S112G which displays a slightly improved (*R*)-enantioselectivity (35% ee) compared to the wild type enzyme (23 % ee). Two further rounds of saturation mutagenesis resulted in the N49V isoform, providing the hydrogenated product in 65% ee.

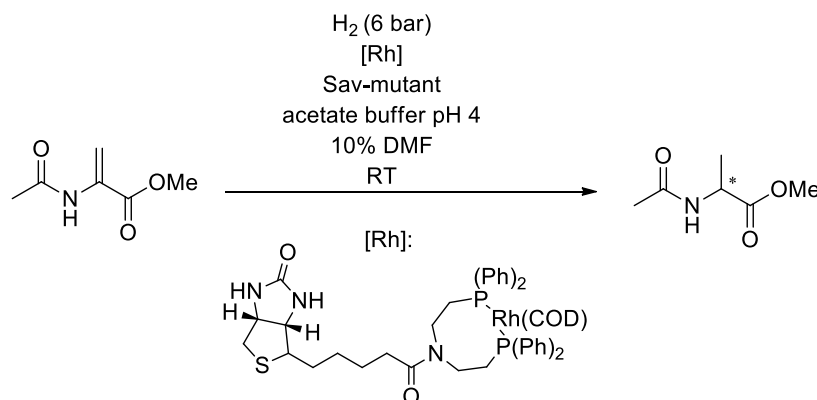


**Fig. 3.2.** Benchmark reaction for the directed evolution of an artificial hydrogenase reported by Reetz et al.<sup>25</sup>



Although the modest selectivity of the final artificial hydrogenase variant is far lower than one would expect for from such an evolutionary approach, this study is noteworthy as it shows that directed evolution in principle can be applied to hybrid catalysts and illustrates the challenges that arise by doing so. The poor result can partially be explained with the fact that only a relatively small library of Sav-isoforms could be employed which is traced back to the poor expression levels of some mutants. This restricts the the screening effort as the bacteria cultures become too large to produce thousands of mutants in parallel (e.g. in microtiter plates). In contrast to natural enzymes, chemical catalysts exhibit lower catalytic activities and therefore larger amounts of protein is required when performing directed evolution of hybrid catalysts. In this context it has also to be considered that the amount of protein cannot be determined for each mutant when generating very large protein libraries and therefore the metal cofactor may be present in an excess compared to the host. Since in this case the outcome of the catalysis would be biased, it has to be ensured that the incorporated metal cofactor is significantly more active than the free one (e.g. through a ligand exchange within the protein scaffold) or that the free metal complex is inactive (e.g. by the presence of an inhibitory ligand that has no access to the protein-embedded metal). Furthermore, catalysis should ideally be performed in crude cell extracts or in living cells. This on one hand avoids the time-consuming purification step of the mutant proteins which significantly expands the size of the library that can be screened. On the other hand, the use of living cells allows to apply selection to identify high-performance (hybrid) catalysts. Although not explicitly stated by Reetz and coworkers, it is likely that the Sav-mutants were -at least partially- purified before being subjected to catalysis. However, performing transition metal catalysis in living systems is indeed a challenging task as the presence of cellular metabolites significantly reduces the activity of the corresponding catalysts and therefore may be the major hurdle when evolving artificial metalloenzymes in a Darwinian approach.<sup>26</sup>

## 3.2 Towards *in vivo* Transition Metal Catalysis

### 3.2.1 Preamble: Comment on Publications

In order to perform directed evolution of artificial transfer hydrogenases or apply organometallic chemistry in context of synthetic biology, the activity of the corresponding catalyst in presence of cellular environment has to be ensured. Furthermore, it has to be considered that the catalyst may interact with different cellular components and therefore displays toxic effects which affect the viability of the cell.

With the aim of performing *in vivo* transition metal catalysis, two main challenges have been identified. First, thiols mainly present in the form of glutathione may inactivate the catalyst. Second, the cellular proteins and metal complexes often suffer from mutual inhibition. This chapter summarizes the efforts to overcome these challenges and presents two possible selection systems which may be applied in the directed evolution of artificial transfer hydrogenases.

#### 3.2.1.1 Neutralizing the Detrimental Effect of Glutathione on Precious Metal Catalysts

Glutathione ( $\gamma$ -L-Glutamyl-L-cysteinylglycine, GSH) is a one electron donor which among other functions serves as a scavenger of reactive oxygen species (ROS) whereby it is oxidised to dimeric glutathione disulfide (GSSG).<sup>27</sup> Due to its high cytosolic concentration (up to 17 mM!),<sup>28</sup> glutathione is one of the main source of free thiol groups and therefore may contribute significantly to the poisoning of soft transition metal catalysts within the cell. Indeed, addition of GSH severely inhibits the catalytic performance of  $[(\eta^5\text{-Cp}^*)\text{Ir}(\text{Biot-}p\text{-L})\text{Cl}]$  as well as the respective hybrid catalysts  $[(\eta^5\text{-Cp}^*)\text{Ir}(\text{Biot-}p\text{-L})\text{Cl}]\text{cS112A}$  and  $[(\eta^5\text{-Cp}^*)\text{Ir}(\text{Biot-}p\text{-L})\text{Cl}]\text{cS112K}$  and no activity towards the reduction of 6,7-dimethoxy-1-methyl-3,4-dihydroisoquinoline was observed. Subsequently, a selection of oxidizing agents and Michael acceptors known to react with the thiol group of GSH were tested to neutralize the detrimental effect of GSH on the

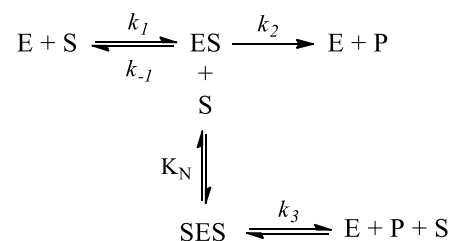
precious metal catalyst. This screening was performed using purified Sav in reactions spiked with GSH and led to the identification of some promising "GSH-neutralizing" reagents. Among these, Diamide (1,1'-azobis(*N,N*-dimethylformamide)) proved to be efficient as well in *E. coli* cell free extracts (cfe) and cell lysates containing Sav-mutants. Thereby, the presence of Sav turned out to be beneficial for the catalytic performance of  $[(\eta^5\text{-Cp}^*)\text{Ir}(\text{Biot-}p\text{-L})\text{H}]$ , affording up to 110 TON in cfe and 86 TON when cell lysate was used as a source of Sav. The results are summarized in section 3.2.2.

### 3.2.1.2 Preventing Mutual Inhibition between Organometallic Catalysts and Cellular Proteins by the Use of Artificial Metalloenzymes

Mutual inhibition between organometallic catalysts and enzymes is a phenomenon which is often observed when combining these two catalytic systems to establish reaction cascades. This may be traced back to interactions between the metal and functional groups of certain amino acids on the surface of proteins.<sup>29</sup> With the aim of performing catalysis *in vivo*, this challenge was addressed in a biomimetic manner. The incorporation of  $[(\eta^5\text{-Cp}^*)\text{Ir}(\text{Biot-}p\text{-L})\text{H}]$  within Sav shields the organometallic moiety and thus prevents inhibitory interactions with natural enzymes. This concept was tested in a benchmark reaction which combined the artificial transfer hydrogenase with evolved monoamine oxidases (MAO) from *Aspergillus niger* to perform concurrent double stereoselective deracemisation of amines. Thereby, the artificial transfer hydrogenase reduces the imine with moderate (*R*)-selectivity whereas the minor (*S*)-amine is converted back to the imine by the highly selective MAO. After several cycles of this process, the (*R*)-amine accumulates up to 99% ee. To prevent deactivation of the Ir-catalyst by hydrogen peroxide generated through the catalytic action of MAO catalase was added to the reaction to decompose this side product. This procedure was successfully applied to several substrates, including 1-methyl-3,4-dihydroisoquinoline, 2-cyclohexyl-1-pyrroline and pseudooxynicotine. The corresponding artificial transfer hydrogenase variants were identified with a screening of Sav-mutants for each substrate. The obtained results indicate

that the artificial transfer hydrogenase may also be a promising catalyst for the reduction of aliphatic imines as up to 86% ee was achieved for the reduction of 2-cyclohexyl-1-pyrroline.

A time plot of the concurrent deracemisation of 1-methyl-3,4-dihydroisoquinoline demonstrates that in the presence of the (*R*)-selective artificial transfer hydrogenase variant  $[(\eta^5\text{-Cp}^*)\text{Ir}(\text{Biot-}p\text{-L})\text{Cl}]\text{C}112\text{T}$  a high enantiomeric excess is more rapidly reached as when the (*S*)-selective artificial transfer hydrogenase  $[(\eta^5\text{-Cp}^*)\text{Ir}(\text{Biot-}p\text{-L})\text{Cl}]\text{C}112\text{K}$  was used. The saturation kinetics of these artificial transfer hydrogenase isoforms revealed that  $[(\eta^5\text{-Cp}^*)\text{Ir}(\text{Biot-}p\text{-L})\text{Cl}]\text{C}112\text{K}$  actually displays a higher  $k_{\text{cat}}$  value than the S112T counterpart but on the same time has a lower affinity for the substrate as reflected by the higher Michaelis constant  $K_M$ . In addition, the S112T-ATHase was found to be prone to significant substrate inhibition. This phenomenon is also observed with natural enzymes at high substrate concentrations and can be explained with the binding of a second substrate molecule in the active site.



whereby  $K_i$  is the dissociation equilibrium constant  $1/K_N$  for the reaction  $\text{SES} \rightleftharpoons \text{S} + \text{ES}$ .<sup>30</sup>

The kinetic profile of the cascade reaction thus can be explained with a combined effect of these kinetic parameters and the selectivity of the ATHases.

Encouraged by these results, the ATHase was used within a more complex reaction cascade and combined with amino acid oxidases. The S112A-ATHase reduces  $\Delta^1$ -piperidine-2-carboxylic acid generated *in situ* from L-lysine by the enzyme L-amino acid oxidase (LAO) from snake venom (*Crotalus atrox*), yielding L-pipecolic acid with moderate enantioselectivity. The latter could be upgraded by addition of a D-amino acid oxidase from pig liver which oxidizes the minor D-pipecolic acid to  $\Delta^1$ -piperidine-2-carboxylic acid.

Again, addition of catalase prevents the deactivation of the metal cofactor by  $\text{H}_2\text{O}_2$  produced by both amino acid oxidases, thus combining the ATHase with three natural enzymes which display complementary and compatible catalytic properties for the production of L-pipecolic acid.

In all presented cascade reactions herein the presence of Sav is crucial to prevent mutual inhibition between the organometallic catalyst and the enzymes. The absence of the host protein leads typically to lower conversions and/or to racemic product. The herein presented strategy thus represents an efficient approach to overcome the incompatibility of both homogenous and bio-catalysts and moreover may allow to perform transition metal catalysis in living cells.

### 3.2.2 Synthetic Cascades are Enabled by Combining Biocatalysts with Artificial Metalloenzymes

Author contribution: Screening of ATHase isoforms for the reduction of 1-methyl-3,4-dihydroisoquinoline and 2-cyclohexyl-1-pyrroline, performing the cascade reactions with 1-methyl-3,4-dihydroisoquinoline, 2-cyclohexyl-1-pyrroline, pseudoxynicotine and lysine (in collaboration with Valentin Köhler), kinetic measurements with the ATHase isoforms for the transfer hydrogenation of 1-methyl-3,4-dihydroisoquinoline.

# Synthetic cascades are enabled by combining biocatalysts with artificial metalloenzymes

V. Köhler<sup>1</sup>, Y. M. Wilson<sup>1</sup>, M. Dürrenberger<sup>1</sup>, D. Ghislieri<sup>2</sup>, E. Churakova<sup>3</sup>, T. Quinto<sup>1</sup>, L. Knörr<sup>1</sup>, D. Häussinger<sup>1</sup>, F. Hollmann<sup>3\*</sup>, N. J. Turner<sup>2\*</sup> and T. R. Ward<sup>1\*</sup>

**Enzymatic catalysis and homogeneous catalysis offer complementary means to address synthetic challenges, both in chemistry and in biology. Despite its attractiveness, the implementation of concurrent cascade reactions that combine an organometallic catalyst with an enzyme has proven challenging because of the mutual inactivation of both catalysts. To address this, we show that incorporation of a  $d^6$ -piano stool complex within a host protein affords an artificial transfer hydrogenase (ATHase) that is fully compatible with and complementary to natural enzymes, thus enabling efficient concurrent tandem catalysis. To illustrate the generality of the approach, the ATHase was combined with various NADH-, FAD- and haem-dependent enzymes, resulting in orthogonal redox cascades. Up to three enzymes were integrated in the cascade and combined with the ATHase with a view to achieving (i) a double stereoselective amine deracemization, (ii) a horseradish peroxidase-coupled readout of the transfer hydrogenase activity towards its genetic optimization, (iii) the formation of L-pipecolic acid from L-lysine and (iv) regeneration of NADH to promote a monooxygenase-catalysed oxyfunctionalization reaction.**

Cellular biochemistry requires the orchestration of metabolic pathways in which many enzyme-catalysed processes are able to function simultaneously, resulting in the production of a wide range of primary and secondary metabolites within the cell. In an attempt to construct artificial cells using the principles of synthetic biology, compartmentalization of cellular processes will need to be mimicked to allow cascade reactions to take place in parallel in an efficient manner<sup>1–6</sup>. Whereas enzymes have evolved in concert and in complex media, and are therefore well suited for cascade reactions, compatibility problems and mutual inactivation are often encountered upon combining chemocatalysts with biocatalysts<sup>7–9</sup>. Such incompatibility may be circumvented by performing cascades in sequential steps or by site-isolation of the individual catalysts through immobilization, heterogeneous or biphasic reaction conditions, encapsulation, and so on<sup>10–24</sup>.

Recently, we have described one approach to cellular compartmentalization in which an *Escherichia coli* cell was engineered to simultaneously express an intracellular enzyme (monoamine oxidase) and also bind palladium nanoparticles in its outer membrane, thereby allowing efficient chemo-enzymatic deracemization of amines<sup>24</sup>. Artificial metalloenzymes resulting from the encapsulation of an organometallic catalyst within a protein scaffold have been shown to combine attractive features of both chemocatalysts and biocatalysts for single-step transformations<sup>25–32</sup>. In the context of concurrent cascade reactions, we reasoned that the artificial cofactor may be effectively shielded by its host protein, thus preventing the mutual inactivation commonly encountered when combining an organometallic catalyst with an enzyme (Fig. 1). To test the validity of the concept, we examined the combination of an artificial transfer-hydrogenase (ATHase) and an oxidase, a catalase, an amino-acid oxidase and a monooxygenase (Fig. 2). For this purpose, we rely on the incorporation of a biotinylated [Cp\*Ir(Biot-*p*-L)Cl] complex within streptavidin (Sav hereafter) as ATHase using sodium formate as hydride source (Figs 1 and 2).

## Results and discussion

**Double stereoselective deracemization of amines.** In recent years, evolved monoamine oxidases (MAO-N from *Aspergillus niger*) have found widespread applications in the synthesis of enantiopure amines<sup>33,34</sup>. For this purpose, a highly (*S*)-selective MAO is combined with a stoichiometric reducing agent (for example, H<sub>3</sub>N·BH<sub>3</sub>)<sup>34</sup> or with a heterogeneous reduction catalyst<sup>24</sup>. Efforts to combine MAO with a homogeneous imine reduction catalyst have proven challenging thus far: indeed, on combining the transfer hydrogenation catalyst [Cp\*Ir(Biot-*p*-L)Cl] with MAO, we observed mutual inactivation (Fig. 1). Only modest levels of amine could be detected starting from the imine, nor could imine be detected in significant amounts starting from the racemic amine (Table 1, entries 1, 2). These observations suggest that the biocatalyst and chemocatalyst are incompatible. In the chemo-enzymatic dynamic kinetic resolution of alcohols and amines, as pioneered by Bäckvall, inactivation may be circumvented by performing the cascade reaction in an organic solvent<sup>21,22</sup>. This strategy effectively provides a phase separation between the highly robust and enantioselective enzyme (for example, CALB) and the organometallic racemization catalyst.

In a biomimetic spirit, we speculated that molecular compartmentalization of the organometallic imine reduction catalyst within a protein scaffold might shield it from the biocatalyst, thus preventing mutual inactivation. With this goal in mind, we set out to investigate the potential of cascade reactions in the presence of ATHase based on the supramolecular incorporation of a catalytically active [Cp\*Ir(biot-*p*-L)Cl] complex within streptavidin (Figs 1, 2). Initially, the individual reaction steps were performed with a **1-red** and **1-ox** (1-methyl-1,2,3,4-tetrahydroisoquinoline and 1-methyl-3,4-dihydroisoquinoline) couple. This led to the identification of [Cp\*Ir(biot-*p*-L)Cl]·Sav S112T (59% enantiomeric excess (e.e.) (*R*)-**red-1**) and [Cp\*Ir(biot-*p*-L)Cl]·Sav S112K (46% e.e. (*S*)-**red-1**) as well as MAO-N-9 for the oxidation of (*S*)-**red-1** (Table 1, entries 3 and 4; Supplementary Tables S2, S5)<sup>35,36</sup>.

<sup>1</sup>Department of Chemistry, University of Basel, Spitalstrasse 51, CH-4056 Basel, Switzerland, <sup>2</sup>School of Chemistry, University of Manchester, Manchester Institute of Biotechnology, 131 Princess Street, Manchester M1 7DN, UK, <sup>3</sup>Department of Biotechnology, Delft University of Technology, Julianalaan 136, 2628BL Delft, The Netherlands. \*e-mail: F.Hollmann@tudelft.nl; Nicholas.Turner@manchester.ac.uk; thomas.ward@unibas.ch

## ARTICLES

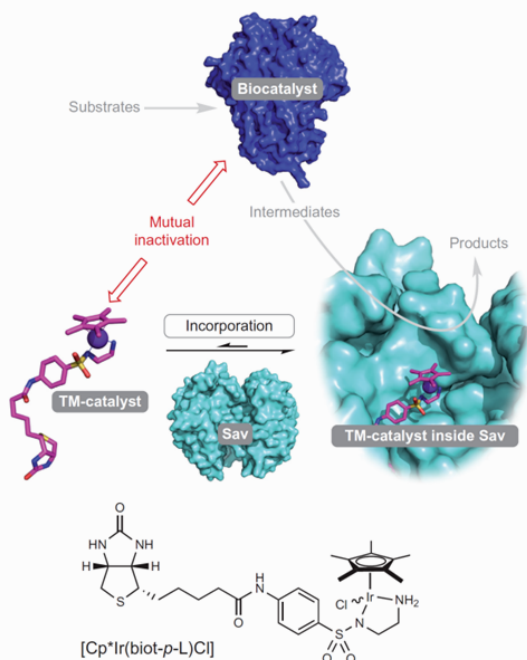


**Figure 1** | Reaction cascades resulting from combining an ATHase with a biocatalyst. The organometallic transfer-hydrogenation catalyst [Cp\*Ir(biot-*p*-L)Cl] and biocatalyst suffer from mutual inactivation, thus precluding the implementation of reaction cascades. Relying on the strength of the biotin-streptavidin interaction, incorporation of the biotin-bearing complex [Cp\*Ir(biot-*p*-L)Cl] within streptavidin (Sav) affords an ATHase that is fully compatible with and complementary to a variety of natural enzymes, thus leading to the development of concurrent orthogonal redox cascades.

On incorporating [Cp\*Ir(biot-*p*-L)Cl] in Sav, only modest ATH activity was observed in the presence of MAO-N-9 (Supplementary Fig. S21). We speculated that the H<sub>2</sub>O<sub>2</sub> produced by MAO as a side product may poison the Ir catalyst (Supplementary Table S7)<sup>37</sup>. Upon the addition of a catalase (from bovine liver), quantitative conversion and 99% e.e. in favour of (*R*)-**1-red** was obtained using 0.5 mol% [Cp\*Ir(biot-*p*-L)Cl]·Sav S112T with 0.19 mg MAO/ml. The orthogonal redox cascade yielded identical results on starting from the racemic amine (*rac*-**1-red**) or from the prochiral imine (**1-ox**; Figs 2, 3; Table 1, compare entries 5 and 6). In stark contrast, only negligible MAO activity could be observed with [Cp\*Ir(biot-*p*-L)Cl], in the presence or absence of catalase, highlighting the beneficial effect of the Sav host protein in effectively site-isolating the reductase and the oxygenase (Table 1, entries 1 and 2; Supplementary Table S6).

We next investigated the influence of the Sav isoform on the rate of the cascade reaction. For this purpose, a moderately (*S*)-selective [Cp\*Ir(biot-*p*-L)Cl]·Sav S112K ATHase was combined with MAO-N-9. Although the reaction with Sav S112K had a faster initial rate, it took significantly longer to reach high enantiomeric excess in favour of the (*R*)-enantiomer: 93% e.e. after 23 h with S112K versus 99% e.e. after 8 h with S112T (Fig. 3b; Table 1, entries 6 and 7). The kinetic profile reflects a combined effect of  $k_{\text{cat}}$ ,  $K_M$ ,  $K_{\text{inhib}}$  and selectivity ( $k_{\text{cat(app)}}$  = 5.4 min<sup>-1</sup> [±0.2 min<sup>-1</sup>];  $K_{\text{M(app)}}$  = 55 mM [±5 mM]) compared to the (*R*)-selective ATHase S112T ( $k_{\text{cat(app)}}$  = 1.09 min<sup>-1</sup> [±0.05 min<sup>-1</sup>],  $K_{\text{M(app)}}$  = 4.5 mM [±0.4 mM] with a  $K_{\text{inhib}}$  of 104 mM [±12 mM]) (Fig. 3c, Supplementary Fig. S19). These

## NATURE CHEMISTRY DOI: 10.1038/NCHEM.1498

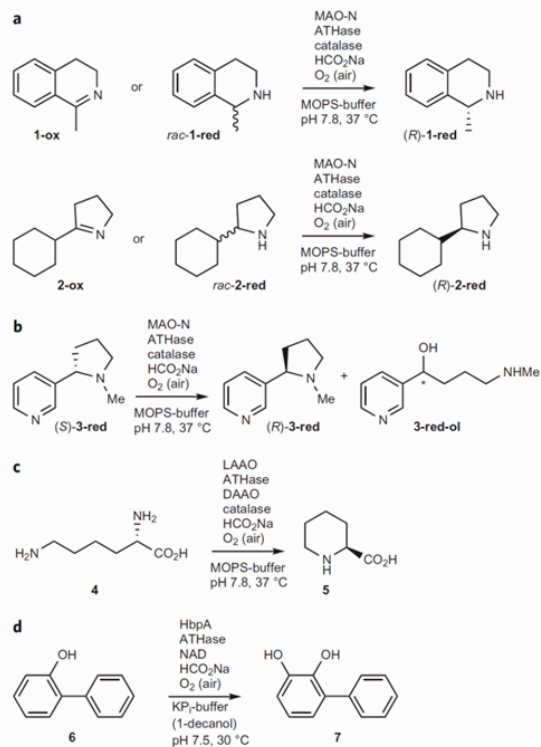


**Figure 2** | Overview of reaction cascades scrutinized in this study. **a**, Reduction of prochiral imines with subsequent deracemization of cyclic amines. **b**, Stereoinversion of natural nicotine, which leads partially to the formation of the chiral alcohol **3-red-ol**. **c**, Formation of L-lysine from L-lysine. **d**, Hydroxylation of 2-hydroxybiphenyl coupled to an ATHase-catalysed NADH regeneration process. MAO-N is a monoamine oxidase variant from *A. niger*. ATHase is an artificial transfer hydrogenase variant, formed by incorporation of [Cp\*Ir(biot-*p*-L)Cl] into a streptavidin variant. LAAO is L-amino acid oxidase from *C. atro*. DAAO is D-amino acid oxidase from porcine kidney. HbpA is 2-hydroxybiphenyl monooxygenase from *P. azaleica*.

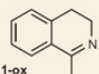
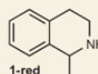
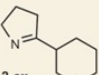
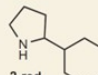
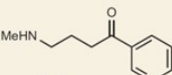
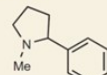
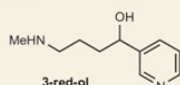
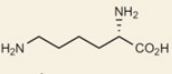
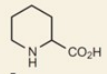
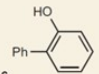
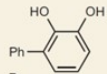
data highlight the versatility of the double stereoselective cascade, with the ATHase and MAO working in concert to expediently produce the enantiopure amine.

These results demonstrate the following: (i) the MAO determines the overall enantioselectivity of the reaction; (ii) a synergistic effect for the matched (*R*)-selective ATHase-(*S*)-selective MAO-N-catalase cascade is operative; (iii) the stereoselectivity of ATHase is unaffected by the presence of both MAO and catalase, as highlighted by the enantioselectivities at the start of the reaction (samples taken after 5 min); (iv) the presence of a His-tag on the MAO-N-9 does not affect the performance of the ATHase, as judged by the initial rates.

**Other amine-imine couples.** To investigate the scope of the concurrent cascade reaction, a secondary amine with purely aliphatic substituents (*rac*-**2-red**) and a tertiary amine (*S*)-**3-red**, as well as their respective oxidation products (**2-ox**, **3-ox**), were subjected to the above enzyme cascade including ATHase. Before this, suitable enzymes for the individual reaction steps (reduction and oxidation) were identified (see Table 1, entries 8 and 9; Supplementary Tables S3 and S4).



**Table 1 | Orthogonal redox cascades combining ATHase with oxidases or oxygenase.**

Entry	Substrate	Product	Sav-mutant	Oxidase/oxygenase	Catalase	Conv. <sup>a</sup> (%)	e.e. (%) (abs.config)
1	 1-ox	 1-red	-	MAO-N-9	Yes	36 <sup>†</sup>	rac.
2	<i>rac</i> -1-red	1-red	-	MAO-N-9	No	<1 <sup>†</sup>	rac.
3	1-ox	1-red	S112T	-	No	>99	59 (R)
4	1-ox	1-red	S112K	-	No	>99	46 (S)
5	<i>rac</i> -1-red	1-red	<b>S112T</b>	<b>MAO-N-9</b>	<b>Yes</b>	<b>&gt;99</b>	<b>&gt;99 (R)</b>
6	1-ox	1-red	<b>S112T</b>	<b>MAO-N-9</b>	<b>Yes</b>	<b>&gt;99</b>	<b>&gt;99 (R)</b> <sup>†</sup>
7	1-ox	1-red	S112K	MAO-N-9	Yes	98	99 (R) <sup>‡</sup>
8	 2-ox	 2-red	S112A	-	No	84 <sup>§</sup>	86 (R)
9	2-ox	2-red	S112A-K121N	-	No	>99 <sup>§</sup>	63 (R)
10	2-ox	2-red	<b>S112A</b>	<b>MAO-N-9</b>	<b>Yes</b>	<b>98<sup>§</sup></b>	<b>99 (R)</b>
11	<i>rac</i> -2-red	2-red	<b>S112A-K121N</b>	<b>MAO-N-9</b>	<b>Yes</b>	<b>99<sup>§</sup></b>	<b>&gt;99 (R)</b>
12	 3-ox	 3-red	S112A-K121T	-	No	76 <sup>‡</sup>	79 (R)
13	3-ox	 3-red-ol	S112G	-	No	79 <sup>*</sup>	30 (ND)
14	( <i>S</i> )-3-red	3-red	<b>S112A-K121T</b>	<b>MAO-N-5</b>	<b>Yes</b>	<b>65<sup>#</sup></b>	<b>&gt;99 (R)</b>
15	 4	 5	-	LAAO	Yes	20	1 (R)
16	4	5	S112A	LAAO	Yes	89	29 (S)
17	( <i>S</i> )-4	5	<b>S112A</b>	<b>LAAO</b> + <b>DAAO</b>	<b>Yes</b>	<b>88<sup>**</sup></b>	<b>86 (S)</b>
18	 6	 7	-	HbpA	No	3	NA
19	6	7	<b>S112A</b>	<b>HbpA</b>	<b>No</b>	<b>&gt;99</b>	<b>NA</b>

The most relevant entries are highlighted in bold. <sup>a</sup>Conversion determined by HPLC or gas chromatography (GC). <sup>†</sup>After 8 h reaction time with 1 mol% ATHase or after 24 h with 0.5 mol%. <sup>‡</sup>After 65 h reaction time with 1 mol% ATHase. <sup>§</sup>Conversion determined by response of 2-ox versus 2-red. <sup>||</sup>Ratio of 3-red to 3-red-ol = 6.6:1, conversion refers to 3-red only. <sup>#</sup>Ratio of 3-red to 3-red-ol = 1:22.8, conversion refers to 3-red-ol only. <sup>\*\*</sup>Additionally ~10% of 3-red-ol were formed. <sup>\*</sup>Determined by 2D NMR. See Methods and Supplementary Information for full experimental details. ND, not determined; NA, not applicable.

In the cascade reaction, the conversion of *rac*-2-red or 2-ox into (*R*)-red-2 was achieved by combining MAO-N-9 with [Cp\*Ir(biot-*p*-L)Cl]-Sav S112A-K121N or [Cp\*Ir(biot-*p*-L)Cl]-Sav S112A and a catalase to afford (*R*)-red-2 (e.e. of 99% (*R*), Table 1, entries 10 and 11). In a preparative deracemization reaction, nearly quantitative yields of red-2 were isolated in 95% e.e. (*R*).

In the case of nicotine red-3, we found that mutations on Sav had a significant influence on product distribution. As reported by Brandänge *et al.*, the tertiary iminium generated upon oxidation of the tertiary amine red-3 exists in equilibrium with the ketoamine ox-3 in aqueous solution<sup>38</sup>. The relative rate of ketoamine versus iminium reduction by the ATHase determines the product distribution 3-red versus 3-red-ol (Table 1, entries 12 and 13). For the reduction step alone, [Cp\*Ir(biot-*p*-L)Cl]-Sav S112A-K121T led to the highest e.e. for nicotine red-3 (79% e.e. (*R*)) with a nicotine red-3 to alcohol red-3-ol ratio of 6.6:1.

For the stereoinversion of (*S*)-nicotine red-3 using the cascade reaction, MAO-N-5 was combined with [Cp\*Ir(biot-*p*-L)Cl]-Sav S112A-K121T and catalase. After 14 h, (*R*)-nicotine was formed from (*S*)-nicotine in >99% e.e. (*R*) at 65% yield, with ~10% yield of alcohol 3-red-ol (35% e.e.; Table 1, entry 14).

**Activity screen of ATHases by a coupled colorimetric assay.** Horseradish peroxidase (HRP) has found broad use in coupled assays, both in medicine and in biotechnology<sup>39</sup>. In this context, a (pro)-dye is rapidly oxidized by HRP, consuming H<sub>2</sub>O<sub>2</sub> and leading to an optical signal. We speculated that substitution of the catalase by HRP may allow the performance of the ATHase in the cascade reaction to be estimated (Fig. 4).

Comparison of the kinetic constants ( $k_{\text{cat}} > 250 \text{ min}^{-1}$ ,  $K_M < 1 \text{ mM}$  for MAO-N-9) indicates that the ATHase step is rate-limiting in the enzyme cascade under the considered reaction conditions (Supplementary Section S2.9). Thus, the HRP-generated optical

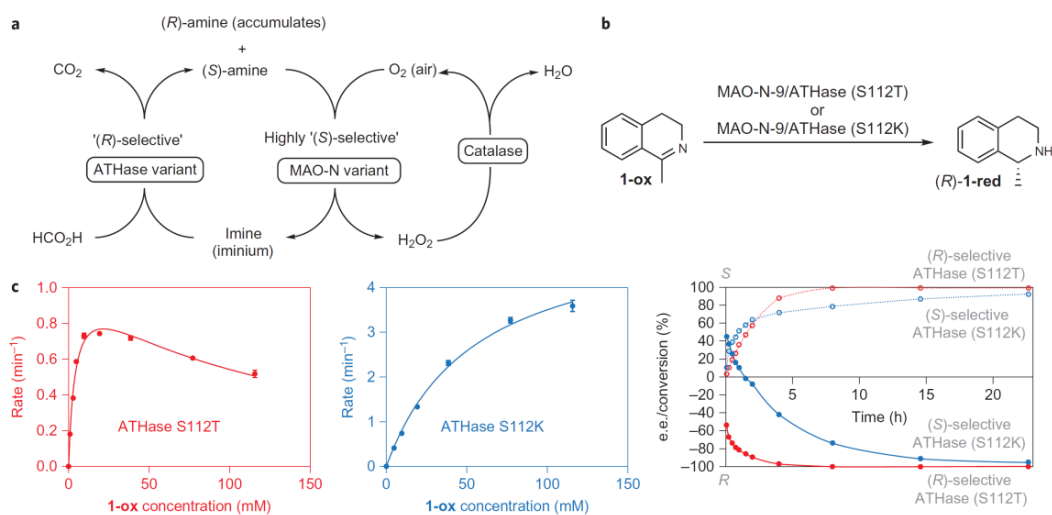


**Figure 3 | Enzyme cascade for the double stereoselective deracemization of amines.** **a**, Schematic representation of the double stereoselective deracemization with MAO-N/ATHase (see Methods and Supplementary Section S2 for experimental details). **b**, Reaction scheme for the production of (R)-1-red via a reaction cascade, and time plot of conversion (dotted lines, empty circles) and enantiomeric excess (solid lines, filled circles) for [Cp\*Ir(biot-*p*-L)Cl]Sav S112T ATHase (red) and [Cp\*Ir(biot-*p*-L)Cl]Sav S112K ATHase (blue). ATHase loading was 1 mol%. **c**, Saturation kinetic curves for [Cp\*Ir(biot-*p*-L)Cl]Sav S112T ATHase (red trace) and [Cp\*Ir(biot-*p*-L)Cl]Sav S112K ATHase (blue trace). Error bars indicate  $\pm 1$  standard deviation, determined from the triplicate measurement of each rate. Although the ATHase rate of the (R)-selective ATHase (S112T variant) is significantly lower than that of the (S)-selective variant (S112K) at the beginning of the reaction, the matched enzyme cascade (that is, S112T MAO-N-9) reaches a high enantiomeric excess in favour of the (R)-amine **1** more rapidly than the mismatched case (that is, S112K MAO-N-9).

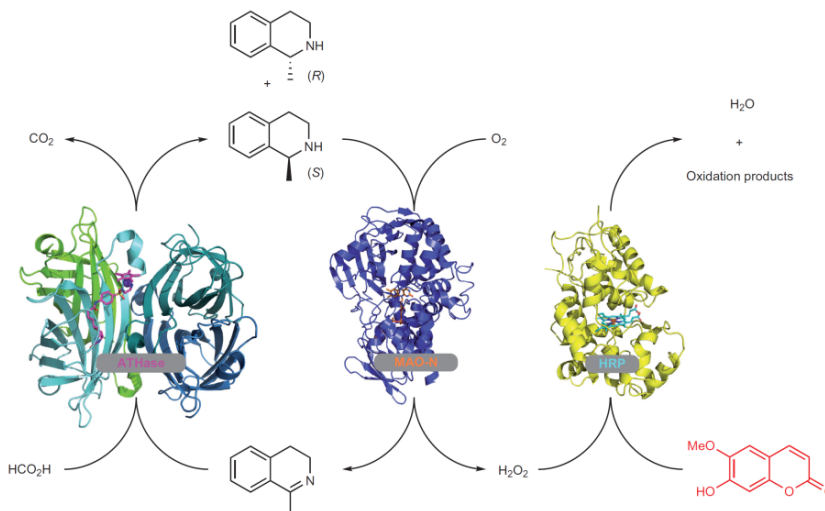


**Figure 4 | Colorimetric assay for the determination of ATHase activity in an enzyme cascade.** The activity of the ATHase in the enzyme cascade is revealed by HRP: the H<sub>2</sub>O<sub>2</sub> generated by MAO-N reacts with a dye (scoipoletin, red) in the presence of HRP and leads to bleaching of scoipoletin.

signature allows comparison of the relative ATHase activities, depending on the Sav isoform.

After screening several dyes/prodyes, we identified scoipoletin as a suitable substrate as it loses its fluorescence upon oxidation: because the MAO-N variant is highly (S)-selective, the optical readout generated by the oxidation of scoipoletin correlates to the

production of (S)-red-1. As the ATHases display modest selectivities ( $E$  values  $\leq 4$ ), sufficient (S)-red-1 is produced to allow the implementation of the coupled assay. By following the decrease in the fluorescence of scoipoletin in the ATHase/MAO/HRP coupled assay, imine-reductases with strongly increased activity (compared to S112T) could be identified. The ATHase [Cp\*Ir(biot-*p*-L)Cl]·

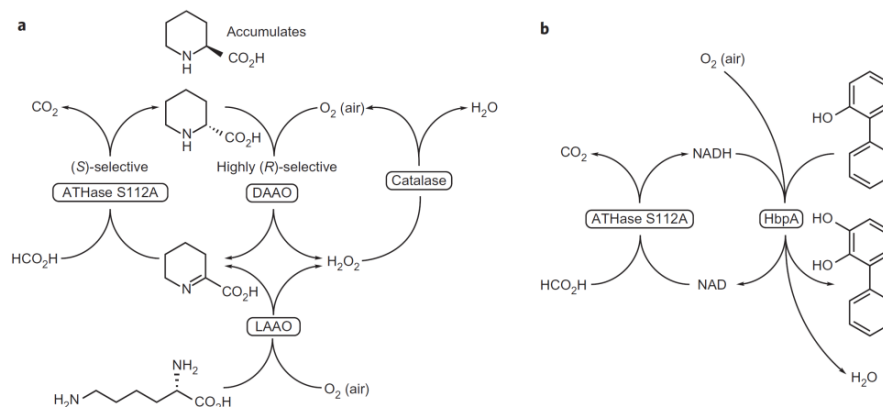


**Figure 5** | Expanding the concept of orthogonal redox cascades to include other enzymes. **a**, Production of L-pipecolic acid from L-lysine requires the combination of an ATHase with an LAAO and a DAAO. Catalase is added to decompose the  $\text{H}_2\text{O}_2$  generated by the AAOs. **b**, Concurrent regeneration of NADH by the ATHase in the presence of a monooxygenase.

K121A displayed kinetic constants of  $k_{\text{cat}(\text{app})} = 20 \text{ min}^{-1}$  ( $\pm 3 \text{ min}^{-1}$ ),  $K_{\text{M}(\text{app})} = 12 \text{ mM}$  ( $\pm 3 \text{ mM}$ ) and  $K_{\text{I}} = 20 \text{ mM}$  ( $\pm 4 \text{ mM}$ ) (Supplementary Fig. S19). The relative order of activities in the assay was in good agreement with the rates determined by high-performance liquid chromatography (HPLC), although for high activities the relative activity was underestimated by the assay (Supplementary Fig. S20).

**Combination of ATHase with amino acid oxidases for the formation of L-pipecolic acid.** Encouraged by the results with MAO, we sought to combine ATHases in more complex cascades with other oxidases. For this purpose, we selected L-lysine (4), which, upon oxidation with an L-amino acid oxidase (LAAO) and reduction with the ATHase, yields pipecolic acid (5). The enantiomeric excess of 5 can be upgraded by combining the LAAO/ATHase/catalase with a D-selective amino acid oxidase (DAAO) (Fig. 5a)<sup>40,41</sup>.

In a first round of screening, the performances of a range of ATHase mutants were screened for the reduction of  $\Delta^1$ -piperidine-2-carboxylic acid generated *in situ* by oxidation of L-lysine with LAAO (from snake venom, *Crotalus atrox*). The Ir-cofactor  $[\text{Cp}^*\text{Ir}(\text{biot-}p\text{-L})\text{Cl}]$  in the absence of Sav showed only a low conversion (TON = 11, turnover number (TON) = moles product/moles catalyst) and led to racemic product, highlighting again the inactivation of the naked catalyst (Table 1, entry 15). In contrast, the ATHase demonstrated promising conversions (up to 90%; TON = 48), albeit with low enantioselectivity. The most (S)-selective mutant (Sav S112A; TON = 47; 29% e.e.) was selected for further studies (Table 1, entry 16; Supplementary Table S8). Combining the system with a DAAO (from porcine kidney) allowed the enantiomeric excess of the L-pipecolic acid to be upgraded by re-oxidizing the D-enantiomer; under the chosen conditions, an enantiomeric excess of 86% in favour of L-4 was obtained (Fig. 5a; Table 1, entry 17). The formation of pipecolic acid was unambiguously established by 2D NMR analysis of the reaction mixtures using L-lysine-2-<sup>13</sup>C as substrate (Supplementary Fig. S22).

**NADH regeneration for monooxygenases.** The chemical and electrochemical recycling of NAD(P)H and analogues has been intensively investigated as an alternative to enzymatic regeneration<sup>12,42–49</sup>. In this context,  $[\text{Cp}^*\text{Rh}(\text{bipy})\text{Cl}]$  has emerged as the redox mediator or catalyst of choice. However, in the presence of the downstream enzyme, mutual inactivation is

commonly encountered<sup>44,45</sup>. To test the validity of the molecular compartmentalization concept outlined in Fig. 1, we investigated the regeneration of NADH in the presence of an NADH-dependent enzyme using an ATHase. Although significantly more active than  $[\text{Cp}^*\text{Rh}(\text{bipy})\text{Cl}]$  for NADH regeneration in the absence of an NADH-dependent enzyme,  $[\text{Cp}^*\text{Ir}(\text{biot-}p\text{-L})\text{Cl}]$  was rapidly deactivated in the presence of 2-hydroxybiphenyl monooxygenase (HbpA from *Pseudomonas azaleica*, an NADH- and FAD-dependent enzyme). In the presence of Sav, however, the mutual inactivation of  $[\text{Cp}^*\text{Ir}(\text{biot-}p\text{-L})\text{Cl}]$  and HbpA was efficiently prevented, and robust hydroxylation activity was achieved (Table 1, compare entries 18 and 19; Fig. 5b). We conclude that Sav shields the ATHase from the downstream enzyme, allowing NADH regeneration with formate as the hydride source ( $K_{\text{M}(\text{app})} = 165 \mu\text{M}$  [ $\pm 6 \mu\text{M}$ ],  $k_{\text{cat}(\text{app})} = 1.37 \text{ min}^{-1}$  [ $\pm 0.01 \text{ min}^{-1}$ ]; Supplementary Fig. S27). Full conversion of 2-hydroxybiphenyl (6) to 2,3-dihydroxybiphenyl (7) was accomplished in 2 h with a crude enzyme extract (Fig. 5b, Table 1, entries 18 and 19; Supplementary Fig. S25).

The system could be run either in the pure aqueous phase or as a biphasic system with 1-decanol functioning as a substrate reservoir and product sink, thereby highlighting the applicability of the ATHase under a variety of reaction conditions. The biphasic system again displayed strong inactivation in the absence of Sav, whereas a TON of >100 (versus  $[\text{Cp}^*\text{Ir}(\text{biot-}p\text{-L})\text{Cl}]$ ) was achieved when Sav was present (Supplementary Fig. S26).

### Outlook

We have demonstrated herein that an ATHase consisting of  $[\text{Cp}^*\text{Ir}(\text{biot-}p\text{-L})\text{Cl}]$  anchored within a streptavidin isoform is complementary and compatible with a variety of redox enzymes relying on NADH,  $\text{FADH}_2$  and haem cofactors. Such artificial metalloenzymes display attractive features that are reminiscent of both biocatalysts and chemocatalysts: precious metal reactivity, genetic optimization potential and well-defined second coordination sphere provided by a protein scaffold. This last feature could be further exploited with a view to achieving the immobilization of the entire enzyme cascade.

To optimize such cascades, directed evolution protocols are highly desirable. With this goal in mind, we have shown that the ATHase can be integrated with a colorimetric coupled assay, leading to the identification of a genetically improved ATHase. These proof-of-principle examples open fascinating perspectives

## ARTICLES

## NATURE CHEMISTRY DOI: 10.1038/NCHEM.1498

towards complementing biocatalytic cascades with molecularly compartmentalized organometallic catalysts.

## Methods

**Typical procedure for a double stereoselective deracemization with MAO-N/ATHase (analytical scale).** The following stock solutions were prepared. Catalase from bovine liver ( $50 \text{ kU ml}^{-1}$ ) was dissolved in MOPS/sodium formate buffer (0.6 M in MOPS, 3.0 M in sodium formate, pH adjusted with aq. KOH to pH 7.8). Sav S112T ( $16.4 \text{ mg ml}^{-1}$ , 0.75 mM free binding sites, assuming three free binding sites per tetramer) was dissolved in the catalase containing buffer.  $[\text{IrCp}^*(\text{biot-}p\text{-L})\text{Cl}]$  was dissolved in DMF (37.5 mM). Affinity purified MAO-N-9 (buffer exchange with MOPS, 0.6 M, pH adjusted with KOH to 7.8) was diluted in MOPS buffer (0.6 M, pH adjusted with KOH to 7.8) to a concentration of  $0.38 \text{ mg ml}^{-1}$ . Substrate stock was prepared by dissolving the hydrochloride of 1-ox in  $\text{H}_2\text{O}$  (1 M). The ATHase was prepared by adding  $[\text{IrCp}^*(\text{biot-}p\text{-L})\text{Cl}]$ -stock ( $10 \mu\text{l ml}^{-1}$ ) to the Sav-stock solution. MAO-N-stock was placed in 1.5 ml PP-tubes (100  $\mu\text{l}$ ) and ATHase was added (100  $\mu\text{l}$ ). The reactions were initiated by addition of substrate stock solution (7.5  $\mu\text{l}$ ) and incubated at  $37^\circ\text{C}$  and 250 r.p.m. in a lysing position. For work-up aq. NaOH solution was added (50  $\mu\text{l}$  of a 10 M solution) and the mixture extracted with  $\text{CH}_2\text{Cl}_2$  (1  $\times$  1 ml). The organic phase was dried over  $\text{Na}_2\text{SO}_4$  and analysed by HPLC (Supplementary Sections S2.3.1 and S2.4.1).

Received 10 May 2012; accepted 10 October 2012;  
published online 25 November 2012

## References

- Wörsdörfer, B., Woycechowsky, K. J. & Hilvert, D. Directed evolution of a protein container. *Science* **331**, 589–592 (2011).
- Choudhary, S., Quin, M. B., Sanders, M. A., Johnson, E. T. & Schmidt-Dannert, C. Engineered protein nano-compartments for targeted enzyme localization. *PLoS ONE* **7**, e33342 (2012).
- Dueber, J. E. *et al.* Synthetic protein scaffolds provide modular control over metabolic flux. *Nature Biotechnol.* **27**, 753–759 (2009).
- Keasling, J. D. Synthetic biology for synthetic chemistry. *ACS Chem. Biol.* **3**, 64–76 (2008).
- Bromley, E. H. C., Channon, K., Moutevelis, E. & Woolfson, D. N. Peptide and protein building blocks for synthetic biology: from programming biomolecules to self-organized biomolecular systems. *ACS Chem. Biol.* **3**, 38–50 (2008).
- Weissman, K. J. & Leadlay, P. F. Combinatorial biosynthesis of reduced polyketides. *Nature Rev. Microbiol.* **3**, 925–936 (2005).
- Mutti, F. G. *et al.* Simultaneous iridium catalysed oxidation and enzymatic reduction employing orthogonal reagents. *Chem. Commun.* **46**, 8046–8048 (2010).
- Haak, R. M. *et al.* Dynamic kinetic resolution of racemic  $\beta$ -haloalcohols: direct access to enantioenriched epoxides. *J. Am. Chem. Soc.* **130**, 13508–13509 (2008).
- Maid, H. *et al.* Iron catalysis for *in situ* regeneration of oxidized cofactors by activation and reduction of molecular oxygen: a synthetic metalloporphyrin as a biomimetic NAD(P)H oxidase. *Angew. Chem. Int. Ed.* **50**, 2397–2400 (2011).
- Wasilke, J.-C., Obrey, S. J., Baker, R. T. & Bazan, G. C. Concurrent tandem catalysis. *Chem. Rev.* **105**, 1001–1020 (2005).
- Zhou, J. Recent advances in multicatalyst promoted asymmetric tandem reactions. *Chem. Asian J.* **5**, 422–434 (2010).
- Betanzos-Lara, S. *et al.* Organometallic ruthenium and iridium transfer-hydrogenation catalysts using coenzyme NADH as a cofactor. *Angew. Chem. Int. Ed.* **51**, 3897–3900 (2012).
- Wingstrand, E., Laurell, A., Fransson, L., Hult, K. & Moberg, C. Minor enantiomer recycling: metal catalyst, organocatalyst and biocatalyst working in concert. *Chem. Eur. J.* **15**, 12107–12113 (2009).
- Simons, C., Hanefeld, U., Arends, I. W. C. E., Maschmeyer, T. & Sheldon, R. A. Towards catalytic cascade reactions: asymmetric synthesis using combined chemo-enzymatic catalysts. *Top. Catal.* **40**, 35–44 (2006).
- Wieczorek, B. Covalent anchoring of a racemization catalyst to CALB-beads: towards dual immobilization of DKR catalysts. *Tetrahedron Lett.* **52**, 1601–1604 (2011).
- Rocha-Martín, J., de las Rivas, B., Muñoz, R., Guisán, J. M. & López-Gallego, F. Rational co-immobilization of bi-enzyme cascades on porous supports and their applications in bio-redox reactions with *in situ* recycling of soluble cofactors. *ChemCatChem* **4**, 1279–1288 (2012).
- Hanefeld, U., Gardossi, L. & Magner, E. Understanding enzyme immobilisation. *Chem. Soc. Rev.* **38**, 453–468 (2009).
- Brady, D. & Jordaán, J. Advances in enzyme immobilisation. *Biotechnol. Lett.* **31**, 1639–1650.
- Mateo, C., Palomo, J. M., Fernandez-Lorente, G., Guisán, J. M. & Fernandez-Lafuente, R. Improvement of enzyme activity, stability and selectivity via immobilization techniques. *Enzyme Microb. Tech.* **40**, 1451–1463 (2007).
- Lopez-Gallego, F. & Schmidt-Dannert, C. Multi-enzymatic synthesis. *Curr. Opin. Chem. Biol.* **14**, 174–183 (2010).
- Pámies, O. & Bäckvall, J.-E. Combination of enzymes and metal catalysts. A powerful approach in asymmetric catalysis. *Chem. Rev.* **103**, 3247–3261 (2003).
- Kim, Y., Park, J. & Kim, M.-J. Dynamic kinetic resolution of amines and amino acids by enzyme-metal cocatalysis. *ChemCatChem* **3**, 271–277 (2011).
- Yusop, R. M., Unciti-Broceta, A., Johansson, E. M. V., Sánchez-Martin, R. M. & Bradley, M. Palladium-mediated intracellular chemistry. *Nature Chem.* **3**, 239–243 (2011).
- Foulkes, J. M., Malone, K. J., Coker, V. S., Turner, N. J. & Lloyd, J. R. Engineering a biometallic whole cell catalyst for enantioselective deracemization reactions. *ACS Catal.* **1**, 1589–1594 (2011).
- Lu, Y., Yeung, N., Sieracki, N. & Marshall, N. M. Design of functional metalloproteins. *Nature* **460**, 855–862 (2009).
- Ward, T. R. Artificial metalloenzymes based on the biotin-avidin technology: enantioselective catalysis and beyond. *Acc. Chem. Res.* **44**, 47–57 (2011).
- Bos, J., Fusetti, F., Driessen, A. J. M. & Roelofs, G. Enantioselective artificial metalloenzymes by creation of a novel active site at the protein dimer interface. *Angew. Chem. Int. Ed.* **51**, 7472–7475 (2012).
- Jing, Q. & Kazlauskas, R. J. Regioselective hydroformylation of styrene using rhodium-substituted carbonic anhydrase. *ChemCatChem* **2**, 953–957 (2010).
- Podtetenieff, J., Taglieber, A., Bill, E., Reijerse, E. J. & Reetz, M. T. An artificial metalloenzyme: creation of a designed copper binding site in a thermostable protein. *Angew. Chem. Int. Ed.* **49**, 5151–5155 (2010).
- Deuss, P. J., den Heeten, R., Laan, W. & Kamer, P. C. J. Bioinspired catalyst design and artificial metalloenzymes. *Chem. Eur. J.* **17**, 4680–4698 (2011).
- Ueno, T., Abe, S., Yokoi, N. & Watanabe, Y. Coordination design of artificial metalloproteins utilizing protein vacant space. *Coord. Chem. Rev.* **251**, 2717–2731 (2007).
- Matsuo, T. *et al.* Meso-unsubstituted iron corrole in hemoproteins: remarkable differences in effects on peroxidase activities between myoglobin and horseradish peroxidase. *J. Am. Chem. Soc.* **131**, 15124–15125 (2009).
- Turner, N. J. Directed evolution drives the next generation of biocatalysts. *Nature Chem. Biol.* **5**, 567–573 (2009).
- Turner, N. J. Enantioselective oxidation of C–O and C–N bonds using oxidases. *Chem. Rev.* **111**, 4073–4087 (2011).
- Dürrenberger, M. *et al.* Artificial transfer hydrogenases for the enantioselective reduction of cyclic imines. *Angew. Chem. Int. Ed.* **50**, 3026–3029 (2011).
- Rowles, I., Malone, K. J., Etchells, L. L., Willies, S. C. & Turner, N. J. Directed evolution of the enzyme monoamine oxidase (MAO-N): highly efficient chemo-enzymatic deracemisation of the alkaloid ( $\pm$ )-crispine A. *ChemCatChem* **4**, 1259–1261 (2012).
- Heiden, Z. M. & Rauchfuss, T. B. Homogeneous catalytic reduction of dioxygen using transfer hydrogenation catalysts. *J. Am. Chem. Soc.* **129**, 14303–14310 (2007).
- Brandänge, S., Lindblom, L., Pilotti, Å. & Rodriguez, B. Ring-chain tautomerism of pseudooxynicotine and some other iminium compounds. *Acta Chem. Scand. B* **37**, 617–622 (1983).
- Truppo, M. D., Escalantes, F. & Turner, N. J. Rapid determination of both the activity and enantioselectivity of ketoreductases. *Angew. Chem. Int. Ed.* **47**, 2639–2641 (2008).
- Yasuda, M., Ueda, M., Muramatsu, H., Mihara, H. & Esaki, N. Enzymatic synthesis of cyclic amino acids by N-methyl-L-amino acid dehydrogenase from *Pseudomonas putida*. *Tetrahedron Asym.* **17**, 1775–1779 (2006).
- Gatto, G. J., Boyne, M. T., Kelleher, N. L. & Walsh, C. T. Biosynthesis of pipercolic acid by RapL, a lysine cyclodeaminase encoded in the rapamycin gene cluster. *J. Am. Chem. Soc.* **128**, 3838–3847 (2006).
- Hollmann, F., Hofstetter, K. & Schmid, A. Non-enzymatic regeneration of nicotinamide and flavin cofactors for monooxygenase catalysis. *Trends Biotechnol.* **24**, 163–171 (2006).
- Hollmann, F., Arends, I. W. C. E. & Buehler, K. Biocatalytic redox reactions for organic synthesis: nonconventional regeneration methods. *ChemCatChem* **2**, 762–782 (2010).
- Poizat, M., Arends, I. W. C. E. & Hollmann, F. On the nature of mutual inactivation between  $[\text{Cp}^*\text{Rh}(\text{bpy})(\text{H}_2\text{O})]^{2+}$  and enzymes — analysis and potential remedies. *J. Mol. Catal. B* **63**, 149–156 (2010).
- Hildebrand, F. & Lütz, S. Stable electroenzymatic processes by catalyst separation. *Chem. Eur. J.* **15**, 4998–5001 (2009).
- Haquette, P. *et al.* Chemically engineered papain as artificial formate dehydrogenase for NAD(P)H regeneration. *Org. Biomol. Chem.* **9**, 5720–5727 (2011).
- Maenaka, Y., Suenobu, T. & Fukuzumi, S. Efficient catalytic interconversion between NADH and  $\text{NAD}^+$  accompanied by generation and consumption of hydrogen with a water-soluble iridium complex at ambient pressure and temperature. *J. Am. Chem. Soc.* **134**, 367–374 (2012).

48. Canivet, J., Süß-Fink, G. & Štěpnička, P. Water-soluble phenanthroline complexes of rhodium, iridium and ruthenium for the regeneration of NADH in the enzymatic reduction of ketones. *Eur. J. Inorg. Chem.* 4736–4742 (2007).
49. Ryan, J. D., Fish, R. H. & Clark, D. S. Engineering cytochrome P450 enzymes for improved activity towards biomimetic 1,4-NADH cofactors. *ChemBioChem* **9**, 2579–2582 (2008).

#### Acknowledgements

This work was supported by the Marie Curie Initial Training Network (Biotrains FP7-ITN-238531). T.R.W. acknowledges financial support from the SNF (Schweizerische Nationalfonds, grant no. 200020\_126366) and the National Centre of Competence in Research Nanosciences. N.J.T. acknowledges the Royal Society for a Wolfson Research Merit Award. F.H. thanks A. Schmid (Dortmund University of Technology) for the kind provision of HbpA. The authors also thank M. Corbett, S. Willies and K. Malone for helpful advice and materials, R. Pfalzberger for help with the graphic material, and Umicore for a precious metal loan.

#### Author contributions

V.K., F.H., N.T. and T.W. conceived the catalytic cascades. V.K., F.H., N.T. and T.W. supervised the project. V.K., Y.W., M.D., D.G., E.C. and T.Q. performed the experiments. V.K., Y.W., M.D., D.G., E.C., T.Q., F.H., N.T. and T.W. analysed the data. V.K., F.H., N.T. and T.W. co-wrote the paper. V.K., Y.W., M.D., D.G. and L.K. contributed materials. D.H. analysed the conversion of <sup>13</sup>C-labelled lysine by 2D NMR.

#### Additional information

Supplementary information and chemical compound information are available in the online version of the paper. Reprints and permission information is available online at <http://www.nature.com/reprints>. Correspondence and requests for materials should be addressed to F.H., N.J.T. and T.R.W.

#### Competing financial interests

The authors declare no competing financial interests.

# Synthetic cascades are enabled by combining biocatalysts with artificial metalloenzymes

V. Köhler, Y. M. Wilson, M. Dürrenberger, D. Ghislieri, E. Churakova, T. Quinto, L. Knörr, D. Häussinger,  
F. Hollmann,\* N. J. Turner,\* and T. R. Ward\*

## Contents

1. General Information .....	3
2. Concurrent catalysis reactions with MAO-N/ATHase .....	4
2.1. MAO-N Protein expression.....	4
2.2. MAO-N Protein purification .....	4
2.3. Reactions on a preparative scale.....	5
2.3.1. Reduction of 1-methyl-3,4-dihydroisoquinoline ( <b>1-ox</b> ) with MAO-N-9/ATHase (S112T) .....	5
2.3.2. Deracemisation of 2-cyclohexylpyrrolidine ( <b>2-red</b> ).....	8
2.3.3. Conversion of ( <i>S</i> )-nicotine ( <b>S-3-red</b> ) with MAO-N-5/ATHase (Sav S112G or Sav S112A-K121T) .....	11
2.4. Reactions with MAO-N /ATHase on an analytical scale .....	17
2.4.1. Substrates <i>rac</i> -1-methyl-1,2,3,4-tetrahydroisoquinoline ( <i>rac</i> - <b>1-red</b> ) and 1-methyl-3,4-dihydroisoquinoline ( <b>1-ox</b> ) .....	17
2.4.2. Substrates <i>rac</i> -2-cyclohexylpyrrolidine ( <i>rac</i> - <b>2-red</b> ) and 2-cyclohexyl-1-pyrroline ( <b>2-ox</b> ) .....	17
2.4.3. Substrates ( <i>S</i> )-nicotine ( <b>S-3-red</b> ) and pseudooxynicotine ( <b>3-ox</b> ) .....	19
2.5. Screening of ATHase variants for the reduction of prochiral substrates .....	20
2.5.1. 1-Methyl-3,4-dihydroisoquinoline ( <b>1-ox</b> ).....	20
2.5.2. 2-Cyclohexyl-1-pyrroline ( <b>2-ox</b> ).....	22

2.5.3. Pseudooxynicotine ( <b>3-ox</b> ).....	23
2.6. Evaluation of MAO-N mutants as whole cell biocatalysts.....	27
2.7. Time course of concurrent catalysis reactions with MAO-N-9/ATHase (Sav S112T or Sav S112K) for the reduction of 1-methyl-3,4-dihydroisoquinoline ( <b>1-ox</b> ).....	28
2.8. Determination of apparent kinetic constants for ATHase (S112T, S112K and K121A) in the reduction of 1-methyl-3,4-dihydroisoquinoline ( <b>1-ox</b> ).....	29
2.9. ATHase plate-based activity assay .....	32
2.9.1. ATHase plate-based activity assay: HPLC-comparison.....	33
2.10. Controls .....	36
2.10.1. Inactivation of MAO-N.....	36
2.10.2. Effect of H <sub>2</sub> O <sub>2</sub> -addition on the catalytic performance of ATHase S112T in the presence and absence of catalase .....	37
2.10.3. Influence of catalase on the reaction with MAO-N and ATHase.....	38
2.10.4. Reversibility of MAO-N inactivation.....	40
3. Deracemisation of pipercolic acid ( <b>5</b> ) with DAAO/ATHase and synthesis of L-pipercolic acid from lysine ( <b>4</b> ) employing LAAO/ATHase/DAAO.....	41
3.1. Screening of ATHase mutants for the reduction of <i>in-situ</i> generated $\Delta^1$ -piperideine-2-carboxylic acid.....	43
3.2. Conversion of L-lysine ( <b>4</b> ) to L-pipercolic acid ( <b>5</b> ): NMR-investigation.....	45
4. NAD reduction and HbpA coupled hydroxylation of 2-hydroxybiphenyl ( <b>6</b> ) .....	47
4.1. HbpA preparation.....	47
4.2. NADH regeneration activity of [Cp*Ir(biot- <i>p</i> -L)Cl], [Cp*Ir(biot- <i>p</i> -L)Cl]-Sav S112A and [Cp*Rh(biot- <i>p</i> -L)Cl].....	48
4.3. Effect of Sav S112A on the mutual deactivation of the Ir-cofactor and HbpA.....	50
4.4. The effect of Sav S112A on the chemoenzymatic hydroxylation of 2-hydroxybiphenyl ( <b>6</b> ) ...	51
4.5. Determination of apparent kinetic constants of ATHase catalysed NAD reduction.....	55
5. References.....	57

## 1. General Information

Chemicals were purchased from Sigma-Aldrich, Acros, Fluka and TCI and used as received. Streptavidin (Sav) mutants were produced, purified and characterised as previously described [1]. The Sav used in this work and on which all variants were based was T7-tagged core Sav described by Gallizia et al. [2] and here we refer to this as wild-type Sav. The corresponding ATHase is also referred to as wild-type (WT). For a detailed synthesis procedure of [Cp\*Ir(biot-*p*-L)Cl] see reference [3]. Commercial enzyme preparations were purchased from Sigma. MAO-N mutants used in this study are described elsewhere [4,5]. *rac*-1-Methyl-1,2,3,4-tetrahydroisoquinoline (**1-red**) was prepared from 1-methyl-3,4-dihydroisoquinoline (**1-ox**) hydrochloride hydrate by reduction with NaBH<sub>4</sub> in MeOH. 2-Cyclohexyl-1-pyrroline (**2-ox**) was prepared according to literature procedures [6]. *rac*-2-Cyclohexylpyrrolidine (**2-red**) was prepared from 2-cyclohexyl-1-pyrroline (**2-ox**) by reduction with NaBH<sub>4</sub> in MeOH. Pseudooxynicotine (**3-ox**) was prepared as described in reference [7]. 2,3-Dihydroxybiphenyl (**7**) was a kind gift from Prof. Dr. Andreas Schmid (TU Dortmund, Dortmund, Germany). L-Lysine-<sup>13</sup>C<sub>2</sub> HCl (99% <sup>13</sup>C) was obtained from Sigma. NMR experiments were performed at 25°C (MeOH calibration) on Bruker Avance III NMR spectrometers operating at 600, 500 or 400 MHz proton frequency. All were equipped with direct (600 and 400 MHz) or inverse (500 MHz) dual channel, broadband probe-heads with z-gradients. Chemical shifts were referenced to residual proton solvent peaks (4.773 ppm for H<sub>2</sub>O, 7.26 for CHCl<sub>3</sub>). The quantitative constant time HSQC experiment was performed using 2048 data points in the F2 and 1024 data points in the F1 dimension, corresponding to acquisition times of 155 ms in F2 and 34 ms in F1. Each increment was recorded with 8 scans resulting in a total experiment time of 2 h 45 min. HPLC measurements were performed on Agilent (or hp) machines equipped with modules from the 1100 and 1200 series and diode array detectors, if not indicated otherwise. HPLC columns were used with the appropriate guard columns, if not indicated otherwise. Column and conditions are indicated for each



compound separately. GC measurements were performed on Agilent GCs of the 6890 series equipped with FIDs.

## 2. Concurrent catalysis reactions with MAO-N/ATHase

### 2.1. MAO-N Protein expression

Aqueous solutions of dithiothreitol (8  $\mu$ L, 200 mM) followed by pET-16b plasmid DNA containing the MAO-N gene variant (2  $\mu$ L, 49–138 ng/ $\mu$ L) were added to ultra competent BL21(DE3)pLysS *E. coli* cells (produced in-house) (100  $\mu$ L). The mixture was stored on ice for 15 min and the transformed cells were plated onto LB-Lennox agar plates containing ampicillin (279  $\mu$ M), chloramphenicol (100  $\mu$ M) and glucose (111 mM), and incubated overnight at 37  $^{\circ}$ C. The culture and preculture media were composed of bactotryptone (from BD, 20 g/L), Na<sub>2</sub>HPO<sub>4</sub> (9.16 mM), KH<sub>2</sub>PO<sub>4</sub> (7.35 mM), NaCl (136.9 mM) and bacto yeast extract (from Merck, 15 g/L). A single colony was inoculated to the preculture medium (50 mL), which contained ampicillin (279  $\mu$ M), chloramphenicol (100  $\mu$ M), and glucose (55.5 mM), and was incubated overnight on an orbital shaker (37  $^{\circ}$ C, 250 rpm). The preculture was diluted 1 to 1000 into fresh media (600 mL), containing ampicillin (279  $\mu$ M), chloramphenicol (100  $\mu$ M) and glucose (1.1 mM). The cells were grown at 30  $^{\circ}$ C until an OD<sub>600</sub> of 2–3 was reached. Expression was induced by addition of isopropyl  $\beta$ -D-1-thiogalactopyranoside (600  $\mu$ L, 1 M). The cells were harvested approximately 10 hours after induction by centrifugation (3600  $\times$  g, 10 min, 4  $^{\circ}$ C). The supernatant was discarded and the pellet was frozen at -20  $^{\circ}$ C until purification. Protein expression was confirmed by SDS-PAGE analysis.

### 2.2. MAO-N Protein purification

The cell pellet was thawed on ice and resuspended in potassium phosphate buffer (100 mM, pH 7.7, 20 mL/g wet cell pellet) containing DNase I (from Roche, 20 U/mL), lysozyme (40 kU/mL) and

phenylmethylsulfonyl fluoride (1 mM). The resuspended cells were incubated at 30 °C, 100 rpm for 30-60 min. The proteic extract was centrifuged ( $18000 \times g$ , 30 min, 4 °C) to remove cell debris and filtered (0.2  $\mu\text{m}$  filters, Sarstedt). The buffers for purification by nickel affinity column (1 mL HiTrap Chelating HP, GE Healthcare) were: buffer A: potassium phosphate buffer (100 mM, pH 7.7) containing sodium chloride (300 mM) and buffer B: potassium phosphate buffer (100 mM, pH 7.7) containing sodium chloride (300 mM) and imidazole (1 M). The column was pre-equilibrated with buffer A before loading of the protein sample. The bound protein was washed with buffer A (minimum wash volume 30 mL), followed by 20 % buffer B (minimum wash volume 10 mL) and eluted in 35 % buffer B. The eluted sample was concentrated to 2.5 mL using a centrifugal filter unit (Amicon Ultra-15, 30000 MWCO, from Millipore,  $3600 \times g$ , 2-5 min) and desalted on a PD-10 desalting column (GE Healthcare) pre-equilibrated with MOPS buffer (25 mL, 0.6 M, pH 7.8). Concentration and filtration were repeated using a fresh filter unit and PD-10 column. The absorbance of the sample at 280 nm was measured using a Nanodrop 1000 (Witec AG). The following factors were used to correct the concentration values obtained from the Nanodrop measurement: 1.691 for MAO-N-9 and 1.787 for MAO-N-5 (calculated from the amino acid sequence using the ExPASy ProtParam tool from the Swiss Institute of Bioinformatics). This corresponds to molar extinction coefficients of  $99350 \text{ M}^{-1}\text{cm}^{-1}$  for MAO-N-5 and  $93850 \text{ M}^{-1}\text{cm}^{-1}$  for MAO-N-9, assuming all cysteine residues are reduced.

## 2.4. Reactions with MAO-N /ATHase on an analytical scale

### 2.4.1. Substrates *rac*-1-methyl-1,2,3,4-tetrahydroisoquinoline (*rac*-1-red) and 1-methyl-3,4-dihydroisoquinoline (1-ox)

The analytical reactions were carried out with the same buffer (consider note regarding buffer C, on page 5 of the SI) and substrate concentrations as described for the preparative reaction. (Initially concentrations were varied to find the optimal reaction conditions.) Analytical reactions were typically conducted in the following format: 100  $\mu$ L ATHase preparation was added to 100  $\mu$ L MAO-N preparation (0.38 mg/mL in 0.6 M MOPS, pH 7.8) in a 1.5 mL PP-tube and the reactions were initiated by the addition of substrate (7.5  $\mu$ L of either a 1 M solution of 1-methyl-3,4-dihydroisoquinoline hydrochloride hydrate in H<sub>2</sub>O, or a 1 M solution of 1-methyl-1,2,3,4-tetrahydroisoquinoline (solution prepared in 1 N HCl). The tubes were incubated in a lying position at 250 rpm and 37 °C for the appropriate time. Subsequently the tube was removed from the incubator and aqueous NaOH (50  $\mu$ L of a 10 N solution) was added, immediately followed by CH<sub>2</sub>Cl<sub>2</sub> (1 mL). Mixing was achieved by means of a vortex mixer. The organic phase was separated, dried with Na<sub>2</sub>SO<sub>4</sub> and analysed by chiral phase HPLC. The experiment cited in the main text in Table 1, entry 5 was carried out with 0.5 mol % ATHase and analysed after 24 hours. For experiments cited in the main text in Table 1, entries 6, 7, see >Time course of concurrent catalysis reactions with MAO-N-9/ATHase (Sav S112T or Sav S112K) in the reduction of 1-methyl-3,4-dihydroisoquinoline (1-ox)<; compare also Table S6.

### 2.4.2. Substrates *rac*-2-cyclohexylpyrrolidine (*rac*-2-red) and 2-cyclohexyl-1-pyrroline (2-ox)

The procedure was similar to that described above for *rac*-1-red and 1-ox. After work-up, conversion was determined in the crude extracts by GC-FID (see above). The total response for amine and imine dropped over the course of the reaction significantly, presumably caused by absorption of the lipophilic substrate and product into the PP-tubes. The preparative reaction showed that high isolated yields can be obtained. For *ee*-determination derivatization was carried out as described above. The experiments cited

in the main text (Table 1, entries 10, 11) were performed with 1 mol % ATHase as follows: Stock solutions: Catalase (27.5 mg, from bovine liver, 11 kU/mg, Sigma C40) was dissolved in MOPS/sodium formate buffer (6.059 mL, 0.6 M in MOPS, 3.0 M in formate, pH adjusted with NaOH to 7.8). Sav S112A (40.4 mg) or Sav S112A-K121N (39.8 mg) was dissolved in the catalase containing buffer (1.230 mL for Sav S112A, 1.213 mL for Sav S112A-K121N).  $[\text{Cp}^*\text{Ir}(\text{biot-}p\text{-L})\text{Cl}]$  (1.82 mg) was dissolved in DMF (30.0  $\mu\text{L}$ ). The ATHase was prepared by adding Ir-stock solution (12.30  $\mu\text{L}$  for Sav S112A, 12.13  $\mu\text{L}$  for Sav S112A-K121N) to the Sav-stock solutions. 2-Cyclohexyl-1-pyrroline and 2-cyclohexylpyrrolidine were dissolved to a final concentration of 1 M in 1.1 N aq. HCl. The amine stock solution remained slightly turbid, but clarified upon standing. Note: Turbidity in the preparation of the stock solutions (amine **2-red** or imine **2-ox**) was observed on other occasions. Purified MAO-N-9 (100  $\mu\text{L}$ , 0.38 mg/mL in 0.6 M MOPS buffer, pH 7.8) was placed in a 1.5 mL PP-tube, ATHase (100  $\mu\text{L}$ ) was added and the reaction initiated by addition of substrate stock solution (7.5  $\mu\text{L}$ ). Workup and analysis was performed after 39 hours as described above (see also Figure S14 for *ee*-determination).

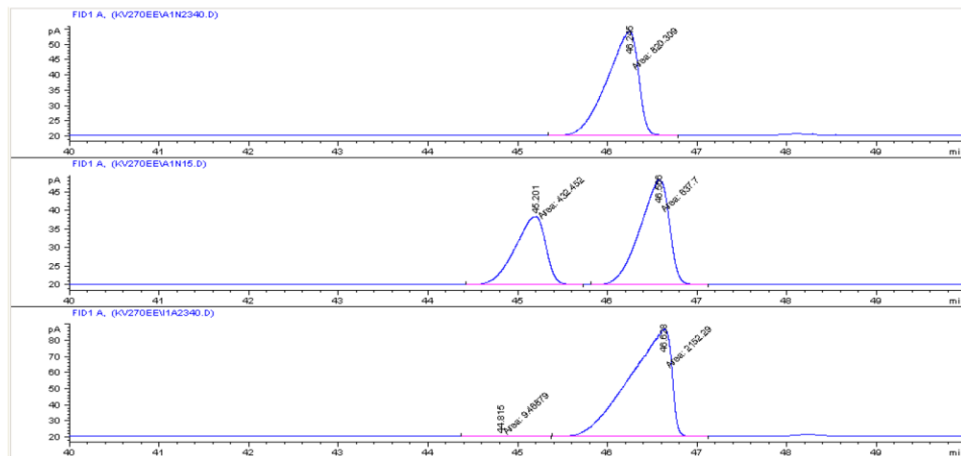


**Figure S14.** Chiral phase GC traces of 2-cyclohexylpyrrolidine deracemisation with ATHase (Sav S112A-K121N) and MAO-N-9 after derivatization with TFAA after 39 hours (top) and after 15 minutes (middle); 2-cyclohexyl-1-pyrroline reduction with ATHase (Sav S112A) and MAO-N-9 after derivatization with TFAA after 39 hours (bottom).

### 2.4.3. Substrates (*S*)-nicotine (*S*)-3-red) and pseudooxynicotine (3-ox)

The procedure was similar to that described above for *rac*-1-methyl-1,2,3,4-tetrahydroisoquinoline and 1-methyl-3,4-dihydroisoquinoline. The stock solution for pseudooxynicotine (1 M) was prepared by dissolving the double HCl salt in H<sub>2</sub>O. Conversion and *ee*-determination were carried out as described above. The experiment cited in the main text (Table 1, entry 14) was performed with 1 mol % ATHase as follows: Stock solutions: Catalase (8.55 mg, from bovine liver, 11 kU/mg, Sigma C40) was dissolved in MOPS/sodium formate buffer (1.881 mL, 0.6 M in MOPS, 3.0 M in formate, pH adjusted with NaOH to 7.8). Sav S112A-K121T (42.0 mg) was dissolved in the catalase containing buffer (1.282 mL). [Cp\*Ir(biot-*p*-L)Cl] (2.11 mg) was dissolved in DMF (35.0  $\mu$ L). The ATHase was prepared by adding Ir-stock solution (12.82  $\mu$ L) to the Sav-stock solution. (*S*)-Nicotine (162.5 mg) was dissolved to a final volume of 1 mL in 1 N HCl. Purified MAO-N-5 (100  $\mu$ L, 1.43 mg/mL in 0.6 M MOPS buffer, pH 7.8) was placed in a 1.5 mL PP-tube, ATHase (100  $\mu$ L) was added and the reaction initiated by addition of substrate stock solution (7.5  $\mu$ L). Workup and analysis was performed after 14 hours as described above (see also Figure S15 for *ee*-determination of nicotine). For conversion determination the sample was additionally run under modified RP-HPLC-conditions (compare preparative reactions): Agilent Eclipse XDB-C18 150  $\times$  4.6 mm, 5  $\mu$ m; solvent A: H<sub>2</sub>O with 0.1 % TFA, solvent B: MeOH with 0.1 % TFA; 0 % B at 0 min, 0 % B at 10 min, 5 % B at 11 min, 5 % B at 21 min, 50 % B at 26 min, 50 % B at 31 min, 0 % B at 36 min, 0 % B at 40 min; 1 mL/min, 25  $^{\circ}$ C, 254 nm; T<sub>R</sub> 3.2 min 4-(methylamino)-1-(3-pyridyl)-1-butanol, 4.4 min nicotine, 28.6 min 2-(3,4-dimethoxyphenyl)ethanol.

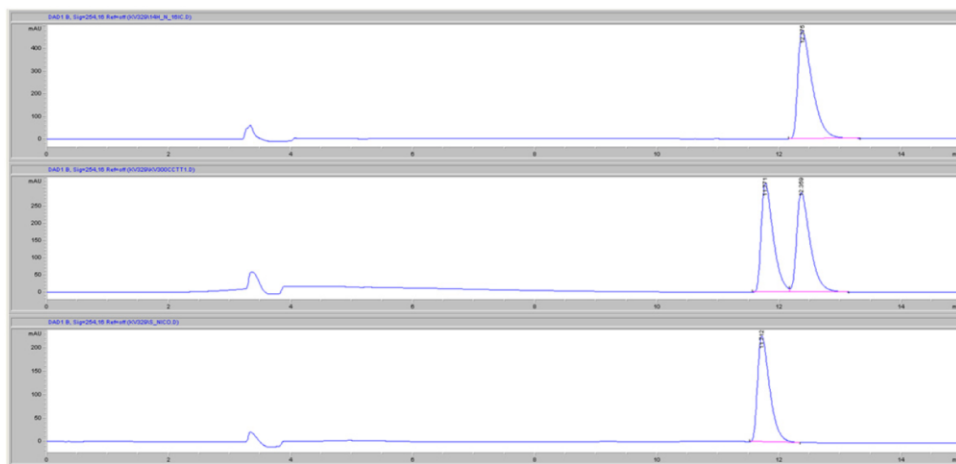


**Figure S15.** Chiral phase HPLC trace of (*S*)-nicotine conversion with MAO-N-5 and ATHase (Sav S112A-K121T) showing the signals of nicotine (top) and for comparison *rac*-nicotine (middle) and natural (*S*)-nicotine (bottom).

## 2.5. Screening of ATHase variants for the reduction of prochiral substrates

### 2.5.1. 1-Methyl-3,4-dihydroisoquinoline (1-ox)

The initial screening protocols for the identification of a suitable ATHase differed for the described substrates in details (compare substrates 2-cyclohexyl-1-pyrroline and pseudoxy nicotine) and are therefore reported individually and comprehensively. The following stock solutions were prepared: Reaction buffer: 0.6 M MOPS, 1.5 M HCO<sub>2</sub>Na, pH adjusted with aqueous KOH to pH 7.8. [IrCp\*(biot-*p*-L)Cl] (e. g. 2.84 mg, 3.53 μmol) was dissolved in DMF (252 μL) resulting in a final concentration of 14 mM. A 1 M solution of the substrate was prepared by dissolving 1-methyl-3,4-dihydroisoquinoline hydrochloride hydrate (200 mg, 1.00 mmol, water content considered in calculation) in water to a total volume of 1 mL. Lyophilised Sav-mutants were weighed into PP-tubes and dissolved in the appropriate volume of reaction buffer to reach a calculated final concentration of 690 μM free biotin binding sites. Free binding sites in the protein preparation were determined by a B4F-assay [8]. Note: in all other

experiments the number of free binding sites in the protein preparation was set arbitrarily to 3 per tetramer to ensure that sufficient free binding sites were present. 200  $\mu\text{L}$  of the protein solutions were transferred to 1.5 mL PP-tubes and 4.93  $\mu\text{L}$  of complex solution was added (this equates to two free binding sites per biotinylated metal complex), followed by mixing by means of a vortex mixer. The reactions were started by addition of substrate stock solution (15  $\mu\text{L}$ ) and the tubes were incubated at 37  $^{\circ}\text{C}$  and 250 rpm. After 20 hours the tubes were removed from the incubator, water (500  $\mu\text{L}$ ) and aqueous NaOH solution (50  $\mu\text{L}$  of a 10 N solution) were added. The resulting solutions were transferred to 2 mL PP-tubes and subsequently extracted with  $\text{CH}_2\text{Cl}_2$  ( $4 \times 1$  mL). The combined organic phases were dried over  $\text{Na}_2\text{SO}_4$  and analysed by chiral phase HPLC (Table S2).

**Table S2.** Screening of ATHase mutants for the reduction of 1-methyl-3,4-dihydroisoquinoline.



entry	Sav-mutant	free binding sites	conversion [%]	ee [%]
1	WT	3.8	100	23 ( <i>R</i> )
2	S112A	3.0	100	50 ( <i>R</i> )
3	S112E	3.4	7	5 ( <i>R</i> )
4	S112K	3.0	100	46 ( <i>S</i> )
5	S112R	3.0	100	15 ( <i>S</i> )
6	S112C	3.9	7	19 ( <i>R</i> )
7	S112L	3.0	100	23 ( <i>R</i> )
8	S112H	3.3	7	6 ( <i>S</i> )
9	S112Q	3.3	99	16 ( <i>R</i> )
10	S112V	3.6	100	57 ( <i>R</i> )
11	S112Y	3.6	100	37 ( <i>R</i> )
12	S112G	3.6	100	23 ( <i>R</i> )
13	S112T	3.3	100	59 ( <i>R</i> )
14	K121A	3.9	100	41 ( <i>R</i> )
15	K121H	3.6	44	6 ( <i>R</i> )
16	S112A-K121G	3.6	100	10 ( <i>R</i> )
17	S11A-K121N	3.6	100	48 ( <i>R</i> )

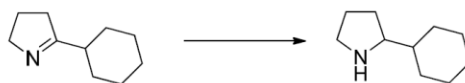
### 2.5.2. 2-Cyclohexyl-1-pyrroline (2-ox)

The following stock solutions were prepared: Reaction buffer: 0.6 M MOPS, 1.5 M HCO<sub>2</sub>Na, pH adjusted with aqueous KOH to pH 7.8. [Cp\*Ir(biot-*p*-L)Cl] (e. g. 2.60 mg, 3.24 μmol) was dissolved in DMF (86.3 μL) resulting in a final concentration of approximately 37.5 mM. A 1 M solution of the substrate was prepared by dissolving 2-cyclohexyl-1-pyrroline (151.3 mg, 1.000 mmol) in 1.1 N HCl to a total volume of 1 mL. Note: the substrate stock solution stayed turbid. Lyophilised Sav-mutants were weighed into PP-tubes and dissolved in the appropriate volume of reaction buffer to reach a calculated final concentration of 375 μM free biotin binding sites (assuming 3 free binding sites per tetramer). Appropriate amounts of complex stock solution were added to reach the desired stoichiometry of 2 free binding sites per complex. The solutions were mixed by means of a vortex mixer and 200 μL of the preformed ATHase transferred to 1.5 mL PP-tubes. The reactions were initiated by addition of substrate stock solution (7.5 μL) and the tubes were incubated at 37 °C and 250 rpm in a lying position. After 20 hours, aqueous NaOH-solution (50 μL of a 10 N solution) was added and the mixtures extracted with CH<sub>2</sub>Cl<sub>2</sub> (1 × 1 mL). The extracts were dried with Na<sub>2</sub>SO<sub>4</sub> and analysed by GC-FID as described for the preparative reaction. The results are summarised in Table S3.



DOI: 10.1038/NCHEM.1498

## SUPPLEMENTARY INFORMATION

**Table S3.** Screening of ATHase mutants for the reduction of 2-cyclohexyl-1-pyrroline.

entry	Sav-mutant	conversion <sup>a)</sup> [%]	ee [%]
1	WT	66	55 ( <i>R</i> )
2	S112A	84	86 ( <i>R</i> )
3	S112K	24	54 ( <i>R</i> )
4	S112L	21	3 ( <i>R</i> )
5	S112H	0	-
6	S112Q	19	61 ( <i>R</i> )
7	S112V	60	78 ( <i>R</i> )
8	S112G	96	8 ( <i>S</i> )
9	S112E	0	-
10	K121A	100	35 ( <i>R</i> )
11	S112A-K121G	88	35 ( <i>R</i> )
12	S11A-K121N	100	63 ( <i>R</i> )
13	S112A-K121T	100	49 ( <i>R</i> )
14	WT	66	55 ( <i>R</i> )

a) Conversion [%] = (area amine × 100)/(area amine + area imine) as determined by GC-FID after extraction.

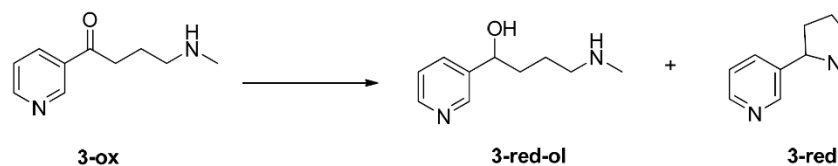
### 2.5.3. Pseudooxynicotine (3-ox)

The following stock solutions were prepared: Reaction buffer: 1.2 M MOPS, 3.0 M HCO<sub>2</sub>Na, pH adjusted with solid NaOH to pH 7.8. [Cp\*Ir(biot-*p*-L)Cl] (3.35 mg, 4.17 μmol) was dissolved in DMF (111.3 μL) resulting in a final concentration of approximately 37.5 mM. The substrate stock solution was prepared by dissolving the double HCl salt of pseudooxynicotine (35.1 mg, 140 μmol) in H<sub>2</sub>O to a total volume of 2 mL resulting in a final concentration of 69.8 mM. Lyophilised Sav-mutants were weighed into PP-tubes and dissolved in the appropriate volume of reaction buffer to reach a final concentration of 750 μM free biotin binding sites (assuming 3 free binding sites per tetramer). Appropriate amounts of complex stock solution were added to reach the desired stoichiometry of 2 free binding sites per complex. The solutions were mixed by means of a vortex mixer and 100 μL of the preformed ATHase transferred to

1.5 mL PP-tubes. The reactions were initiated by addition of substrate stock solution (107.5  $\mu\text{L}$ ) and the tubes were incubated at 37 °C and 250 rpm in a lying position. After 20 hours 2-phenylethanol (50  $\mu\text{L}$  of a 120 mM solution in  $\text{H}_2\text{O}$ ) was added as an internal standard to the reaction mixtures. 125  $\mu\text{L}$  of the resulting solutions were transferred to a separate PP-tube, treated with MeOH (300  $\mu\text{L}$ ) and the resulting mixture centrifuged at 18800  $\times g$ . 200  $\mu\text{L}$  of the supernatant were diluted with 1 mL  $\text{H}_2\text{O}$  and the resulting solution was analysed by reversed phase HPLC as described for reactions on a preparative scale ( $T_{\text{R}}$  2-phenylethanol 14.5 min). The remaining 132.5  $\mu\text{L}$  reaction mixture containing internal standard from above were treated with aqueous NaOH (25  $\mu\text{L}$  of a 10 N solution) and subsequently extracted with  $\text{CH}_2\text{Cl}_2$  (1  $\times$  500  $\mu\text{L}$ ). The organic phase was separated, dried over  $\text{Na}_2\text{SO}_4$  and analysed by chiral phase HPLC as described above. The results are summarised in Table S4. Note: As described above an internal standard was added to determine the conversion. In several cases the combined yield of nicotine and 4-(methylamino)-1-(3-pyridyl)-1-butanol exceeded 100 % and was highest for mutant S112A (121 %). All values were therefore normalised relative to this value. The relative response between alcohol and nicotine was determined in a separate experiment and considered in the calculations. Representative HPLC traces (2D and 3D) are depicted in Figures S16-S18.

DOI: 10.1038/NCHEM.1498

## SUPPLEMENTARY INFORMATION

**Table S4.** Screening of ATHase mutants for the reduction of pseudooxynicotine.

entry	Sav-mutant	HPLC-yield <b>3-red-ol</b> <sup>a)</sup> [%]	HPLC-yield <b>3-red</b> <sup>a)</sup> [%]	<i>ee</i> ( <b>3-red-ol</b> ) <sup>b)</sup> [%]	<i>ee</i> ( <b>3-red</b> ) [%]
1	S112A	41	59	+13	51 ( <i>R</i> )
2	S112A-K121G	29	58	+32	66 ( <i>R</i> )
3	S112A-K121N	14	74	+57	59 ( <i>R</i> )
4	S112A-K121T	11	76	+6	79 ( <i>R</i> )
5	S112K	16	28	n.d.	22 ( <i>S</i> )
6	K121A	51	39	+35	20 ( <i>S</i> )
7	S112C	2	4	n.d.	n.d.
8	S112E	1	1	n.d.	n.d.
9	S112G	79	3	+30	n.d.
10	S112H	1	2	n.d.	n.d.
11	S112L	32	25	n.d.	8 ( <i>S</i> )
12	S112Q	33	15	n.d.	4 ( <i>S</i> )
13	S112R	19	38	n.d.	4 ( <i>S</i> )
14	S112T	45	47	+17	22 ( <i>R</i> )
15	S112V	59	27	+5	11 ( <i>S</i> )
16	S112Y	50	33	-88	15 ( <i>R</i> )
17	WT	38	47	+60	11 ( <i>R</i> )

a) determined with an internal standard by reversed phase HPLC and normalised since some yields exceeded 100 %, see end of experimental procedure above. b) Absolute configuration was not determined; + and - sign are arbitrarily assigned.

**Figure S16.** Entire reversed-phase HPLC-trace (254 nm) for the analysis of the reduction of pseudooxynicotine with ATHase (S112G).

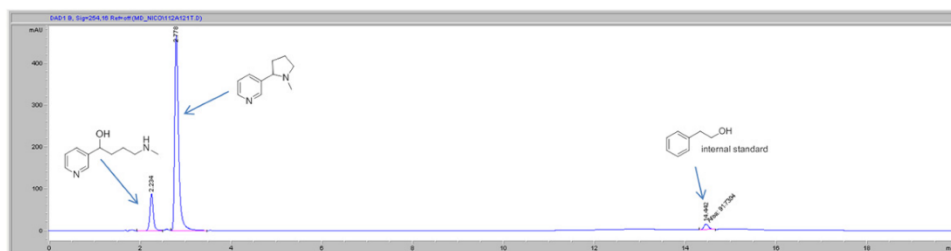


**Figure S17.** Entire reversed-phase HPLC-trace (254 nm) for the analysis of the reduction of pseudooxynicotine with ATHase (S112A-K121T).

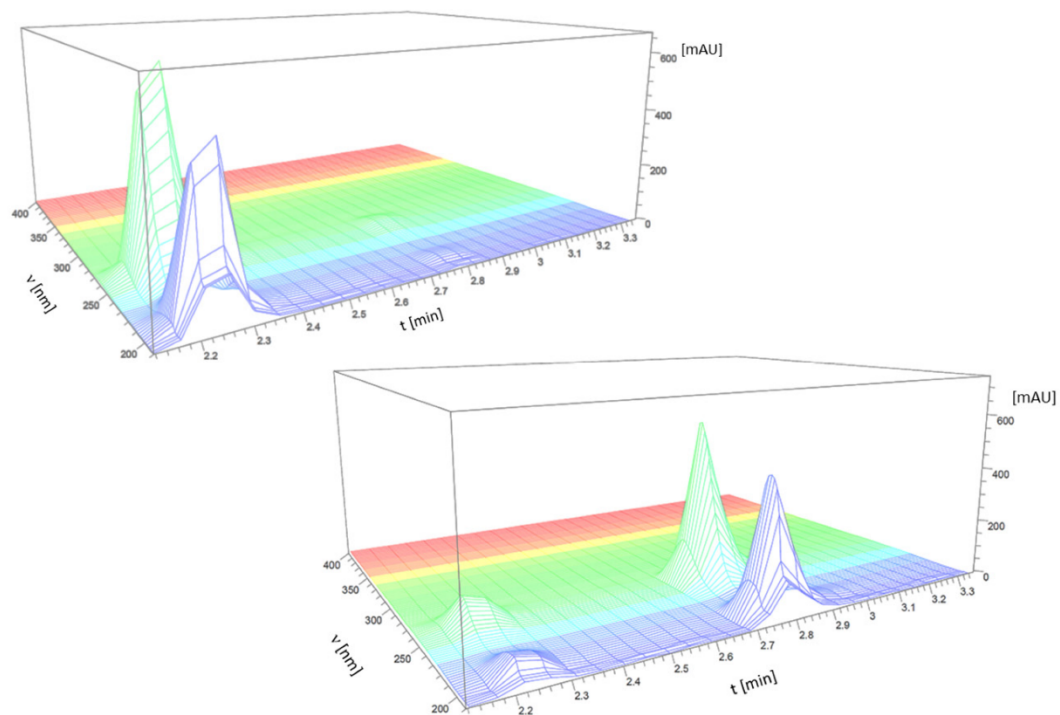


**Figure S18.** Wavelength resolved reversed-phase HPLC chromatograms for the analysis of the reduction of pseudooxynicotine with (top): ATHase (S112G), and (bottom): ATHase (S112A-K121T).

## 2.8. Determination of apparent kinetic constants for ATHase (S112T, S112K and K121A) in the reduction of 1-methyl-3,4-dihydroisoquinoline (1-ox)

Preparation of stock solutions and buffers:

MOPS buffer of 0.6 M, pH adjusted to 7.8 with NaOH.

MOPS/formate buffer: 0.6 M in MOPS, 3.0 M in sodium formate, pH adjusted with NaOH to 7.8.

[Cp\*Ir(biot-*p*-L)Cl]: 1.51 mg [Cp\*Ir(biot-*p*-L)Cl] was dissolved in 200.5  $\mu$ l of degassed DMF (calculated final concentration: 9.38 mM). This stock solution was used for the preparation of the Sav S112T and S112K ATHase (see below). For the preparation of the K121A ATHase the following Ir-complex stock solution was prepared: 1.34 mg [Cp\*Ir(biot-*p*-L)Cl] was dissolved in 711.6  $\mu$ L of degassed DMF (calculated final concentration: 2.34 mM).

1-Methyl-3,4-dihydroisoquinoline: Substrate stock solutions were prepared by dissolving 1-methyl-3,4-dihydroisoquinoline hydrochloride hydrate (315.6 mg, containing 7.8 % water) in MOPS buffer using a 5 mL volumetric flask (final concentration 320 mM). All other substrate solutions were prepared by diluting this stock solution in a 2 mL volumetric flask to the desired concentrations with MOPS buffer.

ATHase: Sav mutants (3 free binding sites per tetramer were assumed) were weighed into 2 mL PP-tubes and dissolved in an appropriate volume of the MOPS/formate buffer (between 1.5 and 1.7 mL). An appropriate volume of the corresponding [Cp\*Ir(biot-*p*-L)Cl] stock solution was added (between 15 and 17  $\mu$ L) and the mixture was vigorously mixed by means of a vortex mixer (calculated final concentrations: 247.5  $\mu$ M Sav monomer, 92.8  $\mu$ M [Cp\*Ir(biot-*p*-L)Cl] for S112T/S112K; 61.9  $\mu$ M Sav monomer, 23.2  $\mu$ M [Cp\*Ir(biot-*p*-L)Cl] for K121A).

500  $\mu$ L of the ATHase stock solution was added to an HPLC-vial and 37.5  $\mu$ L of H<sub>2</sub>O were added. The substrate stock solution and the ATHase stock solution were incubated at 37 °C for 5 minutes. The reaction was started by adding 500  $\mu$ L of the substrate stock solution to the vial and the mixture was shaken at 37 °C and 250 rpm (calculated final concentrations: 119  $\mu$ M Sav monomer, 44.7  $\mu$ M

[Cp\*Ir(biot-*p*-L)Cl)], 0.558 M MOPS, 1.395 M formate for S112T/S112K; 29.8  $\mu$ M Sav monomer, 11.2  $\mu$ M [Cp\*Ir(biot-*p*-L)Cl)], 0.558 M MOPS, 1.395 M formate for K121A). Aliquots of 100  $\mu$ L were taken at 10, 20, 30, 40 and 50 minutes and were added to PP-tubes containing 50  $\mu$ L of a freshly prepared glutathione solution (250 mM) which was found to be an effective quencher of the catalyst. For a given substrate concentration all measurements were performed simultaneously in triplicate (reactions were started staggered every minute).

To the quenched samples was added 25  $\mu$ L of an aqueous 2-(3,4-dimethoxyphenyl)ethanol solution (3 mM) as an internal standard followed by 300  $\mu$ L MeOH before the tubes were centrifuged at 21100  $\times g$  for 1 min at 4  $^{\circ}$ C. 400  $\mu$ L of the supernatant were diluted with 800  $\mu$ L of H<sub>2</sub>O and analysed by RP-HPLC using an Eclipse XDB-C18 column (5  $\mu$ m, 4.6  $\times$  150 mm, Agilent); solvent A: H<sub>2</sub>O with 0.1 % TFA, solvent B: MeCN with 0.1 % TFA; 13 % B at 0 min, 13 % B at 15 min, 90 % B at 20 min, 90 % B at 21 min, 13 % B at 26 min, 13 % B at 31 min; 1 mL/min; 25  $^{\circ}$ C, 210 nm; T<sub>R</sub> 5.8 min (1-methyl-1,2,3,4-tetrahydroisoquinoline), 13.0 min (2-(3,4-dimethoxyphenyl)ethanol).

Product concentrations were calculated under consideration of the calibration curve and plotted against the corresponding reaction times (see above). Initial rates at a given initial substrate concentration were obtained by linear regression of the resulting data points. The average value of these rates was plotted as a function of the substrate concentration, Figures S19. The apparent Michaelis-Menten parameters  $V_{\max}$ ,  $K_m$  and  $K_i$  were obtained applying nonlinear regression (least squares method) using GraphPad Prism 5.0<sup>®</sup> corresponding to the Michaelis-Menten equation [9] in case of S112K or to Haldane's equation for substrate inhibition [10] in case of S112T and K121A.

DOI: 10.1038/NCHEM.1498

## SUPPLEMENTARY INFORMATION

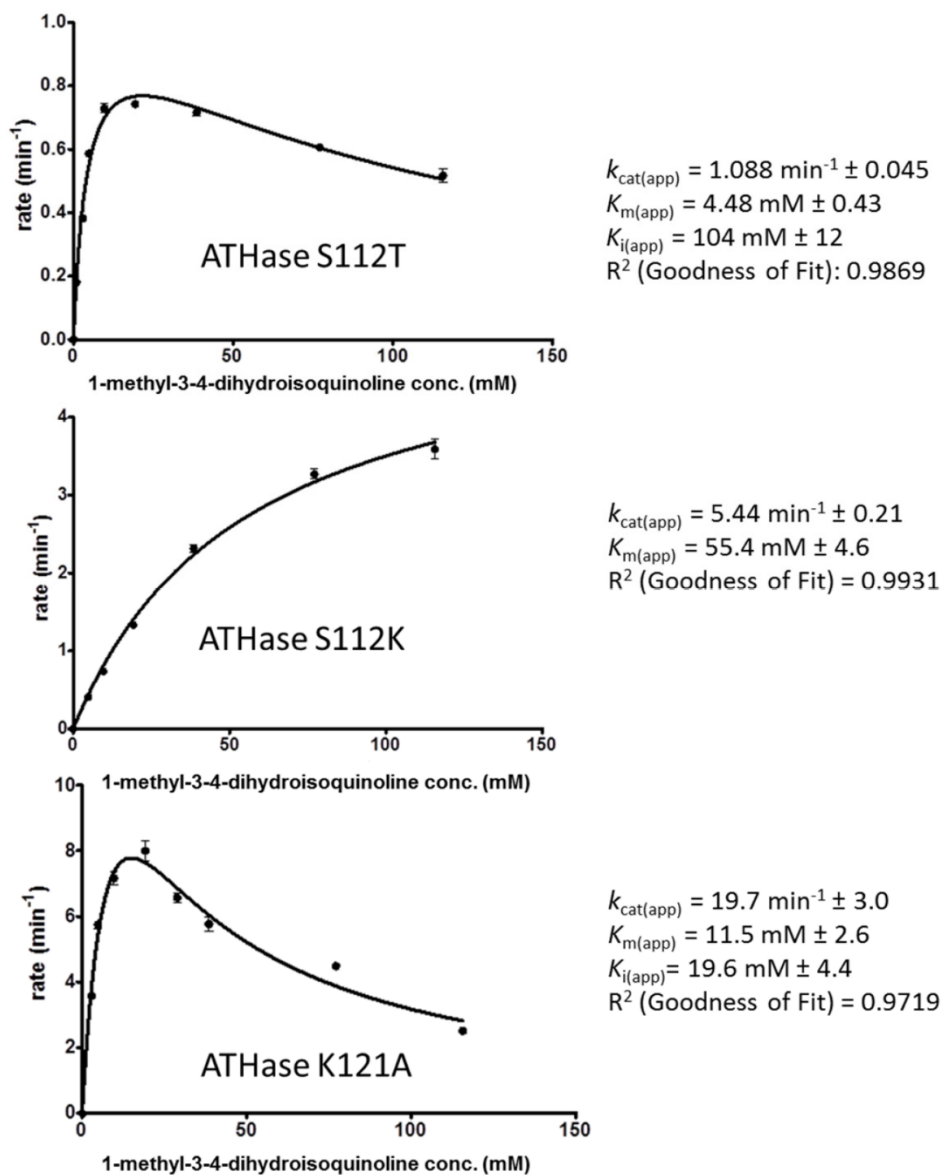


**Figure S19.** Saturation kinetics of ATHases in 1-methyl-3,4-dihydroisoquinoline reduction. Errors bars indicate  $\pm 1$  standard deviation, determined from the triplicate measurement of each rate.

### 3. Deracemisation of pipecolic acid (5) with DAAO/ATHase and synthesis of L-pipecolic acid from lysine (4) employing LAAO/ATHase/DAAO

Buffers and stock solutions:

MOPS buffer of 0.6 M, pH adjusted to 7.8 with NaOH.

MOPS/formate buffer: 0.6 M in MOPS, 3.0 M in sodium formate, pH adjusted with NaOH to 7.8.

Substrate: 36.5 mg of L-lysine hydrochloride (Bachem) was dissolved in a 10 mL volumetric flask in the MOPS/formate buffer and the pH was adjusted to 7.8 using solid NaOH (final concentration: 20 mM L-lysine). The pipecolic acid stock solution was prepared the same way dissolving 12.9 mg of *racemic* pipecolic acid (TCI) in 5 ml of the MOPS/formate buffer.

Sav: 11.0 mg of lyophilised Sav S112A (three free binding sites per tetramer were assumed) was dissolved in 671.5  $\mu$ L of the substrate stock solution (calculated final concentration: 1 mM Sav monomer corresponding to 750  $\mu$ M free biotin binding sites).

[Cp\*Ir(biot-*p*-L)Cl]: 1.20 mg of [Cp\*Ir(biot-*p*-L)Cl] was dissolved in 39.9  $\mu$ L of degassed DMF (final concentration: approximately 37.5 mM [Ir]).

LAAO: 20.1 mg of L-amino acid oxidase (*Crotalus atrox*, 0.17 U/mg solid, Sigma A5147) was dissolved in 342.3  $\mu$ L of the MOPS buffer (final concentration: 10 U/mL L-amino acid oxidase).

DAAO: 1.65 mg D-amino acid oxidase (from porcine kidney, 8.2 U/mg solid, Sigma A5222) was dissolved in 67.6  $\mu$ L of the MOPS buffer (calculated final concentration: 200 U/mL).

Catalase: 1.05 mg of lyophilised catalase (from bovine liver, 11 kU/mg solid, Sigma C40) was dissolved in 1153.8  $\mu$ L of the MOPS buffer (final concentration: 10 kU/mL catalase).

FAD: 1.22 mg of flavin adenine dinucleotide disodium salt hydrate (Sigma) was dissolved in 1470.7  $\mu$ L of the MOPS buffer (final concentration: 1 mM FAD).

The ATHase stock solution was prepared by adding 6.72  $\mu$ L of the [(Cp\*)Ir(biot-*p*-L)Cl] stock solution to the Sav stock solution before the mixture was stirred vigorously by means of a vortex mixer. A slight



turbidity was observed which disappeared upon dilution into the reaction mixture. The reaction mixture was prepared by adding the following stock solutions to a 1.5 mL PP-tube: 50  $\mu\text{L}$  LAAO-stock solution, 10  $\mu\text{L}$  DAAO-stock solution, 20  $\mu\text{L}$  catalase-stock solution and 20  $\mu\text{L}$  FAD-stock solution. Finally, the reaction was started by adding 100  $\mu\text{L}$  of the ATHase stock solution (final reaction volume: 200  $\mu\text{L}$ , calculated final concentrations: 495  $\mu\text{M}$  Sav monomer/371  $\mu\text{M}$  free biotin binding sites, 186  $\mu\text{M}$  [(Cp\*)Ir(biot-*p*-L)Cl], 2.5 U/mL LAAO, 10 U/mL DAAO, 1000 U/mL catalase, 100  $\mu\text{M}$  FAD, 0.597 M MOPS, 1.485 M formate). Tubes were shaken at 37  $^{\circ}\text{C}$  and 250 rpm in an incubator for 20 h.

To the reaction mixture was added 50  $\mu\text{L}$  of an aqueous 1-aminocyclohexanecarboxylic acid (40 mM) as an internal standard followed by 250  $\mu\text{L}$  of MeOH before the tubes were centrifuged at 21100  $\times g$  for 5 min at 4  $^{\circ}\text{C}$ .

200  $\mu\text{L}$  of the supernatant was diluted with 800  $\mu\text{L}$  of a 2 mM aq.  $\text{CuSO}_4$ -solution and the tubes were again centrifuged at 21100  $\times g$  for 5 min at 4  $^{\circ}\text{C}$ .

The supernatant was analysed by reversed phase HPLC using a Chirex 3126 D-penicillamin column (50  $\times$  4.6 mm) with an Agilent XDB-C18 guard column (12.5  $\times$  4.6 mm) and 2 mM aq.  $\text{CuSO}_4$  as an eluent (0.8 mL/min, 25  $^{\circ}\text{C}$ , 247 nm);  $T_R$  7.4 min (L-pipecolic acid), 12.8 min (D-pipecolic acid), 27.1 min (1-aminocyclohexanecarboxylic acid). Alternatively 2 mM  $\text{CuSO}_4$  with 3% MeOH was used as an eluent (see following page for retention times). Conversions were determined with respect to the internal standard peak.

## 5. References

- [1] Köhler, V. *et al.* OsO<sub>4</sub>-Streptavidin: A tunable hybrid catalyst for the enantioselective *cis*-dihydroxylation of olefins. *Angew. Chem. Int. Ed.* **50**, 10863-10866 (2011).
- [2] Gallizia, A. *et al.* Production of a soluble and functional recombinant streptavidin in *Escherichia coli*. *Protein Expres. Purif.* **14**, 192–196 (1998).
- [3] Wilson, Y. M., Dürrenberger, M. & Ward, T. R. Organometallic chemistry in protein scaffolds. *Protein Engineering Handbook*, Volume III, Eds. S. Lutz, U. T. Bornscheuer, Wiley VCH, Weinheim, *in press*.
- [4] Atkin, K. E. *et al.* The structure of monoamine oxidase from *Aspergillus niger* provides a molecular context for improvements in activity obtained by directed evolution. *J. Mol. Biol.* **384**, 1218–1231 (2008).
- [5] Rowles, I., Malone, K. J., Etchells, L. L., Willies, S. C. & Turner, N. J. Directed evolution of the enzyme monoamine oxidase (MAO-N): highly efficient chemo-enzymatic deracemisation of the alkaloid (±)-crispine A. *ChemCatChem*, DOI: 10.1002/cctc.201200202.
- [6] Starr, D. F., Bulbrook, H. & Hixon, R. M. Electron sharing ability of organic radicals VI. Alpha-substituted pyrrolines and pyrrolidines. *J. Am. Chem. Soc.* **54**, 3971-3976 (1932).
- [7] Dunsmore, C. J., Carr, R., Fleming, T. & Turner, N. J. A chemo-enzymatic route to enantiomerically pure cyclic tertiary amines. *J. Am Chem. Soc.* **128**, 2224-2225 (2006).
- [8] Kada, G., Kaiser, K., Falk, H. & Gruber, H. Rapid estimation of avidin and streptavidin by fluorescence quenching or fluorescence polarization. *Biochim. Biophys. Acta, Gen. Subj.* **1427**, 44-48 (1999).
- [9] Michaelis, L. & Menten, M. L. Die kinetik der invertinwirkung. *Biochem. Z.* **49**, 333–369 (1913).
- [10] Haldane, J. *Enzymes*. Longmans, Green and Co., New York (1930).

DOI: 10.1038/NCHEM.1498

## SUPPLEMENTARY INFORMATION

- [11] Vuister, G. W. & Bax, A. Resolution enhancement and spectral editing of uniformly  $^{13}\text{C}$  enriched proteins by homonuclear broadband  $^{13}\text{C}$  decoupling. *J. Magn. Reson.* **98**, 428–435 (1992).
- [12] Schmid, A., Vereyken, V., Held, M. & Witholt, B. Preparative regio- and chemoselective functionalization of hydrocarbons by cell free preparations of 2-hydroxybiphenyl 3-monooxygenase. *J. Mol. Catal. B.* **11**, 455-462 (2001).
- [13] Suske, W. A., *et al.* Purification and characterization of 2-hydroxybiphenyl 3-monooxygenase, a novel NADH-dependent, flavin-containing, aromatic hydroxylase from *Pseudomonas azelaica*, HBP1. *J. Biol. Chem.* **272**, 24257-24265 (1997).
- [14] Dawson, R. M. C., Elliott, D. C., Elliott, W. H. & Jones, K. M. *Data for Biochemical Research*, 3rd Ed., Clarendon Press, Oxford, 122-123 (1986).


### 3.2.3 Neutralizing the Detrimental Effect of Glutathione on Precious Metal Catalysts

Author contribution: all experiments were performed in collaboration with Yvonne M. Wilson and Elisa S. Nogueira.

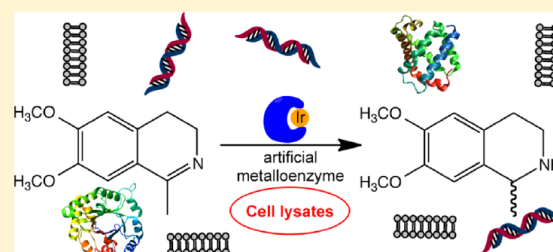
## Neutralizing the Detrimental Effect of Glutathione on Precious Metal Catalysts

Yvonne M. Wilson,<sup>‡,†</sup> Marc Dürrenberger,<sup>‡</sup> Elisa S. Nogueira, and Thomas R. Ward<sup>\*</sup>

Department of Chemistry, University of Basel, Spitalstrasse 51, CH-4056 Basel, Switzerland

 Supporting Information

**ABSTRACT:** We report our efforts to enable transition-metal catalysis in the presence of cellular debris, notably *Escherichia coli* cell free extracts and cell lysates. This challenging goal is hampered by the presence of thiols, mainly present in the form of glutathione (GSH), which poison precious metal catalysts. To overcome this, we evaluated a selection of oxidizing agents and electrophiles toward their potential to neutralize the detrimental effect of GSH on an Ir-based transfer hydrogenation catalyst. While the bare catalyst was severely inhibited by cellular debris, embedding the organometallic moiety within a host protein led to promising results in the presence of some neutralizing agents. In view of its complementary to natural enzymes, the asymmetric imine reductase based on the incorporation of a biotinylated iridium pianostool complex within streptavidin (Sav) isoforms was selected as a model reaction. Compared to purified protein samples, we show that pretreatment of cell free extracts and cell lysates containing Sav mutants with diamide affords up to >100 TON's and only a modest erosion of enantioselectivity.



### ■ INTRODUCTION

In many respects, organometallic- and enzymatic catalysis can be regarded as complementary. Over the past four decades, these two disciplines have by-and-large evolved independently. In recent years, however, there has been an increasing interest in exploiting organometallic catalysis in the context of chemical biology.<sup>1</sup> To achieve this ambitious goal, however, the compatibility of organometallic catalysts within the sea of functionality present in a cell must be ensured.

In recent years, there have been a handful of reports on precious-metal organometallic catalysis within living cells or in the presence of cell lysates.<sup>2</sup> To the best of our knowledge, however, the catalytic efficiency, as reflected by the very high catalyst loading used, remains modest in most cases.<sup>3</sup>

With the aim of improving the catalytic performance in the presence of cellular components, we have identified two potential challenges that may limit the versatility of organometallic catalysis in a cellular environment: (i) the organometallic catalyst and the enzymes present in a cell suffer from mutual inhibition;<sup>4</sup> and (ii) the reduced form of glutathione (GSH hereafter), present in millimolar concentration in cells cultivated under aerobic conditions, may poison the precious transition metals catalysts.

To overcome the mutual inhibition challenge, which may lead to inhibition of both organometallic catalyst and enzyme, we have exploited the potential of artificial metalloenzymes. Such hybrid catalysts result from the incorporation of an organometallic moiety within a protein environment, thus conferring a shielding second coordination sphere, reminiscent of natural enzymes.<sup>5–7</sup> Inspired by the pioneering work of

Wilson and Whitesides,<sup>6a</sup> we rely on the biotin–streptavidin technology to incorporate a biotinylated d<sup>6</sup>-Ir pianostool complex [Cp\*Ir(biot-*p*-L)Cl] within streptavidin (Sav hereafter) to yield an artificial transfer hydrogenase. Genetic optimization revealed that mutation at position S112 offered an attractive means to improve (and revert) the enantioselectivity: [Cp\*Ir(biot-*p*-L)Cl] ⋅ S112A Sav and [Cp\*Ir(biot-*p*-L)Cl] ⋅ S112K Sav yield the opposite enantiomers of salsolidine in 96 and 78% ee under optimized conditions using purified Sav.<sup>6b,8</sup>

Herein, we report our efforts to address *ex vivo* the GSH poisoning of precious-metal organometallic catalysts. For this purpose, we set out to screen a variety of Michael acceptors as well as oxidizing agents known to react with glutathione.

### ■ RESULTS AND DISCUSSION

Inspired by the reports of Meggers<sup>3</sup> Sadler<sup>8</sup> and Teply,<sup>2b</sup> suggesting that d<sup>6</sup>-pianostool complexes are particularly robust scaffolds for reactions within cells or in the presence of cell lysates, we selected the IrCp\*<sup>\*</sup>-catalyzed asymmetric transfer hydrogenation as a benchmark reaction.

For screening purposes, we selected *Escherichia coli* cell-free extracts and cell lysates (see experimental details in the Supporting Information (SI)). Following overexpression of a Sav isoform in the *E. coli* strain BL21(DE3) pLysS, the cell pellet was lysed by freeze–thaw cycles followed by addition of Tris-HCl buffer containing DNase I and phenylmethylsulfonyl-

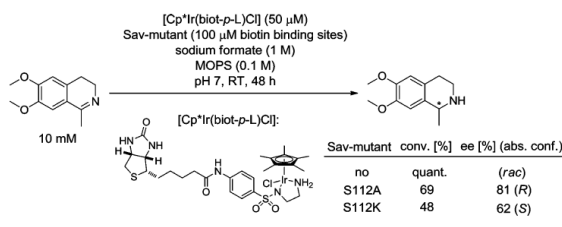
Received: January 20, 2014

Published: June 11, 2014

fluoride as protease inhibitor. Catalysis was either performed in the resulting cell lysate or with dried cell free extract (cfe) obtained by centrifugation and lyophilization of the supernatant to yield a brown powder. The cfe was stored at 4 °C until use. The biotin-binding site concentration of the cell lysates and cfe was determined using the biotin-4-fluorescein assay (see Figure S11).<sup>9</sup> The total thiol concentration of the cfe was estimated to approximately 500  $\mu\text{M}$  using Ellman's reagent.<sup>10</sup> As Sav, which is devoid of cysteines, represents >50% of the proteins present in the cfe, we conclude that most of the cysteines quantified by the Ellman test are contained in the glutathione present in cfe.

For comparison purposes, catalytic transfer hydrogenase experiments using  $[\text{Cp}^*\text{Ir}(\text{biot-}p\text{-L})\text{Cl}]$  were carried out with (i) purified Sav samples, (ii) purified Sav samples spiked with GSH, (iii) cfe containing Sav isoforms, (iv) cfe containing no Sav (resulting from an *E. coli* culture using a plasmid devoid of the Sav gene), and (v) cell lysates containing Sav isoforms. Prior to this study, typical catalysis experiments using purified Sav samples were performed using 250  $\mu\text{M}$   $[\text{Cp}^*\text{Ir}(\text{biot-}p\text{-L})\text{Cl}]$ , 500  $\mu\text{M}$  biotin binding sites (i.e., 125  $\mu\text{M}$  tetrameric Sav), with *in vivo* catalysis in mind, we set out to decrease the catalyst and substrate concentrations. Initial experiments were thus performed using 50  $\mu\text{M}$   $[\text{Cp}^*\text{Ir}(\text{biot-}p\text{-L})\text{Cl}]$ , 100  $\mu\text{M}$  biotin binding sites (i.e. 25  $\mu\text{M}$  tetrameric Sav), 1 M  $\text{HCO}_2\text{Na}$  in MOPS buffer (100 mM, pH 7) (see Scheme 1). For

**Scheme 1. Asymmetric Transfer Hydrogenation Catalyzed by an Artificial Imine Reductase As a Benchmark Reaction to Test the Neutralization of the Detrimental Effect of GSH**



comparison purposes, the imine reduction was performed with  $[\text{Cp}^*\text{Ir}(\text{biot-}p\text{-L})\text{Cl}]$ ;  $[\text{Cp}^*\text{Ir}(\text{biot-}p\text{-L})\text{Cl}]$  C S112A Sav and  $[\text{Cp}^*\text{Ir}(\text{biot-}p\text{-L})\text{Cl}]$  C S112K Sav, Scheme 1. The results are summarized in Table 1.

Catalysis results from experiments performed at 125  $\mu\text{M}$  Sav and 25  $\mu\text{M}$  Sav are similar, suggesting that the ATHase is well suited to operate at low concentrations (Table 1, compare entries 1–3 to 4–6). Upon addition of  $\geq 0.1$  mM GSH (i.e., two equivalents vs Ir), all three catalytic systems were completely inhibited (Table 1, entries 7–18). This emphasizes the severe poisoning effect of GSH toward the catalyst precursor. Substitution of the chloride ligand by a pyridine (i.e.,  $[\text{Cp}^*\text{Ir}(\text{biot-}p\text{-L})\text{pyridine}]$ ), as suggested by Sadler,<sup>8b</sup> did not improve significantly the catalytic performance in the presence of GSH toward the reduction of the salsolidine precursor. In contrast, addition of GSSG had a less negative impact on the reaction, although in the case of the bare Ir-complex and the S112K mutant, the conversions were found to be modest (Table 1, entries 19–21). We thus speculated that oxidizing GSH or derivatizing its thiol function could—at least partially—prevent inhibition of the transfer hydrogenation catalyst.

We selected Michael acceptors and oxidizing agents known to react with GSH to yield the corresponding thioether and disulfide, respectively. The following Michael acceptors were tested: maleinimide **Malln**, 2-bromo-1-phenylethanone **BrPheOne**, phenyl-vinylsulfone **PheViSul**, and 3-phenyl-2-propenenitrile **PhePropNit**. The following oxidizing agents were selected: oxone **Ox**, 1,4-benzoquinone **BQ**,<sup>11</sup>  $\text{K}_3[\text{Fe}(\text{CN})_6]$   $\text{Fe}^{3+}$ ,<sup>12</sup> and diamide **DiAm**,<sup>13</sup> Figure 1. For this purpose, solutions either with or without a Sav isoform were spiked with 2.5 mM GSH and incubated overnight in the presence of different concentrations of a particular GSH neutralizing agent before adding the Ir-catalyst. The reactions were initiated by addition of the imine substrate and run for 2 days (see Table 1 in the SI). The main findings of this screening include: (1)  $\text{Fe}^{3+}$  and **BQ** are not compatible with any of the three catalytic systems; even in the absence of GSH, no or low conversions are observed. (2) **Malln** exhibits limited compatibility with the Ir-catalyst, especially when the latter is embedded within Sav. However, apart from this, **Malln** proved to be a poor GSH neutralizing agent under the selected experimental conditions. (3) **PhePropNit** is most effective when applied at a ratio **PhePropNit**/GSH 2:1. An equimolar amount has no benefit on the reaction, whereas four equivalents led to a decrease in conversion and enantioselectivity in the case of the S112K mutant. (4) Despite the fact that  $\text{H}_2\text{O}_2$  is commonly used to oxidize GSH, we favored **Ox** for this purpose. Indeed, it was found to be more compatible with the experimental setup as the presence of catalases in the cfe lead to significant gushing upon addition of  $\text{H}_2\text{O}_2$ . Strikingly, although **Ox** is a two electron oxidant, its efficacy is most pronounced with four equivalents vs GSH. This behavior may be traced back to the fact that, in the presence of formate, GSH is oxidized to the corresponding sulfonic acid rather than the disulfide GSSG.<sup>14</sup> (5) The most effective GSH neutralizing agents are **BrPheOne**, **PheViSul**, and **DiAm**. Compared to reactions where GSH is absent, all these agents led to comparable conversions and enantioselectivities in most cases when incubated for either 2 or 15 h to GSH-spiked solutions prior to catalysis. Increasing the concentration of the GSH neutralizing agents leads to less consistent results; the outcome of the reaction depends on the Sav mutant (if any) is used. For example, **DiAm** is fully compatible with the artificial metalloenzymes but not with free  $[\text{Cp}^*\text{Ir}(\text{biot-}p\text{-L})\text{Cl}]$  as increasing concentrations led to a decrease in conversion. A similar behavior is observed with **BrPheOne** when no Sav or the S112K mutant was present. On the other hand, **PheViSul** does not affect the free Ir-complex but limited compatibility was observed with the hybrid catalysts especially in absence of GSH.

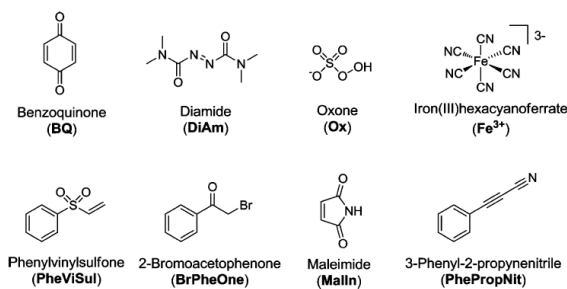
With regard to these results, the following properties of the GSH neutralizing agents have to be considered: (i) efficiency of GSH neutralization; (ii) (mutual) inhibition between the catalyst and the GSH neutralizing agent (compatibility), (iii) inhibition of the catalyst and the product of the GSH neutralization (disulfide and thioether respectively), (iv) reduction of GSSG to GSH by the Ir-catalyst, (v) competing catalytic reduction of the GSH neutralizing agent by the Ir-catalyst when used in excess and vi) derivatization of Sav amino acid side chains by the Michael acceptors.

Next, the most promising glutathione neutralizing agents **BrPheOne**, **PheViSul**, and **DiAm** were tested in the presence of cell free extracts, Figure 2. While the bare catalyst was inactive, up to 22 turnovers (i.e., 11% conversion at 0.5 mol %

**Table 1.** Catalysis with Purified Sav at Low Catalyst Concentration and in the Presence of GSH and GSSG at RT (for further details see SI)

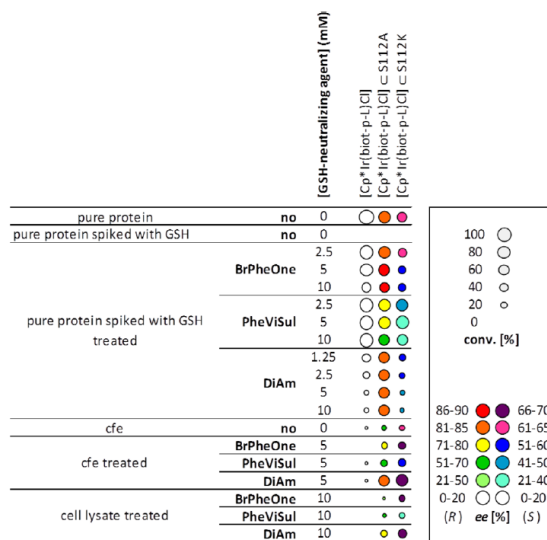
entry	Sav mutant	[Sav] ( $\mu\text{M}$ )	[Ir] ( $\mu\text{M}$ )	[formate] (M)	[GSH] (mM)	[GSSG] (mM)	[substrate] (mM)	time (h)	conversion <sup>b</sup> (%)	ee <sup>a,b</sup> (%)
1	no	125	250	3	0	0	50	4.5	quant.	0
2	S112A	125	250	3	0	0	50	4.5	89 $\pm$ 1	90 $\pm$ 1
3	S112K	125	250	3	0	0	50	4.5	70 $\pm$ 3	-75 $\pm$ 1
4	no	25	50	1	0	0	10	48	quant.	0
5	S112A	25	50	1	0	0	10	48	69 $\pm$ 5	81 $\pm$ 1
6	S112K	25	50	1	0	0	10	48	48 $\pm$ 1	-62 $\pm$ 2
7	no	25	50	1	0.025	0	10	48	92 $\pm$ 2	0
8	no	25	50	1	0.05	0	10	48	59 $\pm$ 4	0
9	no	25	50	1	0.1	0	10	48	0	-
10	no	25	50	1	2.5	0	10	48	0	0
11	S112A	25	50	1	0.025	0	10	48	56 $\pm$ 2	83 $\pm$ 1
12	S112A	25	50	1	0.05	0	10	48	37 $\pm$ 3	83 $\pm$ 2
13	S112A	25	50	1	0.1	0	10	48	0	-
14	S112A	25	50	1	2.5	0	10	48	0	0
15	S112K	25	50	1	0.025	0	10	48	23 $\pm$ 2	-60 $\pm$ 2
16	S112K	25	50	1	0.05	0	10	48	9 $\pm$ 5	-55 $\pm$ 3
17	S112K	25	50	1	0.1	0	10	48	0	-
18	S112K	25	50	1	2.5	0	10	48	0	0
19	no	25	50	1	0	2.5	10	48	19 $\pm$ 1	0
20	S112A	25	50	1	0	2.5	10	48	50 $\pm$ 1	84 $\pm$ 2
21	S112K	25	50	1	0	2.5	10	48	15 $\pm$ 1	-47 $\pm$ 3

<sup>a</sup>Positive ee values correspond to (*R*)-salsolidine, and negative ee values correspond to (*S*)-salsolidine. <sup>b</sup>The  $\pm$  values represent standard deviations resulting from triplicate measurements. GSH: reduced form of glutathione; GSSG: oxidized form of glutathione (glutathione disulfide).

**Figure 1.** Stoichiometric reagents tested to neutralize glutathione (top oxidizing agents, bottom Michael acceptors).

catalyst loading) were obtained for the  $[\text{Cp}^*\text{Ir}(\text{biot-}p\text{-L})\text{Cl}] \text{Cl}$  S112A Sav variant without pretreatment of the cfe with a GSH neutralizing agent. This clearly demonstrates the efficacy of the second coordination sphere to protect the precious metal from cell debris, Table 2 entries 5 and 6. In the presence of a GSH neutralizing agent, the catalytic performance could be improved significantly for the artificial metalloenzyme. **DiAm** proved most effective at concentrations of 5–10 mM leading up to 110 turnovers in case of the S112A mutant and 96 turnovers with the S112K mutant (Table 2, entry 14 and 15). This amounts to up to 72% recovery of the original activity of these catalysts, without loss of selectivity. Reducing the preincubation time to 2 h yielded nearly identical results (Table 2, entry 16 and 17). On the other hand, none of the three GSH neutralizing agents had a beneficial effect on the bare Ir-complex in cfe's: conversions do not exceed 5% (Table 2, entry 7, 10 and 13).

Recent saturation kinetic studies demonstrate that the  $[\text{Cp}^*\text{Ir}(\text{biot-}p\text{-L})\text{Cl}] \text{Cl}$  S112A Sav ATHase exhibits higher reaction rates than its  $[\text{Cp}^*\text{Ir}(\text{biot-}p\text{-L})\text{Cl}] \text{Cl}$  S112K Sav counterpart ( $k_{\text{cat}} = 11.4 \text{ min}^{-1}$  vs  $k_{\text{cat}} = 2.6 \text{ min}^{-1}$ ). Although

**Figure 2.** Fingerprint representation of ATHase activity in the presence of GSH neutralizing agents.

these kinetic profiles are reflected in the initial screening experiments in the presence of purified Sav, the S112K variant generally yields better conversions in the presence of pretreated cfe. Assuming that the neutralization of GSH in the cellular environment is as efficient as in the presence of purified protein, this finding suggests that GSH may be the main but not the sole inhibitor of the precious metal catalyst. Considering the propensity of precious metals to interact with guanine in oligonucleotides,<sup>15</sup> we speculate that the cationic lysine residue at position S121 K interacts with the

Table 2. Selected Results Obtained from Catalysis in the Presence of Cell Free Extracts (cfe) and Cell Lysates<sup>a</sup>

entry	Sav mutant	origin	GSH neutralizing agent	concentration (mM)	preincubation time (h)	conversion <sup>c</sup> (%)	ee <sup>b,c</sup> (%)
1	no	–	no	–	–	98 ± 1	0
2	S112A	purified	no	–	–	95 ± 3	82 ± 2
3	S112K	purified	no	–	–	67 ± 3	–64 ± 3
4	no	cfe <sup>d</sup>	no	–	–	2 ± 1	o
5	S112A	cfe	no	–	–	11 ± 2	68 ± 2
6	S112K	cfe	no	–	–	8 ± 2	–55 ± 5
7	no	cfe <sup>d</sup>	BrAcPhe	5	15	0	–
8	S112A	cfe	BrAcPhe	5	15	20 ± 1	74 ± 3
9	S112K	cfe	BrAcPhe	5	15	25 ± 3	–62 ± 6
10	no	cfe <sup>d</sup>	PheViSul	5	15	2 ± 1	0
11	S112A	cfe	PheViSul	5	15	22 ± 5	62 ± 3
12	S112K	cfe	PheViSul	5	15	32 ± 1	–44 ± 6
13	no	cfe <sup>d</sup>	DiAm	10	15	4 ± 1	0
14	S112A	cfe	DiAm	5	15	55 ± 6	83 ± 2
15	S112K	cfe	DiAm	5	15	48 ± 5	–60 ± 4
16	S112A	cfe	DiAm	10	2	49 ± 10	85 ± 1
17	S112K	cfe	DiAm	10	2	42 ± 1	–64 ± 6
18	no	cell lysate	no	–	–	0	–
19	S112A	cell lysate	no	–	–	0	–
20	S112K	cell lysate	no	–	–	0	–
21	S112A	cell lysate	BrAcPhe	10	15	6 ± 1	59 ± 17
22	S112K	cell lysate	BrAcPhe	10	15	31 ± 12	–66 ± 1
23	S112A	cell lysate	PheViSul	10	15	9 ± 1	54 ± 11
24	S112K	cell lysate	PheViSul	10	15	20 ± 5	–42 ± 6
25	no	cell lysate <sup>d</sup>	DiAm	10	15	<1	n.d.
26	S112A	cell lysate	DiAm	10	15	22 ± 3	70 ± 6
27	S112K	cell lysate	DiAm	10	15	43 ± 7	–68 ± 1

<sup>a</sup>All reactions were performed with 50  $\mu$ M [Cp\*Ir(biot-*p*-L)Cl], 25  $\mu$ M tetrameric Sav, 0.6 M MOPS pH 7, and 3 M sodium formate at RT for 48 h (see SI for details). <sup>b</sup>Positive ee values correspond to (*R*)-salsolidine and negative ee values correspond to (*S*)-salsolidine. <sup>c</sup>The  $\pm$  values represent standard deviations resulting from triplicate measurements. <sup>d</sup>cfe containing no Sav resulting from an *E. coli* culture using an plasmid devoid of the Sav gene.

phosphate of the (oligo)nucleotide, hampering N<sup>7</sup> guanine coordination to the iridium moiety with this mutant.

Encouraged by these findings, we tested the ATHase with cell lysates (see SI for a detailed procedure). Again here, the best results were achieved with **DiAm** yielding up to 44 turnovers (S112A) and 86 (S112K) turnovers, respectively (Table 2, entry 26 and 27). Besides the lower conversions obtained compared to experiments performed with cfe, in the case of the S112A-ATHase also a slight decrease of enantioselectivity was observed. The S112K mutant shows no degradation in agreement with the assumption that the latter better protects the Ir-center from inhibitors.

## OUTLOOK

From the data presented in this study, we conclude that diamide **DiAm** is a promising GSH oxidizing agent which is shown to be compatible with organometallic catalysis on cell free extracts as well as cell lysates. This important finding will allow us to apply directed evolution protocols to optimize the performance of artificial transfer hydrogenases with crude cellular extracts.

With the ultimate goal of performing precious metal catalysis *in vivo*, it is noteworthy that Kosower has shown that diamide **DiAm** is compatible with living cells, including *E. coli*, neither causing lysis nor death.<sup>13,16</sup> The next challenge is to engineer a transport of the abiotic metal cofactor within *E. coli* expressing Sav to ultimately perform catalysis *in vivo*.

## ASSOCIATED CONTENT

### Supporting Information

General procedure for the preparation of cell free extracts and cell lysates, experimental details, and additional data. This material is available free of charge via the Internet at <http://pubs.acs.org>

## AUTHOR INFORMATION

### Corresponding Author

thomas.ward@unibas.ch

### Author Contributions

<sup>‡</sup>These authors contributed equally.

### Notes

The authors declare no competing financial interest.

<sup>†</sup>Deceased on January 22, 2014.

## ACKNOWLEDGMENTS

T.R.W. thanks the Swiss National Science Foundation (grant 200020\_144354) and the EU (ITN Biotrains FP7-ITN-238531 for a Marie Curie fellowship to ESN) for financial support. Prof. C. R. Cantor is thanked for the streptavidin gene and Umicore precious metal chemistry for a loan of iridium. T.R.W. thanks Prof. F. Seebeck for insightful comments. M.D. thanks Fabian Schwizer for help with Figure 2.



## REFERENCES

- (1) (a) Prescher, J. A.; Bertozzi, C. R. *Nat. Chem. Biol.* **2005**, *1*, 13. (b) Sletten, E. M.; Bertozzi, C. R. *Angew. Chem., Int. Ed.* **2009**, *48*, 6974. (c) Stephanopoulos, N.; Francis, M. B. *Nat. Chem. Biol.* **2011**, *7*, 876.
- (2) (a) Streu, C.; Meggers, E. *Angew. Chem., Int. Ed.* **2006**, *45*, 5645. (b) driaenssens, L.; Severa, L.; Vávra, J.; Šalová, T.; Hývl, J.; Čížková, M.; Pohl, R.; Šaman, D.; Teplý, F. *Collect. Czech. Chem. Commun.* **2009**, *74*, 1023. (c) Yusop, R. M.; Unciti-Broceta, A.; Johansson, E. M. V.; Sánchez-Martín, R. M.; Bradley, M. *Nat. Chem.* **2011**, *3*, 239. (d) Sasmal, P. K.; Carregal-Romero, S.; Han, A. A.; Streu, C. N.; Lin, Z.; Namikawa, K.; Elliott, S. L.; Köster, R. W.; Parak, W. J.; Meggers, E. *ChemBioChem* **2012**, *13*, 1116. (e) Do, J. H.; Kim, H. N.; Yoon, J.; Kim, J. S.; Kim, H.-J. *Org. Lett.* **2010**, *12*, 932. (f) Chalker, J.; Wood, C.; Davis, B. J. *Am. Chem. Soc.* **2009**, *131*, 16346. (g) Lin, Y. A.; Chalker, J. M.; Davis, B. J. *ChemBioChem* **2009**, *10*, 959. (h) Giannini, F.; Süß-Fink, G.; Furrer, J. *Inorg. Chem.* **2011**, *50*, 10552. (i) Soriano del Amo, D.; Wang, W.; Jiang, H. J. *Am. Chem. Soc.* **2010**, *132*, 16894. (j) Lee, Y.; Umeano, A.; Balskus, E. P. *Angew. Chem., Int. Ed.* **2013**, *52*, 11800. (k) Ball, Z. T. *Acc. Chem. Res.* **2013**, *46*, 560. (l) Li, N.; Lim, R. K. V.; Edwardraja, S.; Lin, Q. J. *Am. Chem. Soc.* **2011**, *133*, 15316. (m) Li, J.; Yu, J.; Zhao, J.; Wang, J.; Zheng, S.; Lin, S.; Chen, L.; Yang, M.; Jia, S.; Zhang, X.; Chen, P. R. *Nat. Chem.* **2014**, *6*, 352.
- (3) Sasmal, P. K.; Streu, C. N.; Meggers, E. *Chem. Commun.* **2013**, 49, 1581.
- (4) Poizat, M.; Arends, I. W. C. E.; Hollmann, F. *J. Mol. Catal. B: Enzym.* **2010**, *63*, 149.
- (5) (a) Rosati, F.; Roelfes, G. *ChemCatChem.* **2010**, *2*, 916. (b) Deuss, P. J.; den Heeten, R.; Laan, W.; Kamer, P. C. *Chem.—Eur. J.* **2011**, *17*, 4680. (c) Ringenberg, M. R.; Ward, T. R. *Chem. Commun.* **2011**, 47, 8470. (d) Ward, T. R. *Acc. Chem. Res.* **2011**, *44*, 47.
- (6) (a) Wilson, M. E.; Whitesides, G. M. *J. Am. Chem. Soc.* **1978**, *100*, 306. (b) Koehler, V.; Wilson, Y. M.; Dürrenberger, M.; Ghislieri, D.; Churakova, E.; Quinto, T.; Knörr, L.; Häussinger, D.; Hollmann, F.; Turner, N. J.; Ward, T. R. *Nat. Chem.* **2013**, *5*, 93.
- (7) Wang, Z. J.; Clary, K. N.; Bergman, R. G.; Raymond, K. N.; Toste, F. D. *Nat. Chem.* **2013**, *5*, 100.
- (8) (a) Dougan, S. J.; Habtemariam, A.; McHale, S. E.; Parsons, S.; Sadler, P. J. *Proc. Natl. Acad. Sci. U. S. A.* **2008**, *105*, 11628. (b) Liu, Z.; Romero-Canelón, I.; Qamar, B.; Hearn, J. M.; Habtemariam, A.; Barry, N. P. E.; Pizarro, A. M.; Clarkson, G. J.; Sadler, P. J. *Angew. Chem., Int. Ed.* **2014**, *53*, 3941.
- (9) (a) Kada, G.; Kaiser, K.; Falk, H.; Gruber, H. J. *Biochim. Biophys. Acta* **1999**, *1427*, 44. (b) Humbert, N.; Zocchi, A.; Ward, T. R. *Electrophoresis* **2005**, *26*, 47.
- (10) Riddles, P. W. *Anal. Biochem.* **1979**, *94*, 75.
- (11) Lau, S. S.; Hill, B. A.; Highet, R. J.; Monks, T. J. *Mol. Pharmacol.* **1988**, *34*, 829.
- (12) Stochel, G.; Martinez, P.; Van Eldik, R. J. *Inorg. Biochem.* **1994**, *54*, 131.
- (13) Wax, R.; Rosenberg, E.; Kosower, N. S.; Kosower, E. M. J. *Bacteriol.* **1970**, *101*, 1092.
- (14) Calam, D. H.; Waley, S. G. *Biochem. J.* **1962**, *85*, 417.
- (15) Wang, F.; Xu, J.; Wu, K.; Weidt, S. K.; Mackay, C. L.; Langridge-Smith, P. R. R.; Sadler, P. J. *Dalton Trans.* **2013**, 42, 3188.
- (16) Kosower, E. M.; Kosower, N. S. *Nature* **1969**, *224*, 117.

## Neutralizing the Detrimental Effect of Glutathione on Precious Metal Catalysts

Yvonne M. Wilson<sup>††</sup>, Marc Dürrenberger<sup>‡</sup>, Elisa S. Nogueira and Thomas R. Ward<sup>\*</sup>

Department of Chemistry, University of Basel, Spitalstrasse 51, CH-4056 Basel, Switzerland

### Supporting Information

**General Considerations** 6,7-dimethoxy-1-methyl-3,4-dihydroisoquinoline, glutathione, Maleimide, 2-bromo-1-phenylethanone, Oxone, Phenylvinyl sulfone, diamide, 3-phenyl-2-propynenitrile, benzoquinone and  $\text{K}_3\text{Fe}^{\text{III}}(\text{CN})_6$  were purchased from commercial suppliers and used as received. Streptavidin (Sav) mutants were produced, purified and characterized as previously described [1]. The Sav used in this work and on which all variants were based was T7-tagged core Sav described by Gallizia *et al.* [2] and herein we refer to it as wild-type Sav. The corresponding ATHase is also referred to as wild-type (WT). For a detailed synthesis procedure of  $[\text{Cp}^*\text{Ir}(\text{Biot-}p\text{-L})\text{Cl}]$ , see reference [3]. HPLC measurements were performed on Agilent machines equipped with modules from the 1100 and 1200 series and diode array detectors. HPLC columns were used with the appropriate guard columns.

**Stock solutions and buffers** MOPS/formate buffer: 3-(*N*-morpholino)propanesulfonic acid and sodium formate were dissolved in milliQ water to the desired concentrations (see below) and the pH was adjusted by addition of NaOH.

–S2–

Ir-complex: [Cp\*Ir(biot-*p*-L)Cl] was dissolved in DMF to a final concentration of 2 mM. This solution was prepared freshly for each experiment.

Substrate: 6,7-dimethoxy-1-methyl-3,4-dihydroisoquinoline (164.2 mg) was dissolved in water (2 ml) to a final concentration of 400 mM.

Glutathione: Reduced glutathione was dissolved in milliQ water to the desired final concentration (see below). This solution was prepared freshly for each experiment.

GSH neutralizing agents: Maleinimide, 2-bromo-1-phenylethanone, Phenylvinyl sulfone, diamide, 3-phenyl-2-propynenitrile and benzoquinone were dissolved in DMF to a final concentration of 200 mM.

Oxone and  $K_3Fe^{III}(CN)_6$  were dissolved in milliQ water to a final concentration of 200 mM.

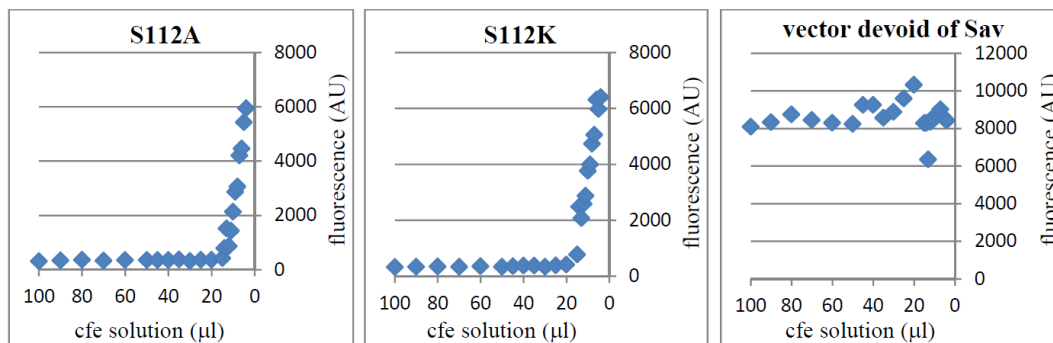
These solutions were prepared freshly for each experiment.

**Preparation of cell free extracts (cfe) and cell lysates** *E. coli* cells (BL21(DE3)pLysS) containing either a pET11b-T7Sav-plasmid including the gene for Sav-S112A or -S112K, respectively, were grown in LB medium containing 34  $\mu$ g/ml chloramphenicol and 100  $\mu$ g/ml ampicillin (1 L culture) at 37 °C until an  $OD_{600}$  of 0.8-1 was reached. Expression was induced by adding IPTG (400  $\mu$  M final concentration). The cultures were shaken for 3.5 hours at 37 °C, and cells were harvested by centrifugation (3846 x *g*) for 10 minutes at 4 °C. To the pellet (between 2.5 and 3 g per liter) was added Tris-HCl buffer (20 mM, pH 7.4) containing 1 mM PMSF (5-10 ml according to have a final concentration of 28.6  $\mu$ M tetrameric Sav) as well as DNaseI (Roche, small tip of spatula, some 1000 U) before shaking at room temperature for 1 h. The resulting cell lysate was stored at -20 °C.

Cfe was prepared by centrifugation of the cell lysate for 10 minutes and lyophilizing the frozen supernatant to obtain beige to brown powder which was stored at 4 °C. The content of Sav was determined using a biotin-4-fluorescein titration assay (see below). [4]

**Biotin-4-fluorescein assay** Cfe was dissolved in 100 mM phosphate buffer pH 7 (5 mg/ml) and decreasing volumes of this solution (100 to 4  $\mu$ l) were added to microtiter plate wells (Nunclon) each containing 10  $\mu$ l of a 40  $\mu$ M biotin-4-fluorescein solution (prepared by dilution of a 0.6 M stock solution in DMSO with phosphate buffer). The final volume of 120  $\mu$ l was adjusted by addition of phosphate buffer in each well before the fluorescence was detected in a plate reader (Tecan Sapphire,  $\lambda_{\text{ex}} = 485$  nm,  $\lambda_{\text{abs}} = 520$  nm). The fluorescence was then plotted as a function of the amount of cfe solution added to each well and the concentration of biotin binding sites was calculated from the volume at the equivalence point (where the concentration of Sav free binding sites is equal to the biotin-4-fluorescein concentration, see below). The content of Sav in cell lysates was determined from diluted (1:2-1:4) supernatants of centrifuged samples as described above.

**Figure S11** Determination of Sav biotin binding capacity of cell free extracts using biotin-4-fluorescein. Upon incorporation within Sav isoforms, the fluorescence is quenched. Once all biotin-binding sites are saturated, the excess biotin-4-fluorescein leads to fluorescence.



**Ellman's assay** 2.5 ml of a reaction buffer containing 100 mM phosphate (pH 8) and 1 mM EDTA was treated with 50  $\mu$ l of a 5,5'-dithio-*bis*-(2-nitrobenzoic acid) solution (10 mM in reaction buffer) as well as 250  $\mu$ l cfe solution (20 mg/ml in reaction buffer) and incubated for 30 min at RT before the absorbance at

-S4-

412 nm was measured. The thiol concentration was calculated using a molar extinction coefficient of  $14150 \text{ M}^{-1}\text{cm}^{-1}$ . [5]

**General set up for reactions using purified Sav mutants** Lyophilized Sav was dissolved in MOPS/formate buffer containing 0.2 M MOPS and 2 M sodium formate (pH 7) to a final concentration of 50  $\mu\text{M}$  tetrameric Sav (the average number of free binding sites per Sav tetramer was determined with a biotin-4-fluorescein assay [4]). 100  $\mu\text{l}$  of this solution were added to a glass tube equipped with a mechanical stirrer followed by addition of water (50  $\mu\text{l}$ ), glutathione stock solution (16.7  $\mu\text{M}$ , 30  $\mu\text{l}$ ), DMF (between 0 and 10  $\mu\text{l}$ ) and GSH neutralizing agent stock solution (between 0 and 10  $\mu\text{l}$  corresponding to the desired final concentration). This mixture was then stirred for 2 or 15 hours at room temperature before the Ir-complex stock solution was added (5  $\mu\text{l}$ ). After 5 minutes, the reaction was initiated by adding the substrate stock solution (5  $\mu\text{l}$ ), and the mixture was stirred for 48 hours at room temperature (final volume: 200  $\mu\text{l}$ ; final concentrations: 50  $\mu\text{M}$  [ $\text{Cp}^*\text{Ir}(\text{biot-}p\text{-L})\text{Cl}$ ], 25  $\mu\text{M}$  Sav, 0.1M MOPS, 1 M formate, 2.5 mM glutathione, between 1.25 and 10 mM glutathione neutralizing agent, 7.5 % (v/v) DMF). The set up for reactions without Sav was identical, except that MOPS/formate buffer containing no Sav was used.

**General set up for reactions using cell free extracts** Cfe was dissolved in MOPS formate buffer containing 0.686 M MOPS and 3.429 M sodium formate (pH 7) to a concentration of 22.9 mg/ml (corresponds to 28.6  $\mu\text{M}$  tetrameric Sav). 175  $\mu\text{l}$  of this slightly turbid solution was added to a glass tube equipped with a mechanical stirrer followed by addition of water (5  $\mu\text{l}$ ), DMF (between 0 and 10  $\mu\text{l}$ ) and GSH neutralizing agent stock solution (between 0 and 10  $\mu\text{l}$  corresponding to the desired final concentration). The mixture was then stirred for 15 hours and the reaction was started as described above (final volume: 200  $\mu\text{l}$ ; final concentrations: 50  $\mu\text{M}$  [ $\text{Cp}^*\text{Ir}(\text{biot-}p\text{-L})\text{Cl}$ ], 25  $\mu\text{M}$  Sav, 0.6 M MOPS, 3 M formate, between 1.25 and 10 mM glutathione neutralizing agent, 7.5 % v/v DMF).

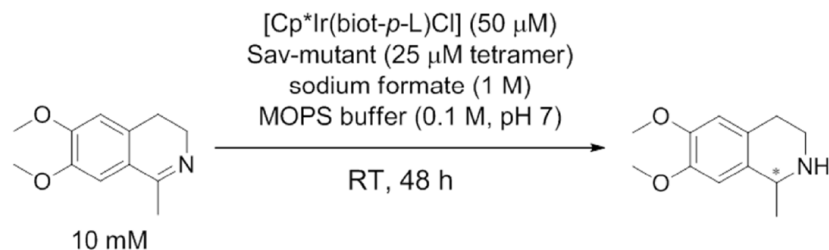
-55-

**General set up for reactions using lysed cells** To cell lysates was added MOPS and sodium formate to a concentration of 0.686 M and 3.429 M, respectively, and the mixture was stirred by means of a vortex mixer until the MOPS and formate were completely dissolved. The pH was adjusted to 7 by addition of NaOH, and reactions were performed with 175  $\mu$ l of the resulting mixture as described for catalysis with cfe (see above). Final volume: 200  $\mu$ l; final concentrations: 50  $\mu$ M [Cp\*Ir(biot-*p*-L)Cl], 25  $\mu$ M Sav, 0.6 M MOPS, 3 M formate, 17.5 mM Tris, 0.875 mM PMSF, between 0.1 and 10 mM glutathione neutralizing agent, 7.5 % (v/v) DMF)

**Work up and analysis** To the reaction mixtures milliQ water (500  $\mu$ l) was added followed by addition of 20% NaOH (50  $\mu$ l). The mixture was then extracted two times with dichloromethane (1 ml), the combined organic fractions were collected in a PP tube containing anhydrous sodium sulfate, centrifuged (18800 x g) for 5 minutes and the supernatant was analyzed by chiral HPLC using a Chiralpak IC column (5  $\mu$ m, 4.6 mm · 25 mm) and dichloromethane containing 1% isopropanol and 0.06% diethylamine as an eluent; 1 ml/min; 25 °C, 280 nm,  $T_R$  8.5 min ((*S*)- 6,7-dimethoxy-1-methyl-1,2,3,4-tetrahydroisoquinoline), 9.8 min (6,7-dimethoxy-1-methyl-3,4-dihydroisoquinoline), 14.6 ((*R*)- 6,7-dimethoxy-1-methyl-1,2,3,4-tetrahydroisoquinoline, referred to as salsolidine). Yields were calculated under consideration of a response factor of 1.95.

-S6-

**Table S11** Reproduction of catalysis with purified Sav spiked glutathione, and the GSH neutralizing agents



Sav-mutant	[GSH] (mM)	GSH neutralizing agent	[GSH neutralizing agent] (mM)	incubation time (h)	conv. (%)	ee (%)	abs. conf.
no	2.5	<b>MalIn</b>	2.5	15	24	0	<i>rac</i>
no	2.5	<b>MalIn</b>	5	15	20	0	<i>rac</i>
no	2.5	<b>MalIn</b>	10	15	7	0	<i>rac</i>
S112A	2.5	<b>MalIn</b>	2.5	15	12	80	( <i>R</i> )
S112A	2.5	<b>MalIn</b>	5	15	2	75	( <i>R</i> )
S112A	2.5	<b>MalIn</b>	10	15	2	59	( <i>R</i> )
S112K	2.5	<b>MalIn</b>	2.5	15	5	46	( <i>S</i> )
S112K	2.5	<b>MalIn</b>	5	15	4	46	( <i>S</i> )
S112K	2.5	<b>MalIn</b>	10	15	5	20	( <i>S</i> )
no	0	<b>MalIn</b>	2.5	15	100	0	<i>rac</i>
no	0	<b>MalIn</b>	5	15	99	0	<i>rac</i>
no	0	<b>MalIn</b>	10	15	85	0	<i>rac</i>
S112A	0	<b>MalIn</b>	2.5	15	22	65	( <i>R</i> )
S112A	0	<b>MalIn</b>	5	15	15	60	( <i>R</i> )
S112A	0	<b>MalIn</b>	10	15	8	56	( <i>R</i> )
S112K	0	<b>MalIn</b>	2.5	15	26	26	( <i>S</i> )
S112K	0	<b>MalIn</b>	5	15	20	20	( <i>S</i> )
S112K	0	<b>MalIn</b>	10	15	13	13	( <i>S</i> )
no	2.5	<b>BroPheOne</b>	2.5	15	92	0	<i>rac</i>
no	2.5	<b>BroPheOne</b>	5	15	77	0	<i>rac</i>
no	2.5	<b>BroPheOne</b>	10	15	49	0	<i>rac</i>
no	2.5	<b>BroPheOne</b>	2.5	2	94	0	<i>rac</i>
no	2.5	<b>BroPheOne</b>	5	2	95	0	<i>rac</i>
no	2.5	<b>BroPheOne</b>	10	2	88	0	<i>rac</i>
S112A	2.5	<b>BroPheOne</b>	2.5	15	71	84	( <i>R</i> )
S112A	2.5	<b>BroPheOne</b>	5	15	65	86	( <i>R</i> )
S112A	2.5	<b>BroPheOne</b>	10	15	58	87	( <i>R</i> )
S112A	2.5	<b>BroPheOne</b>	2.5	2	68	85	( <i>R</i> )
S112A	2.5	<b>BroPheOne</b>	5	2	68	86	( <i>R</i> )
S112A	2.5	<b>BroPheOne</b>	10	2	62	87	( <i>R</i> )
S112K	2.5	<b>BroPheOne</b>	2.5	15	40	63	( <i>S</i> )
S112K	2.5	<b>BroPheOne</b>	5	15	34	59	( <i>S</i> )

-57-

S112K	2.5	<b>BroPheOne</b>	10	15	29	51	(S)
S112K	2.5	<b>BroPheOne</b>	2.5	2	34	58	(S)
S112K	2.5	<b>BroPheOne</b>	5	2	24	54	(S)
S112K	2.5	<b>BroPheOne</b>	10	2	29	51	(S)
no	0	<b>BroPheOne</b>	2.5	15	96	0	<i>rac</i>
no	0	<b>BroPheOne</b>	5	15	74	0	<i>rac</i>
no	0	<b>BroPheOne</b>	10	15	54	0	<i>rac</i>
S112A	0	<b>BroPheOne</b>	2.5	15	72	83	(R)
S112A	0	<b>BroPheOne</b>	5	15	74	84	(R)
S112A	0	<b>BroPheOne</b>	10	15	67	83	(R)
S112K	0	<b>BroPheOne</b>	2.5	15	45	58	(S)
S112K	0	<b>BroPheOne</b>	5	15	45	53	(S)
S112K	0	<b>BroPheOne</b>	10	15	37	41	(S)
no	2.5	<b>PheViSul</b>	2.5	15	98	0	<i>rac</i>
no	2.5	<b>PheViSul</b>	5	15	99	0	<i>rac</i>
no	2.5	<b>PheViSul</b>	10	15	98	0	<i>rac</i>
no	2.5	<b>PheViSul</b>	2.5	2	79	0	<i>rac</i>
no	2.5	<b>PheViSul</b>	5	2	97	0	<i>rac</i>
no	2.5	<b>PheViSul</b>	10	2	86	0	<i>rac</i>
S112A	2.5	<b>PheViSul</b>	2.5	15	78	80	(R)
S112A	2.5	<b>PheViSul</b>	5	15	86	64	(R)
S112A	2.5	<b>PheViSul</b>	10	15	91	55	(R)
S112A	2.5	<b>PheViSul</b>	2.5	2	71	79	(R)
S112A	2.5	<b>PheViSul</b>	5	2	69	73	(R)
S112A	2.5	<b>PheViSul</b>	10	2	44	59	(R)
S112K	2.5	<b>PheViSul</b>	2.5	15	61	58	(S)
S112K	2.5	<b>PheViSul</b>	5	15	88	21	(S)
S112K	2.5	<b>PheViSul</b>	10	15	63	28	(S)
S112K	2.5	<b>PheViSul</b>	2.5	2	43	52	(S)
S112K	2.5	<b>PheViSul</b>	5	2	63	38	(S)
S112K	2.5	<b>PheViSul</b>	10	2	53	29	(S)
no	0	<b>PheViSul</b>	2.5	15	100	0	<i>rac</i>
no	0	<b>PheViSul</b>	5	15	99	0	<i>rac</i>
no	0	<b>PheViSul</b>	10	15	100	0	<i>rac</i>
S112A	0	<b>PheViSul</b>	2.5	15	64	83	(R)
S112A	0	<b>PheViSul</b>	5	15	52	84	(R)
S112A	0	<b>PheViSul</b>	10	15	10	83	(R)
S112K	0	<b>PheViSul</b>	2.5	15	65	58	(S)
S112K	0	<b>PheViSul</b>	5	15	38	53	(S)
S112K	0	<b>PheViSul</b>	10	15	18	41	(S)
no	2.5	<b>Ox</b>	2.5	15	0	0	-
no	2.5	<b>Ox</b>	5	15	0	0	-
no	2.5	<b>Ox</b>	10	15	27	0	<i>rac</i>
S112A	2.5	<b>Ox</b>	2.5	15	0	0	-
S112A	2.5	<b>Ox</b>	5	15	0	0	-
S112A	2.5	<b>Ox</b>	10	15	55	80	(R)
S112K	2.5	<b>Ox</b>	2.5	15	0	0	-
S112K	2.5	<b>Ox</b>	5	15	0	0	-
S112K	2.5	<b>Ox</b>	10	15	22	43	(S)
no	0	<b>Ox</b>	2.5	15	100	0	<i>rac</i>
no	0	<b>Ox</b>	5	15	100	0	<i>rac</i>



-58-

no	0	<b>Ox</b>	10	15	99	0	<i>rac</i>
S112A	0	<b>Ox</b>	2.5	15	87	78	( <i>R</i> )
S112A	0	<b>Ox</b>	5	15	89	77	( <i>R</i> )
S112A	0	<b>Ox</b>	10	15	90	77	( <i>R</i> )
S112K	0	<b>Ox</b>	2.5	15	57	49	( <i>S</i> )
S112K	0	<b>Ox</b>	5	15	57	44	( <i>S</i> )
S112K	0	<b>Ox</b>	10	15	53	40	( <i>S</i> )
no	2.5	<b>Fe<sup>3+</sup></b>	2.5	15	0	0	-
no	2.5	<b>Fe<sup>3+</sup></b>	5	15	0	0	-
no	2.5	<b>Fe<sup>3+</sup></b>	10	15	0	0	-
S112A	2.5	<b>Fe<sup>3+</sup></b>	2.5	15	0	0	-
S112A	2.5	<b>Fe<sup>3+</sup></b>	5	15	0	0	-
S112A	2.5	<b>Fe<sup>3+</sup></b>	10	15	0	0	-
S112K	2.5	<b>Fe<sup>3+</sup></b>	2.5	15	0	0	-
S112K	2.5	<b>Fe<sup>3+</sup></b>	5	15	0	0	-
S112K	2.5	<b>Fe<sup>3+</sup></b>	10	15	0	0	-
no	0	<b>Fe<sup>3+</sup></b>	2.5	15	0	0	-
no	0	<b>Fe<sup>3+</sup></b>	5	15	0	0	-
no	0	<b>Fe<sup>3+</sup></b>	10	15	0	0	-
S112A	0	<b>Fe<sup>3+</sup></b>	2.5	15	0	0	-
S112A	0	<b>Fe<sup>3+</sup></b>	5	15	0	0	-
S112A	0	<b>Fe<sup>3+</sup></b>	10	15	0	0	-
S112K	0	<b>Fe<sup>3+</sup></b>	2.5	15	0	0	-
S112K	0	<b>Fe<sup>3+</sup></b>	5	15	0	0	-
S112K	0	<b>Fe<sup>3+</sup></b>	10	15	0	0	-
no	2.5	<b>PhePropNit</b>	2.5	15	0	0	-
no	2.5	<b>PhePropNit</b>	5	15	94	0	<i>rac</i>
no	2.5	<b>PhePropNit</b>	10	15	87	0	<i>rac</i>
S112A	2.5	<b>PhePropNit</b>	2.5	15	0	0	( <i>R</i> )
S112A	2.5	<b>PhePropNit</b>	5	15	57	82	( <i>R</i> )
S112A	2.5	<b>PhePropNit</b>	10	15	40	84	( <i>R</i> )
S112K	2.5	<b>PhePropNit</b>	2.5	15	0	0	-
S112K	2.5	<b>PhePropNit</b>	5	15	30	52	( <i>S</i> )
S112K	2.5	<b>PhePropNit</b>	10	15	13	39	( <i>S</i> )
no	0	<b>PhePropNit</b>	2.5	15	98	0	<i>rac</i>
no	0	<b>PhePropNit</b>	5	15	99	0	<i>rac</i>
no	0	<b>PhePropNit</b>	10	15	68	0	<i>rac</i>
S112A	0	<b>PhePropNit</b>	2.5	15	73	83	( <i>R</i> )
S112A	0	<b>PhePropNit</b>	5	15	74	84	( <i>R</i> )
S112A	0	<b>PhePropNit</b>	10	15	33	86	( <i>R</i> )
S112K	0	<b>PhePropNit</b>	2.5	15	54	60	( <i>S</i> )
S112K	0	<b>PhePropNit</b>	5	15	46	57	( <i>S</i> )
S112K	0	<b>PhePropNit</b>	10	15	23	50	( <i>S</i> )
no	2.5	<b>BQ</b>	1.25	15	2	0	<i>rac</i>
no	2.5	<b>BQ</b>	2.5	15	2	0	<i>rac</i>
no	2.5	<b>BQ</b>	5	15	1	0	<i>rac</i>
no	2.5	<b>BQ</b>	10	15	2	0	<i>rac</i>
S112A	2.5	<b>BQ</b>	1.25	15	6	77	( <i>R</i> )
S112A	2.5	<b>BQ</b>	2.5	15	5	73	( <i>R</i> )
S112A	2.5	<b>BQ</b>	5	15	5	63	( <i>R</i> )
S112A	2.5	<b>BQ</b>	10	15	12	46	( <i>R</i> )

S112K	2.5	<b>BQ</b>	1.25	15	6	51	(S)
S112K	2.5	<b>BQ</b>	2.5	15	5	48	(S)
S112K	2.5	<b>BQ</b>	5	15	4	18	(S)
S112K	2.5	<b>BQ</b>	10	15	11	10	(S)
no	0	<b>BQ</b>	1.25	15	14	0	<i>rac</i>
no	0	<b>BQ</b>	2.5	15	13	0	<i>rac</i>
no	0	<b>BQ</b>	5	15	14	0	<i>rac</i>
no	0	<b>BQ</b>	10	15	17	0	<i>rac</i>
S112A	0	<b>BQ</b>	1.25	15	16	55	(R)
S112A	0	<b>BQ</b>	2.5	15	20	46	(R)
S112A	0	<b>BQ</b>	5	15	20	32	(R)
S112A	0	<b>BQ</b>	10	15	39	21	(R)
S112K	0	<b>BQ</b>	1.25	15	17	14	(S)
S112K	0	<b>BQ</b>	2.5	15	21	4	(S)
S112K	0	<b>BQ</b>	5	15	30	2	(S)
S112K	0	<b>BQ</b>	10	15	39	2	(S)
no	2.5	<b>DiAm</b>	1.25	15	33	0	<i>rac</i>
no	2.5	<b>DiAm</b>	2.5	15	22	0	<i>rac</i>
no	2.5	<b>DiAm</b>	5	15	16	0	<i>rac</i>
no	2.5	<b>DiAm</b>	10	15	14	0	<i>rac</i>
no	2.5	<b>DiAm</b>	1.25	2	27	0	<i>rac</i>
no	2.5	<b>DiAm</b>	2.5	2	12	0	<i>rac</i>
no	2.5	<b>DiAm</b>	5	2	8	0	<i>rac</i>
no	2.5	<b>DiAm</b>	10	2	7	0	<i>rac</i>
S112A	2.5	<b>DiAm</b>	1.25	15	64	84	(R)
S112A	2.5	<b>DiAm</b>	2.5	15	64	85	(R)
S112A	2.5	<b>DiAm</b>	5	15	63	84	(R)
S112A	2.5	<b>DiAm</b>	10	15	58	83	(R)
S112A	2.5	<b>DiAm</b>	1.25	2	65	82	(R)
S112A	2.5	<b>DiAm</b>	2.5	2	60	82	(R)
S112A	2.5	<b>DiAm</b>	5	2	53	82	(R)
S112A	2.5	<b>DiAm</b>	10	2	45	82	(R)
S112K	2.5	<b>DiAm</b>	1.25	15	24	55	(S)
S112K	2.5	<b>DiAm</b>	2.5	15	18	53	(S)
S112K	2.5	<b>DiAm</b>	5	15	13	50	(S)
S112K	2.5	<b>DiAm</b>	10	15	9	47	(S)
S112K	2.5	<b>DiAm</b>	1.25	2	17	49	(S)
S112K	2.5	<b>DiAm</b>	2.5	2	7	37	(S)
S112K	2.5	<b>DiAm</b>	5	2	4	30	(S)
S112K	2.5	<b>DiAm</b>	10	2	3	19	(S)
no	0	<b>DiAm</b>	10	15	100	0	<i>rac</i>
S112A	0	<b>DiAm</b>	10	15	71	82	(R)
S112K	0	<b>DiAm</b>	10	15	45	60	(S)

## References

- [1] Köhler, V. *et al.* OsO<sub>4</sub>/Streptavidin: A tunable hybrid catalyst for the enantioselective *cis*-dihydroxylation of olefins. *Angew. Chem. Int. Ed.* **2011**, *50*, 10863-10866.

-S10-

- [2] Gallizia, A. *et al.* Production of a soluble and functional recombinant streptavidin in *Escherichia coli*. *Protein Expres. Purif.* **1998**, *14*, 192–196.
- [3] Wilson, Y. M., Dürrenberger, M., Ward, T. R. Organometallic chemistry in protein scaffolds. *Protein Engineering Handbook*, Volume III, Eds. S. Lutz, U. T. Bornscheuer, Wiley VCH, Weinheim.
- [4] Kada G. *et al.* Rapid estimation of avidin and streptavidin by fluorescence quenching or fluorescence polarization. *BiochemBiophysActa* **1999**, *1427*, 33
- [5] Riddles, P.W. *et al.* (1979) Ellman's reagent: 5, 5'-dithiobis(2-nitrobenzoic acid) - a reexamination. *Anal Biochem* **1979**, *94*, 75.

### 3.2.4 Appendix

When considering directed evolution of protein-derived catalysts (i.e. enzymes or hybrid catalysts), a suitable method has to be identified which allows to detect the catalytic activity of the desired transformation for a large number of mutants. Two strategies are usually applied for this purpose: high-throughput screening and selection (see section 3.1.1.1). In the case where catalysis is performed in living cells, the latter methodology can be used to screen for catalytic activity.

Two reactions were devised which may be applied in a selection mechanism for the directed evolution of ATHases and their feasibility was tested in context of initial experiments. Both approaches rely on the reduction of 1,4-unsaturated carbonyl compounds. Several studies showed that transfer hydrogenation is an effective catalytic method for this purpose.<sup>30</sup> Additionally, prior studies within the Ward group revealed that enones are suitable substrates for ATHases.<sup>31</sup> However, as the corresponding transformations are not enantioselective they serve only as a method to screen for ATHase activity.

#### 3.2.4.1 ATHase-mediated Generation of Amino Acids from Enone Precursors

Two amino acid precursors were synthesized, namely **1** and **3** (see experimental part for a detailed synthetic procedure). The 1,4-reduction of these compounds yields the corresponding saturated  $\beta$ -keto acids **2a** and **4a** which may be prone to transamination by intracellular transaminases, thus affording leucine and valine (Figure 3.3). In a quantitative reaction (25 mg), both compounds were subjected to transfer hydrogenation using 1 mol%  $[(\eta^5\text{-Cp}^*)\text{M}(\text{Biot-}p\text{-L})\text{Cl}]$  ( $\text{M} = \text{Rh, Ir}$ ) and 2 equivalents of sodium formate (100 mM) within a period of 10 hours. The  $^1\text{H-NMR}$ -spectra of the isolated product mixtures revealed that transfer hydrogenation of **1** yielded the unsaturated hydroxylic acid **2b** (approximately 25% yield) whereas the desired unsaturated product **2a** resulting from 1,4-reduction was not detected. In contrast, reduction of **3** produced almost exclusively the desired  $\beta$ -keto acid **4a** in near quantitative yield. Thereby, the Rh-catalyst seems to be slightly more selective with respect to 1,4-reduction as no alcohol formation could be observed

whereas in case of the Ir-complex traces of the fully reduced compound **3c** was detected. The lower reactivity of **1** results possibly from the increased steric demand of this substrate.

Initial experiments with some Sav-mutants showed that compound **3** is also reduced by  $[(\eta^5\text{-Cp}^*)\text{M}(\text{Biot-}p\text{-L})\text{Cl}]$  when incorporated in the host protein at low formate concentrations. As judged from GC-traces, in all cases the valine precursor **4a** was found to be one of the main products. However, further conclusions concerning the dependence of the Sav-mutant on the chemoselectivity of this reaction are hard to be drawn as additional peaks in the GC-spectra corresponding to unidentified compounds were present and the used analytical GC-method did not allow to quantify the (derivatized) reaction products. Further experiments showed that the valine precursor **4a** is indeed transaminated in presence of *E. coli* cell free extracts. However, attempts to generate valine with the ATHase in presence of cell free extracts failed so far.

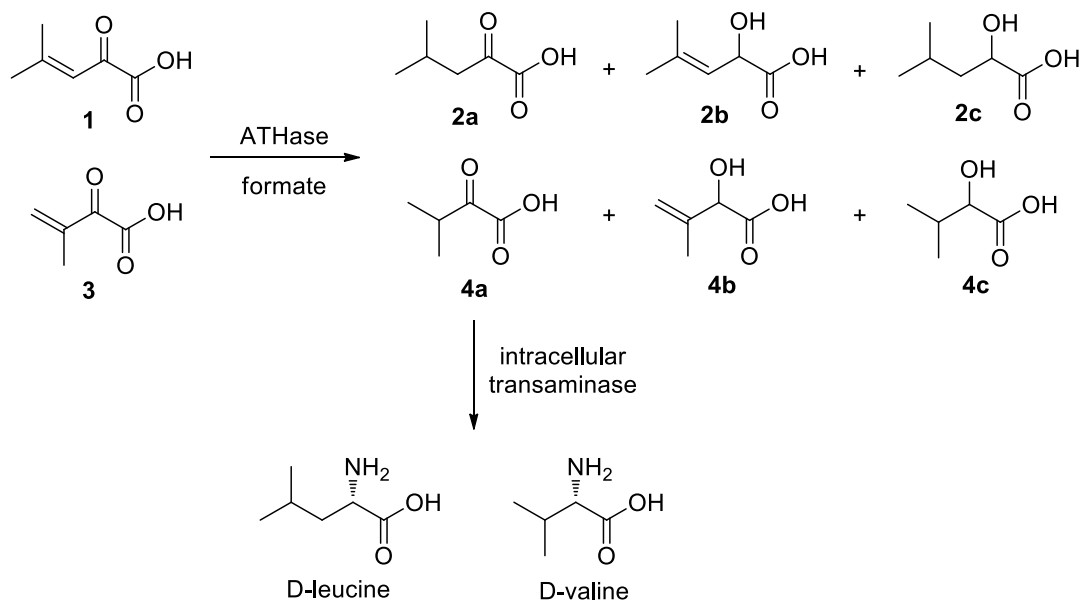


**Fig. 3.3.** ATHase mediated generation of amino acid precursors as a selection strategy.

## 3.2.4.2 ATHase-mediated Degradation of an Antibiotic

Bacteria expressing a Sav-mutant that in combination with the artificial metal cofactor provides an efficient hybrid catalyst for the degradation of an antibiotic would experience an advantage to survive in presence of the drug. Based on this idea fluoroquinolones were tested as substrates of the ATHase. Members of this antibiotic class inhibits two essential enzymes (DNA-gyrase and topoisomerase IV) associated with the replication of the bacterial genome and is widely used to treat infections of various gram-negative bacteria including *E. coli*.<sup>32</sup> The structural core element of all fluoroquinolons exhibits an enone moiety prone to 1,4-reduction by reactive hydride species.<sup>33</sup> The resulting intermediate decarboxylates spontaneously to yield an inactive form of the antibiotic as reflected by the much higher minimal inhibitory concentrations (MIC) of this derivative, thus providing a potential selection mechanism.<sup>34</sup> As a color change to yellow occurs upon reduction, this system on the same time may afford a screening method for the ATHase activity. However, initial results with purified protein showed modest activity of different ATHase-variants based on  $[(\eta^5\text{-Cp}^*)\text{M}(\text{biot-}p\text{-L})\text{Cl}]$  ( $\text{M} = \text{Rh, Ir}$ ) towards Enrofloxacin (see experimental part).

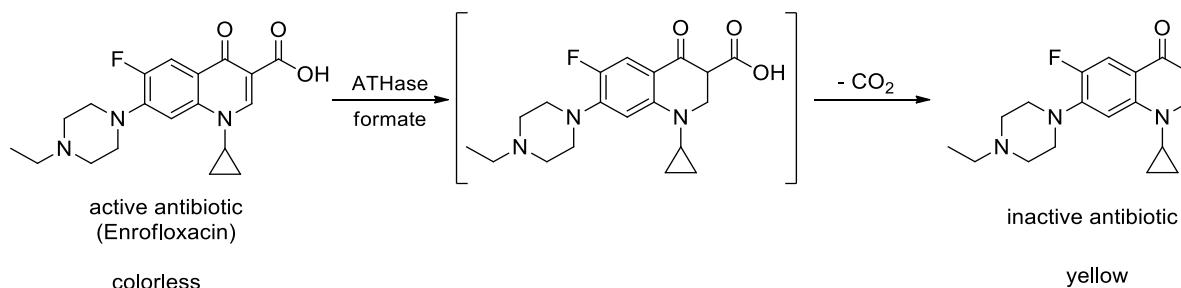


**Fig. 3.4.** ATHase-mediated degradation of fluoroquinolone antibiotics as a potential selection mechanism.

Further studies in collaboration with Seraina Blümli (master thesis) revealed that catalysts obtained from combination of the biotinylated metal precursor  $[\eta^5\text{-Cp}^*\text{IrCl}_2]_2$  with different bidentate ligands as well as the respective ATHase variants are more active towards the reduction of this particular substrate, achieving up to 50 TON in case of the K121A-variant (see figure 3.5).<sup>35</sup> Additionally, a colorimetric assay could be developed which allows to monitor the reaction in a parallel manner.

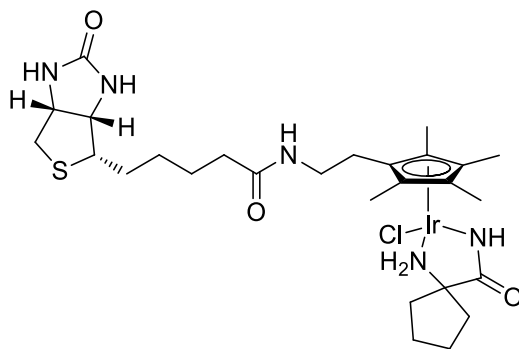


**Fig. 3.5.** "Second generation" transfer hydrogenation catalyst displaying improved catalytic activity towards the reduction of Enrofloxacin within Sav-mutants. The catalyst was prepared *in situ* from  $[\eta^5\text{-Cp}^*\text{IrCl}_2]_2$  and 1-amino cyclopentane carboximide.<sup>35</sup>

### 3.3 Conclusions and Outlook

The implementation of a directed evolution protocol for artificial metalloenzymes may further tune these hybrid catalysts and therefore is highly desirable. However, this implies the performance of transition metal catalysis in a cellular environment. Artificial transfer hydrogenases based on the biotin-(Strept)avidin technology for the enantioselective reduction of imines served as a corresponding model system to address two major issues in this context. First, the incorporation of a homogenous metal catalyst within a host protein effectively prevents mutual inhibition between the organometallic moiety and several natural enzymes. Second, an effective reagent was identified to neutralize the dentrimetal effect of glutathione on precious metal catalysts.

Further efforts include the realization of *in vivo* catalysis. For this purpose, the integrity of the cell has to be ensured. Initial experiments indicate that the reaction conditions under which the ATHase operates for the reduction of imines are not compatible with bacterial cells (in particular the high formate concentrations). Cell lysis was observed within a short period of time when incubated with the corresponding reaction buffer. Therefore, enones may be more suitable substrates as it was illustrated that some of these compounds are reduced more effectively at much lower formate concentrations. Alternatively, a formate-independent reaction could be applied. Ikariya showed that  $[(\eta^6\text{-arene})\text{Ru}(\text{R,R-TsDPEN})]$  complexes catalyse the enantioselective 1,4-addition of malonates to enones.<sup>37</sup>

In addition, the uptake of the metal cofactor into the cell has to be ensured. Otherwise, an expression system has to be developed where the Sav-mutants are displayed on the cell surface or are secreted into the growth medium. However, respective systems are under investigation currently within the Ward-group.



### 3.4 References

- 1) Otten, L.G.; Quax, W.J. *Biomolecular Engineering*, **2005**, *22*, 1.
- 2) Arnold, F.H. *Acc. Chem. Res.* **1998**, *31*, 125.
- 3.a) Neylon C. *Nucl. Acids Res.* **2004**, *32*, 1448. b) Lutz S.; Patrick W.M. *Curr. Opin. Biotechnol.* **2004**, *15*, 291.
- 4.a) Stemmer, W.P.C. *Nature* **1994**, *370*, 389. b) Crameri, A.; Raillard, S.; Bermudez, E.; Stemmer, W.P.C. *Nature* **1998**, *391*, 288. c) Coco, W.M.; Levinson, W.E.; Crist, M.J.; Hektor, H.J.; Darzins, A.; Pienkos, P.T.; Squires, C.H.; Monticello, D.J. *Nat. Biotech.* **2001**, *19*, 354.
- 5.a) Pelletier, J.N. *Nat. Biotech.* **2001**, *19*, 314.
- 6.a) Aharoni, A.; Griffiths, A.D.; Tawfik, D.S. *Curr. Op. Chem. Biol.* **2005**, *9*, 210. b) Wahler, D.; Reymond, J.L. *Curr. Opin. Biotechnol.* **2001**, *12*, 535.
- 7) Boersma, Y.L.; J. Dröge, M.J.; Quax, W.J. *FEBS J.* **2007**, *274*, 2181.
- 8) Kurioka, M.; Matsuda, M. *Anal. Biochem.* **1976**, *75*, 281.
- 9) Reetz, M.T.; Daligault, B.; Brunner, B.; Hinrichs, A.; Deege, A. *Angew. Chem. Int. Ed. Engl.* **2004**, *43*, 4078.
- 10) Reetz, M.T.; Eipper, A.; Tielmann, P.; Mynott, R. *Adv. Synth. Catal.* **2002**, *344*, 1008.
- 11) Reetz, M.T.; Becker, M.H.; Klein, H.W.; Stöckigt, D. *Angew. Chem. Int. Ed.* **1999**, *38*, 1758.
- 12) Reetz, M.T., Kühling, S.; Wilensek, S.; Husmann, H.; Hermes, M. *Catal. Today* **2001**, *67*, 389.
- 13) Ding, K.; Ishii, A.; Mikami, K. *Angew. Chem. Int. Ed. Engl.* **1999**, *38*, 497.
- 14.a) Fernandez-Alvaro, E.; Snajdrova, R.; Jochens, H.; Davids, T.; Böttcher, D.; Bornscheuer, U.T. *Angew. Chem. Int. Ed.* **2011**, *50*, 8584. b) Farinas, E.T. *Comb. Chem. High Throughput Screen* **2006**, *9*, 321.
- 15) Taylor, S.V.; Kast, P.; Hilvert, D. *Angew. Chem. Int. Ed.* **2001**, *40*, 3310.
- 16.a) Reetz, M.T.; Höbenreich, H.; Soni, P.; Fernandez, L. *Chem. Commun.* **2008**, 5502.
- 17.a) Cipolla, L. *Comb. Chem. High Throughput* **2004**, *7*, 101. b) Griffiths, J.S.; Cheriyan, M.; Corbell, J.B.; Pocivavsek, L.; Fierke, C.A.; Toone, E.J. *Bioorg. Med. Chem. Lett.* **2004**, *12*, 4067.
- 18) Zhao, H.; Arnold, F.H. *Curr. Op. Struc. Biol.* **1997**, *7*, 480.

- 19) Giver, L.; Gershenson, A.; Freskgard, P.O.; Arnold, F.H. *Proc. Natl. Acad. Sci.* **1998**, *95*, 12809.
- 20) You, L.; Arnold, F.H. *Prot. Eng.* **1994**, *9*, 77.
- 21) Valderrama, B. *FASEB J.* **2006**, *20*, 1233.
- 22) Gülich, S.; Linhult, M.; Stahl, S.; Hober, S. *Protein Eng.* **2002**, *15*, 835.
- 23.a) Jaeger, K.E.; Eggert, T. *Curr. Op. Biotechnol.* **2004**, *15*, 305. b) Yano, T.; Oue, S.; Kagamiyama, H. *Proc. Natl. Acad. Sci.* **1998**, *95*, 5511
- 24.a) Hult, K.; Berglund, P. *Curr. Op. Biotechnol.* **2003**, *14*, 395. b) Cherry, J.R.; Fidantsef, A.L. *Curr. Op. Biotechnol.* **2003**, *14*, 438.
- 25.a) Reetz, M.T.; Peyralans, J.J.P.; Maichele, A.; Fu, Y.; Maywald, M. *Chem. Commun.* **2006**, 4318. b) Reetz, M.T.; Rentzsch, M.; Pletsch, A.; Maywald, M.; Maiwald, P.; Peyralans, J.J.P.; Maichele, A.; Fu, Y.; Jiao, N.; Hollmann, F.; Mondiere, R.; Taglieber, A. *Tetrahedron* **2007**, *63*, 6404.
- 26) Sasmal, P.K.; Streu, C.N.; Meggers, E. *Chem. Commun.* **2013**, *49*, 1581.
- 27) Pompella, A.; Visvikis, A.; Paolicchi, A.; Tata, V.; Casini, A.F. *Biochem. Pharmacol.* **2003**, *66*, 1499.
- 28) Bennett, B.D.; Kimball, E.H.; Gao, M.; Osterhout, R.; Van Dien, S.J.; Rabinowitz, J.D. *Nat. Chem. Biol.* **2009**, *5*, 593.
- 29) Poizat, M.; Arends, I. W. C. E.; Hollmann, F. *J. Mol. Catal. B: Enzym.* **2010**, *63*, 149.
- 30.a) Reed, M.C.; Lieb, A.; Nijhout, H.F. *Bioessays* **2010**, *32*, 422. b) Haldane, J. *Enzymes*, **1930** New York, Longmans, Green and Co.
- 30.a) Baan, Z.; Finta, Z.; Keglevich, I.; Hermecz, I. *Green Chem.* **2009**, *11*, 1937. b) Doi, T.; Fukuyuma, T.; Horiguchi, J.; Okamura, T.; Ryu, I. *Synlett* **2006**, 721. c) Sharma, A.; Kumar, V.; Shina, A.K.; *Adv. Synth. Catal.* **2006**, *348*, 354. d) Sakaguchi, S.; Yamaga, T.; Ishii, Y. *J. Org. Chem.* **2001**, *66*, 4710. e) Li, X.; Li, L.; Tang, Y.; Zhong, L.; Cun, L.; Zhu, J.; Liao, J.; Deng, J. *J. Org. Chem.* **2010**, *75*, 2981. f) Hannedouche, J.; Kenny, J.A.; Walsgroove, T.; Wills, M. *Synlett* **2002**, 263. g) Naskar, S.; Bhattacharjee, M. *Tetrahedron Lett.* **2007**, *48*, 465. h) Gong, X.; Zhang, H.; Li, X.; *Tetrahedron Lett.* **2011**, *52*, 5596. j) Tang, L.; Lin, Z.; Wang, Q.; Wang, X.; Cun, L.; Yuan, J.; Deng, J. *Tetrahedron Lett.* **2012**, *53*, 3828. i) Bizet, Y.; Pannecoucke, Y.; Renaud, J.L.; Cahard, D. *Adv. Synth. Catal.* **2013**, 355, 1394.
- 31) Heinisch, T.; Langowska, K.; Tanner, P.; Reymond, J.L.; Meier, W.; Palivan, C.; Ward, T.R. *ChemCatChem* **2013**, *5*, 720.

- 32.a) Ronald, A. R.; Low, D. E. *Fluoroquinolone Antibiotics*; Birkhauser Verlag, Basel, **2003**; (b) Domagala, J. M.; Hanna, L. D.; Heifetz, C. L.; Huff, M. P.; Mich, T. F.; Sanchez, P.; Solomon, M. *J. Med. Chem.* **1986**, *29*, 394.
- 33) Kondo, H.; Sakamoto, F.; Kawakami, K.; Tsukamoto, G. *J. Med. Chem.* **1988**, *31*, 221.
- 34) Nguyen, S.T.; Ding, X.; Butler, M.M.; Tashjian, T.F.; Peet, N.P.; Bowlin, T.L. *Bioorg. Med. Chem. Lett.* **2011**, *21*, 5961.
- 35) Zimbron, J.M.; Heinisch, T.; Schmid, M.; Hamels, D.; Nogueira, E.S.; Schirmer, T.; Ward, T.R. *J. Am. Chem. Soc.* **2013**, *3*, 720.
- 36) Blümli, S. Master Thesis, Universität Basel **2013**
- 37) Watanabe, M.; Murata, K.; Ikariya, T. *J. Am. Chem. Soc.* **2003**, *125*, 7508



## Chapter 4: Experimental Part

### 4.1 General Information

#### 4.1.1 Reagents and Solvents

Commercial reagents were purchased at the highest degree of purity available and used without further purification. For analytical high performance liquid chromatography (HPLC) solvents with a corresponding HPLC-grade were used. Buffers were prepared with MiliQ-grade water obtained from a Barnstead ultrapure water system.

#### 4.1.2 Materials

For thin layer chromatography Merck silica gel 60 F<sub>254</sub> plates were used. Flash chromatography was performed with Merck silica gel 60 (particle size 40-63  $\mu\text{m}$ ).

#### 4.1.3 Analytical Methods

##### 4.1.3.1 Nuclear Magnetic Resonance (NMR)

<sup>1</sup>H and <sup>13</sup>C spectra were recorded on Bruker Avance DRX-500 or DPX-400 MHz spectrometers. The HMBC-experiment was performed on a DRX-600 spectrometer. All devices were equipped with direct

(600 and 400 MHz) or inverse (500 MHz) dual channel, broadband probe-heads with  $z$ -gradients. The NMR experiments were performed at 25°C (MeOH calibration). Chemical shifts ( $\delta$ ) are reported in ppm with respect tetramethylsilane (TMS). Coupling constants ( $J$ ) are reported in Hertz (Hz).

#### 4.1.3.2 Mass spectrometry (MS)

Mass spectra were recorded on an Esquire 3000 plus (Bruker) applying electron spray ionisation (ESI). High resolution mass spectrometry (HRMS) was performed at the University of Fribourg with a Bruker FTMS 4.7T BioAPEX II device.

#### 4.1.3.3. Elementary Analysis

Elementary analysis was performed on an Analysator 240 from Perkin-Elmer or a vario MICRO cube from Elementar.

#### 4.1.3.4 High Performance Liquid Chromatography (HPLC)

HPLC measurements were performed on Agilent (or hp) machines equipped with modules from the 1100 and 1200 series and diode array detectors (UV-detection). HPLC columns were used with the appropriate guard columns. Column and conditions are indicated for each compound separately.

#### 4.1.3.5 Gas Chromatography (GC)

GC measurements were performed on Agilent GCs of the 6890 series equipped with FIDs. Column and conditions are indicated for each compound separately.

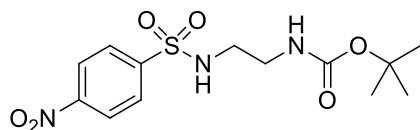
#### 4.1.3.6 Circular Dichroism (CD)

CD-spectra were obtained from a Chirascan spectrophotometer from Applied Photophysics Ltd (United Kingdom).

## 4.2 Synthesis

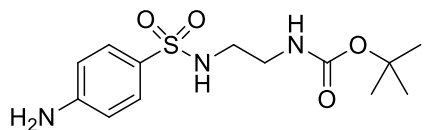
### 4.2.1 Synthesis of $[(\eta^5\text{-Cp}^*)\text{M}(\text{biot-}p\text{-L})\text{Cl}]$ (M = Rh, Ir)

#### 4.2.1.1 *N*-Boc-*N'*-(4-Nitrophenylsulfonyl)-ethylenediamine



A solution of 4-Nitrophenylsulfonyl chloride (7.26 g, 32.8 mmol, 1.05 eq) in 250 ml  $\text{CH}_2\text{Cl}_2$  was added dropwise to a solution of *N*-Boc-ethylamine (5 g, 31.2 mmol, 1 eq) and  $\text{Et}_3\text{N}$  (8.7 ml, 62.4 mmol, 2 eq) in  $\text{CH}_2\text{Cl}_2$  (800 ml) at 0 °C. The resulting yellow mixture was stirred over night at RT, was then concentrated to 250 ml and washed three times with water (60 ml). The organic phase was dried over  $\text{Na}_2\text{SO}_4$  and evaporated under reduced pressure to obtain a yellowish solid. The crude product was recrystallised from hot ethyl acetate yielding colorless needles (7.74 g, 72% yield).

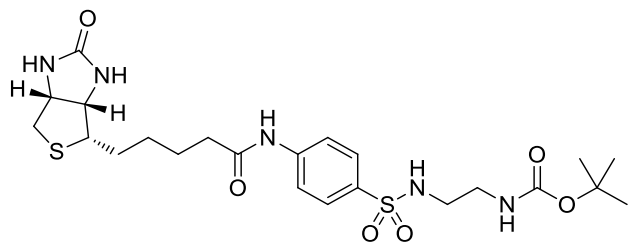
$^1\text{H}$  NMR (400 MHz,  $\text{MeOH-}D_4$ ):  $\delta$  1.40 (s, 9H; tBu), 2.99 (m, 2H; ethylenediamine- $\text{CH}_2$ ), 3.09 (m, 2H; ethylenediamine- $\text{CH}_2$ ), 8.07 (d, 2H,  $J = 8.91$  Hz; ArH), 8.41 (d, 2H,  $J = 8.91$  Hz; ArH)

4.2.1.2 *N*-Boc-*N'*-(4-Aminophenylsulfonyl)-ethylenediamine

An autoclave containing a suspension of Pd/C (5%, 1.1 g) in methanol (60 ml) was charged with *N*-Boc-*N'*-(4-Nitrophenylsulfonyl)-ethylenediamine (7 g, 20.3 mol), purged 3 times with H<sub>2</sub> and then filled with H<sub>2</sub> (15 bars). The mixture was stirred at RT overnight and filtered 3 times through a celite plug. The solvent was removed under reduced pressure to obtain the product as a white powder which was used without further purification (5.8 g, 96 % yield).

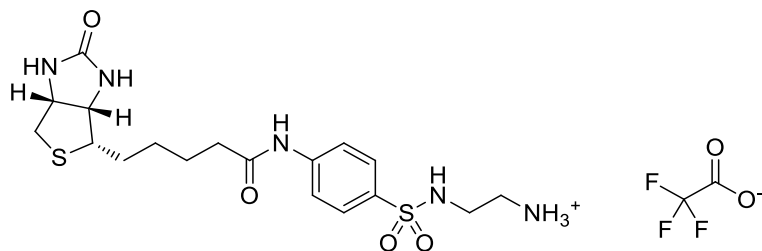
<sup>1</sup>H NMR (400 MHz, MeOH-D<sub>4</sub>): δ 1.41 (s, 9H; tBu), 2.84 (m, 2H; ethylenediamine-CH<sub>2</sub>), 3.08 (m, 2H; ethylenediamine-CH<sub>2</sub>), 6.68 (d, 2H, *J* = 8.7 Hz; ArH), 7.50 (m, 2H, *J* = 8.7 Hz; ArH).



4.2.1.3 *N*-Boc-*N'*-(4-Biotinamidophenylsulfonyl)-ethylenediamine

To a suspension of crude *N*-Boc-*N'*-(4-Aminophenylsulfonyl)-ethylenediamine (5 g, 15.8 mmol, 1 eq), biotin (3.95 g, 16.2 mmol, 1.02 eq) and 2-chloro-4,6-dimethoxy-1,3,5-triazine (2.95 g, 15.9 mmol, 1.06 eq) in acetonitrile (300 ml) was added *N*-methylmorpholine (2.62 ml, 23.8 mmol, 1.5 eq) and the mixture was stirred for 24 h at RT and then heated to reflux for 3 h. After cooling to RT, water was added (90 ml) and the resulting yellowish solution was concentrated under reduced pressure to afford a brownish solid which was filtered and washed with CH<sub>2</sub>Cl<sub>2</sub>. The crude product was purified by flash chromatography using EtOAc/MeOH 8:1 as an eluent.

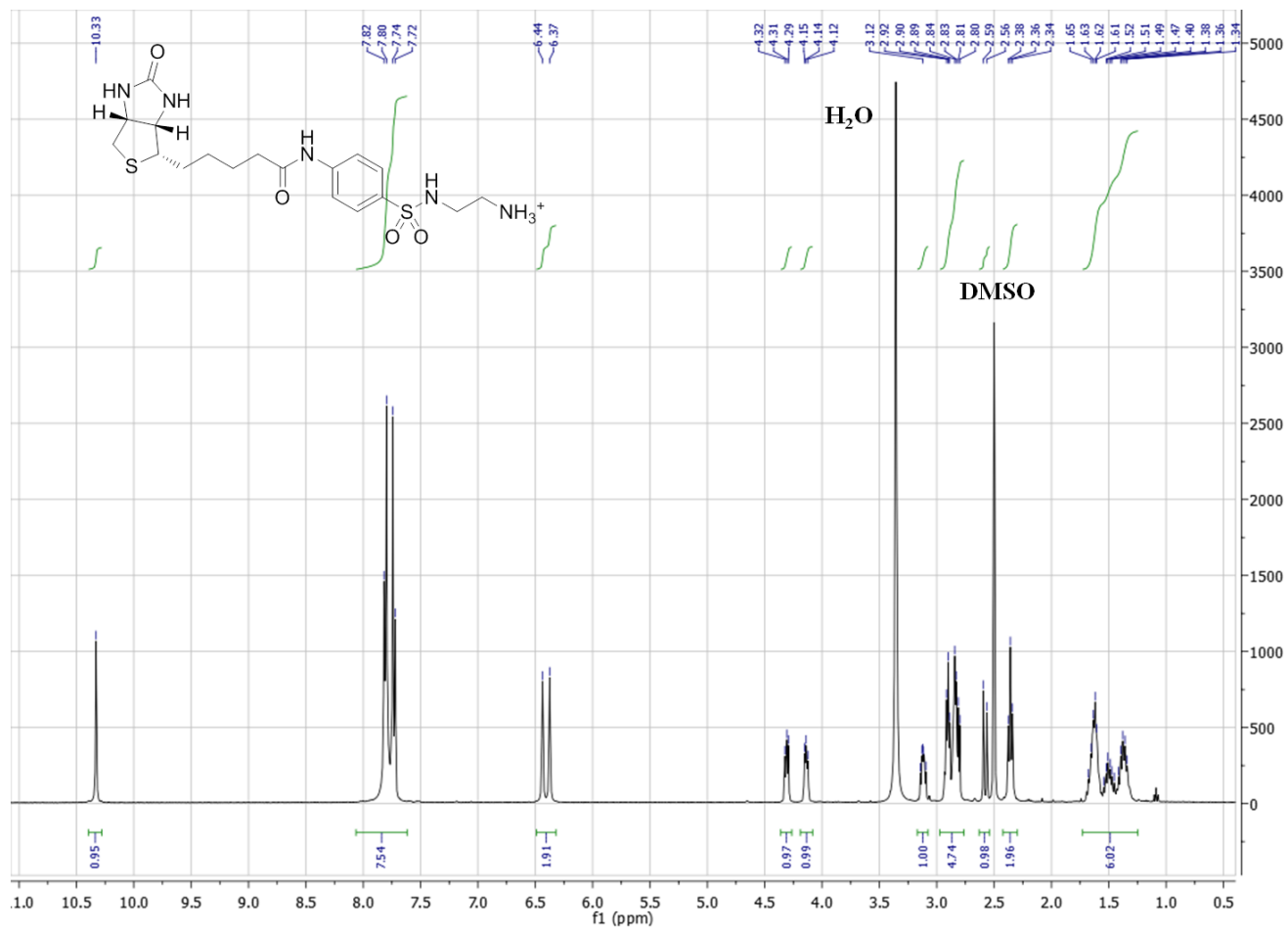
<sup>1</sup>H NMR (400 MHz, DMSO-d<sub>6</sub>): δ 1.25-1.70 (m, 15H; valeryl-CH<sub>2</sub>, tBu), 2.36 (m, 2H; valeryl-CH<sub>2</sub>-CO), 2.59 (d, 1H, *J* = 12.46 Hz; thiophene-CH<sub>2</sub>), 2.72 (m, 2H; ethylenediamine-CH<sub>2</sub>), 2.83 (dd, 1H, *J* = 5.09 Hz; thiophene-CH<sub>2</sub>), 2.94 (m, 2H; ethylenediamine-CH<sub>2</sub>), 3.12 (m, 1H; thiophene-H), 4.15 (m, 1H; ureido-CH), 4.32 (m, 1H; ureido-CH), 6.37 (br s, 1H; ureido-NH), 6.45 (br s, 1H; ureido-NH), 6.76 (t, 1H, *J* = 5.23 Hz; ethylenediamine-NH), 7.51 (t, 1H, *J* = 5.75 Hz; ethylenediamine-NH), 7.71 (d, 2H, *J* = 8.77 Hz; ArH), 7.78 (d, 2H, *J* = 8.77 Hz; ArH), 10.27 (s, 1H; CO-NH-Ar).

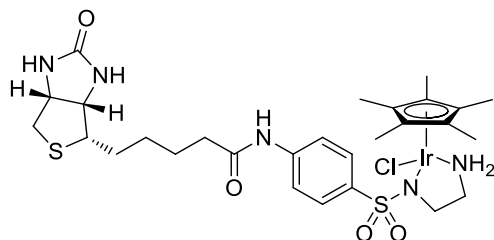
4.2.1.4 *N*'-(4-Biotinamidophenylsulfonyl)-ethylenediamine TFA salt

To a suspension of *N*-Boc-*N*'-(4-Biotinamidophenylsulfonyl)-ethylenediamine (1 g, 1.85 mmol, 1 eq) in dry CH<sub>2</sub>Cl<sub>2</sub> (90 ml) was added dropwise trifluoroacetic acid (2.1 ml, 27.8 mmol, 15 eq) at 0°C. The resulting yellowish solution was stirred for 6 h at RT and was then evaporated to dryness to obtain a brownish oil. The crude product was dissolved in MeOH and ether was added until a white precipitate formed which was collected by filtration and dried under reduced pressure (710 mg, 70 % yield).

<sup>1</sup>H NMR (400 MHz, DMSO-*d*<sub>6</sub>): δ 1.3-1.75 (m, 6H; valeryl-CH<sub>2</sub>), 2.37 (m, 2H; valeryl-CH<sub>2</sub>-CO), 2.58 (d, 1H, *J* = 12.51 Hz; thiophene-CH<sub>2</sub>), 2.8-2.95 (m, 5H; ethylenediamine-CH<sub>2</sub>; thiophene-CH<sub>2</sub>), 3.13 (m, 1H; thiophene-H), 4.15 (m, 1H; ureido-CH), 4.31 (m, 1H; ureido-CH), 6.38 (br s, 1H; ureido-NH), 6.45 (br s, 1H; ureido-NH), 7.7-7.9 (m, 8H; ArH, ethylenediamine-SO<sub>2</sub>-NH, ethylenediamine-NH<sub>3</sub><sup>+</sup>), 10.34 (s, 1H; CO-NH-Ar).

ESI-MS (pos. mode): *m/z* 442.2 ([M<sup>+</sup>]).



4.2.1.5  $[(\eta^5\text{-Cp}^*)\text{Ir}(\text{biot-}p\text{-L})\text{Cl}]$ 

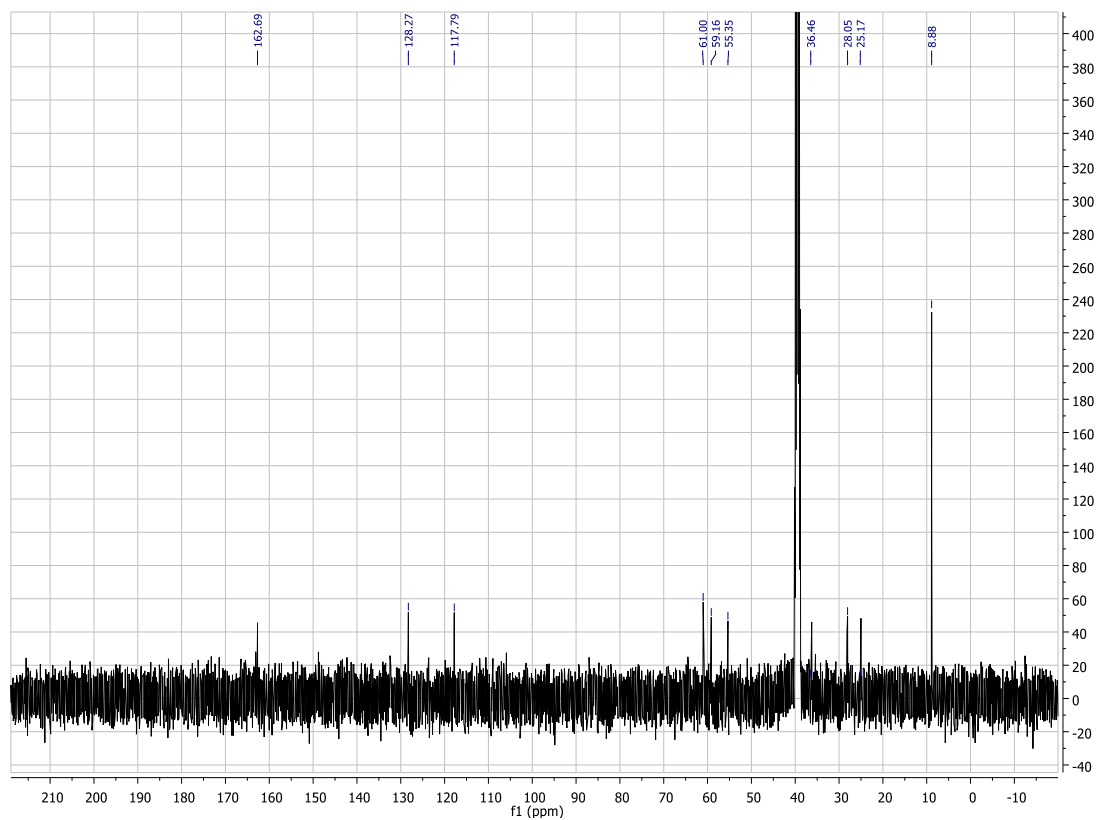
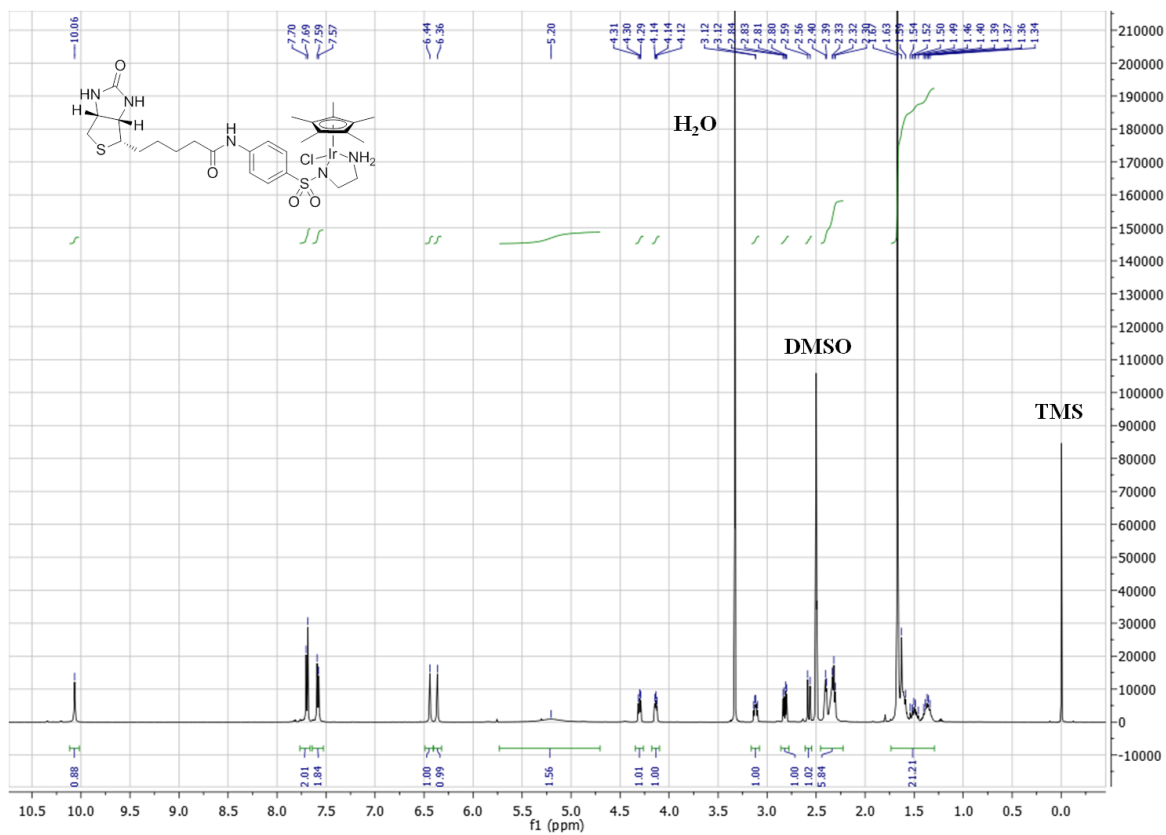
To a mixture of *N*'-(4-Biotinamidophenylsulfonyl)-ethylenediamine TFA salt (200 mg, 0.36 mmol, 1 eq) and  $[(\eta^5\text{-Cp}^*)\text{IrCl}_2]_2$  (136.4 mg, 0.171 mmol, 0.475 eq) in  $\text{CH}_2\text{Cl}_2$  (30 ml) was added  $\text{Et}_3\text{N}$  (251  $\mu\text{l}$ , 1.8 mmol, 5 eq) whereupon a color change from orange to dark brown and finally to yellow was observed. After stirring for 24 h at room temperature, the resulting yellow precipitate was filtered off, washed with  $\text{CH}_2\text{Cl}_2$  (3 x 5 ml) and water (3 x 4 ml) and dried *in vacuo* to obtain the pure product as a bright yellow solid (211 mg, 73% yield).

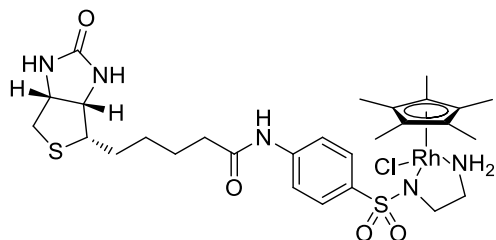
$^1\text{H}$  NMR (500 MHz,  $\text{DMSO-d}_6$ ):  $\delta$  1.25-1.75 (m, 21H; valeryl- $\text{CH}_2$ ,  $\text{Cp}^*$ ), 2.25-2.45 (m, 6H; valeryl- $\text{CH}_2\text{-CO}$ , ethylenediamine- $\text{CH}_2$ ), 2.57 (d, 1H,  $J = 12.51$  Hz; thiophene- $\text{CH}_2$ ), 2.82 (dd, 1H,  $J = 5.15$  Hz), 3.12 (m, 1H; thiophene-H), 4.14 (m, 1H; ureido-CH), 4.31 (m, 1H; ureido-CH), 5.21 (br s, 2H; ethylenediamine- $\text{NH}_2$ ), 6.37 (br s, 1H; ureido-NH), 6.44 (br s, 1H; ureido-NH), 7.59 (d, 2H,  $J = 8.64$  Hz; ArH), 7.7 (d, 2H,  $J = 8.64$  Hz; ArH), 10.05 (br s, 1H; CO-NH-Ar).

$^{13}\text{C}$  NMR (400 MHz,  $\text{DMSO-d}_6$ ):  $\delta$  8.88, 25.17, 28.05, 36.45, 55.35, 59.16, 61.00, 117.79, 128.27, 162.69 (due to the limited solubility of the compound in  $\text{DMSO}$  the intensity of some signals is too small to be detected).

ESI-MS (pos. mode):  $m/z$  768.22 ( $[\text{M-Cl}]^+$ ), 384.18 ( $[\text{M-Cl}]^{2+}$ ), 256.14 ( $[\text{M-Cl}]^{3+}$ )

Anal. Calcd for  $\text{C}_{28}\text{H}_{41}\text{ClIrN}_5\text{O}_4\text{S}_2$ : C, 41.86 %; H, 5.14 %; N, 8.72 %; found: C, 41.63 %; H, 5.15 %; N, 8.54 %.



4.2.1.5  $[(\eta^5\text{-Cp}^*)\text{Rh}(\text{biot-}p\text{-L})\text{Cl}]$ 

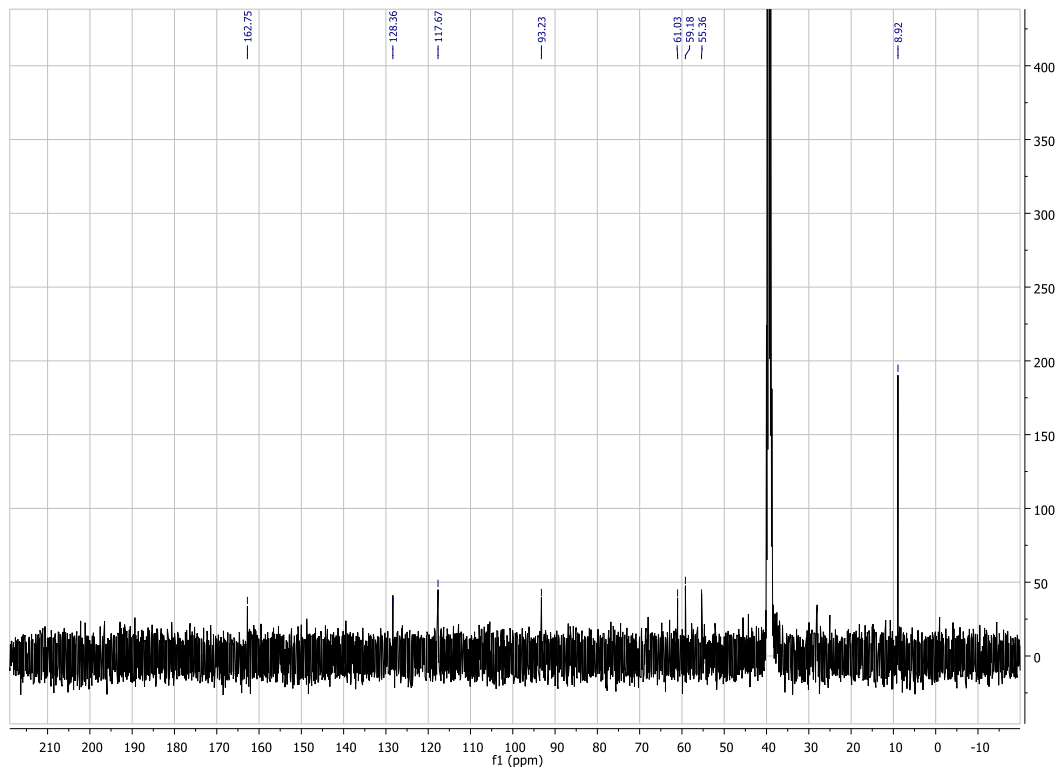
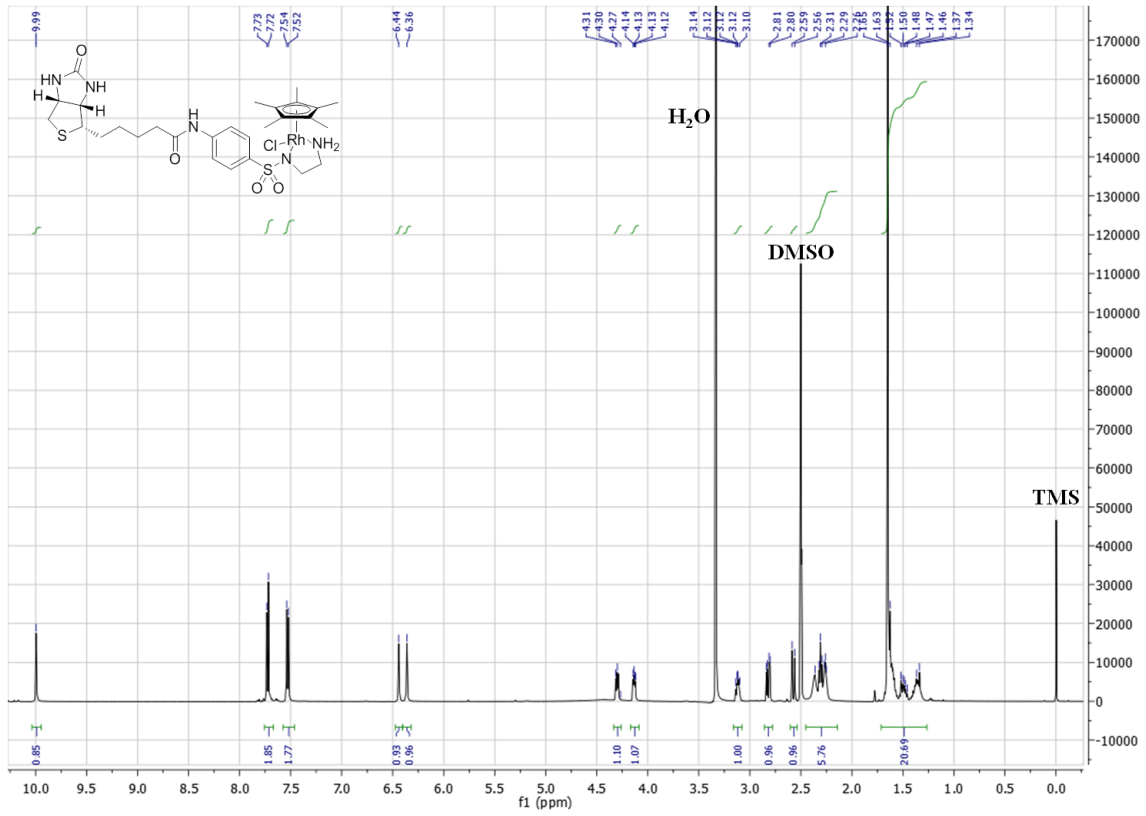
$[(\eta^5\text{-Cp}^*)\text{Rh}(\text{biot-}p\text{-L})\text{Cl}]$  was synthesized applying the same procedure as for  $[(\eta^5\text{-Cp}^*)\text{Ir}(\text{biot-}p\text{-L})\text{Cl}]$  (see above) using  $[(\eta^5\text{-Cp}^*)\text{RhCl}_2]_2$  (53.5 mg, 0.0865 mmol, 0.48 eq), *N'*-(4-Biotinamidophenylsulfonyl)-ethylenediamine TFA salt (100 mg, 0.18 mmol, 1 eq) and  $\text{NEt}_3$  (125  $\mu\text{l}$ , 0.9 mmol, 5 eq) to obtain the complex as an orange solid (76 mg, 58 % yield).

$^1\text{H}$  NMR (500 MHz,  $\text{DMSO-d}_6$ ):  $\delta$  1.25-1.75 (m, 21H; valeryl- $\text{CH}_2$ ,  $\text{Cp}^*$ ), 2.2-2.45 (m, 6H; valeryl- $\text{CH}_2\text{-CO}$ , ethylenediamine- $\text{CH}_2$ ), 2.57 (d, 1H,  $J = 12.02$  Hz; thiophene- $\text{CH}_2$ ), 2.82 (dd, 1H,  $J = 5.07$  Hz), 3.12 (m, 1H; thiophene-H), 4.13 (m, 1H; ureido-CH), 4.30 (m, 1H; ureido-CH), 6.36 (br s, 1H; ureido-NH), 6.44 (br s, 1H; ureido-NH), 7.53 (d, 2H,  $J = 8.07$  Hz; ArH), 7.72 (d, 2H,  $J = 8.63$  Hz; ArH), 10.0 (br s, 1H;  $\text{CO-NH-Ar}$ ).

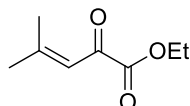
$^{13}\text{C}$  NMR (400 MHz,  $\text{DMSO-d}_6$ ):  $\delta$  8.92, 55.36, 59.18, 61.03, 93.23, 117.67, 128.36, 162.75 (due to the limited solubility of the compound in  $\text{DMSO}$  the intensity of some signals is too small to be detected).

ESI-MS (pos. mode):  $m/z$  678.27 ( $[\text{M-Cl}]^+$ )

Anal. Calcd for  $\text{C}_{28}\text{H}_{41}\text{ClRhN}_5\text{O}_4\text{S}_2$ : C, 47.77 %; H, 6.08 %; N, 9.60 %; found: C, 47.93 %; H, 6.21 %; N, 9.87 %.



## 4.2.2 Synthesis of Amino Acid Precursors

4.2.2.1 Ethyl 4-methyl-2-oxopent-3-enoate<sup>1</sup>

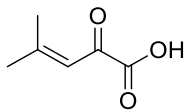
A solution of diethyl oxalate (3 g, 20.5 mmol, 1 eq), dry diethyl ether (20 ml) and dry THF (20 ml) was placed in a three necked flask equipped with a mechanical stirrer, a thermometer, a dropping funnel and an inlet tube for N<sub>2</sub> supply. The mixture was cooled to -78 °C and 2-methyl-1-propenyl magnesium bromide (50 ml of a 0.5 M solution, 24.5 mmol, 1.2 eq) in THF was added via the dropping funnel within a period of 30 minutes. After stirring for one hour the reaction was quenched with 2 N H<sub>2</sub>SO<sub>4</sub> (30 ml) and the mixture was extracted with diethyl ether (3 x 50 ml). The combined organic fractions were washed with brine (75 ml), dried over Na<sub>2</sub>SO<sub>4</sub> and filtered. The solvent was evaporated under reduced pressure to afford a yellowish oil which was purified by flash chromatography using cyclohexanes/dichloromethane 1:1 as an eluent. The product still contained some diethyl oxalate.

<sup>1</sup>H NMR (400 MHz, CDCl<sub>3</sub>): δ 1.37 (t, 3H, *J* = 7.3 Hz), 2.03 (d, 3H, *J* = 1.4 Hz), 2.24 (d, 3H, *J* = 0.67 Hz), 4.31 (q, 2H, *J* = 7.3 Hz), 6.76 (m, 1H).

<sup>13</sup>C NMR (400 MHz, CDCl<sub>3</sub>): δ 13.97, 21.73, 28.37, 62.11, 119.18, 164.35, 173.15, 197.20.



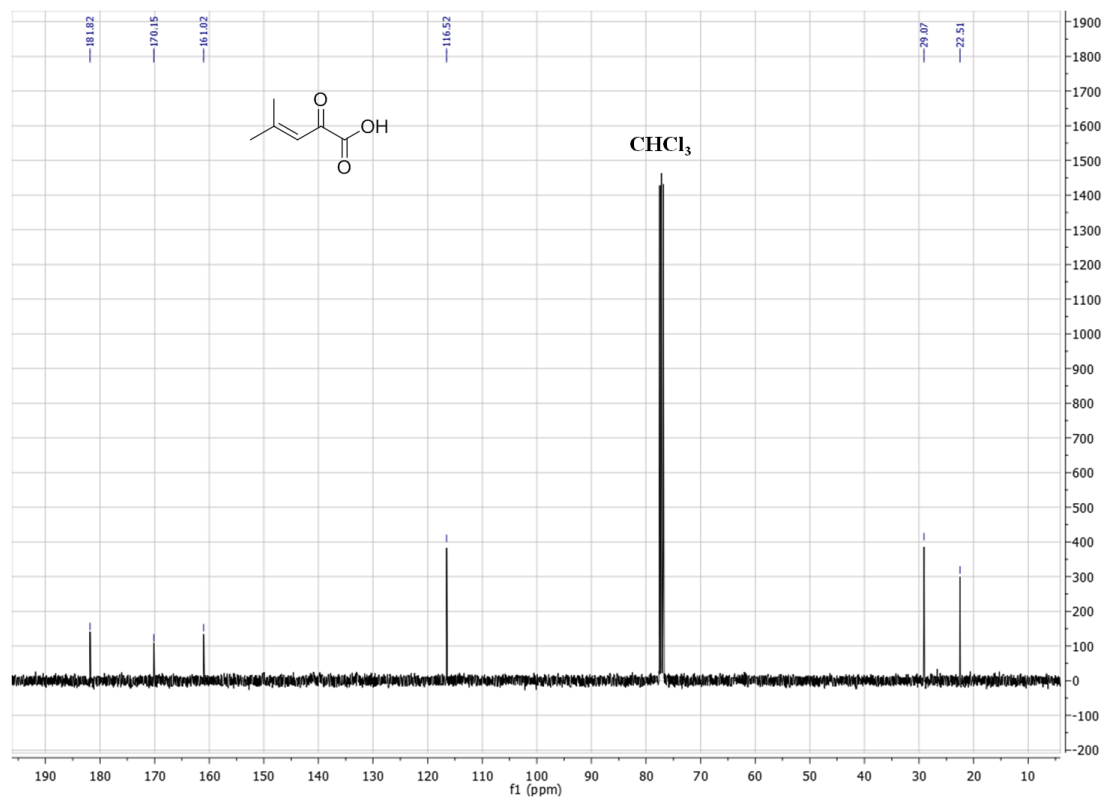
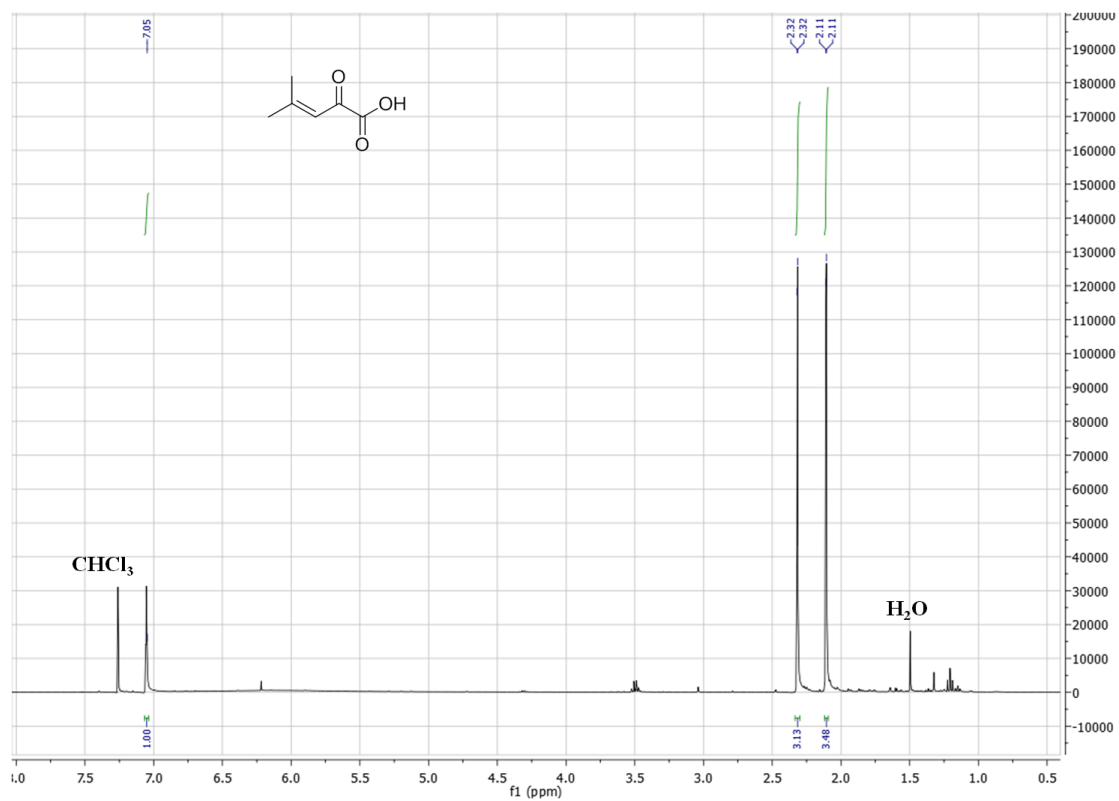
#### 4.2.2.2 4-methyl-2-oxopent-3-enoic acid<sup>2</sup>

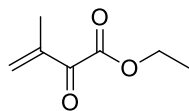


Ethyl 4-methyl-2-oxopent-3-enoate (2 g, 12.8 mmol) was dissolved in ethanol (15 ml) and the solution was added to aq. NaOH (0.1 M, 135 ml) in a round-bottomed flask equipped with a mechanical stirrer. After stirring for 12 hours, the reaction mixture was acidified with 1 M HCl and extracted with diethyl ether (4 x 150 ml). The combined organic fractions were dried over Na<sub>2</sub>SO<sub>4</sub> and filtered. The solvent was evaporated to yield the crude product as a colorless oil which was purified by flash chromatography using EtOAc/AcOH 98:2 as an eluent (0.68 g, 42% yield).

<sup>1</sup>H NMR (400 MHz, CDCl<sub>3</sub>): δ 2.11 (d, 3H, *J* = 1.23 Hz), 2.32 (d, 3H, *J* = 1.06 Hz), 7.05 (m, 1H).

<sup>13</sup>C NMR (400 MHz, CDCl<sub>3</sub>): δ 22.51, 29.07, 116.52, 161.02, 170.15, 181.82.

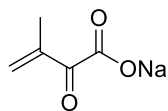


4.2.2.3 Ethyl 3-methyl-2-oxobut-3-enoate<sup>1</sup>

A solution of diethyloxalate (3.65 g, 25 mmol, 1eq), dry diethyl ether (25 ml) and dry THF (25 ml) was placed in a three necked flask equipped with a mechanical stirrer, a thermometer, a dropping funnel and an inlet tube for N<sub>2</sub> supply. The mixture was cooled to -78 °C and isoprenyl magnesium bromide (60 ml of a 0.5 M solution, 30 mmol, 1.2 eq) in THF was added via the dropping funnel within a period of 30 minutes. The progress of the reaction was monitored by GC. If some diethyloxalate remained in the reaction mixture, 2 mmol of the Grignard-reagent was added. After completion of the reaction, 2 N H<sub>2</sub>SO<sub>4</sub> (30 ml) was added before the mixture was extracted with diethyl ether (3 x 60 ml). The combined organic fractions were washed with brine (80 ml), dried over Na<sub>2</sub>SO<sub>4</sub> and filtered. The organic solvent was evaporated under reduced pressure to afford a yellowish oil (3.07 g, 86% yield).

<sup>1</sup>H NMR (400 MHz, CDCl<sub>3</sub>): δ 1.31 (t, 3H, *J* = 7.0 Hz), 1.87 (m, 3H), 4.23 (q, 2H, *J* 7.0 Hz), 6.03 (m, 1H), 6.12 (m, 1H).

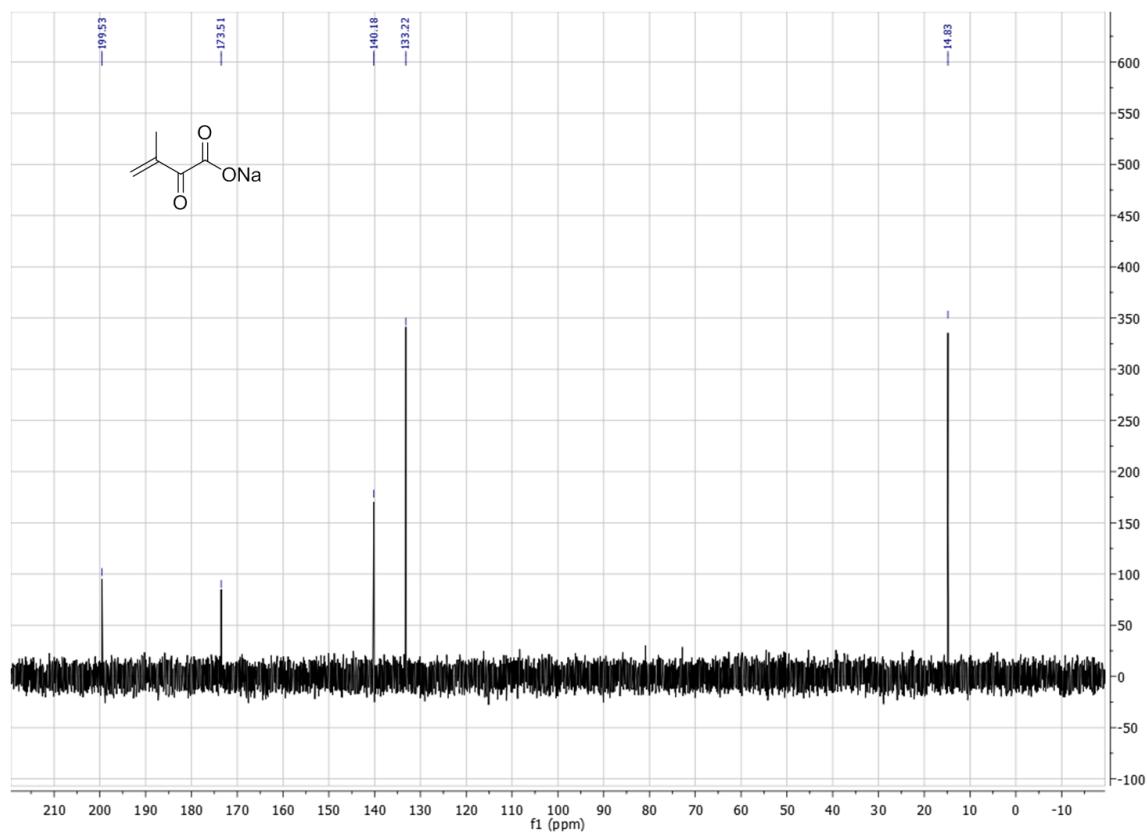
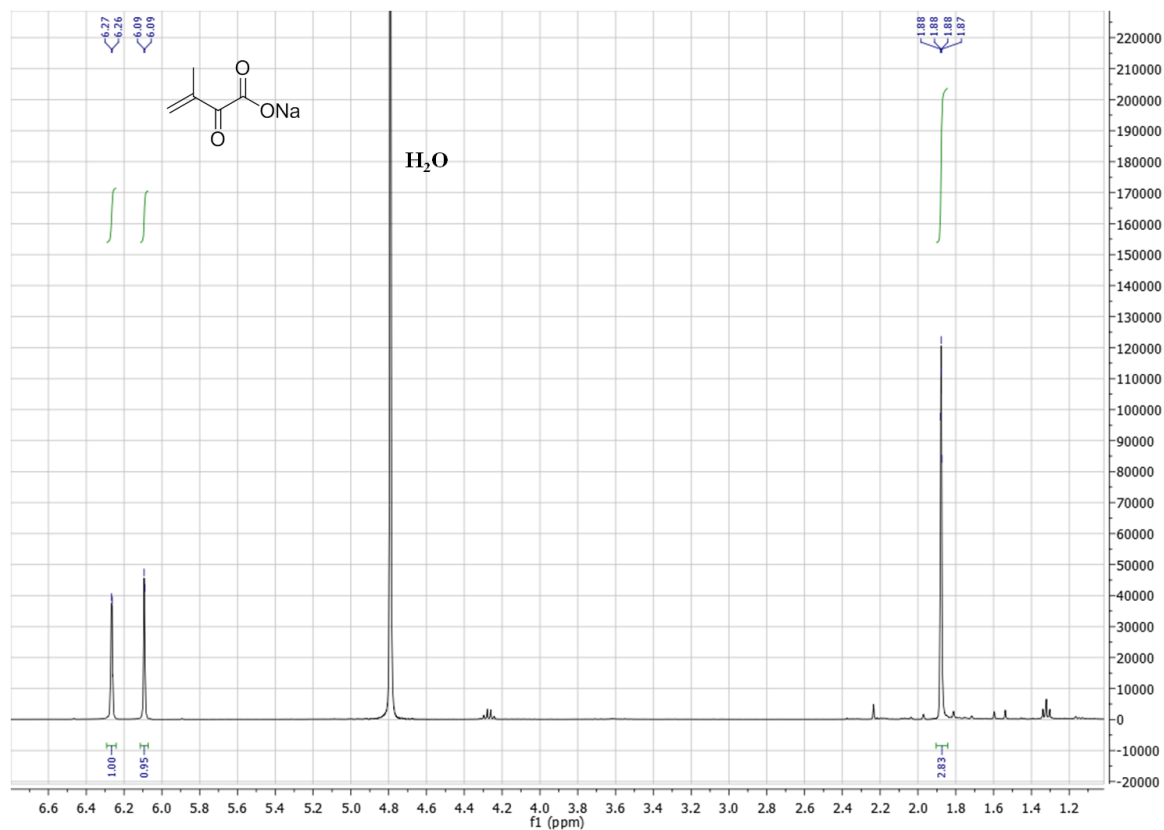
<sup>13</sup>C NMR (400 MHz, CDCl<sub>3</sub>): 13.96, 15.82, 61.91, 132.35, 140.43, 164.01, 188.73.

4.2.2.4 3-methyl-2-oxobut-3-enoate sodium salt<sup>3</sup>

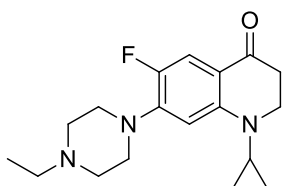
Ethyl 3-methyl-2-oxobut-3-enoate (0.43 g, 3 mmol, 1 eq), water (24 ml) and ethanol (2.5 ml) were placed in a round-bottomed flask equipped with a mechanical stirrer. 1 M aqueous NaOH (2.7 ml, 2.7 mmol, 0.9 eq) was added and the mixture was stirred over night. The resulting clear solution was then extracted with dichloromethane (12 ml) and diethyl ether (12 ml) and concentrated under reduced pressure. The resulting solid was washed with acetone and dried *in vacuo* to obtain the product as a white solid (0.25 g, 63% yield).

<sup>1</sup>H NMR (400 MHz, CDCl<sub>3</sub>): δ 1.88 (m, 3H), 6.09 (m, 1H), 6.27 (m, 1H).

<sup>13</sup>C NMR (400 MHz, CDCl<sub>3</sub>): 14.83, 133.22, 140.18, 173.51, 199.53.

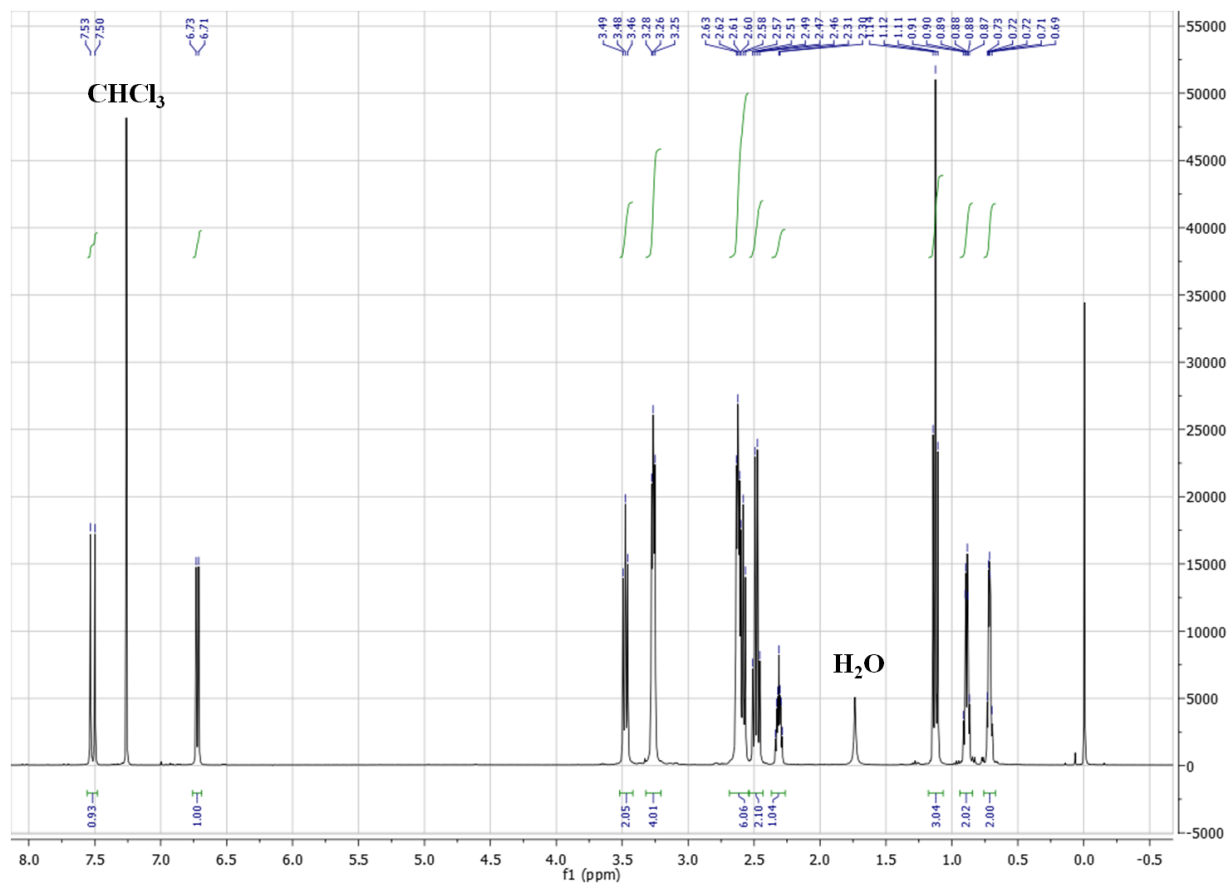


## 4.2.3 Synthesis of Reference Compound

4.2.3.1 1-cyclopropyl-7-(4-ethylpiperazin-1-yl)-6-fluoro-2,3-dihydroquinolin-4(1H)-one (reduced Enrofloxacin)<sup>4</sup>

Enrofloxacin (0.5 g, 1.4 mmol, 1eq) and dry methanol (20 ml) were placed in a round-bottomed flask equipped with a mechanical stirrer. To the suspension was added NaBH<sub>4</sub> (0.21 g, 5.6 mmol, 4 eq) in portions whereupon the reaction mixture immediately turned into a yellow solution. After stirring for 10 minutes, a catalytic amount of *p*-toluenesulfonic acid (small tip of a spatula) was added and the solution was heated to 65 °C for 45 minutes. The solvent was evaporated under reduced pressure and the resulting residue was dissolved in chloroform. The solution was washed with water, dried over Na<sub>2</sub>SO<sub>4</sub>, filtered and evaporated under reduced pressure to obtain the product as yellow prisms which were not further purified (0.345 g, 78% yield).

<sup>1</sup>H NMR (400 MHz, CDCl<sub>3</sub>): δ 0.72 (m, 2H), 0.9 (m, 2H), 1.13 (t, 3H, *J* = 7.2 Hz), 2.32 (m, 1H), 2.49 (q, 2H, *J* = 7.3 Hz), 2.56-2.65 (m, 6H), 3.27 (t, 4H, *J* = 4.8 Hz), 3.48, (t, 2H, *J* = 6.6 Hz), 6.73 (d, 1H, *J* = 7.6 Hz), 7.52 (d, 1H, *J* = 13.5 Hz).



### 4.3 HABA and CD-Titrations

#### 4.3.1 HABA-titration

Sav-mutants were dissolved in phosphate buffer (20 mM, pH 7) to a tetrameric concentration of 8  $\mu\text{M}$ . The solution was added to a quartz cuvette (2.4 ml) and treated with 0.3 ml of a 2-(4-hydroxyphenylazo)benzoic acid solution (HABA, 9.6 mM in phosphate buffer pH 7). To this mixture was added stepwise 5  $\mu\text{L}$  of either a biotin solution (0.96 mM in phosphate buffer) or 1.7  $\mu\text{L}$  of a  $[(\eta^5\text{-Cp}^*)\text{Ir}(\text{biot-}p\text{-L})\text{Cl}]$  solution (2.9 mM in DMF), corresponding to 0.25 equivalents vs. Sav tetramer. The solution was mixed at each step by means of pipetting up and down. After 5 minutes, the absorbance at 506 nm was measured.

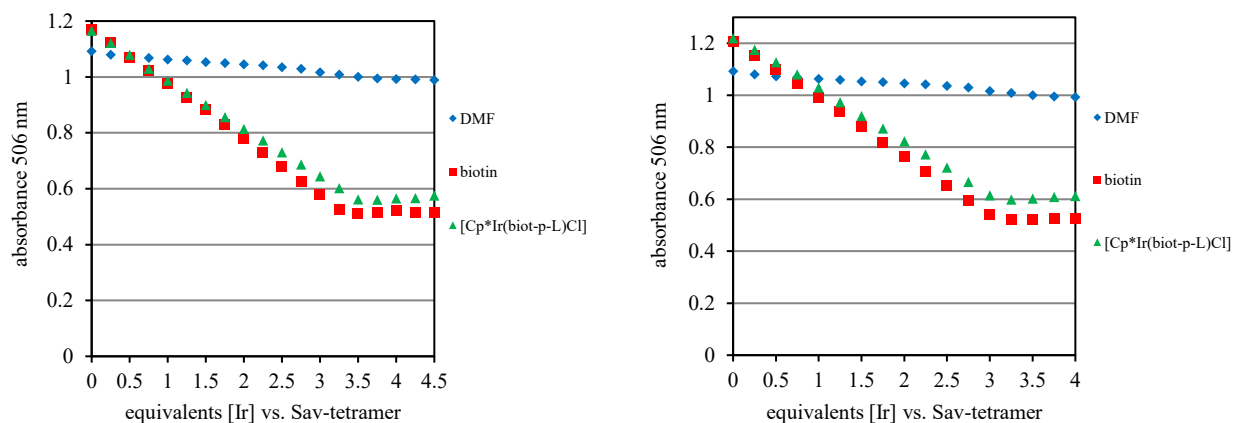


**Fig. 4.1.** Titration of HABA-saturated Sav-S112A (right) and S112K (left) with biotin (red trace) and  $[(\eta^5\text{-Cp}^*)\text{Ir}(\text{biot-}p\text{-L})\text{Cl}]$  (green trace). HABA ( $K_a \approx 10^4$ ) is displaced from Sav by a biotinylated probe whereupon the absorption maximum  $\lambda_{\text{max}}$  of the dye is shifted from 506 to 350 nm.<sup>5</sup> The equivalence point is slightly below 4 due to residual biotin or impurities in the protein preparation. As can be appreciated, DMF used as a co-solvent only displaces HABA marginally.



#### 4.3.2 CD-titration of $[(\eta^5\text{-Cp}^*)\text{Ir}(\text{biot-}p\text{-L})\text{Cl}]$ towards Sav-S112A and Sav-S112K

Streptavidin mutants were dissolved in MOPS-buffer (0.6 M, pH 7) to a tetrameric concentration of 25  $\mu\text{M}$  and the resulting solution (2.5 ml) was added to a quartz cuvette (path length: 1 cm).  $[(\eta^5\text{-Cp}^*)\text{Ir}(\text{biot-}p\text{-L})\text{Cl}]$  was dissolved in DMF to a final concentration of 37.5 mM and 2  $\mu\text{l}$  of this solution (corresponds to 0.5 equivalents  $[\text{Ir}]$  vs. Sav-tetramer) was added stepwise to the Sav-solution. The solution was mixed at each step by means of pipetting up and down. After 5 minutes, the CD-spectrum was measured in duplicate at 25  $^\circ\text{C}$  (scan range: 220-500 nm, step resolution: 1 nm, measuring time/wavelength: 1 s).

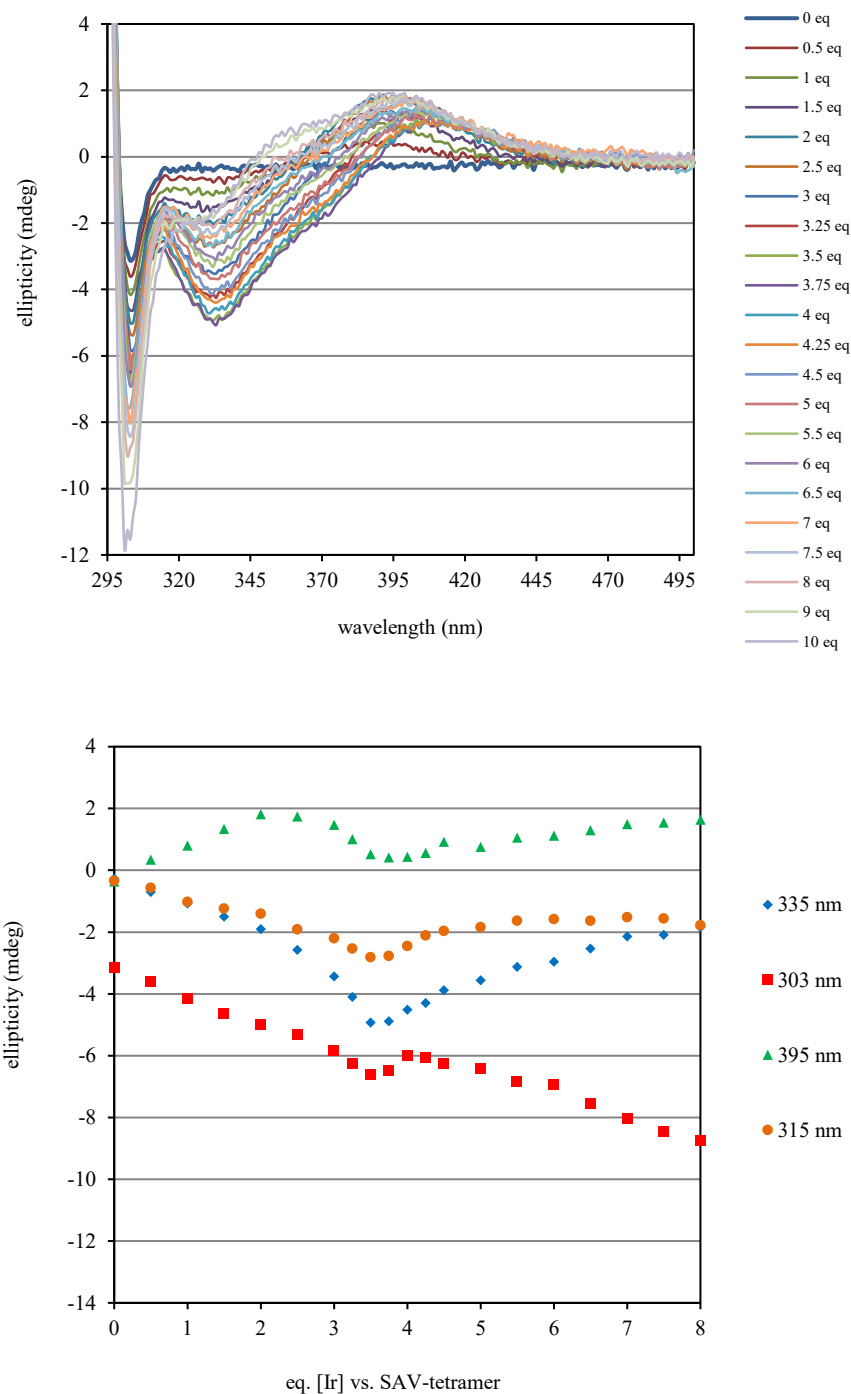


**Fig. 4.2.** CD-spectra resulting from stepwise addition of  $[(\eta^5\text{-Cp}^*)\text{Ir}(\text{biot-}p\text{-L})\text{Cl}]$  to Sav-S112A (top). A signal arises in the near UV region which is absent in the protein (bold line). The CD-signal at selected wavelengths as a function of the [Ir]/Sav ratio (bottom) indicates the accommodation of the metal complex in each biotin binding site of the Sav-tetramer.

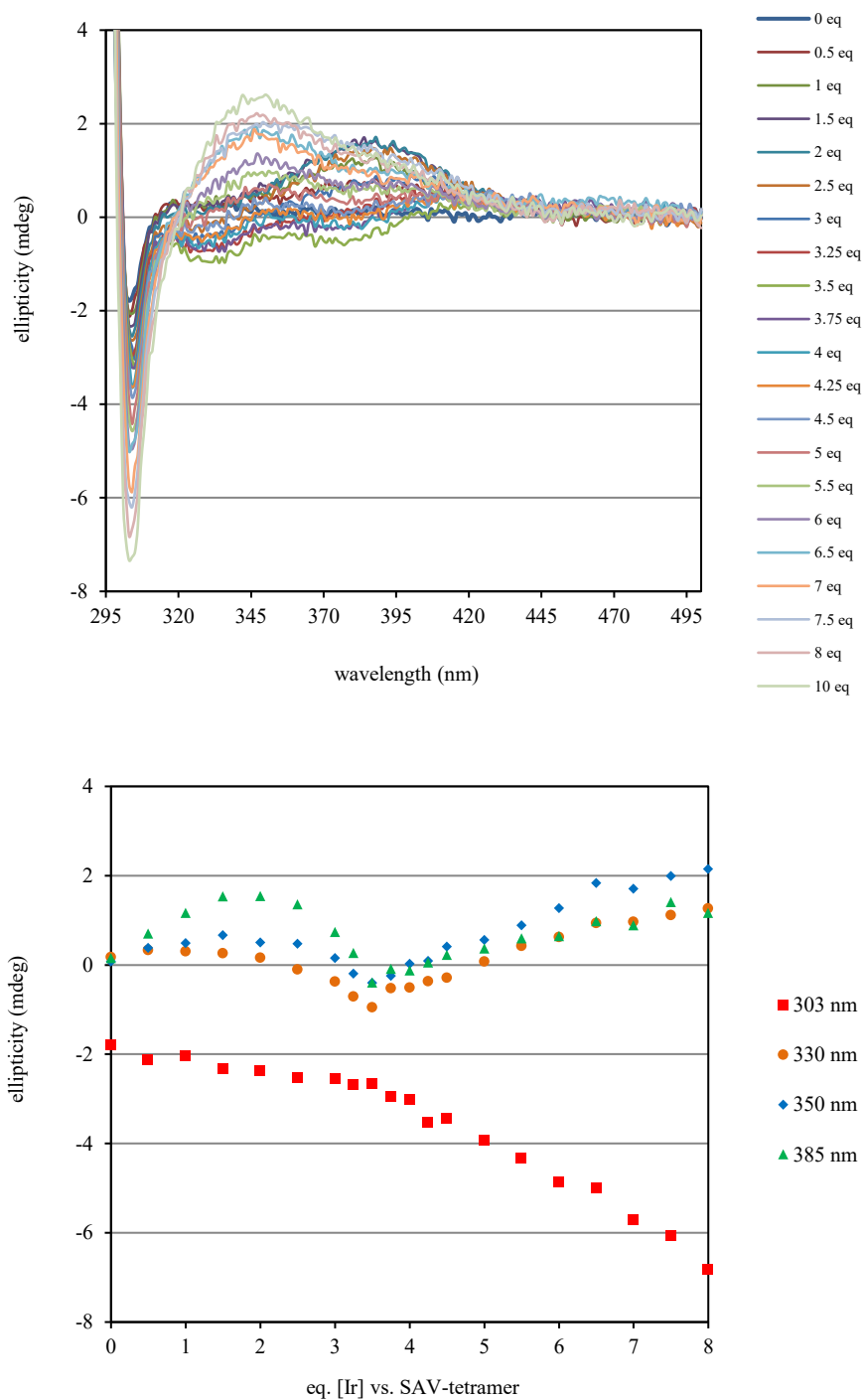


**Fig. 4.3.** CD-spectra resulting from stepwise addition of  $[(\eta^5\text{-Cp}^*)\text{Ir}(\text{biot-}p\text{-L})\text{Cl}]$  to Sav-S112K (top). A signal arises in the near UV region which is absent in the protein (bold line). The CD-signal at selected wavelengths as a function of the [Ir]/Sav ratio (bottom) indicates the accommodation of the metal complex in each biotin binding site of the Sav-tetramer.

### 4.3 NMR experiments to Elucidate the Behavior of 6,7-dimethoxy-1-methyl-3,4-dihydroisoquinoline in Aqueous Solution

All NMR experiments were performed at 25 °C on a Bruker Avance III NMR spectrometer operating at 600.13 MHz, equipped with BBFO smart probe with *z*-axis pulsed field gradients. Chemical shifts were referenced to residual solvent peaks.

The 1D <sup>1</sup>H and <sup>13</sup>C spectra were recorded applying water suppression using excitation sculpting with gradients. The HMBC spectra were recorded using a standard pulse sequence with presaturation pulses for water suppression.

#### 4.3.1 HMBC experiment to confirm the ring-closed structure

The NMR samples contained 80 mM 6,7-dimethoxy-1-methyl-3,4-dihydroisoquinoline, 160 mM phosphate and 5% D<sub>2</sub>O. The pH was adjusted by addition of either an aqueous NaOH or a HCl solution (0.25 M). Measurements were performed at pH 2.5 and 11.5.

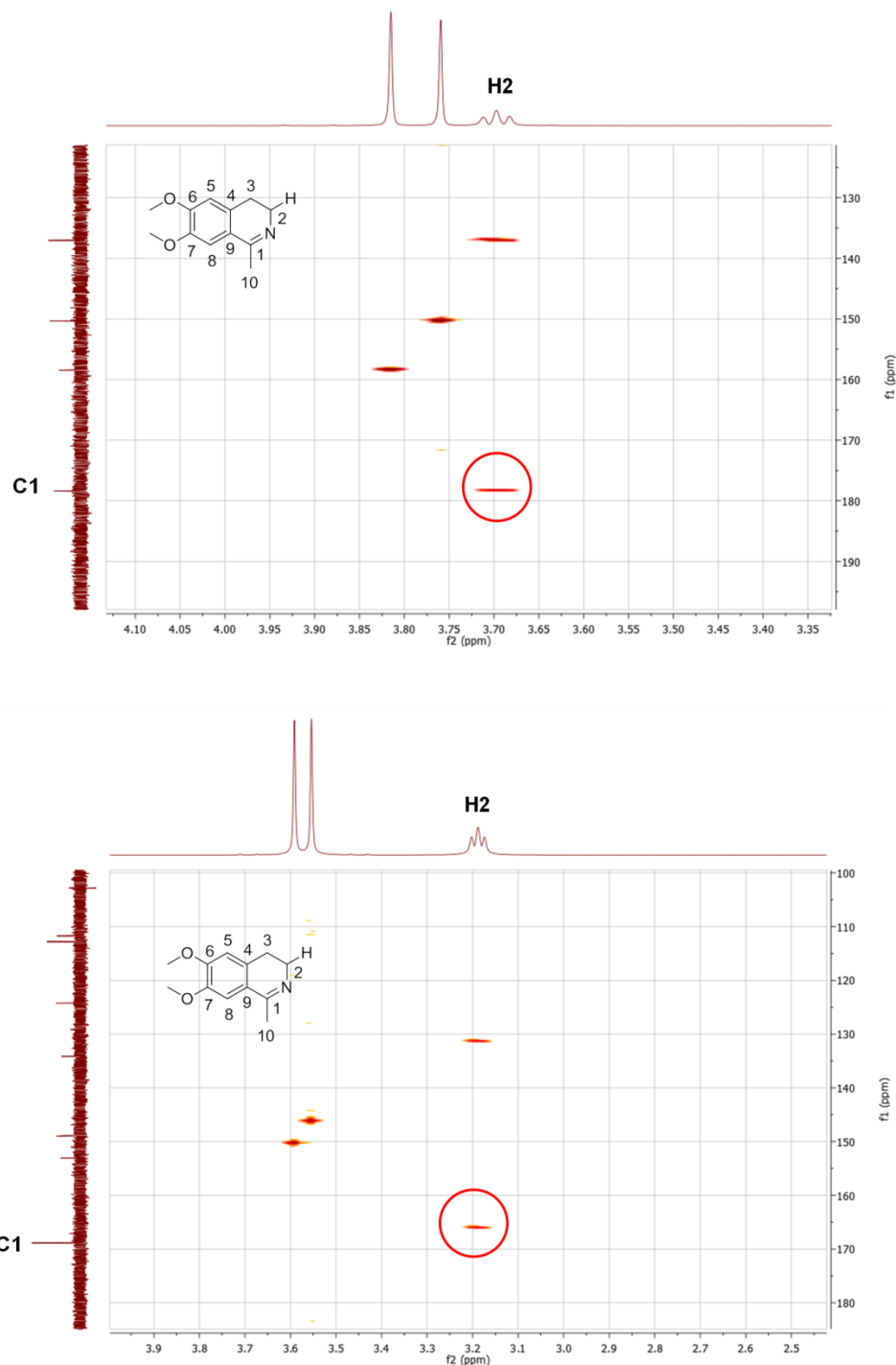


**Fig. 4.3.** Two dimensional HMBC spectra of 6,7-dimethoxy-1-methyl-3,4-dihydroisoquinoline in water at pH 2.5 (top) and 11.5 (bottom). The highlighted cross peaks correspond to a  $^3J$  coupling between carbon C1 and hydrogen H2, indicating that the compound is present as an imine in both cases. The  $^5J$  coupling in the open ketone form would result in a much less intensive or absent signal. The chemical shift of C1 further suggests the presence of an imine rather than a ketone.

4.3.2  $^1\text{H}$  and  $^{13}\text{C}$  NMR measurements to determine the  $\text{pK}_a$  value

The  $\text{pK}_a$  of 6,7-dimethoxy-1-methyl-3,4-dihydroisoquinoline was determined by measuring the  $^1\text{H}$  and  $^{13}\text{C}$  spectra at different pH values in water.

The NMR samples contained 6,7-dimethoxy-1-methyl-3,4-dihydroisoquinoline (80 mM), sodium chloride (150 mM), 3-(trimethylsilyl)-2,2',3,3'-tetradeuteropropionic acid (2 mM) as an internal standard and 5%  $\text{D}_2\text{O}$ . For each measurement at a particular pH value a new sample was prepared. The pH was adjusted by addition of either an aqueous NaOH or a HCl solution (0.25 M).

The chemical shifts of selected  $^1\text{H}$  and  $^{13}\text{C}$  nuclei were plotted as a function of the pH and the resulting data points were fitted according to the following equation<sup>6</sup>:

$$\text{pH} = \text{pK}_a - \log \frac{\frac{\delta_{\text{BH}^+} - \delta_{\text{obs}}}{\delta_{\text{BH}^+} - \delta_{\text{B}}}}{1 - \left( \frac{\delta_{\text{BH}^+} - \delta_{\text{obs}}}{\delta_{\text{BH}^+} - \delta_{\text{obs}}} \right)}$$

where  $\delta_{\text{BH}^+}$  is the chemical shift of the completely protonated form (in the sample at the lowest pH value),  $\delta_{\text{B}}$  is the chemical shift of the completely deprotonated form (in the sample of the highest pH value) and  $\delta_{\text{obs}}$  is the observed chemical shift (see table 4.1).

pH	chemical shift $\delta$ (ppm)				
	H2	H10	C1	C6	C8
3.02	3.86	2.76	178.4	158.5	114.9
5.13	3.86	2.76	178.4	158.5	114.9
7.09	3.85	2.75	178.2	158.4	114.8
7.72	3.83	2.72	177.6	158	114.6
8.18	3.77	2.65	176.5	157.4	114.2
8.46	3.72	2.58	175.5	156.8	113.5
8.7	3.66	2.51	174.4	156.2	113.1
8.91	3.6	2.45	173.3	155.6	112.8
9.13	3.55	2.38	172.2	155	112.4
9.4	3.49	2.31	171	154.3	112.1
9.78	3.43	2.24	170	153.7	111.7
10.74	3.38	2.18	169	153.2	111.7
10.87	3.38	2.18	169	153.1	111.7
11.35	3.37	2.17	168.9	153.1	111.7
11.64	3.37	2.17	168.9	153.1	111.7

**Table 4.1.** Chemical shifts of selected  $^1\text{H}$  and  $^{13}\text{C}$  nuclei of 6,7-dimethoxy-1-methyl-3,4-dihydroisoquinoline at different pH values. The values are referenced with respect to 3-(trimethylsilyl)-2,2',3,3'-tetradeuteropropionic acid.

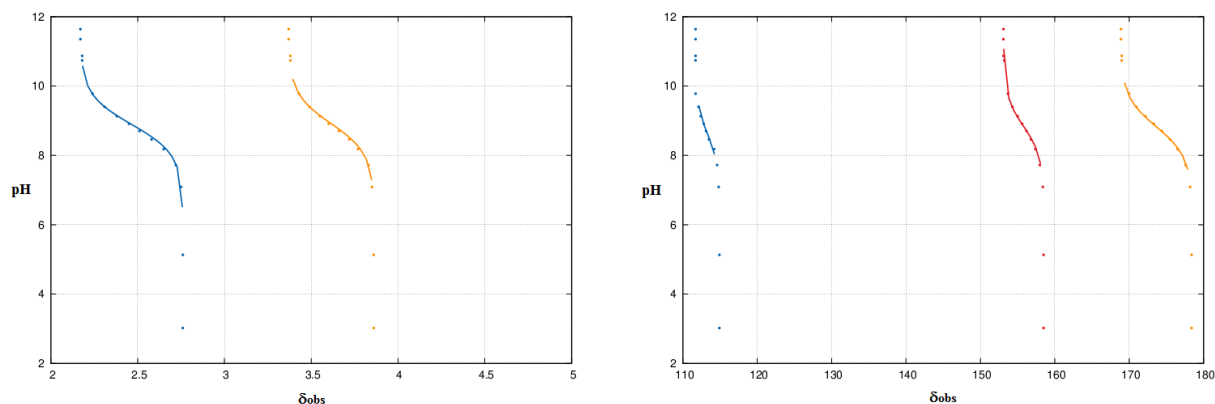
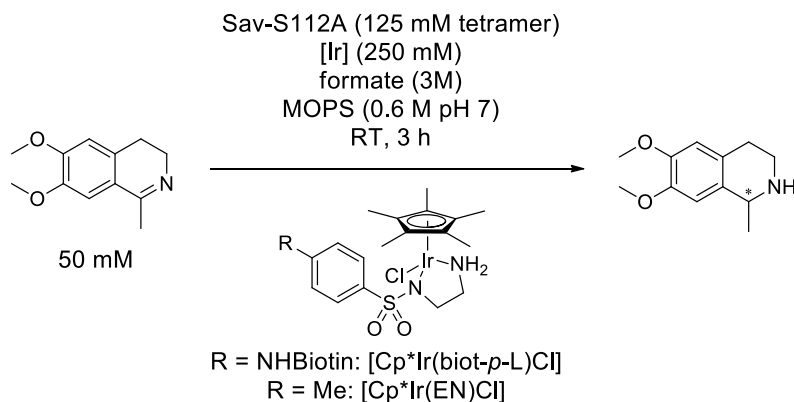


**Fig. 4.4.** Chemical shifts of selected  $^1\text{H}$  (left) and  $^{13}\text{C}$  (right) nuclei as a function of the pH. The data points were fitted as described (solid lines). The corresponding  $pK_a$  values are: (•) H10: 8.99, (•) H2: 8.91; (•) C8: 8.61, (•) C6: 8.83, (•) C1: 8.82.

## 4.4 Catalysis

### 4.4.1 Control Experiments



Buffers were prepared by dissolving MOPS (3-morpholinopropane-1-sulfonic acid) and sodium formate in water to a final concentration of 0.69 and 3.43 M, respectively. The pH was adjusted to 7 using NaOH.  $[(\eta^5\text{-Cp}^*)\text{Ir}(\text{biot-}p\text{-L})\text{Cl}]$  and  $[(\eta^5\text{-Cp}^*)\text{Ir}(\text{TsEN})\text{Cl}]$  were dissolved in DMF to a final concentration of 10 mM. The biotinylated ligand (*N*<sup>7</sup>-(4-Biotinamidophenylsulfonyl)-ethylenediamine TFA salt) and biotin were dissolved in miliQ water to a final concentration of 10 mM. The substrate (6,7-dimethoxy-1-methyl-3,4-dihydroisoquinoline) was dissolved in miliQ water to a final concentration of 1 M.

Streptavidin S112A (if present in the reaction) was dissolved in the MOPS/formate buffer to a final concentration of 571  $\mu\text{M}$  biotin binding sites. According to the experiment (see below), to 175  $\mu\text{l}$  of this solution was added either the  $[(\eta^5\text{-Cp}^*)\text{Ir}(\text{biot-}p\text{-L})\text{Cl}]$  or the  $[(\eta^5\text{-Cp}^*)\text{Ir}(\text{TsEN})\text{Cl}]$  stock solution (5  $\mu\text{l}$ ), the ligand stock solution (5  $\mu\text{l}$ ) and/or the biotin stock solution (10  $\mu\text{l}$ ). If required, the final volume was adjusted by addition of water. The mixtures were stirred for 5 minutes before the reactions were initiated by addition of the substrate stock solution (10  $\mu\text{l}$ ) and stirred.



Final volume: 200  $\mu$ l, final concentrations: 0.6 M MOPS, 3 M formate, 500  $\mu$ M Sav biotin binding sites (if present), 250  $\mu$ M  $[(\eta^5\text{-Cp}^*)\text{Ir}(\text{biot-}p\text{-L})\text{Cl}]$  or  $[(\eta^5\text{-Cp}^*)\text{Ir}(\text{TsEN})\text{Cl}]$ , 250  $\mu$ M biotinylated ligand (if present), 500  $\mu$ M biotin (if present), 50 mM substrate.

Work up and analysis:

To the reaction mixtures water (500  $\mu$ l) was added followed by 20% NaOH (50  $\mu$ l). The mixture was then extracted two times with dichloromethane (1 ml), the combined organic fractions were collected in a PP tube containing anhydrous sodium sulfate, centrifuged (18800 x g) for 5 minutes and the supernatant was analyzed by chiral HPLC using a Chiralpak IC column (5  $\mu$ m, 4.6 mm  $\cdot$  25 mm) and dichloromethane containing 1 % isopropanol and 0.06 % diethylamine as an eluent; 1 ml/min; 25  $^{\circ}$ C, 280 nm,  $T_R$  8.5 min ((*S*)-6,7-dimethoxy-1-methyl-1,2,3,4-tetrahydroisoquinoline), 9.8 min (6,7-dimethoxy-1-methyl-3,4-dihydroisoquinoline), 14.6 ((*R*)-6,7-dimethoxy-1-methyl-1,2,3,4-tetrahydroisoquinoline, referred to as salsolidine). Yields were calculated under consideration of a response factor of 1.95.

ID	Sav-S112A	$[(\eta^5\text{-Cp}^*)\text{Ir}(\text{biot-}p\text{-L})\text{Cl}]$	$[(\eta^5\text{-Cp}^*)\text{Ir}(\text{TsEN})\text{Cl}]$	biotinylated ligand	biotin	conv. (%)	ee (%)
1	yes	yes	no	no	no	75	91 ( <i>R</i> )
2	no	yes	no	no	no	95	<i>rac</i>
3	yes	no	no	no	no	0	-
4	yes	no	yes	no	no	4	<i>rac</i>
5	no	no	yes	no	no	98	<i>rac</i>
6	yes	no	no	yes	no	0	-
7	yes	yes	no	no	yes	35	14 ( <i>R</i> )

**Table 4.2.** Controll experiments elucidating that the biotinylated Ir-complex is incorporated within Sav during catalysis and that the host protein induces the enantioselectivity (TsEN = tosylate ethylenediamine).

4.4.2 pH-dependence of  $[(\eta^5\text{-Cp}^*)\text{Ir}(\text{biot-}p\text{-L})\text{Cl}]$ 

Buffers were prepared by dissolving MOPS and sodium formate in MiliQ water to a final concentration of 0.65 and 3.24 M, respectively. The pH was adjusted using conc.  $\text{H}_2\text{SO}_4$  or  $\text{NaOH}$ .  $[(\eta^5\text{-Cp}^*)\text{Ir}(\text{biot-}p\text{-L})\text{Cl}]$  was dissolved in DMF to a final concentration of 5 mM. 6,7-dimethoxy-1-methyl-3,4-dihydroisoquinoline was dissolved in miliQ water to a final concentration of 1 M.

Streptavidin mutants (if present in the reaction) were dissolved in the appropriate MOPS/formate buffer to a final concentration of 270  $\mu\text{M}$  biotin binding sites. To 185  $\mu\text{l}$  of this solution was added  $[(\eta^5\text{-Cp}^*)\text{Ir}(\text{biot-}p\text{-L})\text{Cl}]$  stock solution (5  $\mu\text{l}$ ) and the mixtures were stirred for 5 minutes. The reactions were initiated by addition of the substrate stock solution (10  $\mu\text{l}$ ).

Final volume: 200  $\mu\text{l}$ , final concentrations: 0.6 M MOPS, 3 M formate, 250  $\mu\text{M}$  Sav biotin binding sites, 125  $\mu\text{M}$   $[(\eta^5\text{-Cp}^*)\text{Ir}(\text{biot-}p\text{-L})\text{Cl}]$ , 50 mM substrate.

The work up of the reactions was performed as described in section 4.4.1.

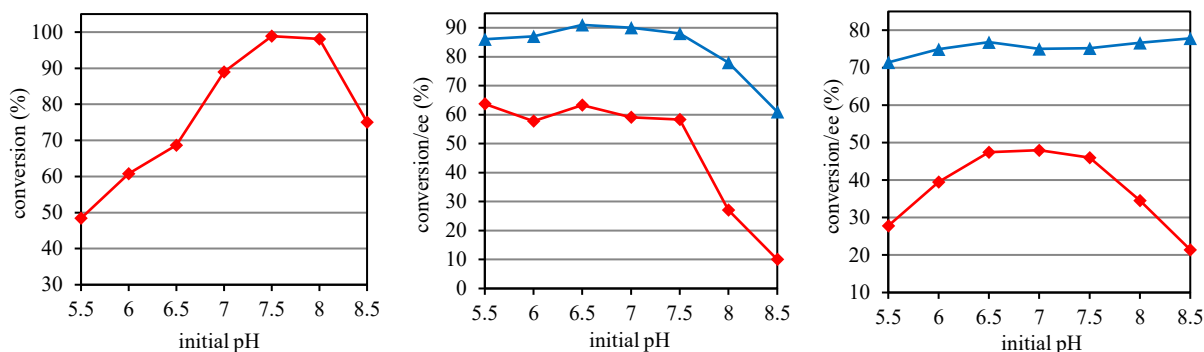
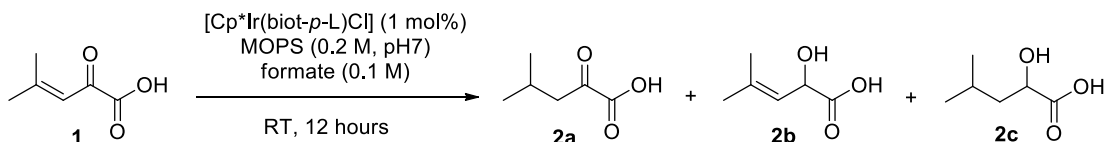


**Fig. 4.5.** pH profiles of  $[(\eta^5\text{-Cp}^*)\text{Ir}(\text{biot-}p\text{-L})\text{Cl}]$  in the transfer hydrogenation of 6,7-dimethoxy-1-methyl-3,4-dihydroisoquinoline. Red data points: conversion, blue data points: enantiomeric excess. Left: free complex after 3 hours, middle:  $[(\eta^5\text{-Cp}^*)\text{Ir}(\text{biot-}p\text{-L})\text{Cl}]\subset\text{Sav-S112A}$  after 3 hours, right:  $[(\eta^5\text{-Cp}^*)\text{Ir}(\text{biot-}p\text{-L})\text{Cl}]\subset\text{Sav-S112K}$  after 6 hours.

## 4.4.3 Transfer Hydrogenation of Amino Acid Precursors

## 4.4.3.1 4-methyl-2-oxopent-3-enoic acid (quantitative reaction)



4-methyl-2-oxopent-3-enoic acid **1** (25 mg, 0.195 mmol) was dissolved in 4 ml of the reaction buffer containing MOPS (0.2 M, pH 7) and sodium formate (0.1 M) and the solution was added to a round bottomed flask equipped with a mechanical stirrer. The reaction was initiated by addition of 50  $\mu\text{l}$  of a  $[(\eta^5\text{-Cp}^*)\text{Ir}(\text{biot-}p\text{-L})\text{Cl}]$  stock solution (40 mM in DMF). After stirring over night, the reaction mixture was acidified with 1 N  $\text{H}_2\text{SO}_4$  and extracted with dichloromethane (4 x 15 ml). The combined organic extracts were dried over  $\text{Na}_2\text{SO}_4$ , filtered and the solvent was evaporated under reduced pressure to obtain colorless oil (21.7 mg).

$^1\text{H}$  NMR (400 MHz,  $\text{CDCl}_3$ ):  $\delta$  1.78 (d, 1.5 H,  $J = 1.3$  Hz), 1.8 (d, 1.5 H,  $J = 1.1$  Hz), 2.1 (d, 3H,  $J = 1.1$  Hz), 1.31 (d, 3H,  $J = 1.1$  Hz), 4.9 (d, 0.5 H,  $J = 8.9$  Hz), 5.19-5.24 (m, 0.5 H).

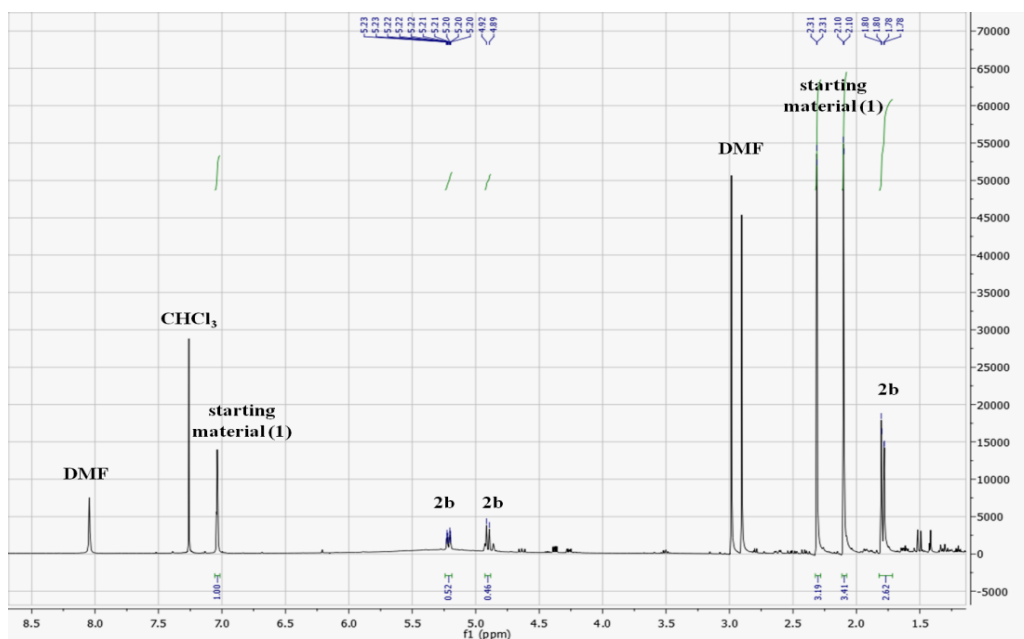
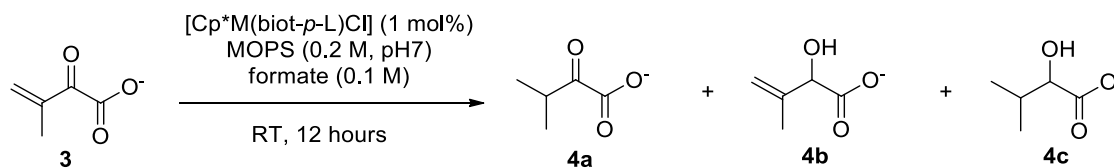


**Fig. 4.6.**  $^1\text{H}$  spectra of the crude reaction mixture resulting from the transfer hydrogenation of 4-methyl-2-oxopent-3-enoic acid with  $[(\eta^5\text{-Cp}^*)\text{Ir}(\text{biot-}p\text{-L})\text{Cl}]$ . The signals from the product **2b** are assigned according to ref. 7.

## 4.4.3.2 3-methyl-2-oxobut-3-enoate (quantitative reaction)



The reaction was performed as described in section 4.4.3.1 with 3-methyl-2-oxobut-3-enoate sodium salt **3** (25 mg, 0.184 mmol) using either 1 mol%  $[(\eta^5\text{-Cp}^*)\text{Ir}(\text{biot-}p\text{-L})\text{Cl}]$  or  $[(\eta^5\text{-Cp}^*)\text{Rh}(\text{biot-}p\text{-L})\text{Cl}]$ .

Reaction with  $[(\eta^5\text{-Cp}^*)\text{Ir}(\text{biot-}p\text{-L})\text{Cl}]$ :

The corresponding acid of **4a** was obtained as a colorless oil (17.7 mg).

$^1\text{H NMR}$  (400 MHz,  $\text{CDCl}_3$ ):  $\delta$  1.15 (s, 3 H), 1.17 (s, 3 H), 3.31 (m, 1H).

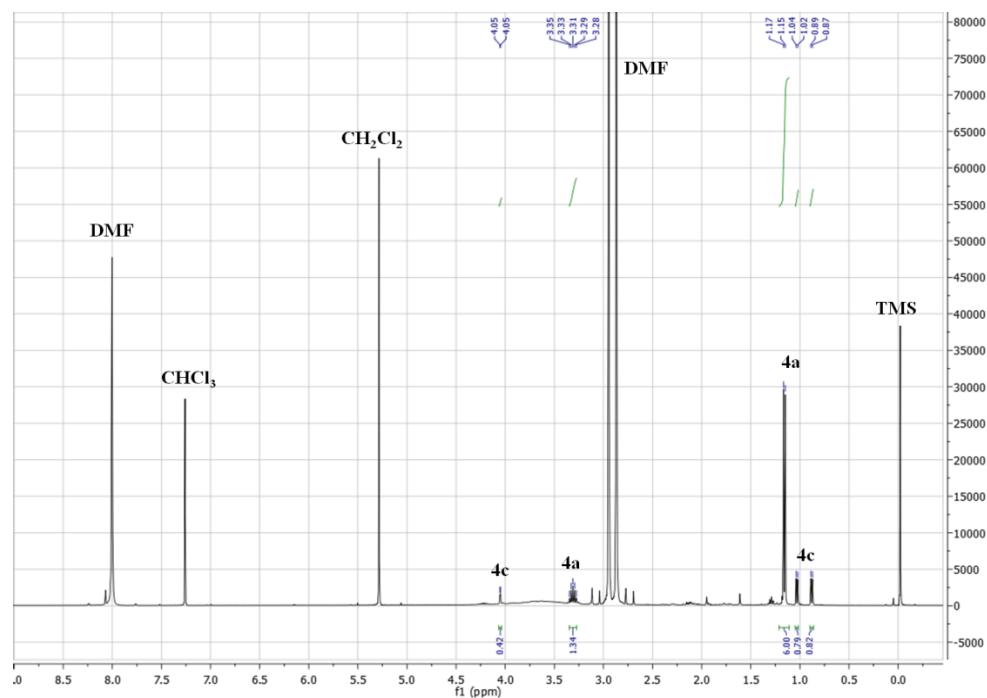


**Fig. 4.7.**  $^1\text{H}$  spectrum of the crude reaction mixture from the transfer hydrogenation of 3-methyl-2-oxobut-3-enoate with  $[(\eta^5\text{-Cp}^*)\text{Ir}(\text{biot-}p\text{-L})\text{Cl}]$ . The small peaks at 4.05 and 0.89 ppm are assigned to product **4c**.

Reaction with  $[(\eta^5\text{-Cp}^*)\text{Rh}(\text{biot-}p\text{-L})\text{Cl}]$ :

The corresponding acid of **4a** was obtained as a colorless oil (19.1 mg).

$^1\text{H NMR}$  (400 MHz,  $\text{CDCl}_3$ ):  $\delta$  1.16 (s, 3 H), 1.18 (s, 3 H), 3.33 (m, 1H).

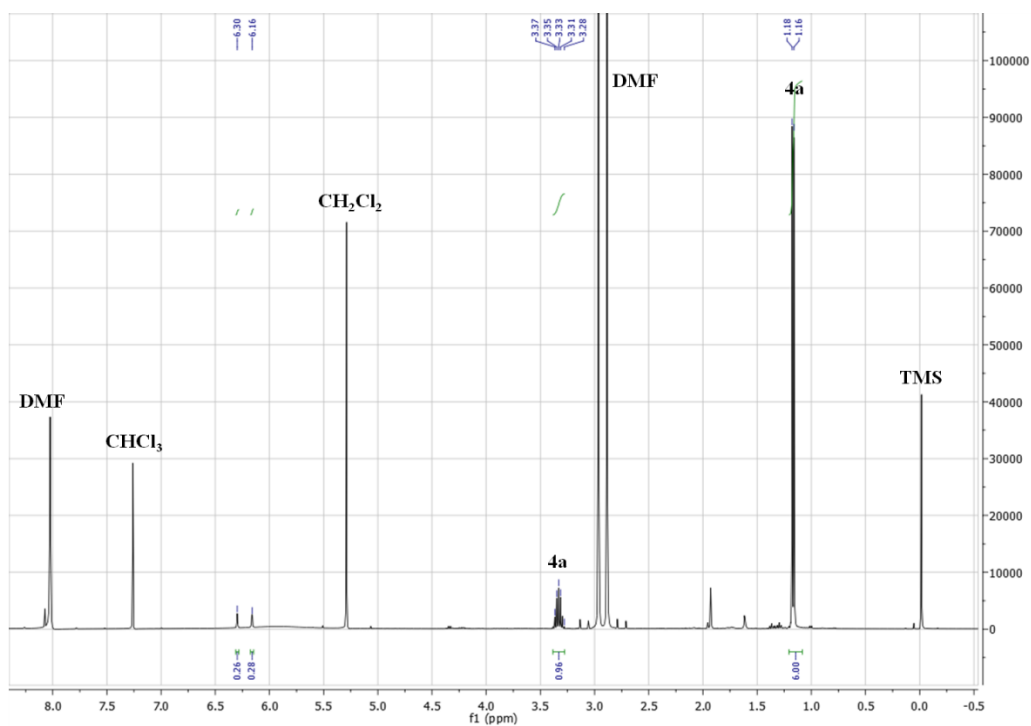
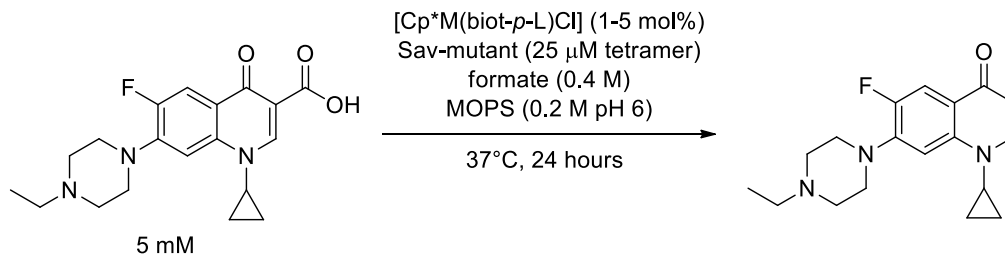


**Fig. 4.8.**  $^1\text{H}$  spectrum of the crude reaction mixture from the transfer hydrogenation of 3-methyl-2-oxobut-3-enoate with  $[(\eta^5\text{-Cp}^*)\text{Rh}(\text{biot-}p\text{-L})\text{Cl}]$ .

## 4.4.4 Transfer Hydrogenation of Enrofloxacin



The reaction buffer was prepared by dissolving MOPS and sodium formate in water to a final concentration of 0.4 and 0.8 M, respectively. The pH was adjusted with NaOH.  $[(\eta^5\text{-Cp}^*)\text{M}(\text{biot-}p\text{-L})\text{Cl}]$  (M = Rh, Ir) was dissolved in DMF to a final concentration of 4 mM. Enrofloxacin was dissolved in 12.5 M  $\text{H}_2\text{SO}_4$  to a final concentration of 10 mM. Enrofloxacin was dissolved in 12.5 M  $\text{H}_2\text{SO}_4$  to a final concentration of 10 mM. Sav-mutants (if present in the reaction) were dissolved in the reaction buffer to a final concentration of 200  $\mu\text{M}$  biotin binding sites. 100  $\mu\text{l}$  of this solution was transferred to a PP-tube and an appropriate volume of the metal complex stock solution was added. The reaction was initiated by addition of 100  $\mu\text{l}$  of the substrate stock solution and the mixtures were shaken at 37°C for 24 hours in an incubator (final concentrations: 0.2 M MOPS, 0.4 M formate, 100  $\mu\text{M}$  Sav biotin binding sites, 50-250  $\mu\text{M}$   $[(\eta^5\text{-Cp}^*)\text{M}(\text{biot-}p\text{-L})\text{Cl}]$ , 5 mM Enrofloxacin).

Work up and analysis:

The reactions were quenched by addition of 50  $\mu\text{l}$  of a glutathione solution (250 mM). 50  $\mu\text{l}$  of an acetophenone solution (35 mM in water) was added as an internal standard followed by 300  $\mu\text{l}$  water. 200  $\mu\text{l}$  of this solution was further diluted with 800  $\mu\text{l}$  water and analysed by RP-HPLC using an Eclipse XDB-C18 column (4.6 x 150 mm, particle size: 5  $\mu\text{m}$ ); solvent A: water containing 0.1% TFA, solvent B: acetonitrile; 5% B at 0 min, 30% B at 20 min, 80% B at 22 min, 80% B at 25 min, 5 % B at 5 min, 5% B at 5 min; 1 ml/min; 40°C, 254 nm; 14.9 min Enrofloxacin, 16.5 min standard, 17.7 min product.

Conversions were determined under consideration of a correlation curve obtained from plotting the ratio of the peak areas of the product and the standard as a function of the concentration the product (correlation factor: 0.1505,  $R^2 = 0.9997$ ).

entry	SAV-mutant	metal complex	[M] (mM)	conv. (%)
1	no	Ir	0.05	5
2	no	Ir	0.1	7
3	no	Ir	0.25	9
4	no	Rh	0.05	5
5	no	Rh	0.1	10
6	no	Rh	0.25	19
7	WT	Ir	0.1	6
8	S112A	Ir	0.1	9
9	S112K	Ir	0.1	2
10	K121A	Ir	0.1	10
11	S112A-K121G	Ir	0.1	9
12	WT	Rh	0.1	1
13	S112A	Rh	0.1	5
14	S112K	Rh	0.1	2
15	K121A	Rh	0.1	4
16	S112A-K121G	Rh	0.1	4

**Table 4.3.** Initial results obtained in the transfer hydrogenation of Enrofloxacin using  $[(\eta^5\text{-Cp}^*)\text{M}(\text{biot-}p\text{-L})\text{Cl}]$  (M = Rh, Ir) and respective ATHases.

## 4.5 References

- 1) Rambaud, M.; Bakasse, M.; Duguay, G.; Villieras, J. *Synthesis* **1988**, 7, 564.
- 2) Casy, G.; Lee, T.V.; Lovell, H.; Nichols, B.J.; Sessions, R.B.; Holbrook, J.B. *Chem. Soc., Chem. Commun.* **1992**, 924.
- 3) Casy, G.; Lee, T.V., Lovell, H. *Tetrahedron Lett.* **1992**; 33, 817.
- 4) Kondo, H.; Sakamoto, F.; Kawakami, K.; Tsukamoto, G. *J. Med. Chem.* **1988**, 31, 221.
- 5) Green, N.M. *Methods Enzymol.* **1990**, 184, 51.
- 6) Handloser, C.S.; Chakrabarty, M.R.; Mosher, M.W. *Journal of Chemical Education* **1973**, 50, 511.
- 7) Okrasa, K.; Levy, C.; Wilding, M.; Goodall, M.; Baudendistel, N.; Hauer, B.; Leys, D.; Micklefield, J. *Angew. Chem. Int. Ed.* **2009**, 48, 7691.



## Appendix

### List of publications

**Dürrenberger, M.**; Heinisch, T.; Wilson, Y.M.; Rossel, T.; Nogueira, E.; Knörr, L.; Mutschler, A.; Kersten, K.; Malcolm, J.Z.; Pierron, J.; Schirmer, T.; Ward, T.R. *Angew. Chem. Int. Ed.* **2011**, *50*, 3026.

Köhler, V.; Wilson, Y. M.; **Dürrenberger, M.**; Ghislieri, D.; Churakova, E.; Quinto, T.; Knörr, L.; Häussinger, D.; Hollmann, F.; Turner, N. J.; Ward, T. R. *Nat. Chem.* **2013**, *5*, 93.

Schwizer, F.; Köhler, V.; **Dürrenberger, M.**; Knörr, L.; Ward, T.R. *ACS Catal.* **2013**, *3*, 1752.

Nogueira, E.; Schleier, T.; **Dürrenberger, M.**; Ballmer-Hofer, K.; Ward, T.R.; Jaussi, R. *Prot. Expr. Purif.*, **2014**, *93*, 54.

**Dürrenberger, M.**; Ward, T.R. *Curr. Op. Chem. Bio.*, **2014**, *19*, 99.

Wilson, Y.M.; **Dürrenberger, M.**; Nogueira, E.; Ward, T. R., *J. Am. Chem. Soc.* **2014**, *136*, 8928.

Munoz, V.; **Dürrenberger, M.**; Heinisch, T.; Schirmer, T.; Ward, T.R.; Maréchal, J.D. *J. Am. Chem. Soc.* **2014**, *136*, 15676.

Heinisch, T.; Pellizzoni, M.; **Dürrenberger, M.**; Tinberg, C.E.; Köhler, V.; Klehr, J.; Häussinger, D.; Baker, D.; Ward, T.R. *J. Am. Chem. Soc.* **2015**, *137*, 1041

